สารต้านมะเร็งและต้านการสร้างหลอดเลือดใหม่จากราเอนโดไฟต์ที่แยกได้จากพืชป่าชายเลนไทย

นางสาวสุพิชชา โชคไพบูลย์

วิทยานิพนธ์นี้เป็นส่วนหนึ่งของการศึกษาตามหลักสูตรปริญญาวิทยาศาสตรดุษฎีบัณฑิต
สาขาวิชาเทคโนโลยีชีวภาพ
คณะวิทยาศาสตร์ จุฬาลงกรณ์มหาวิทยาลัย
ปีการศึกษา 2558

ANTICANCER AND ANTIANGIOGENIC AGENTS FROM ENDOPHYTIC FUNGI ISOLATED FROM THAI MANGROVE PLANTS

Miss Supichar Chokpaiboon

A Dissertation Submitted in Partial Fulfillment of the Requirements
for the Degree of Doctor of Philosophy Program in Biotechnology
Faculty of Science
Chulalongkorn University
Academic Year 2015

Thesis Title	ANTICANCER AND ANTIANGIOGENIC AGENTS FROM ENDOPHYTIC FUNGI ISOLATED FROM THAI MANGROVE PLANTS
By	Miss Supichar Chokpaiboon
Field of Study	Biotechnology
Thesis Advisor	Assistant Professor Khanitha Pudhom, Ph.D.
Thesis Co-Advisor	Taridaporn Buajarean, Ph.D.

Accepted by the Faculty of Science, Chulalongkorn University in Partial Fulfillment of the Requirements for the Doctoral Degree

.....Dean of the Faculty of Science
(Associate Professor Polkit Sangvanich, Ph.D.)

THESIS COMMITTEE

.....Chairman
(Associate Professor Vudhichai Parasuk, Ph.D.)

.....Thesis Advisor
(Assistant Professor Khanitha Pudhom, Ph.D.)

.....Thesis Co-Advisor
(Taridaporn Buajarean, Ph.D.)

.....Examiner
(Associate Professor Chanpen Chanchao, Ph.D.)

.....Examiner
(Assistant Professor Pattara Thiraphibundet, Ph.D.)

.....External Examiner
(Professor Apichart Suksamrarn)

สุพิชชา โชคไพบูลย์ : สารต้านมะเร็งและต้านการสร้างหลอดเลือดใหม่จากราเอนโดไฟต์ที่แยกได้จากพืชป่าชายเลนไทย (ANTICANCER AND ANTIANGIOGENIC AGENTS FROM ENDOPHYTIC FUNGI ISOLATED FROM THAI MANGROVE PLANTS) อ.ที่ปรึกษาวิทยานิพนธ์หลัก: ผศ. ดร. ขนิษฐา พุดหอม, อ.ที่ปรึกษาวิทยานิพนธ์ร่วม: ดร. ธริดาพร บัวเจริญ, 231 หน้า.

จากการนำส่วนสกัดเอธิลแอซิเทตของราเอนโดไฟต์ *Rhytidhysteron rufulum* จากพังกาหัวสุมดอกแดงที่เพาะเลี้ยงใน Sabouraud dextrose broth มาทำการแยกให้บริสุทธิ์ พบสารอนุพันธ์โครโมนใหม่ 5 ชนิด คือ rhytidchromone A-E (1-5), สารอนุพันธ์ไอโซคูมารินใหม่ 1 ชนิด (6) และสารที่มีการรายงานมาก่อนอีก 1 ชนิด คือ **α**-D-galacto pyranoside methyl (7) เมื่อนำสารเหล่านี้มาทดสอบฤทธิ์ยับยั้งเซลล์มะเร็งตับ, มะเร็งกระเพาะอาหาร, มะเร็งเต้านมและมะเร็งปากมดลูก พบว่า rhytidchromone A (1), B (2), D, (4) และ E (5) แสดงฤทธิ์ยับยั้งเซลล์มะเร็ง โดยมีค่า IC_{50} อยู่ระหว่าง 16.0-29.3 μM ตามลำดับ ขณะที่สาร 3, 6 และ 7 ไม่มีฤทธิ์ยับยั้งเซลล์มะเร็ง นอกจากนี้ได้นำส่วนสกัดของเอธิลแอซิเทตของราเอนโดไฟต์ basidiomycetous จากตะบูนขาวที่เพาะเลี้ยงใน corn steep broth มาทำการแยกให้บริสุทธิ์ พบว่าได้สารเซสควิเทอร์พีนชนิดใหม่ 1 ชนิด คือ merulin D (11) และสารที่มีการรายงานมาก่อนอีก 4 ชนิด คือ merulin A-C (8-10) และ steperoxide A (12) เมื่อนำสารเหล่านี้มาทดสอบฤทธิ์ต้านการสร้างหลอดเลือดใหม่ พบว่าสาร 10 สามารถยับยั้งการสร้างหลอดเลือดใหม่ได้ดีมากทั้งในระดับ *ex vivo* และ *in vivo* ซึ่งเป็นผลมาจากการยับยั้งการเพิ่มจำนวน (proliferation) ของเซลล์เยื่อบุผนังหลอดเลือด (HUVEC) เป็นหลัก ซึ่งสอดคล้องกับการยับยั้งการเกิด phosphorylation ของ Erk1/2 นอกจากการศึกษาราเอนโดไฟต์จากพืชป่าชายเลน ยังได้นำราทะเล *Astrophaeriella nypae* ที่แยกได้จากต้นจากมาเพาะเลี้ยงใน LCN medium ซึ่งเมื่อนำส่วนสกัดเอธิลแอซิเทตมาแยกให้บริสุทธิ์พบว่า ได้สารใหม่ 3 ชนิด คือ astronypyrone (13), astronyquinone (14) และ astronyurea (15) และสารที่มีการรายงานมาก่อนอีก 4 ชนิด คือ xestodecalactone A (16), B (17), coryoctalactone B (18) และ dimethoxy-*O*-methylpulvinone (19) ได้นำสาร 14, 16 และ 19 มาทดสอบฤทธิ์ยับยั้งเชื้อมาลาเรีย และความเป็นพิษต่อเซลล์ปกติ พบว่า มีเพียงสาร 19 สามารถยับยั้งเชื้อมาลาเรียสายพันธุ์ดื้อยา *Plasmodium falciparum* K1 strain โดยมีค่า IC_{50} เป็น 16.9 μM โดยไม่แสดงความเป็นพิษต่อเซลล์ปกติ

สาขาวิชา เทคโนโลยีชีวภาพ ลายมือชื่อนิสิต .....

ปีการศึกษา 2558 ลายมือชื่อ อ.ที่ปรึกษาหลัก .....

ลายมือชื่อ อ.ที่ปรึกษาร่วม .....

5373913723 : MAJOR BIOTECHNOLOGY

KEYWORDS: FUNGAL METABOLITES / ANTI-ANGIOGENIC / CYTOTOXICITY

SUPICHAR CHOKPAIBOON: ANTICANCER AND ANTIANGIOGENIC AGENTS FROM ENDOPHYTIC FUNGI ISOLATED FROM THAI MANGROVE PLANTS. ADVISOR: ASST. PROF. KHANITHA PUDHOM, Ph.D., CO-ADVISOR: TARIDAPORN BUAJAREAN, Ph.D., 231 pp.

Chromatographic fractionation of EtOAc crude extracts of an endophytic fungus, *Rhytidhysteron rufulum* isolated from *Bruguiera gymnorrhiza* cultured on Sabouraud dextrose broth led to the isolation of five new chromone derivatives, rhytidchromones A-E (1-5), one new isocoumarin derivative (6) and one known **α**-D-galacto pyranoside methyl (7). All compounds were evaluated for cytotoxic effect against four human tumor cell lines: hepato carcinoma (Hep-G2), gastric carcinoma (KATO-3), human breast cancer (MCF-7) and cervical carcinoma (CaSki). Rhytidchromones A (1), B (2), D (4) and E (5) showed cytotoxicity against Hep-G2, KATO-3, MCF-7 and CaSki with IC_{50} ranging of 16.0-29.3 μM, while compounds 3, 6 and 7 did not show any significant activity against all tested cell lines. Additionally, purification of EtOAc crude extract of basidiomycetous fungus from X*ylocarpus granatum* Koenig cultured on corn steep broth by chromatographic technique led to the isolation of one new chamigrane endoperoxide, merulin D (11), and four known derivatives, merulins A-C (8-10) and steperoxide A (12). All isolated compounds were evaluated for their anti-angiogenic activity. Only compound 10 displayed promising activity in both *ex vivo* and *in vivo* models. It was found that the activity of 10 was mainly resulted from the suppression of endothelial cell (HUVEC) proliferation and its effect is mediated by reduction in the phosphorylation of Erk1/2. Moreover, a marine-derived fungus *Astrophaeriella nypae* BCC 3553, isolated from *Nypa fruticans* was cultivated in LCN medium. Purification of its EtOAc crude extracts led to the isolation of three new secondary metabolites, astronypyrone (13), astronyquinone (14) and astronyurea (15), along with four known compounds, xestodecalactones A and B (16-17), coryotalactone B (18), and dimethoxy-*O*-methylpulvinone (19). Compounds 14, 16 and 19 were evaluated for their antimalarial activity and toxicity on normal cell lines. Only 19 exhibited antimalarial activity against *Plasmodium falciparum* K1 strain with an IC_{50} value of 16.9 μM, without toxicity to normal cells.

Field of Study: Biotechnology
Academic Year: 2015

Student's Signature .....
Advisor's Signature .....
Co-Advisor's Signature .....

ACKNOWLEDGEMENTS

I would like to express my sincere gratitude to my mentor, Assistant Professor Dr. Khanitha Pudhom, for her excellent, her valuable guidance, which motivated me to pass through this course successfully. I also would like to express my respect and gratitude to my co-advisor, Dr. Taridaporn Buajarean, for kind supervision and kind suggestions.

Many thanks to the thesis committees, Associate Professor Vudhichai Parasuk, Department of Chemistry, Faculty of Science, Chulalongkorn University; the thesis examiners : Associate Professor Dr. Chanpen Chanchao, Department of Biology, Faculty of Science, Chulalongkorn University, Assistant Professor Pattara Thiraphibundet, Faculty of Science, Department of Chemistry, Faculty of Science, Chulalongkorn University and Professor Dr. Apichart Suksumrarn, Department of Chemistry, Faculty of Science, Ramkhamhaeng University, for their invaluable discussion and suggestion.

I wish to thank the Thailand Graduate Institute of Science and Technology (TGIST; Grant No. TGIST 01-53-011) of the National Science and Technology Development Agency (NSTDA) for providing scholarship. I would like to thank the staff of Bioresource Research Laboratory. I would like to thank Mr. Nattawut Boonyuen, Fungal Biodiversity Laboratory, for fungal identification. I am also grateful to the National Center for Genetic Engineering and Biotechnology (BIOTEC) for supporting all technical facilities.

I wish to thank The 90th Anniversary of Chulalongkorn University Fund (Ratchadaphiseksomphot Endowment Fund) for granting partial financial support to conduct this research. I am grateful to Dr. Thapong Teerawatananond, Department of Chemistry, Faculty of Science and Technology, Valaya Alongkorn Rajabhat University who kindly performed the X-ray crystallographic analysis. I would like to thank Associate Professor Dr. Kiminori Matsubara, Department of Human Life Science Education, Graduate School of Education, Hiroshima University, Japan for anti-angioganic activity.

I wish to thank my laboratory colleagues at room 1532 for their help and friendship,

Finally, I would like to dedicate my work to my parent for their endless and unfailing love.

CONTENTS

Page

Page

Page

Page

Page

LIST OF TABLES

Page

Page

LIST OF FIGURES

Page

Page

Page

Page

Page

LIST OF SCHEMES

Page

LIST OF ABBREVIATIONS

J	Coupling constant
δ	Chemical shift
δ_H	Chemical shift of proton
δ_C	Chemical shift of carbon
s	Singlet (for NMR spectra)
d	Doublet (for NMR spectra)
dd	Doublet of doublet (for NMR spectra)
ddd	Doublet of doublet of doublet (for NMR spectra)
dddd	Doublet of doublet of doublet of doublet (for NMR spectra)
t	Triplet (for NMR spectra)
m	Multiplet (for NMR spectra)
q	Quartet (for NMR spectra)
brs	Broad singlet (for NMR spectra)
brd	Broad doublet (for NMR spectra)
qC	Quaternary carbon
calcd.	Calculated
^{1}H NMR	Proton nuclear magnetic resonance
^{13}C NMR	Carbon-13 nuclear magnetic resonance
2D NMR	Two dimensional nuclear magnetic resonance

^{1}H-^{1}H COSY	Homonuclear (proton-proton) correlation spectroscopy
NOESY	Nuclear overhauser effect spectroscopy
HSQC	Heteronuclear single quantum coherence
HMBC	Heteronuclear multiple bond correlation
ORTEP	Oak ridge thermal ellipsoid plot
HRESIMS	High resolution electrospray ionization mass spectrometry
ESIMS	Electrospray ionization mass spectrometry
CC	Column chromatography
TLC	Thin layer chromatography
MIC	Minimum inhibitory concentration
IC_{50}	Half maximal inhibitory concentration
$CDCl_3$	Deuterated chloroform
CD_3OD	Deuterated methanol
$(CD_3)_2SO$	Deuterated dimethyl sulfoxide
MeOH	Methanol
EtOH	Ethanol
$CHCl_3$	Chloroform
CH_2Cl_2	Dichloromethane
EtOAc	Ethyl acetate
DMSO	Dimethylsulfoxide

KBr	Potassium bromide
$(NH_4)_6Mo_7O_{24}$	Ammonium molybdate
H_2SO_4	Sulfuric acid
SiO_2	Silicon dioxide
g	Gram (s)
mg	Milligram (s)
mL	Milliliter (s)
μg	Microgram (s)
μL	Microliter (s)
μM	Micromolar
mM	Millimolar
L	Liter (s)
M	Molar
min	Minute
h	Hour
rpm	Round per minute
m	Meter (s)
mm	Millimeter (s)
cm	Centimeter (s)
nm	Nanometer

Hz	Hertz
MHz	Megahertz
cm^{-1}	Reciprocal centimeter (unit of wave number)
ppm	part per million
NMR	Nuclear magnetic resonance
MS	Mass spectrometry
IR	Infared
UV	Ultraviolet
m.p.	Melting point
α	Alpha
β	Beta
γ	Gamma
Δ	Delta
m/z	Mass to charge ratio
$[M+H]^+$	Protonated molecule
$[M+Na]^+$	Pseudomolecular ion
$[\alpha]_D^{20}$	Specific rotation at 20 $^{\circ}C$ and sodium D line (589 nm)
λ_{max}	Wavelength of maximum absorption
c	Concentration
ε	Molar extinction coefficient

Å	Angstrom
°C	Degree celcius
deg.	Degree
spp.	Species
No.	Number
ATCC	American type culture collection

CHAPTER I

INTRODUCTION

1.1 Cancer

Global cancer rates have been increasing largely due to an aging population and lifestyle changes in the developing world. The most significant risk factor for developing cancer is old age although it is possible for cancer to strike at any age. In 2012, about 14.1 million new cases of cancer happened worldwide by causing about 8.2 million deaths or 14.6% of all human deaths [1].

Cancer is a group of more than 100 different diseases since it can begin almost anywhere in the body. Two key appearances of this disease are the uncontrolled growth of the cells in the human body and the ability of those cells to migrate from the original site and spread to distant sites. Normally, cancer cells can breakdown away from on original mass of cells; then spread from its original site by local spread, lymphatic spread to regional lymph nodes or by blood to distant sites. The process of cancer cells leaving an area and growing in another body area is termed metastatic spread or metastasis (Figure 1.1). When cancer spreads by a haematogenous route, it generally spreads all above the body. The signs of metastatic cancers rely on the location of the tumor, and can include expanded lymph nodes, increased liver or increased spleen, that can be felt in the abdomen, pain or break of affected bones, and neurological symptoms, where they can again repeat the uncontrolled growth cycle [2].

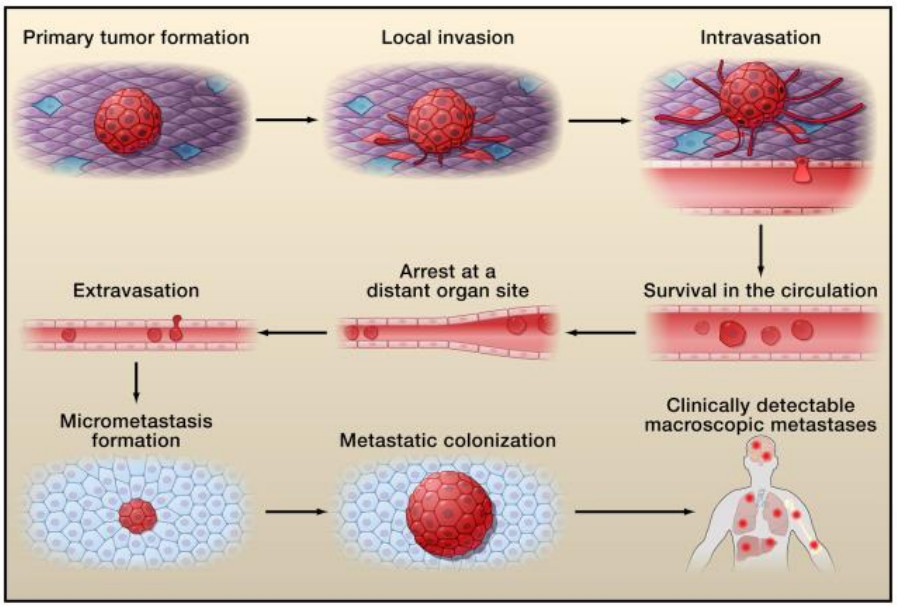

Figure1.1 The invasion–metastasis cascade [3]

There are about 100 types of cancer and the symptoms and treatment of each varies from the other. The most common types of cancer in males are lung, prostate, colorectal, and stomach cancer, while those in females, are breast, colorectal, lung, and cervical cancer. Furthermore, cancers of the kidneys, ovaries, uterus, pancreas, bladder, rectum, blood (leukemia), and lymph nodes (lymphoma) are shown in Figure 1.2

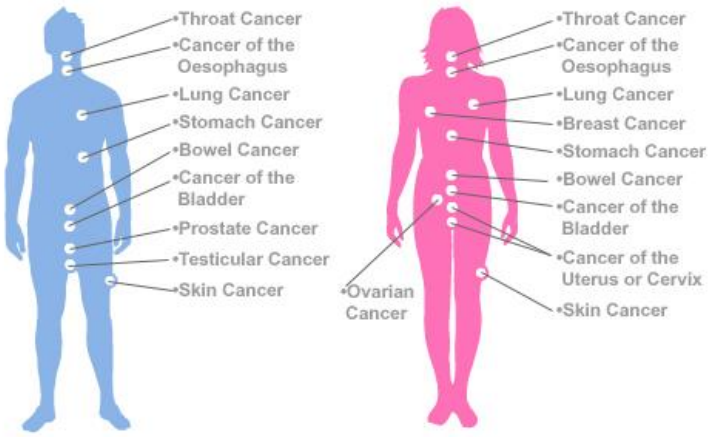

Figure 1.2 Types of cancer.
(http://www.doctorshangout.com/profiles/blogs/cancer-treatment)

The great majority of cancers, 90–95% of cases, are due to environmental factors. The remaining 5–10% is due to inherited genetics. Environmental factors include lifestyle, economic, behavioral factors, and pollution. The factors contributing to cancer death contain tobacco (25–30%), diet and obesity (30–35%), infections (15-20%), radiation (10%), stress, lack of physical activity, and environmental pollutants.

1.2 Treatment of cancer

Several treatment choices for cancer include surgery, chemotherapy, radiation therapy, hormonal therapy, targeted therapy and palliative care, depending on the type and the stage of the cancer. Chemotherapy is one of the major ways for treatment of cancer patients; it mainly contains cytotoxic drugs, and can kill fast proliferating cells which are a common feature of all cancer types. However, there are some limitations the chemotherapy can also kill the normal fast dividing cells and cause serious side effects in patients. Targeted therapies have been develop, which target a specific molecule or pathway differentially expressed in cancer cells [2].

Despite many anticancer drugs have been discovered and developed to use in clinical treatments over the last decades, most of available drugs are non-selective cytotoxic molecules which provoke severe adverse effects, as well as drug resistance. Therefore the discovery and development of new effective chemotherapeutic agents are still required in the fight against cancer. The best promising anticancer drugs from natural resource is Paclitaxel (trade name Taxol®, Figure 1.3), a diterpenoid originally isolated from yew tree (*Taxus brevifolia*). It caused more believe and interest than any other new drug since its discovery. This compound is unique model of action inhibits with the development of cancer cells, intersecting their growth and spreading. USFDA (United States Food and Drug Administration) has accepted taxol for the treatment of advanced breast cancer, lung cancer, and ovarian cancer.

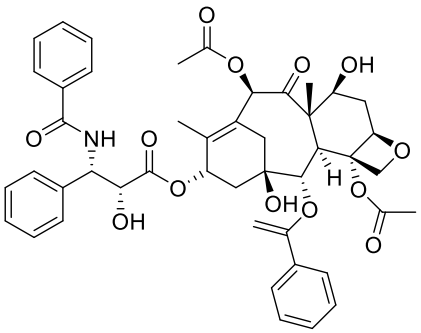

Figure 1.3 Structure of Taxol®

Although numerous plants species have been reported to produce camptothecin important drug from natural resources for cancer treatment is an alkaloid the major practical sources of this compound are from stem bark of two tree species, namely, *Camptotheca acuminata* Decaisne and *Nothapodytes nimmoniana*. Now, the heavy requirement for camptothecin (Figure 1.4) has caused in wide harvesting of these trees in China and India. The endophytic fungi have generated a great deal of attention for the potential role they could play in as important alternative sources of novel plant metabolites. Camptothecin obtained firstly from the endophytic fungi *Fusarium solani*, isolated the wood of *Camptotheca acuminate* in China [4]. It is an important precursor for the synthesis of the clinically useful anticancer drugs including topotecan and irinotecan [5].

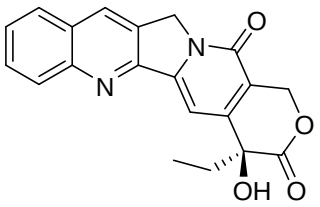

Figure 1.4 Structure of Camtothecin

Doxorubicin (trade name Adriamycin®, Figure 1.5) or hydroxyldaunorubicin is a chemotherapy drug used to treat many types of cancer. Doxorubicin was isolated from soil-based microbe *Streptomyces peucetius*. It is commonly used to treat some leukemias, Hodgkin's lymphoma, as well as cancers of the bladder, breast, stomach,

lung, ovaries, thyroid, soft tissue sarcoma and multiple myeloma. It can reduce or stop the growth of cancer cells. One way that doxorubicin works is by blocking an enzyme called topoisomerase 2 which cancer cells need in order to divide and grow. Doxorubicin may be used in combination with other chemotherapy drugs. Frequently used doxorubicin-containing treatments are CA (cyclophosphamide, Adriamycin), TAC (Taxotere, CA), ABVD (Adriamycin, Bleomycin, Vinblastine, Dacarbazine), BEACOPP, CHOP (Cyclophosphamide, Adriamycin, Vincristine, Prednisone) and FAC (5-Fluorouracil, Adriamycin, Cyclophosphamide) [6].

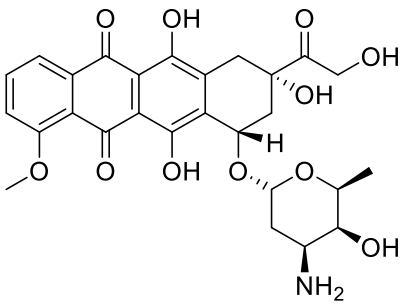

Figure 1.5 Structure of Doxorubicin

Vincristine (trade name Oncovin®, Vincasar Pfs®, Figure 1.6) was isolated from *Catharanthus rose*is, a chemotherapy used to treat several neoplasms, particularly the leukemia and lymphomas thyroid cancer and brain tumors. It works by inhibiting mitosis, causing the cells to die. Vincristine can bind to the tubulin protein, stop the cell from separating [7].

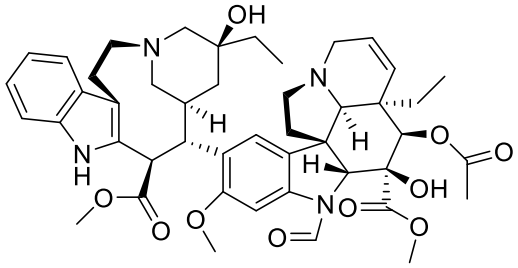

Figure 1.6 Structure of Vincristine

1.3 Natural products: The best sources of drugs and drug leads

Natural products continue to play an important role in the discovery and development of new chemical entities as drug-lead compounds. Considerable attempt is being expended by many groups worldwide on the isolation of natural products from earthly and marine macro- and microorganisms [8]. All living organisms produce many metabolites consisting of primary metabolites which are essential for growth, development and reproduction. Secondary metabolites which are not essential for existence and do not effect in immediate death but they are more in long-term damage of the organism's survivability and often play an important role in medicine, chemicals and flavoring. These compounds are extremely varied group of natural products synthesized by plants, fungi, bacteria, algae, and animals.

All over the ages of humans have trusted on nature for their basic needs which include the medicines for treatment of a wide spectrum of diseases. Plants, in particular, have formed the basis of cultured traditional medicine systems, with the earliest records, dating from around 2600 BCE, documenting the uses of around 1000 plant-derived materials in Mesopotamia [9]. Plants are continued to play an essential role in healthcare, and their use by different nations has been widely known. The World Health Organization (WHO) assessed in 1985 that the people trusted on plant traditional medicines for their preliminary treatment. Although plant products also play an important, however more indirect role in the treatment of the remaining people who mainly reside in developed countries.

The medicinal plants from the wild for extraction of products of interest have led to the loss of certain number of species making them either susceptible or extinct and the limitations associated with the yield and weakness of plant species as sources of novel metabolites. Microorganisms help to the ultimate, readily renewable, reproducible, and inexhaustible source of novel structures bearing pharmaceutical industrial. Among them, fungi are one of the most recognized as a main source of secondary metabolites with biological activities, such as anti-bacterial, anti-cancer, and anti-inflammatory activities.

Fungi play a crucial role in this field after the discovery of penicillin produced by *Penicillium notatum*, one of soil fungus, discovered by Prof. Alexander Fleming in 1928. Fungi have been playing an important role as source of drugs and drug lead compounds [10]. Penicillins are still broadly used today. Further, Artemisinin (antimalarial compound) originally obtained from an *Artemisia annua* were found in mycelial extract from the endophytic fungus *Colletotrichum* sp.[11]. Griseofulvin is one of the first antifungal natural products, derived from *Penicillium griseofulvum* and is commonly used to treat fungal infections of the skin, hair, and nails [12]. Lovastatin, a drug used for lowing cholesterol, is produced by the fungus in the genus *Aspergillus* [13]. Cyclosporine is an immunosuppressant drug which is widely used in post-allogeneic organ transplant. This drug is also obtained from a fungus, *Tolypocladium inflatum* [14].

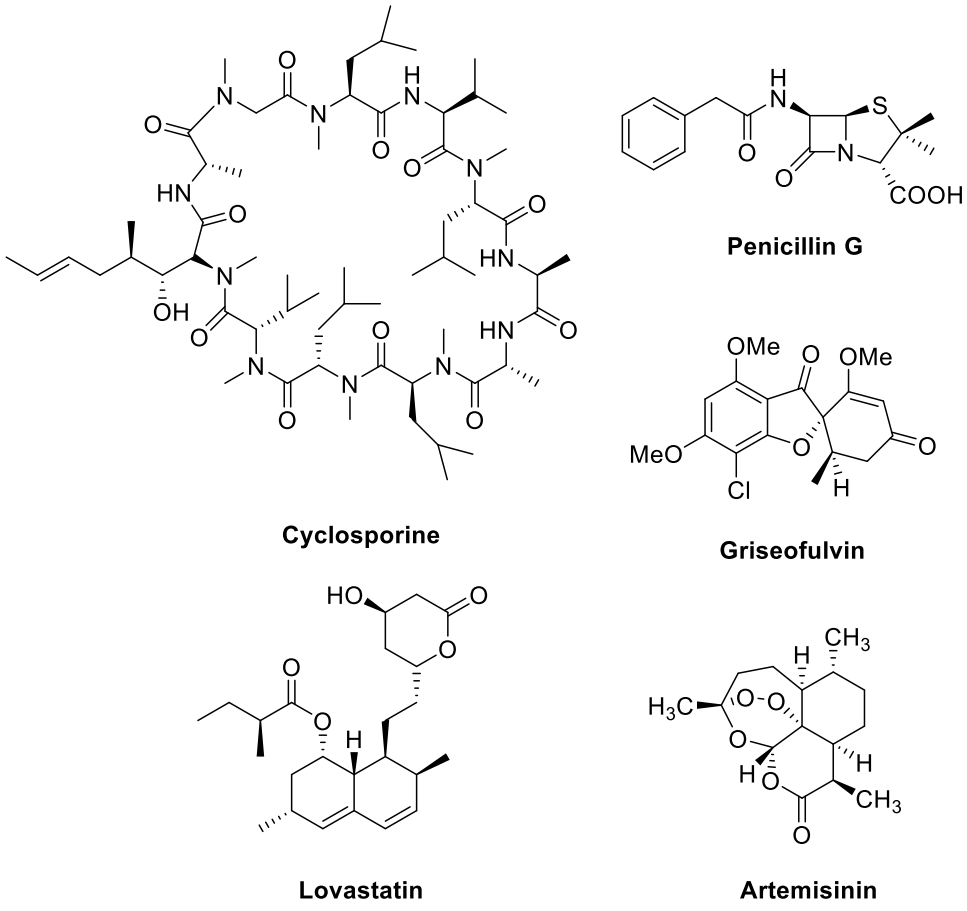

Figure 1.7 Structures of penicillin G, artemisinin, griseofulvin, lovastatin and cyclosporine

Over the last decade, numerous researchers have also reported a large number of structurally new secondary metabolites with biological activity produced by fungi isolated from many species of earthly plants. The potential of fungi as promising sources of bioactive natural products continues to appeal broad attention, since some of which are promising candidates for drug development or agrochemical applications. Among plant-derived fungi, those associated with mangrove trees have received much attention from natural product researchers due to the unique ecosystem. In addition to growing in tropical areas which provide great biodiversity, mangroves have to deal with changing tides and broad ranges of salinity, temperature, and moisture as well as a number of other environment factors. Thus, marine-derived fungi and mangrove-derived endophytic fungi are also potential as hopeful sources of diverse and structurally unique bioactive natural products.

1.4 Bioactive compounds form fungi

Research on natural products from fungi is increasing study them among the world's greatest resources for new biodiversity as well as chemodiversity. Examples of recent publications of bioactive compounds from marine and mangrove-derived fungi are listed as follows:

1.4.1 Cytotoxic activities

In 2011, Liu and co-workers described the isolation and determination of eight new α-pyrone derivatives, namely, nigerapyrones A-H and along with two known congeners, asnipyrones A and B, from *Aspergillus niger* MA-132, an endophytic fungus obtained from the fresh tissue of the mangrove plant *Avicennia marina*. The cytotoxicities against DU145, HeLa, HepG2, MCF-7, NCI-H460, A549, MDA-MB-231, and SW1990 tumor cell lines were determined. Nigerapyrone E showed cytotoxicities against SW1990, MDA-MB-231, and A549 cell lines with IC_{50} values of 38.0, 48.0, and 43.0 μM, respectively. Nigerapyrone B and asnipyrone A showed selective activity against the HepG2 and A549 cell line with an IC_{50} value of 62.0 μM , respectively and

nigerapyrone D showed moderate or weak activity against the MCF-7, HepG2, and A549 cell lines, with IC_{50} values of 121.0, 81.0, and 81.0 μM [15].

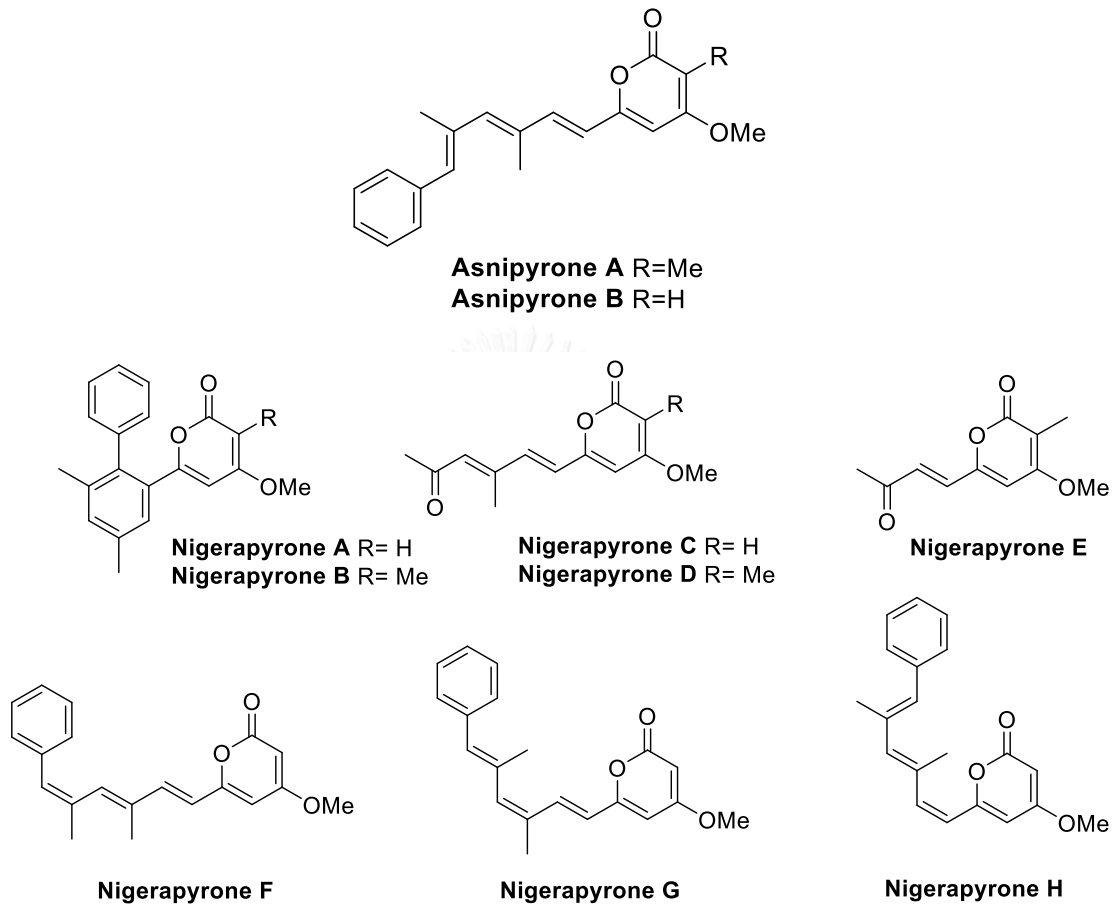

Figure 1.8 Structures of α-pyrone derivatives from *A. niger* MA-132

In 2012, Ding and co-workers determined the chemical constituents of the mangrove-derived *Fusarium incarnatum* (HKI0504) isolated from *Aegiceras corniculatum*, were obtained several unusual alkaloids, *N*-2-methylpropyl-2-methylbutenamide, 2-acetyl-1,2,3,4-tetrahydro-β-carboline, fusarine, fusamine, and 3-(1-aminoethylidene)-6-methyl-2H-pyran-2,4(3H)-dione. 2-Acetyl-1,2,3,4-tetrahydro-β-carboline, fusamine, and 3-(1-aminoethylidene)-6-methyl-2H-pyran-2,4(3H)-dione exhibited antiproliferative activities against HUVEC and K-562 (human chronic myeloid

leukemia cells) with GI_{50} values ranging from 9 to 41.1 μM and HeLa human cell lines with CC_{50} values ranging from 23.3 to 103.6 μM [16].

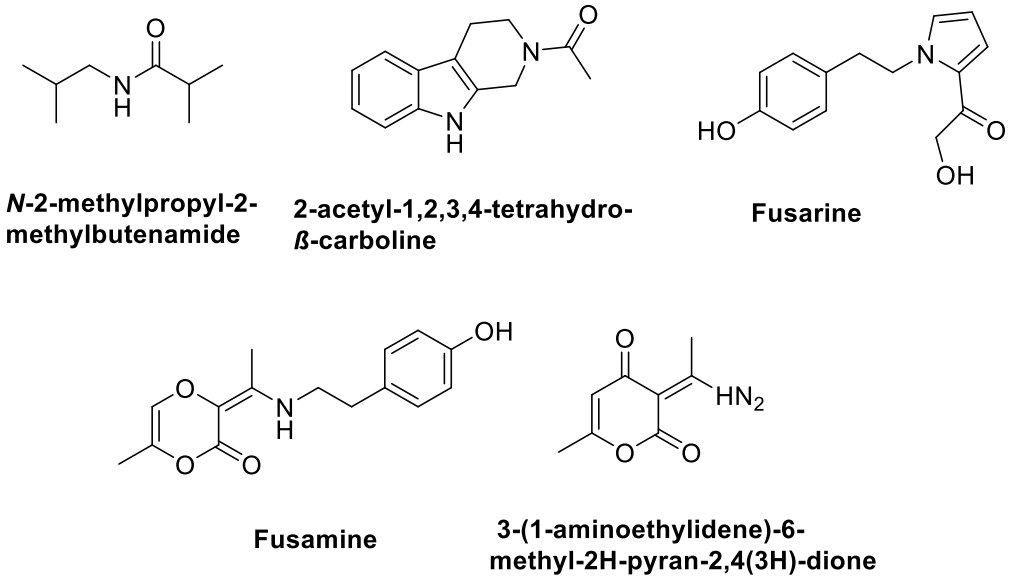

***N*-2-methylpropyl-2-methylbutenamide**

2-acetyl-1,2,3,4-tetrahydro-ß-carboline

Fusarine

Fusamine

3-(1-aminoethylidene)-6-methyl-2H-pyran-2,4(3H)-dione

Figure 1.9 Structures of sesquiterpenoids from *Diaporthe* sp.

In 2014, Wang and co-workers reported that six new disulfide-bridged diketopiperazine derivatives, brocazines A–F, along with epicorazine A and phomazine C, were isolated and identified from the cytotoxic extract of *Penicillium brocae* MA-231, an endophytic fungus obtained from the fresh tissue of the mangrove plant *Avicennia marina*. Brocazines A, B, E, and F showed cytotoxic activities against Du145, Hela, HepG2, MCF-7, NCI-H460, SGC-7901, SW1990, SW480, and U251 cell lines with IC_{50} values ranging from 0.9 to 9.0 μM. However, brocazine C and D did not show any activity toward all of the nine all cell lines [17].

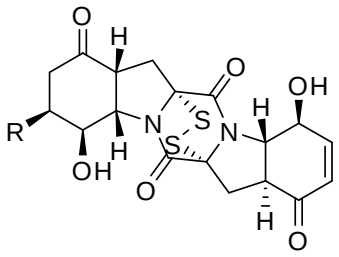

Brocazine A R=OMe
Brocazine B R=H

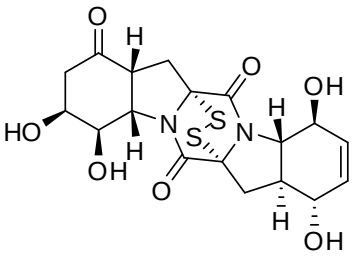

Brocazine C

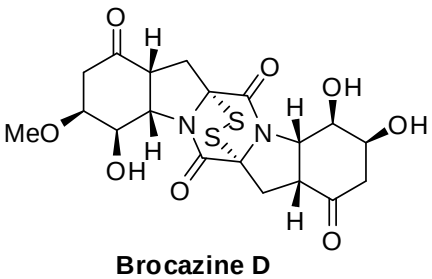

Brocazine D

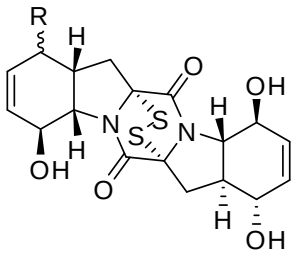

Brocazine E R=αOH, βH
Brocazine F R= =O

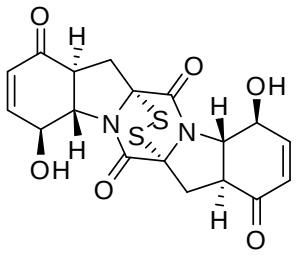

Epicorazine A

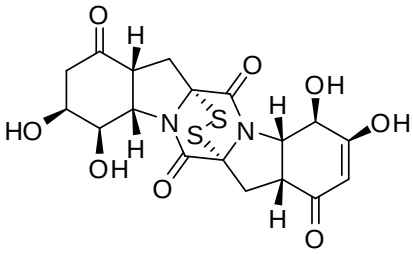

Phomazine C

Figure 1.10 Structures of disulfide-bridged diketopiperazine derivatives from *P. brocae* MA-231

Recently, we found three new spirobisnaphthalenes, rhytidones A-C from the mangrove-derived fungus *Rhytidhysteron* sp., and five known derivatives, MK3018, palmarumycin CR1, CJ-12,372, 4-O-methyl-CJ-12,372 and 4-O-methyl-CJ-12,371. Rhytidone C, MK3018 and palmarumycin CR1 displayed cytotoxicity against both cancer cell lines, MCF-7 and CaSki, while rhytidone B was active only on CaSKi with IC_{50} value of 22.8 μM [18].

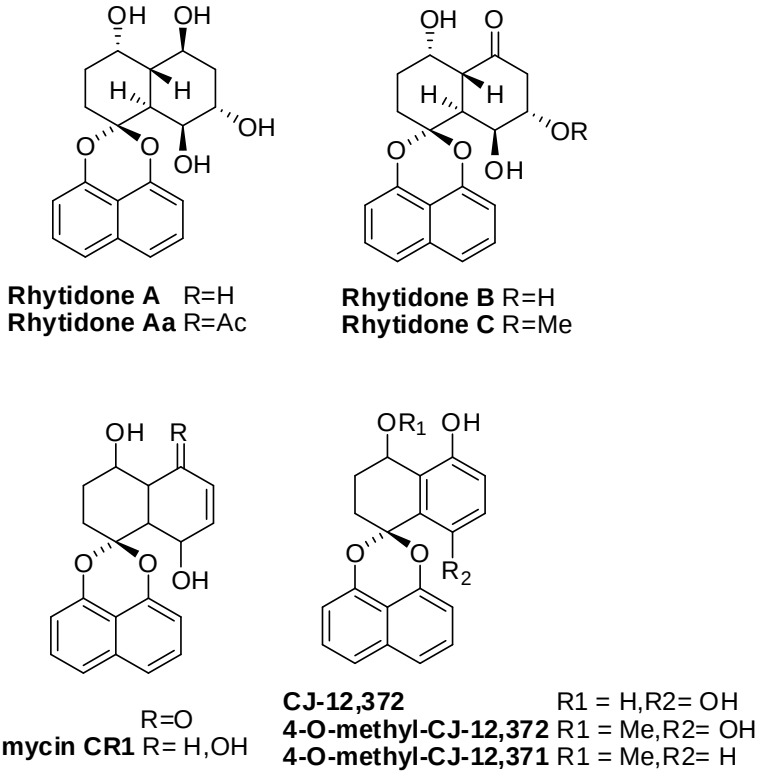

Figure 1.11 Structures of spirobisnapthalenes from *Rhytidhysteron* sp.

1.4.2 Anti-angiogenic activities

Angiogenesis is an important process of new blood vessels. Angiogenesis have been recognized as very important for the growth and spread of cancer. A blood source is required for tumors to the growth and it must continuously stimulate the growth of new capillary blood vessels for the tumor itself to grow. Also, the new blood vessels embedded in a tumor afford a door for tumor cells to arrive the circulation and to metastasize to distant sites, such as liver, lung, or bone.

In 2012, Koyama and co-workers reported that four novel benzo[j]fluoranthene derivatives, hypoxylonols C-F, have been isolated from the *Hypoxylon truncatum*, together with two known derivatives, hypoxylonols A and B. Hypoxylonols D and E showed antiproliferative activity against HUVECs and HUAECs with IC_{50} values of 6.9, 7.4, 6.1 and 4.1 μM, respectively [19].

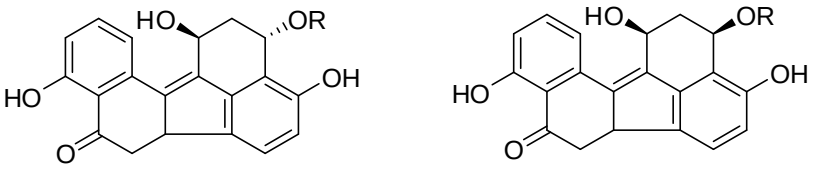

Hypoxylonol A R=CH_2CH_3
Hypoxylonol B R=CH_3
Hypoxylonol C R=h

Hypoxylonol D R=CH_2CH_3
Hypoxylonol E R=CH_3
Hypoxylonol F R=h

Figure 1.12 Structures of benzo[j]fluoranthene derivatives from *H. truncatum*

1.4.3 Antimalarial activities

Malaria represents a major threat to global health provision; it is the most aggressive parasitic infection in people. Each year over half a million people die of malaria. Malaria is endemic in more than 100 countries in world; making it the most exposed continent, but Asia, Oceania, and Central and South America are also under severe threat. Most seriously affected are developing nations, which suffer from a weak healthcare system [20].

In 2011, Plubrukarn and co-workers reported that know kabiramide G and the new kabiramides J and K, were isolated from the sponge *Pachastrissa nux*, along with the previously reported kabiramides B-D. All of the isolated macrolides showed moderate to strong antimalarial, especially kabiramide G showed antimalarial activity against *Plasmodium falciparum* K1 with an IC_{50} value of 0.7 μg/mL [21].

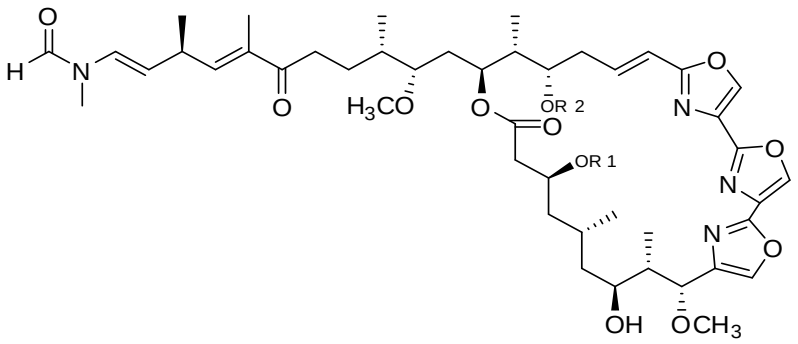

Kabiramide G R1=$CONH_2$, R2=CH_3
Kabiramide J R1=$CONH_2$, R2= H
Kabiramide K R1=H, R2= CH_3

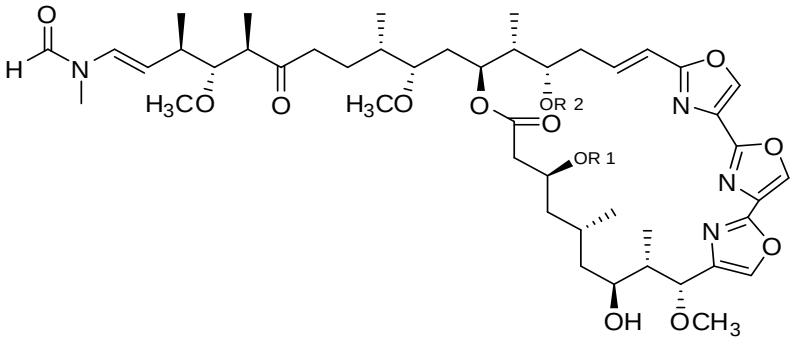

Kabiramide B R1=$CONH_2$, R2= H
Kabiramide C R1=$CONH_2$, R2= CH_3
Kabiramide D R1=H, R2= CH_3

Figure 1.13 Structures of kabiramides the sponge *Pachastrissa nux*

Recently fungi have played a crucial role in drug discovery due to their great biodiversity [22]. As part of our ongoing efforts to investigate Thai natural products potential for use as cancer treatments, the present study focuses on the isolation and characterization of the secondary metabolites of endophytic fungi obtained from Thai mangroves and marine fungi, and on the assessment of their cytotoxicity against cancer cell lines, the inhibition of angiogenesis and antimalarial activity against *Plasmodium falciparum* K1. Furthermore, the investigation on which signaling pathways are involved in their activity will further be performed to clarify the action mechanism.

The present research comprised of these parts into the following three parts as follows;

1. Metabolites from to Thai mangrove-derived endophytic fungi.

2. Sesquiterpenes from a mangrove-derived basidiomycetous fungus and their anti-angiogenic activity

3. Metabolites from a marine-derived fungus *Astrosphaeriella Nypae*

CHAPTER II

Metabolites from Thai mangrove-derived endophytic fungi

2.1 Introduction

2.1.1 Endophytic fungi

Endophytic fungus is the fungus which exits in living plant tissues (Figure 2.1). These fungi usually inhabit within their host plant without causing any disease symptoms. Thus, these class microorganisms have been considered as plant mutualists. In their symbiosis, the host plant (macrophyte) defends and feeds the endophyte, while the fungi produce secondary metabolites, low molecular weight compounds not essential for their growth, to enhance the growth and competitiveness of the host and to protect plant from herbivores and pathogens in nature. This complex relationship continues to present an exciting boundary yet to be discovered as such host plant represent single ecological functions for varied communities of symbiotic microbes giving rise to complex interactions of plant[23].

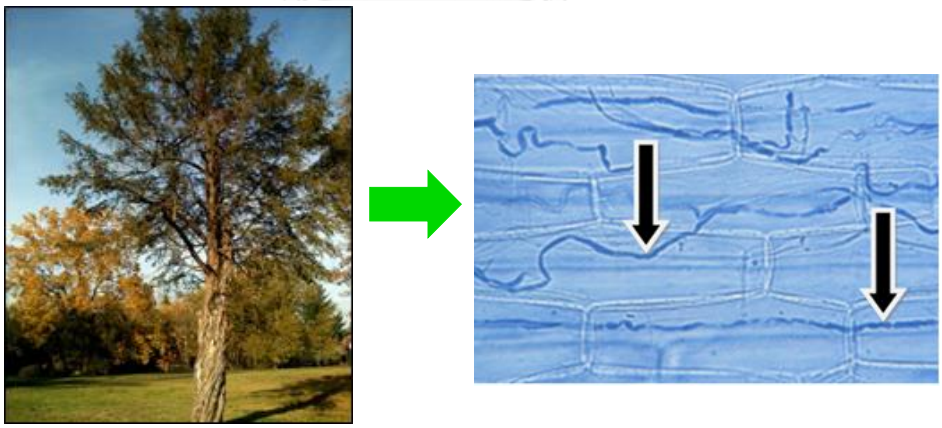

Figure 2.1 Endophytic fungal hyphae in plant cells
(http://taxol.weebly.com/about-the-tree.html),
(http://www.peg.ethz.ch/research/Interactions/index_EN)

Practically all medicinal plants are recognized to have potential endophytic fungi to directly produce bioactive metabolites, since, in their symbiosis with host plant; these fungi produce bioactive substances (plant growth regulatory, antibacterial, antifungal, antiviral, and insecticidal, etc.) to support the survival of their host plants. Moreover, natural products from fungal endophytes have been proved to have a broad spectrum of bioactive compounds and can be collected into several groups with; alkaloids, steroids, terpenoids, flavonoids, glycosides, xanthones, isocoumarins, quinones, phenyl propanoids, lignans, aliphatic metabolites, lactones etc [24]. The bioactive metabolites produced by endophytes associated with medicinal plants can be exploited for curing many diseases and for agrochemical applications.

Oocydin A (Figure 2.2) has the properties of a chlorinated macrocyclic lactone. It shows a potent antifungal. Oocydin A was isolated from *Serratia marcescens*, collected from an aquatic plant, *Rhyncholacis penicillata.* Presently, oocydin A is being considered for agriculture use to control the ever-threatening presence of oomyceteous fungi [25].

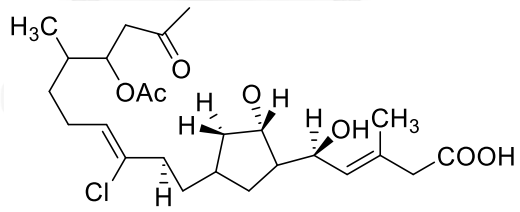

Figure 2.2 Structure of oocydin A

Pestacin and isopestacin (Figure 2.3), a group of structure likeness to the flavonoids and effectiveness for group of free-radical-scavengers, showed to surpass the anti-oxidant activity of trolox (a vitamin E derivative) by at least one order of magnitude, as measured by the total oxyradical scavenging capacity (TOSC) assay. Pestacin and isopestacin were obtained from *Pestalotiopsis microspora*, an

endophyte of *Terminalia morobensis* living the Sepik River drainage of Papua New Guinea [24].

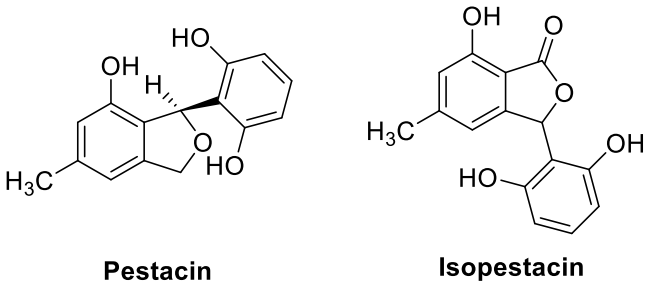

Pestacin **Isopestacin**

Figure 2.3 Structures of pestacin and isopestacin

L-783,281 (Figure 2.4) isolated from *Pseudomassaria* sp. obtained from leaves of an undetermined plant collected near Kinshasa, Democratic Republic of Congo, was shown to be a biofactory of nonpeptidal insulin mimetic. Its discovery prompted quite a revolutionary notion in the therapy of diabetes, namely: an orally administered activator of the human insulin receptor [25].

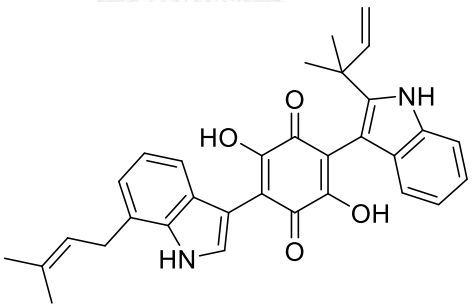

L-783,281

Figure 2.4 Structure of L-783,281

Furthermore, the discovery of endophytic fungi and host plants with capacity to produce the same compounds has shifted the focus of new drug sources from plants to fungi. The most famous example is paclitaxel (trade name Taxol®, Figure 2.5), a texane diterpenoid isolated from bark of a Taxus plant, *Taxus brevifolia* (Figure

2.5), the world's first billion dollar anticancer drug killing tumor cells by enhancing the assembly of microtubules and inhibiting their depolymerisation, and it is used to treat of cancers with: ovarian, breast, lung and pancreatic cancer among others [26]. However, taxol has estimated that harvesting of 38,000 yew trees is required to generate 25 kg of taxol to treat 12,000 patients. One-kilogram paclitaxel is produced when extraction from 10,000-kg bark. This method cannot meet its increasing demand on the market because yews grow very slowly and are a rare and endangered species belonging to first-level conservation plants. Later, increasing efforts have been made to develop alternative means of taxol production [27]. In 1993, Prof. Stierle found an endophytic fungus, *Taxomyces andreanae*, isolated from the Taxus plant, could also produce taxol in good yield, microbe fermentation would thus be a very promising method to increase the production scale of taxol [28]. In addition, it was further found that taxol could be produced by other strains of endophytic fungi, for example, *Fusarium oxysporum* from a mangrove plant *Rhizophora annamalayana*, *Seimatoantlerium nepalense* from *T. wallachianaand*, Himalayan yew tree, and *Tubercularia sp*. strain TF5 from *T. mairei*, Chinese southern yew tree [29].

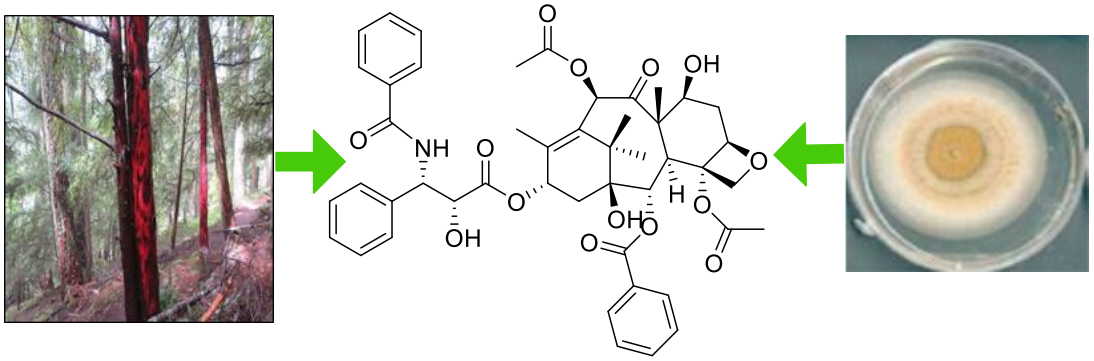

Figure 2.5 Taxus plant, Taxol and *T. andreanae* (http://www.blackdiamondnow.net/black-diamond-now/2012/06/pacific-yew-the-tree-that-fights-cancer.html)

With the discovery of the taxol-producing endophytic fungi from the host plant, it prompted natural product researchers to look for other fungal strains being able to produce drugs as their host plants do.

Podophyllotoxin (Figure 2.6) is the clinically relevant mainly to useful anticancer and antiviral activities and also valued as the precursor to useful anticancer drug like etoposide, teniposide and etophophos phosphate. Originally, podophyllotoxin was extracted from the roots and rhizomes of *Podophyllum* species. Caused by ever increasing demand for podophyllotoxin, because the plant is grows slowly. However, new ways for total synthesis of podophyllotoxin have been exposed but these are not economically possible due to low yield. Many efforts have been put in the past several years to improve its production from different podophyllotoxin producing plant species. Agricultural manufacture of podophyllum has been unsuccessful since the plant requires several factors proper climatic conditions, entire biochemical pathway, including key enzyme and the genetic blueprint involved in podophyllotoxin biosynthesis, is not known yet. Later, alternative methods for production of podophyllotoxin through endophytic fungi are being vigourously explored such as from endophytic *Phialocephala fortinii* from rhizomes of the plant *Podophyllum peltatum* (Mayapple plant) [30].

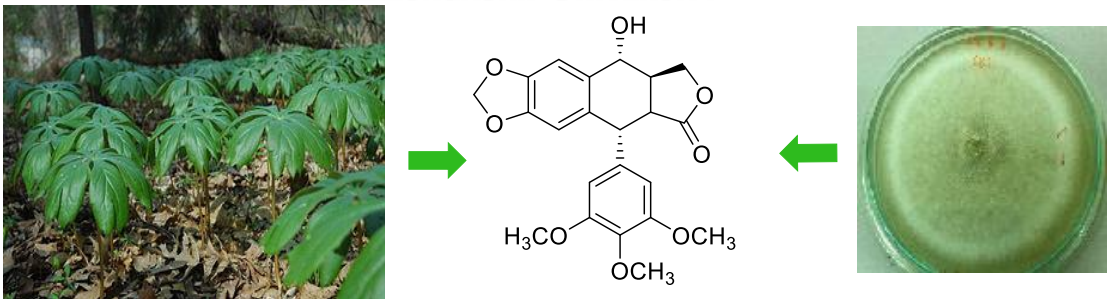

Figure 2.6 Mayapple plant, podophyllotoxin and *P. fortinii* (https://en.wikipedia.org/wiki/File:Podophyllum_peltatum_Single_Leaf.JPG)

As aforementioned, endophytic fungi can be a consistent source for industrial and pharmacological keys of bioactive metabolites used in treatment of diseases along with several industrial applications. The fungi may effect in procedures to produce biologically active agents for biological utilization on a large commercial scale as they are easily cultured in laboratory and fermenters in place of harvesting plants which provide the safety for the environmental biodiversity [4].

2.1.2 Mangrove-derived fungi as sources of bioactive compounds

Endophytic fungi have been proved to be a prolific source for the discovery of structurally interesting and biologically active secondary metabolites, some of which are promising candidates for drug development or agrochemical applications. Among plant-derived fungi, those associated with mangrove trees have received much attention from natural product researchers due to the unique ecosystem[31]. In addition to growing in tropical areas which provide great biodiversity, mangroves have to deal with changing tides and broad ranges of salinity, temperature, and moisture as well as a number of other environment factors. It is reasonable to expect they must be home to a great variety of specific microorganisms including fungi.

In 2009, Xu and co-workers reported the isolation and characterization of six new chromones, named pestalotiopsones A-F from the mycelia and culture filtrate of the mangrove endophytic fungus *Pestalotiopsis* sp., obtained from leaves of the Chinese mangrove plant *Rhizophora mucronata.* Pestalotiopsone F exhibited moderate cytotoxicity against the murine cancer cell line L5178Y with an EC_{50} value of 8.9 μg/mL, whereas the other investigated compounds were proved to be inactive [32].

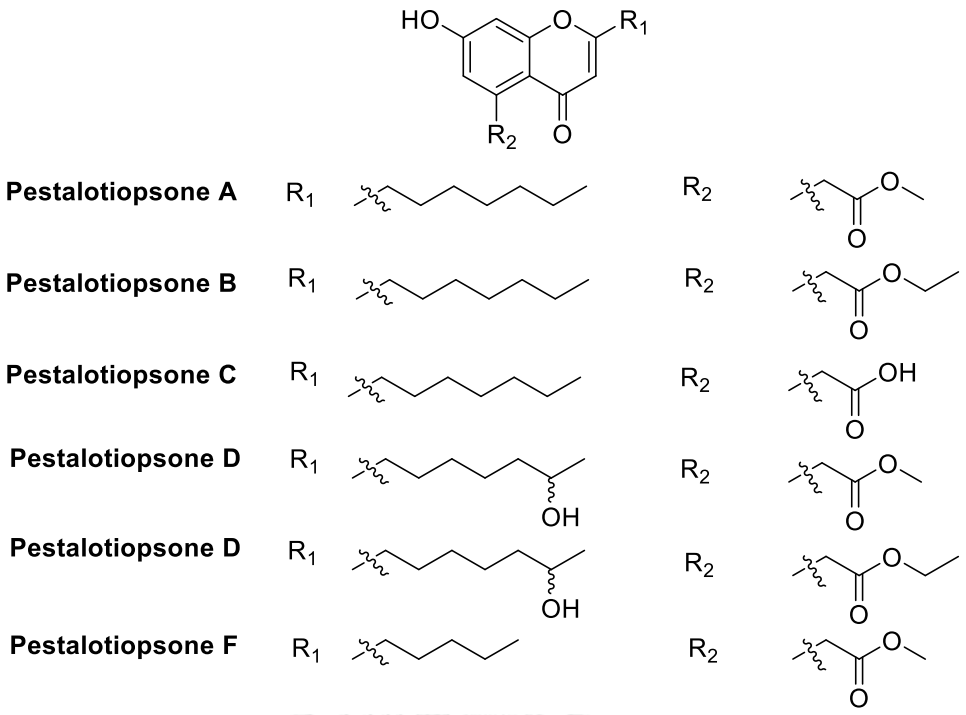

Figure 2.7 Secondary metabolites of the fungus *Pestalotiopsis* sp.

In 2011, Lin and co-workers reported that six secondary metabolites, including three new azaphilones (chermesinones A-C), three new *p*-terphenyls (6'–*O*-desmethylterphenyllin, 3-hydroxy-6'-*O*-desmethylterphenyllin, 3''-deoxy-6'-*O*-desmethylcandidusin B, were isolated from the culture of the mangrove endophytic fungus *Penicillium chermesinum* (ZH4-E2). Chermesinone A showed a mild inhibitory effect on α-glucosidase with an IC_{50} value of 24.5 *μ*M, while 6'–*O*-desmethylterphenyllin and 3-hydroxy-6'-*O*-desmethylterphenyllin exhibited strong inhibitory effects with IC_{50} values of 0.9 and 4.9 *μ*M, respectively. Furthermore, 3''-deoxy-6'-*O*-desmethylcandidusin B showed inhibitory activity toward acetylcholinesterase with an IC_{50} value of 7.8 *μ*M [33].

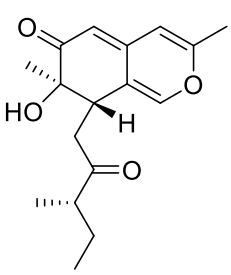

Chermesinone A

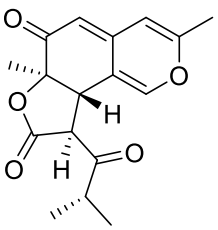

Chermesinone B

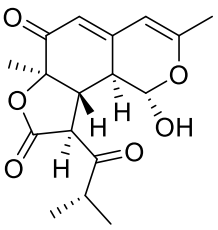

Chermesinone C

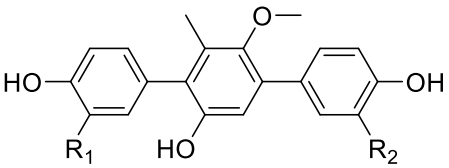

6'-*O*-desmethylterphenyllin
R1=H, R2=H
3-hydroxy-6'-*O*-desmethylterphenyllin
R1=OH, R2=H

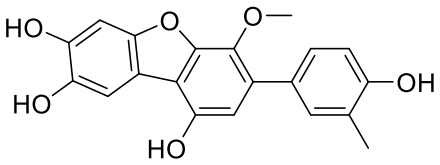

3''-deoxy-6'-*O*-desmethylcandidusin B

Figure 2.8 Secondary metabolites of the fungus *P.chermesinum* (ZH4-E2)

In 2013, She and co-workers found two new asperterpenols A and B, two novel sesterterpenoids with an unusual 5/8/6/6 tetracyclic ring skeleton, were isolated from a mangrove endophytic fungus *Aspergillus* sp. 085242. Both compounds could inhibit acetylcholinesterase with IC_{50} values of 2.3 and 3.0 μM, respectively [34].

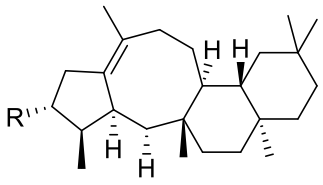

Asperterpenol A R=H
Asperterpenol B R=OH

Figure 2.9 Secondary metabolites of the fungus *Aspergillus* sp. 085242

In 2013, Wang and co-workers reported that six new 4-phenyl-3,4-dihydroquinolone derivatives, namely aniduquinolones A–C, 6-deoxyaflaquinolone E, isoaflaquinolone E, and 14-hydroxyaflaquinolone F, as well as one related known aflaquinolone A, were isolated from the culture of *Aspergillus nidulans* MA-143, an endophytic fungus from the fresh leaves of the marine mangrove plant *Rhizophora stylosa*. All compounds were examined for brine shrimp lethality against *Artemia salina*. Aniduquinolones B and C, and aflaquinolone A exhibited modest activity with LD_{50} values of 7.1, 4.5, and 5.5 μM, respectively [35].

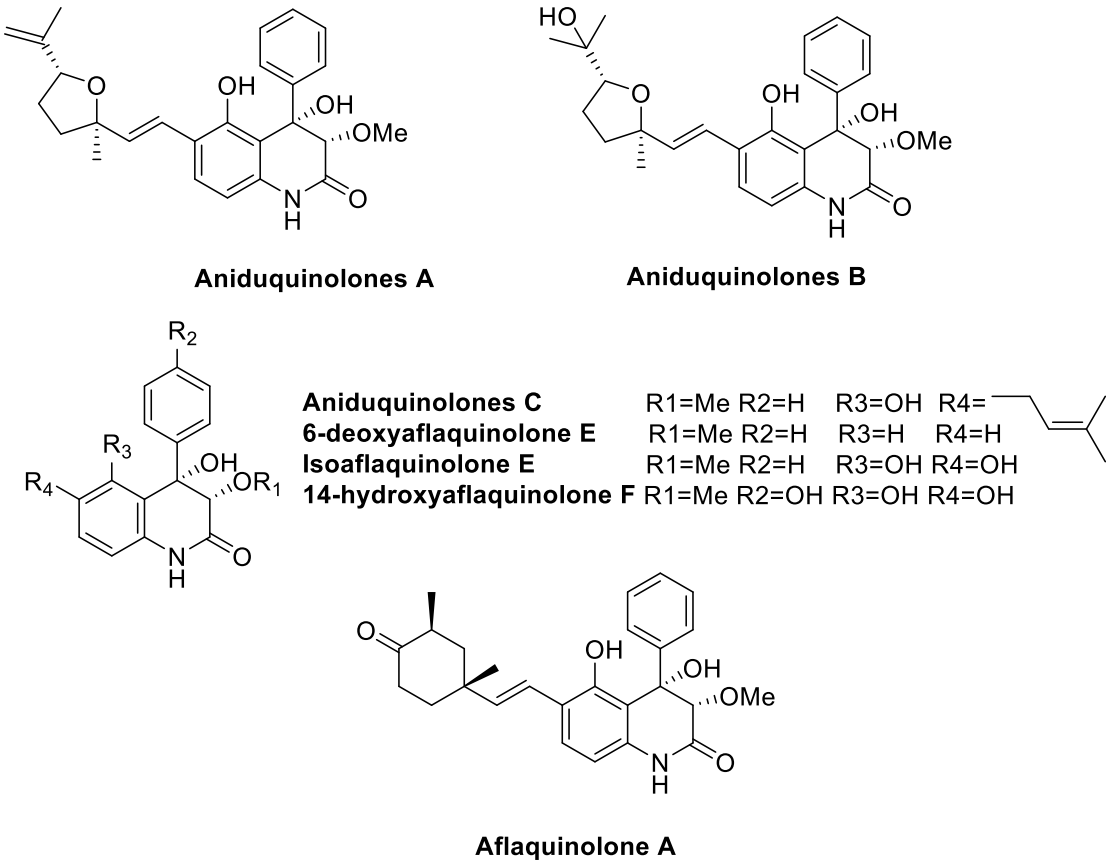

Figure 2.10 Secondary metabolites of the fungus *A. nidulans* MA-143

In 2014, Guo and co-workers reported that a novel pyrrolizidine alkaloid, penibruguieramine A and three known compounds, namely scalusamide A, meleagrin and roquefortine F were isolated from the endophytic fungus *Penicillium* sp. GD6, associated with the Chinese mangrove *Bruguiera gymnorrhiza*. Roquefortine F showed potent cytotoxic activity against two tumor cell lines, HL60 and A549, with IC_{50} values of 9.7 and 8.3 μM, respectively [36].

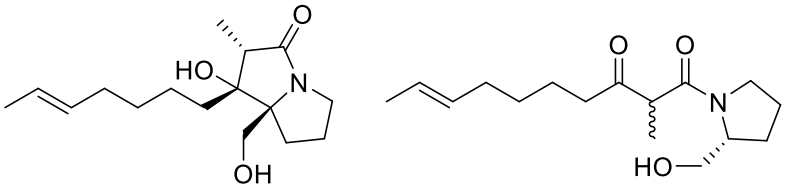

Penibruguieramine A

Scalusamide A

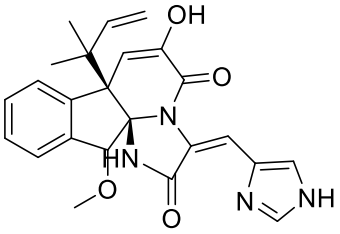

Meleagrin

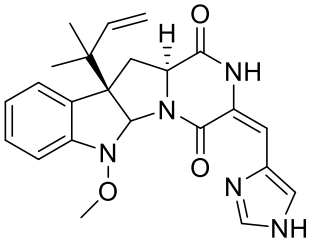

Roquefortine F

Figure 2.11 Secondary metabolites of the fungus *Penicillium* sp. GD6

In 2014, She and co-workers found that five new compounds, pinazaphilones A and B, two phenolic compounds: 4'-(S)-(3,5-dihydroxyphenyl)-4'-hydroxy-6'-methylcyclopent-1'-en-5'-one, 6'-methyl-[1,1'-biphenyl]-3,3',4',5-tetraol, and penicidone D, five known compounds, sch 1385568, (±)-penifupyrone, 3-*O*-methylfunicone, 5-methylbenzene-1,3-diol and 2,4-dihydroxy-6-methylbenzoic acid were obtained from the culture of the endophytic fungus *Penicillium* sp. HN29-3B1, which was isolated from a fresh branch of the mangrove plant *Cerbera manghas* collected from the South China Sea. All compounds were tested for their *in vitro* inhibitory activities against **α**-glucosidase. Pinazaphilone B, sch 1385568, 6'-methyl-

[1,1'-biphenyl]-3,3',4',5-tetraol, and (±)-penifupyrone exhibited significant inhibitory activities against α-glucosidase with IC_{50} values 28.0 ± 0.2, 16.6 ± 0.5, 2.2 ± 0.1 and 14.4 ± 0.5 μM, respectively [37].

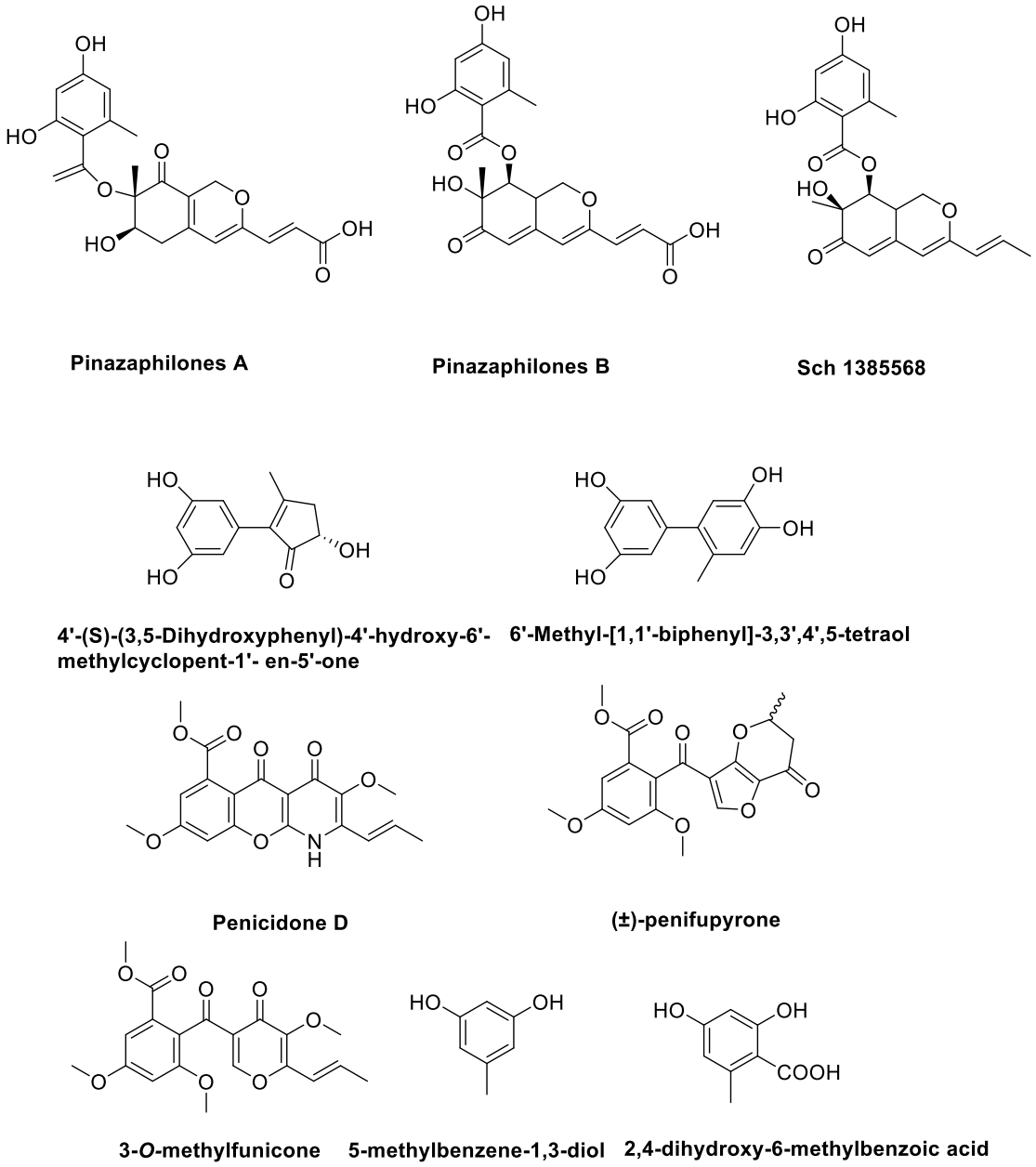

Figure 2.12 Secondary metabolites of the fungus *Penicillium* sp. HN29-3B1

2.2 General Experimental Procedures

2.2.1 Thin-layer chromatography (TLC)

Thin-layer chromatography (TLC) was carried out on a silica gel F254 coated on aluminium sheet (Merck). Detection was visualized under ultraviolet light at wavelengths of 254 and 356 nm and dipped with $(NH_4)_6Mo_7O_{24}$ solution in 5% H_2SO_4 /EtOH.

2.2.2 Column chromatography

Column chromatography (CC) was performed using Sephadex LH-20 (Pharmacia Code No. 17-0090-01) and Silica gel 60H (Merck code No. 7734 and No. 9385) as packing materials.

2.2.3 Nuclear magnetic resonance spectroscopy (NMR)

The NMR spectra were recorded in $CDCl_3$, acetone-d_6, using a Bruker DRX 400 (400 MHz for ^1H, 100 MHz for ^{13}C) and a Bruker AV500D (500 MHz for ^1H, 125 MHz for ^{13}C) spectrometers.

2.2.4 Mass spectrometry (MS)

ESI-TOF mass spectra and HRESIMS were measured with a Bruker microOTOF mass spectrometer.

2.2.5 Ultraviolet-visible measurements (UV-vis)

UV-vis spectra were recorded in MeOH on a Spekol 1200 (Analytic JENA) and a GBC Cintra 404 UV-Visible spectrophotometers.

2.2.6 Fourier transform infared spectroscopy (FT-IR)

The FT-IR spectra were recorded on a Bruker ALPHA spectrometer and a PerkinElmer Spotlight 300 IR imaging system.

2.2.7 Melting points

Melting points were taken on a Buchi M565 digital melting point apparatus.

2.2.8 Optical rotation

Optical rotations were measured with a sodium D line (589 nm) JASCO P-1010 digital polarimeter equipped with a 1 mL cell (cell length 0.1 dm) and a JASCO P-1030 digital polarimeters equipped with a 1 mL cell (cell length 0.1 dm).

2.2.9 High performance liquid chromatography (HPLC)

High performance liquid chromatography (HPLC) was performed using a Water system (Waters 600 HPLC pump and Waters 2996 Photodiode array detector). Column Waters NovaPak C_{18} (3.9 × 150 mm, 4 µm) was used for analysis, GL Science column C_{18} (20 × 250 mm, 3 µm) were used for separation and Dionex-Ultimate 3000 series equipped with a binary pump, an auto sampler, and diode array detector. Column SunFire C_{18} (19 × 150 mm, 5 µm) were used for separation.

2.2.10 Chemicals

All solvents used in this research such as hexane, dichloromethane (CH_2Cl_2), acetone, ethyl acetate (EtOAc) and methanol (MeOH) were commercial grade and purified prior to use by distillation.

2.3 Plant sample Collection

Healthy leaves of seven species of Thai mangroves, including *Lumnitzera racemosa, Tradescantia spathacea, Xylocarpus granatum, Azima sarmentosa, Bruguiera gymnorrhiza, Bruguier cylindrical* and *Solanum trilobatum* were collected in July 2012 from Pak Nam Pran, Prachuap Khiri Khan Province, Thailand.

2.4 Isolation of Fungal endophyte

Healthy leaves were washed in tap water and dry, then the leaves were surface-sterilized with 70% EtOH for 1 min, 6% NaOCl solution for 5 min, and sterile distilled H_2O for 1 min (twice). The surface-sterilized leaves were cut into small pieces (ca. 5 mm in length) using a sterile blade and placed on sterile water agar plates, then incubation at room temperature until the hypha of the fungus grew out from the plant tissue. The hypha tip of each fungus was cut by a sterile pipette and moved on a potato dextrose agar (PDA) plate. After incubation at room temperature for 7-14 days, culture purity was determined from colony morphology.

A total of 64 pure isolates, sixteen isolates were obtained from *L. racemosa*, 12 isolates were isolated from *T. spathacea,* 8 isolates were obtained from *X. granatum*, 2 isolates were obtained from *A. sarmentosa*, 10 isolates were obtained from *B. gymnorrhiza*, 8 isolates were obtained from *B. cylindrical* and 8 isolates were obtained from *S. trilobatum.*

2.5 Screening of endophytic fungal isolates for the interesting metabolite production

Based on different morphology of fungi, 64 isolates were selected for cultivation on three types of media; Sabouraud dextrose broth (SDB), corn steep broth medium and yeast extract sucrose broth (YEB). Selected endophytic fungi were grown in 200 mL Erlenmeyer flasks, containing 100 mL of each culture medium. After culture for 21 days at room temperature, total of 192 culture broths were

extracted with EtOAc, and the crude extracts were examined by ^{1}H NMR spectroscopy.

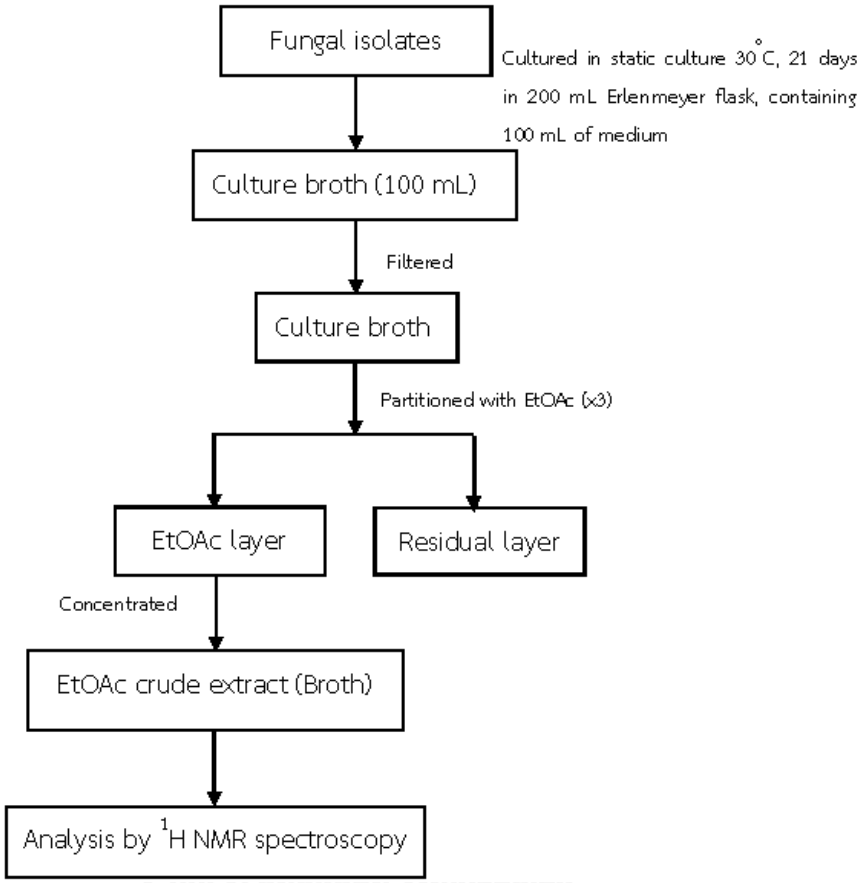

Scheme 2.1 General procedure for selecting endophytic fungi

2.6 Large scale cultivation and extraction of selected fungus BG2Y

Based on ^{1}H NMR data analysis, one fungal strain BG2Y, obtained from *B. gymnorrhiza*, was selected for the further step. The fungus was grown-up on PDA plate at room temperature for 7 days. Subsequently, six fragments (6x6 mm^{2}) of the grown culture were cut and inoculated into 1,000 mL Erlenmeyer flasks (x50)

containing 200 mL of SDB at room temperature for 21 days under static conditions. The culture broth was filtered through five layers of sheet cloth which were comprehensively pressed. The filtrate was extracted with an equal volume of ethyl acetate (EtOAc) for 3 times. The organic layers were combined and evaporated under reduced pressure to yield broth EtOAc crude extract.

After filtration to separate between broth and mycelia, mycelia were soaked in MeOH for 2 days, and then the MeOH soluble fraction was collected by filtering through sheet cloth (five layers). The filtrate was extracted with an equal volume of hexane for 3 times. The MeOH layers were combined and evaporated in vaccuo and the residue was partitioned between EtOAc and H_2O, and then extracted with an equal volume of EtOAc for 3 times. The EtOAc soluble fraction was evaporated under reduced pressure to yield the mycelial EtOAc extract (Scheme 2.2).

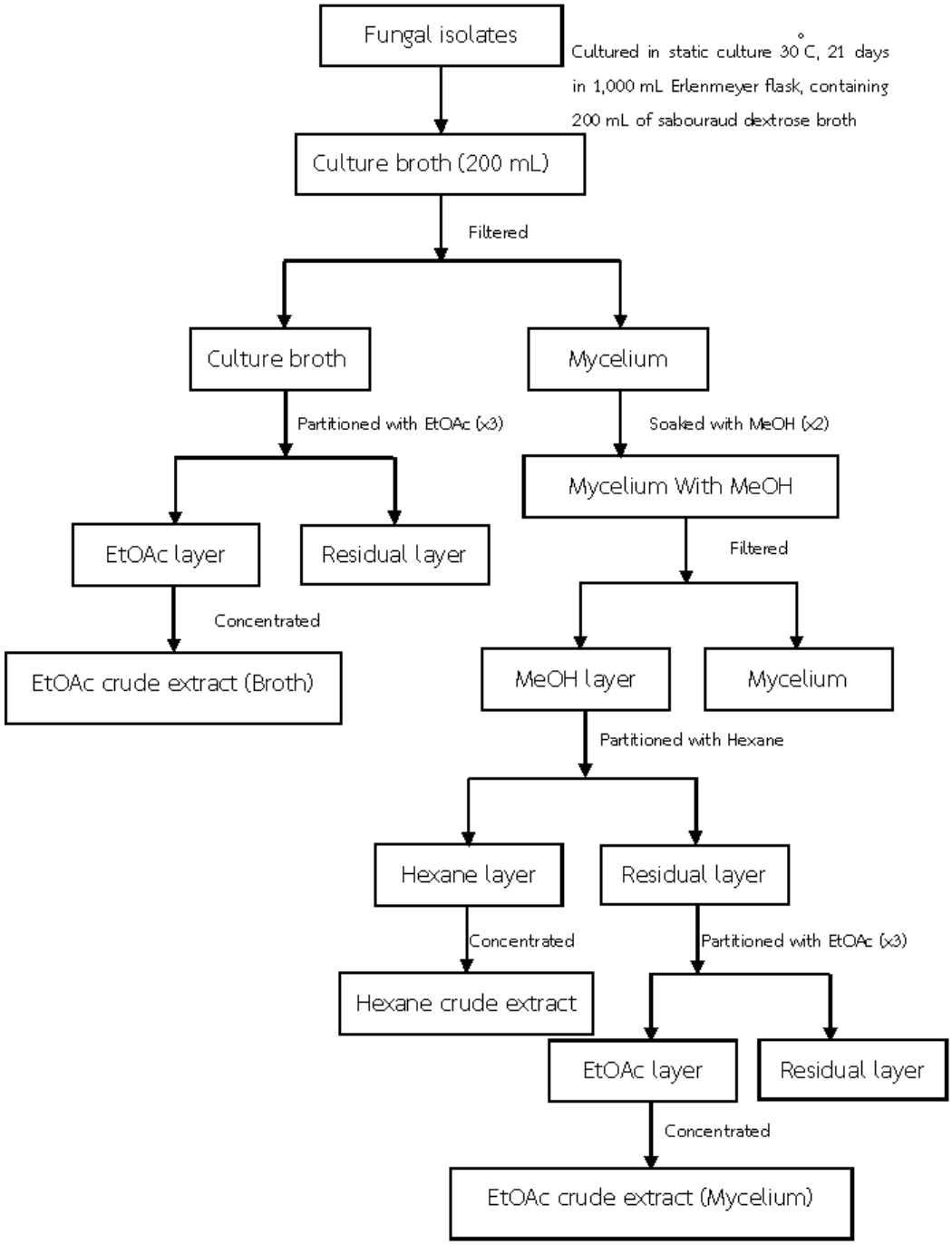

Scheme 2.2 Preparation of EtOAc crude extracts of broth and mycelium of selected fungi

2.7 Isolation of secondary metabolites of the fungus BG2Y

According to the procedure in 2.6, the EtOAc crude extracts of culture broth and mycelium of fungus BG2Y were obtained in amounts of 4.62 g and 0.87 g, respectively.

The broth crude extract (4.62 g) was subjected to Sephadex LH20 column chromatography and eluted with MeOH to yield five fractions (A-E). Fraction C (3.58 g) was further rechomatographed by Sephadex LH20 column chromatography (using 100% MeOH) to yield six subfractions (C1-C6). Subfractions C4 (0.36 g) was subjected to flash column chromatography on silica gel (EtOAc:hexane, 1:1) to yield nine subfractions (C4a-C4i) while subfractions C4b (72.00 mg) were further purified by Sephadex LH20 column chromatography and eluted with MeOH to yield compound **1**, (28.70 mg). Fraction C2f (95.00 mg) was fractionated by silica gel column chromatography (MeOH:CH_2Cl_2, 5:95) and then rechomatographed over reverse phase C18 (MeOH:H_2O, 30:70) to afford compound **2**, (4.50 mg). Fraction C2c (0.12 mg) was fractionated by silica gel column chromatography (MeOH:CH_2Cl_2, 5:95) and then rechomatographed over reverse phase C18 (using 30:70 of MeOH : H_2O) to give compound **3,** (4.00 mg). Fraction C5 (1.63 g) was subjected to silica gel column chromatography (EtOAc:Hexane, 2:3) and then rechomatographed by Sephadex LH20 column chromatography and eluted with MeOH to afford compound **4**, (4.00 mg).

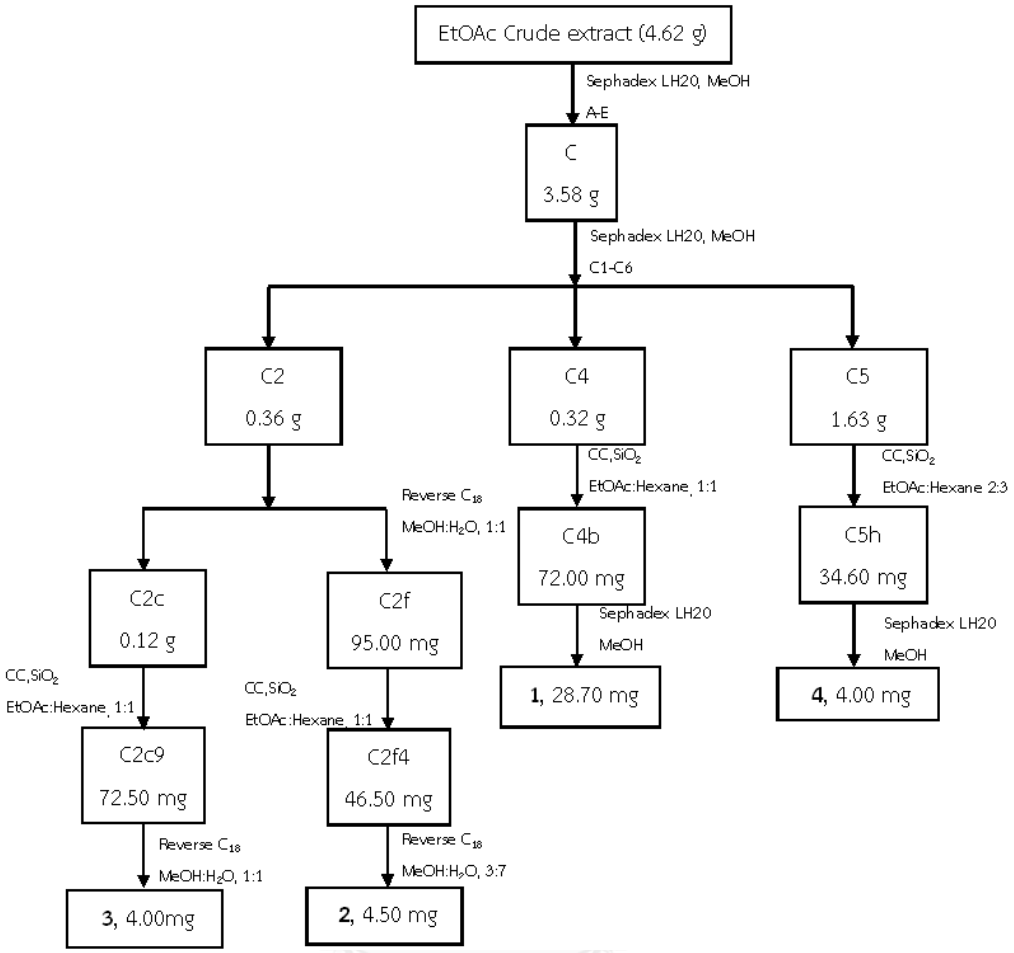

Scheme 2.3 Isolation of metabolites from fungal BG2Y broth EtOAc crude extract

The mycelium EtOAc crude extract was also subjected to Sephadex LH20 column chromatography and eluted with MeOH to yield six fractions (A-F). Fraction C (0.18 g) was subjected to reverse phase C18 (MeOH:H_2O, 50:50) and then subfractions C2 and C3 (0.12 g) were combined and further purified by rechomatographed by silica gel column chromatography (MeOH:CH_2Cl_2, 5:95) to yield compound **7**, (11.40 mg). Fraction C7 (49.10 mg) was subjected to flash column chromatography on silica gel column chromatography (MeOH:CH_2Cl_2, 5:95) to afford compound **5**, (4.00 mg). Fraction E (0.24 g) was subjected to reverse phase C18 (MeOH : H_2O, 50:50) twice to obtain compound **6,** (7.20 mg).

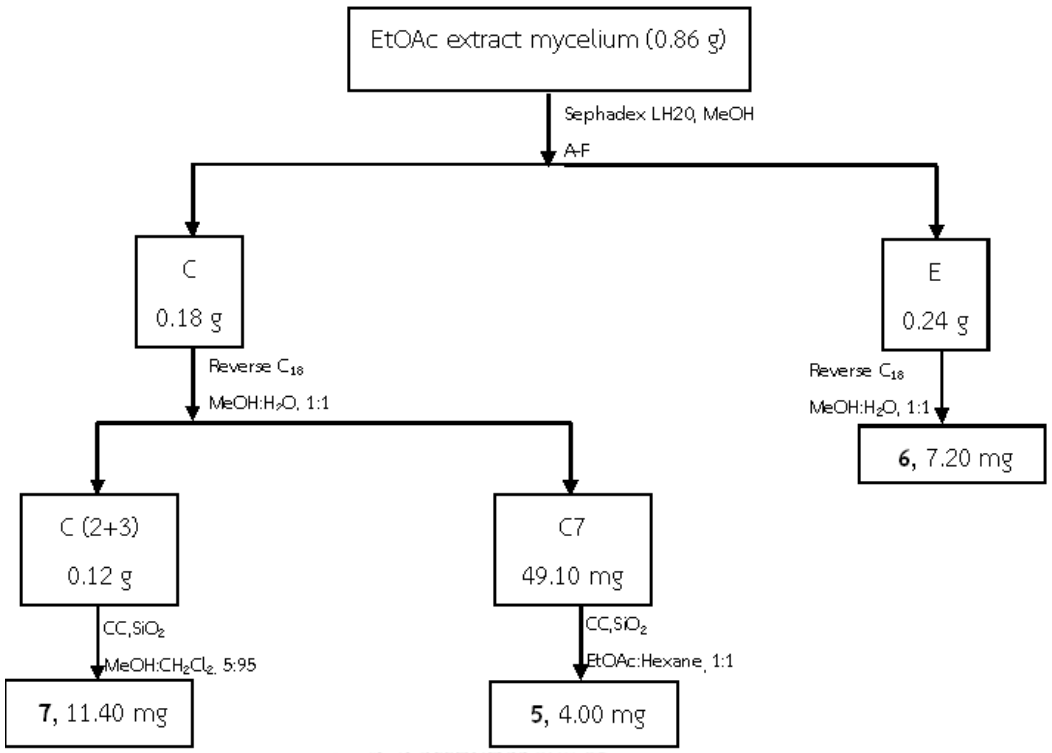

Scheme 2.4 Isolation of metabolites from fungal BG2Y mycelium EtOAc crude extract

2.8 X-ray crystallography Analysis of compound 1

Compound **1** was recrystallized from MeOH and the single-crystal X-ray diffraction data were collected at 298 K on a Bruker APEX-II CCD diffractometer with Mo Kα radiation (λ = 0.71073 Å). The crystal structure was solved by direct methods using SHELXS-97 and refined with full-matrix least-squares on all F^2 data using SHELXS-97 to final *R* values. All hydrogen atoms were added at calculated position and refined using a rigid model.

2.9 Classification of selected endophytic fungus

Selected fungal strains BG2Y was taxonomically identified by Mr.Nattawut Boonyuen, Phylogenetics and Mycology Laboratories Central Research Unit BIOTEC, National Center for Genetic Engineering and Biotechnology, Pathum Thani, Thailand.

The fungus was grown on potato dextrose broth. After cultivation for 7 days, 50 mg of fresh fungal mycelia were harvested, washed twice with normal saline solution, and homogenated in 250 μL of sterile water. The mycelia homogenate was applied evenly to an FTA card matrix, allowed to dry at room temperature, and a 2-mm disk containing the fungal mycelia was punched from the FTA card. Total cellular DNA of fungal mycelia on the disk was extracted and purified using the FTA® Plant Kit (Whatman®) according to the manufacturer's instruction. The disk was transferred to a PCR tube and the ITS1-5.8S-ITS2 ribosomal RNA gene region of fungal genomic DNA was amplified using the ITS5 (GGAAGTAAAAGTCGTAACAAGG) and ITS4 (TCCTCCGCTTATTGATATGC) primers. PCR amplification was performed in a 50 μL reaction volume which contained Taq PCR Master Mix (USB Corp., USA) using an automated thermal cycler (Mastercycler gradient, Eppendorf, Hamburg, Germany). The thermocycling program was as follows: 3 min at 95°C followed by 30 cycles of 50 s at 95°C, 40 s at 45°C and 50 s at 72°C, with a final extension period of 10 min at 72°C. The PCR products were purified and directly subjected to sequencing in both directions primed with either of the two primers used to originally amplify the fragment. The DNA sequence of ITS1-5.8S-ITS2 rRNA gene obtained was used as query sequence to search for similar sequences in GenBank using BLASTIN 2.2.18. DNA sequence similarity was determined by the ClustalW 2 multiple sequence alignment program. The fungus was identified based on the ITS1-5.8S-ITS2 sequence, which were amplified using universal primers ITS1, ITS4 and ITS5. A BLAST search was employed to obtain the closest-matching sequences in the GenBank database. This partial of the 18S sequence, complete ITS1-5.8S-ITS2 sequences, and partial of the 28S sequence of rRNA gene.

For fungal taxonomic comparison with known sequences, databank queries using the Basic Local Alignment Search Tool (BLAST) were performed via the website of the National Center for Biotechnology Information (NCBI, http://www.ncbi.nlm.nih.gov/) and CBS-KNAW Fungal Biodiversity Centre (http://www.cbs.knaw.nl/). Based on partial 28S rRNA analyses using universal fungal primers (LROR and LR7).

2.10 Cytotoxic activity

Bioassay of cytotoxicity activity was performed *in vitro* by MTT (3-(4,5-dimethylthiazol-2-yl)-2,5-diphynyltrazolium bromide) calorimetric method against hepato carcinoma (Hep-G2), gastric carcinoma (KATO-3), human breast cancer (MCF-7) and cervical carcinoma (CaSki). In principle, the viable cell number/well was directly proportional to the production of formazan, followed by solubilization, and could be measured spectrophotometrically.

The human cancer cell line was harvested from exponential-phase maintenance cultures (T-25 cm^2 flask), counted by trypan blue exclusion, seed cells in a 96-well culture plates at a density of $1x10^5$ cells/well in 200 μL of culture medium without compounds to be tested. Cells were cultured in a 5% CO_2 incubator at 37 $^{\circ}C$, 100% relative humidity for 24 h. Culture medium containing the sample was dispensed into the appropriate wells (control cells group, N = 3; each sample treatment group, N = 3). Peripheral wells of each plate (lacking cells) were utilized for sample blank (N = 3) and medium/DMSO blank (N = 3) “background” determination. Culture plates were then incubated for 3 days prior to the addition of tetrazolium reagent. MTT stock solution in a concentration of 5 mg/mL in PBS was sterilized by filtering through 0.45 μL filter units. MTT working solution was prepared just prior to culture application by dilution of MTT stock 1:5 (V/V) in prepared standard culture medium. The freshly prepared MTT reagent in a volume of 10 μL was added into each well and mixed gently for 1 minute on an orbital shaker. The cells were further incubated for 4 h at 37ºC in a 5% CO_2 incubator. After incubation, the formazan produced in the cells will capture as dark crystals in the bottom of the wells. All of the culture medium supernatant was removed from wells and 150 μL of

DMSO was added to dissolve the resulting formazan. Samples in the culture plate were mixed for 5 minutes on an orbital shaker. Subsequently, 25 μL of 0.1 M Glycine pH 10.5 was added and the culture plate was shaken for 5 minutes. Following formazan solubilization, the absorbance was measured using a microculture plate reader at 540 nm (single wavelength, calibration factor = 1.00).

2.11. Results and Discussion

2.11.1 Pure isolates of endophytic fungi

Based on different morphology of fungi, a total of 64 pure isolates of endophytic fungi were obtained from seven species of Thai mangrove plants, including *Lumnitzera racemosa*, *Tradescantia spathacea*, *Xylocarpus granatum*, *Azima sarmentosa*, *Bruguiera gymnorrhiza*, *Bruguier cylindrical* and *Solanum trilobatum*. The numbers of isolated strains from each plant are shown in Table 2.1. All isolated fungi are given their host plant name; LR from *L. racemosa*, TS from *T. spathacea*, XG from *X. granatum,* AS from *A. sarmentosa,* BG from *B. gymnorrhiza,* BC from *B. cylindrical*, and ST from *S. trilobatum*.

Table 2.1 Isolation of fungal endophytes

Plant	Fungal Code	Numbers of Isolates
Lumnitzera racemosa (ฝาดดอกขาว)	LR	16
Tradescantia spathacea (ว่านกาบหอย)	TS	12
Xylocarpus granatum (ตะบูนขาว)	XG	8
Azima sarmentosa (หนามพุงดอ)	AS	2
Bruguiera gymnorrhiza (พังกาหัวสุมดอกแดง)	BG	10
Bruguier cylindrical (ถั่วขาว)	BC	8
Solanum trilobatum (มะแว้ง)	ST	8

After isolation of endophytic fungi, all pure strains were placed on potato dextrose agar (PDA) until grown fully on petri dish, to observe their morphological characteristics including colony, color, produced pigment and sporulation. The characteristics of each strain are shown in Figures 2.13 to 2.19.

	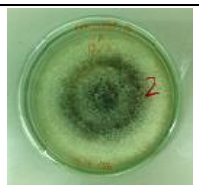	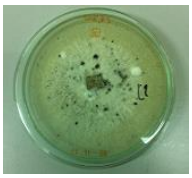	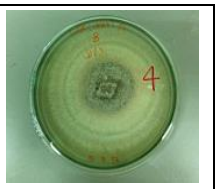
LR1L	LR2L	LR3L	LR4L
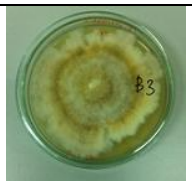	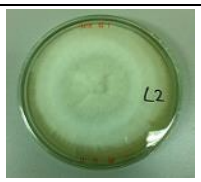	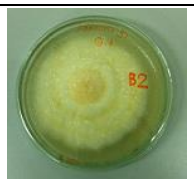	
LR5L	LR6L	LR7L	LR8L
	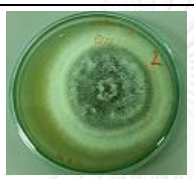		
LR9L	LR10L	LR11L	LR12L
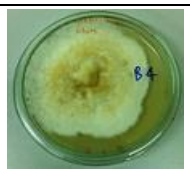		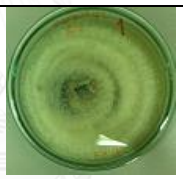	
LR13L	LR14L	LR15L	LR16L

Figure 2.13 Isolated endophytic fungi from *L. racemosa*

		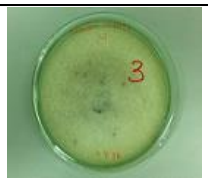	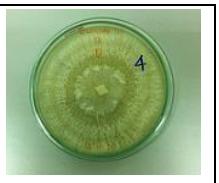
TS1L	TS2L	TS3L	TS4L
	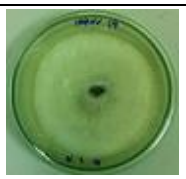		
TS5L	TS6L	TS7L	TS8L
		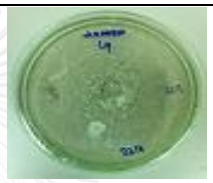	
TS9L	TS10L	TS11L	TS12L

Figure 2.14 Isolated endophytic fungi from *T. spathacea*

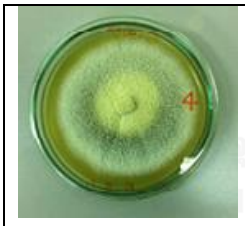	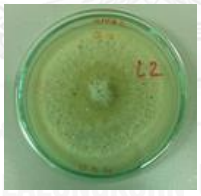	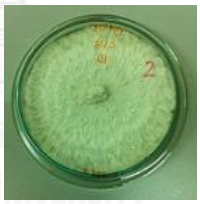	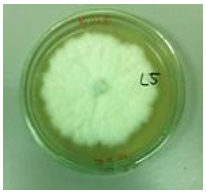
XG1L	XG2L	XG3L	XG4L
	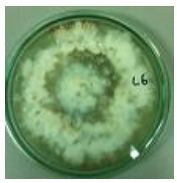		
XG5L	XG6L	XG7L	XG8L

Figure 2.15 Isolated endophytic fungi from *X. granatum*

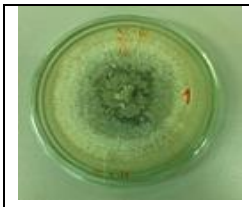	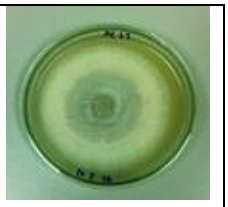
AS1L	AS2L

Figure 2.16 Isolated endophytic fungi from *A. sarmentosa*

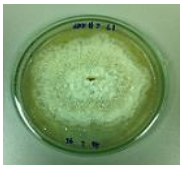		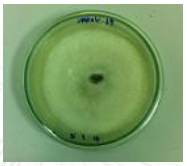	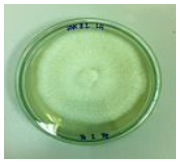	
BG1Y	BG2Y	BG3Y	BG4Y	BG5Y
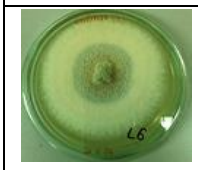	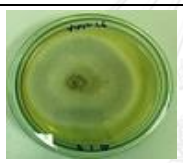	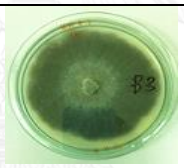	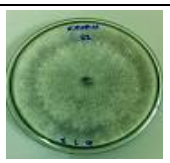	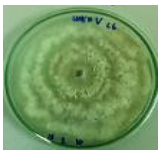
BG6Y	BG7Y	BG8Y	BG9Y	BG10Y

Figure 2.17 Isolated endophytic fungi from *B. gymnorrhiza*

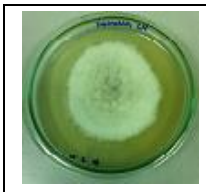		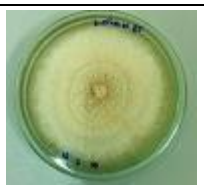	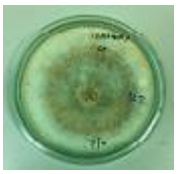
BC1B	BC2B	BC3B	BC4B
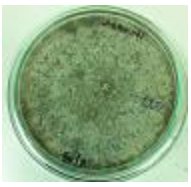	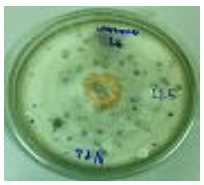		
BC5B	BC6B	BC7B	BC8B

Figure 2.18 Isolated endophytic fungi from *B. cylindrical*

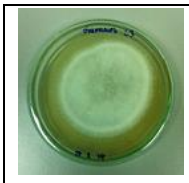	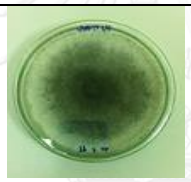	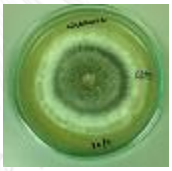	
ST1L	ST2L	ST3L	ST4L
		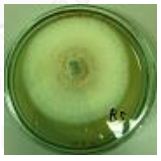	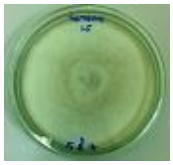
ST5L	ST6L	ST7L	ST8L

Figure 2.19 Isolated endophytic fungi from *S. trilobatum*

2.11.2 Selected mangrove-derived endophytic fungus

Ordinarily, type of media might affect the metabolite production of each fungus. In this study, cultivation of each isolated endophyte on three types of media, including Sabouraud dextrose broth (SDB), corn steep broth medium and yeast extract sucrose broth (YEB) were carried out. After cultivation for 21 days,

followed by extraction according to Scheme 2.1, the EtOAc crude extract (broth) of each fungal strain cultured on each medium was subjected to the analysis by ^{1}H NMR spectroscopy. Accordingly, fungal strain BG2Y grown on SDB, was selected to cultivate in large scale (10 L) for isolating bioactive metabolites in the further step, due to the signals of various functionalities including aromatic (6-8 ppm), olefinic (5-6 ppm) and oxygenated (3-4 ppm) protons as shown in Figures 2.20 and 2.21.

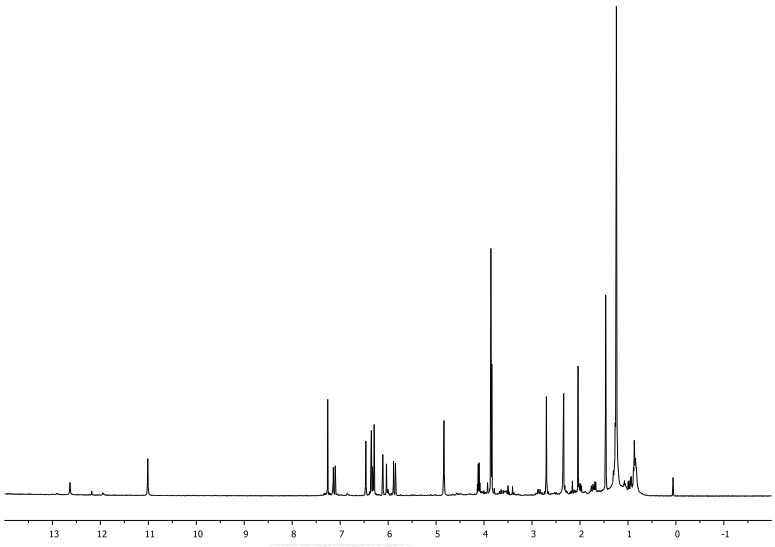

Figure 2.20 ^{1}H NMR spectrum of EtOAc extract (broth) of fungus BG2Y grown on SDB media

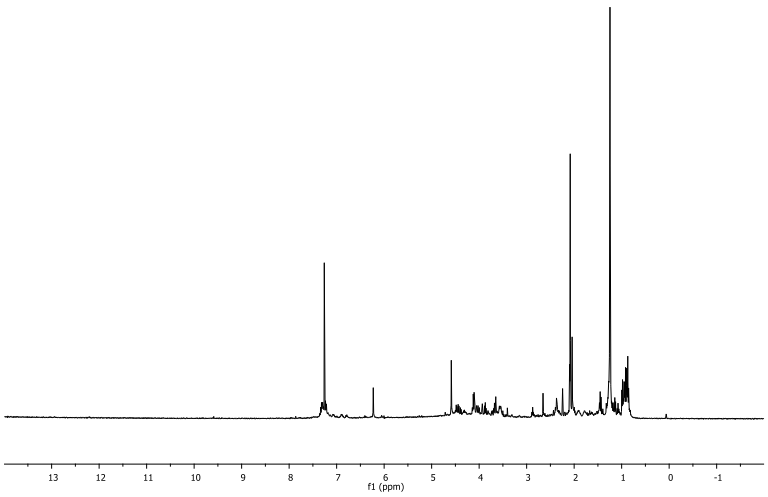

Figure 2.21 ^{1}H NMR spectrum of EtOAc extract (mycelium) of fungus BG2Y grown on SDB media

2.11.3 Classification of the endophytic fungal isolate BG2Y

Selected fungal strains BG2Y was taxonomically identified with molecular method by Mr.Nattawut Boonyuen, Phylogenetics and Mycology Laboratories Central Research Unit BIOTEC, National Center for Genetic Engineering and Biotechnology, Pathum Thani, Thailand.

For fungal taxonomic comparison with known sequences, databank queries using the Basic Local Alignment Search Tool (BLAST) were performed via the website of the National Center for Biotechnology Information (NCBI, http://www.ncbi.nlm.nih.gov/) and CBS-KNAW Fungal Biodiversity Centre (http://www.cbs.knaw.nl/). Based on partial 28S rRNA analyses using universal fungal primers (LROR and LR7), its sequence with 1356 nucleotides showed 95-96% identity with the 20 closest fungal match at NCBI and CBS-KNAW Fungal Biodiversity Centre. They are belonged within class Dothideomycetes; sub-class Pleosporomycetidae; order Hysteriales and family Hysteriaceae (**Table 2.2**). As a result, BG2Y was molecularly classified and grouped in Hysteriaceae as the family position.

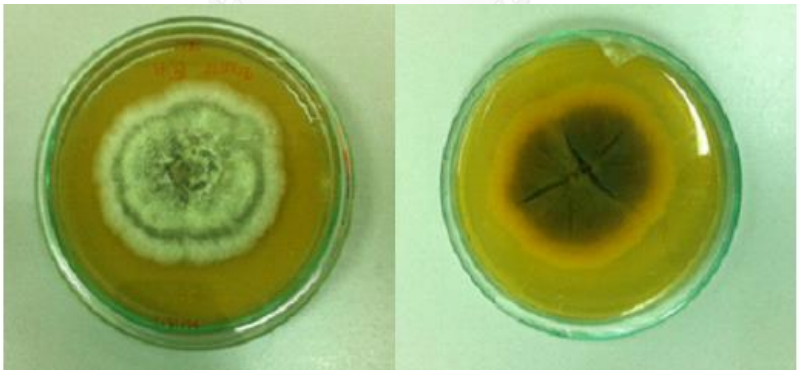

Figure 2.22 Colony morphology of the fungus BG2Y on PDA

Table 2.2 Twenty fungal names with closest BLAST match based on 28S large subunit ribosomal RNA gene, partial sequence.

Fungal name and original code	%Identity	Accession	Taxonomic position
Gloniopsis praelonga CMW:19983	97%	FJ161193.2	Family Hysteriaceae
Gloniopsis praelonga CBS:112415	97%	FJ161173.2	Family Hysteriaceae
Gloniopsis praelonga CBS:123337	97%	FJ161195.2	Family Hysteriaceae
Chaetophoma sp. CBS 119963	96%	EU754143.1	Family Hysteriaceae
Gloniopsis subrugosa CBS:123346	96%	FJ161210.2	Family Hysteriaceae
Rhytidhysteron rufulum isolate AFTOL-ID 2109	96%	FJ469672.1	Family Hysteriaceae
Psiloglonium araucanum CMW:18760	96%	FJ161192.2	Family Hysteriaceae
Psiloglonium araucanum CBS:112412	96%	FJ161172.2	Family Hysteriaceae
Rhytidhysteron rufulum strain EB 0383	96%	GU397353.1	Family Hysteriaceae
Psiloglonium araucanum CMW:17941	96%	FJ161190.2	Family Hysteriaceae
Rhytidhysteron rufulum strain EB 0384	96%	GU397354.1	Family Hysteriaceae
Hysterium angustatum CBS:236.34	95%	FJ161180.2	Family Hysteriaceae
Hysterium angustatum CBS:123334	95%	FJ161207.2	Family Hysteriaceae
Rhytidhysteron rufulum strain EB 0382	95%	GU397352.1	Family Hysteriaceae
Gloniopsis praelonga CMW:18053	95%	FJ161191.2	Family Hysteriaceae
Hysterobrevium mori CBS:123335	95%	FJ161202.2	Family Hysteriaceae
Hysterobrevium mori CBS:123564	95%	FJ161198.2	Family Hysteriaceae
Hysterobrevium mori CBS:123563	95%	FJ161196.2	Family Hysteriaceae

Fungal name and original code	%Identity	Accession	Taxonomic position
Hysterobrevium smilacis CBS:200.34	95%	FJ161177.2	Family Hysteriaceae
Hysterobrevium smilacis CBS:114601	95%	FJ161174.2	Family Hysteriaceae

For the internal transcribed spacer (ITS1-5.8S-ITS2) rDNA amplified by ITS1 and ITS4 primer, sequence produced the same BLAST results was pairwise aligned using the program BioEdit (BioEdit 7.05; http://www.mbio.ncsu.edu/BioEdit/bioedit.html) and the similarity was calculated as shown in Table 2.2. Our result demonstrated a high similarities of 98–99% with *Rhytidhysteron rufulum* strain FMR 8743 (GenBank accession number AM711974). Thus, the fungus was then identified as *Rhytidhysteron rufulum*.

***Rhytidhysteron rufulum* AM71197**
GGATCATTACCAAAGGATCGCGAGGCGCGAGGGGGTAGGAACTAACCGCTCGATCGGTGGACCGT
ACCCATAGAATGCCGTCCTCCGGGGGCTCGCGGCT

***Rhytidhysteron rufulum* BG2Y**
GGATCATTACCAAAGGATGGCGAGGCGGGAGGGGGTAGGAACTAACCACCCGGCCGGTGGACCGT
GCCCATAGAATGGCGTCCTCCGGGGGGTCGCGGCT

***Rhytidhysteron rufulum* AM71197**
TGCCGCGCCCTAGAGGCCTCCTAGGGGGCTTCTCGCGTCCTCGCTTTCCACAACCTTCACCCTTGATT
ACCCTAGCCTTGTTGCCTCGGCGGGTCCGCCC

***Rhytidhysteron rufulum* BG2Y**
TGCCGCGCCCTAGAGGCCTCCTAGGGGGCTTCTCCCGCTCTCGCATTCCACAACCTTCACCCTTGATT
ACCATAGCCCGGTTGCCTCGGCGGGTCCGCCC

***Rhytidhysteron rufulum* AM71197**

GCCAGAGGACACAACCTAAACTACTGTTGTAAACGGCGAAGTCTGAGCTACAAAGCAATTGTTTAAA
ACTTTCAACAACGGATCTCTTGGTTCTGGCATC

***Rhytidhysteron rufulum* BG2Y**
GCCAGAGGACTTTGACTAAACCACTGTTGATAACGGCGGCGTCTGAGCTACAAAGCAATTGTTTAAA
ACTTTCAACAACGGATCTCTTGGTTCTGGCATC
***Rhytidhysteron rufulum* AM71197**
GATGAAGAACGCAGCGAAATGCGATAAGTAGTGTGAATTGCAGAATTCAGTGAATCATCGAATCTTT
GAACGCACATTGCGCCCTTTGGCATCCCGAAGG

***Rhytidhysteron rufulum* BG2Y**
GATGAAGAACGCAGCGAAATGCGATAAGTAGTGTGAATTGCAGAATTCAGTGAATCATCGAATCTTT
GAACGCACATTGCGCCCTTTGGCATCCCGAAGG

***Rhytidhysteron rufulum* AM71197**
GCATGCCTGTTCGAGCGTCATTTCACCAATCAAGCCTGGCTTGGTGTTGGGTGCCGTCCCGCCTCCCG
CGCGCGGACGCTCCCTAAAATCATCGGCGGTG

***Rhytidhysteron rufulum* BG2Y**
GCATGCCTGTTCGAGCGTCATTTCACCGATCAAGCCTGGCTTGGTGTTGGGTGCCGTCCCGCCTTCCG
CGCGTGGACGCTCCCTAAAATCATCGGCGGTG

***Rhytidhysteron rufulum* AM71197**
CAGCACCGGCTTCGAGCGCAGCAGATGTTCGCTTGGGGCCCGGTGCGGCAGCGGCCGCGACGACA
ACCTCTAGGTGAC

***Rhytidhysteron rufulum* BG2Y**
CAGCACCGGCTTCGAGCGCAGCAGATGTTCGCTTGGGGCCCGGTGGGGCAGCGGCCGCGACGACA
ACCTCTAGGTGAC

Figure 2.23 Pairwise alignment between fragments of the ITS1-5.8S-ITS2 from *Rhytidhysteron rufulum*, BG2Y and representative fungal species (*Rhytidhysteron rufulum* AM71197), showing the sequences of primers ITS1 and ITS4.

In Figure 2.24, ITS nucleotide sequence of BG2Y was precisely indicated and verified the components, which are present within each sequence: the partial 18S rRNA, ITS1, 5.8S rRNA, ITS2, the partial 28S rRNA. Both the 28SrDNA and ITS rDNA of 2B have been submitted to GenBank with the accession number KP994148 and KP994147, respectively.

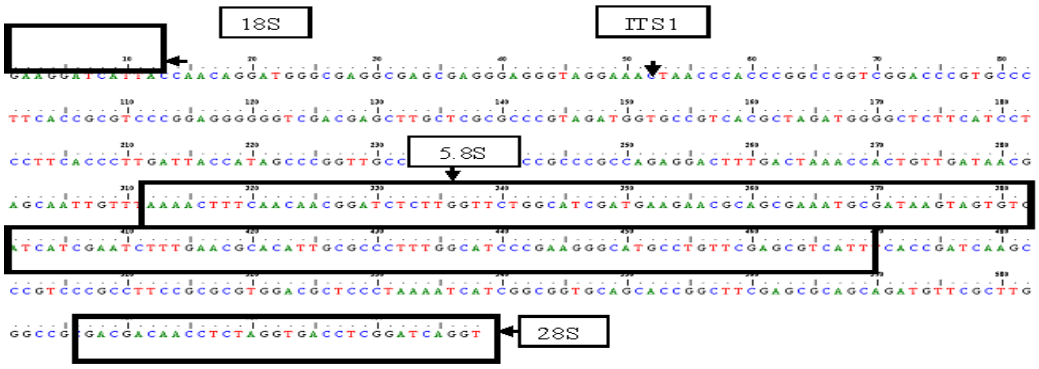

Figure 2.24 Nucleotide sequences of the partial 18S rRNA gene, complete ITS1-5.8S-ITS2, and partial 28S rRNA gene of the fungus BG2Y

2.11.4 Secondary metabolites of the fungus *Rhytidhysteron rufulum* (BG2Y)

The chromatographic fractionation of EtOAc crude extracts of culture broth and mycelium of *R. rufulum* on SDB medium led to the isolation of six new (**1-6**), and one known compound (**7**). Compounds **1-4** were isolated from the EtOAc crude extract of culture broth, while compounds **5-7** were isolated from the EtOAc crude extract of mycelium, as well as compound **1** was isolated as major metabolite. The structures of all isolated compounds are shown in Figure 2.25.

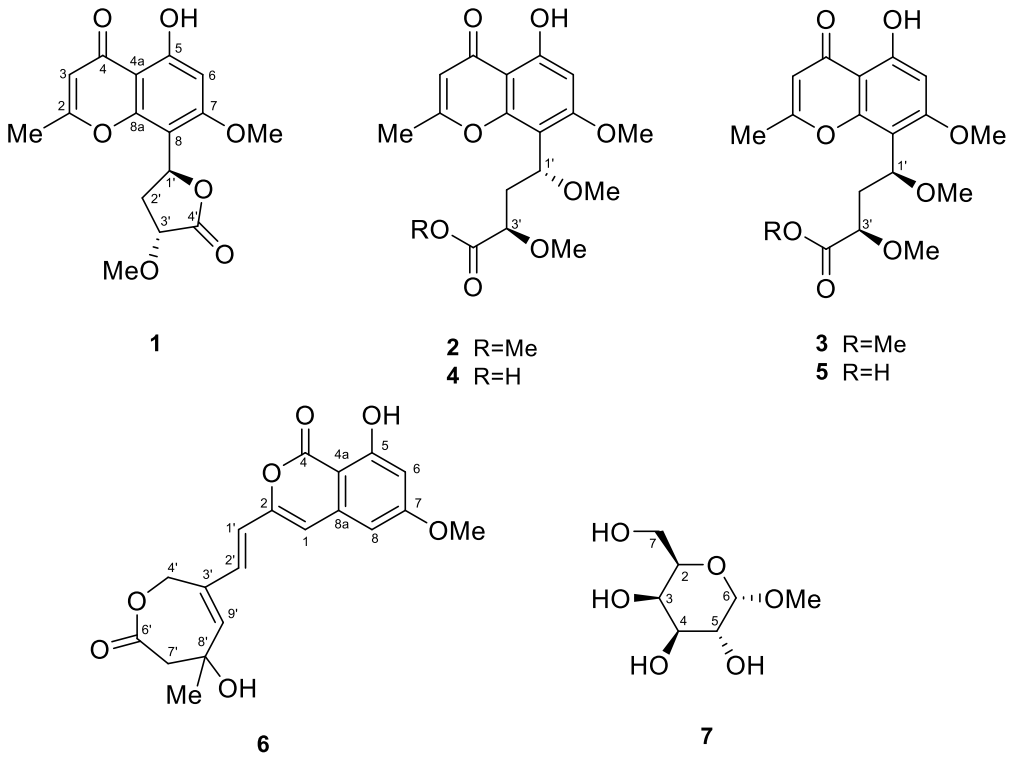

Figure 2.25 Structures of compounds **1**-**7**

Compound **1** was obtained as colorless crystals, mp 149-150 °C, $[\alpha]^{20}_{D}$ -10.8 (*c* 0.1, MeOH), UV (MeOH) λ_{max} (log ε) 237 (3.53) nm, 255 (3.48) nm, 290 (3.20) nm and 319 (3.06) nm, IR (neat) υ_{max} 3346, 1732, 1640, 1423, 1212 cm^{-1}. Its molecular formula was established as $C_{16}H_{16}O_7$ by HRESIMS data (*m/z* 343.0784 $[M+Na]^+$, calcd 343.0788), displaying nine degrees of unsaturation. The NMR spectra contained signals for one phenolic proton bonded to a carbonyl group (δ_H 13.04 s), one aromatic proton (δ_H 6.36 s) attributed to a pentasubstituted aromatic ring, one olefinic proton (δ_H 6.04 s) assigned to a trisubstituted olefin, two methoxy singlets (δ_H 3.64 and 3.89), and one methyl singlet (δ_H 2.35). Analysis of ^{13}C NMR and HSQC NMR data of **1** exposed the presence of one conjugated ketone carbonyl (δ_C182.5), one ester carbonyl (δ_C 174.9), six quaternary carbons (δ_C 167.1, 163.4, 162.9, 155.7, 104.9 and 103.4), four methines (δ_C 108.7, 95.2, 76.1 and 69.2), two methoxys (δ_C 58.6 and 56.3), one methylene (δ_C 33.6) and one methyl (δ_C 20.4). Furthermore, the UV

absorption maxima at 237, 255, 290 and 319 indicated that **1** should be a chromone derivative. According to its double bond equivalent (DBE), the seven units of unsaturation for a chromone skeleton and one unit for ester carbonyl, suggested that compound **1** contains an additional ring in the structure. The ^{1}H–^{1}H COSY spectrum revealed the existence of one isolated spin systems, CH-1'–CH_2-2'–CH-3', as well as the HMBC cross-peaks from H-1' (δ_H 6.00, dd, *J*=7.2, 9.6 Hz) and H-3' (δ_H 4.29, t, *J*=10.0 Hz) to an ester carbonyl at δ_C 174.9 (C-4') led to the corroboration of the γ-lactone ring. Further HMBC correlation from H-1' to C-7, C-8, and C-8a indicated that C-1' oxymethine of the γ-lactone ring was attached on C-8 of the chromone nucleus. One methoxy group (δ_H 3.64, δ_C 58.6) was located on C-3' due to its HMBC correlation with C-3', whereas another methoxy group (δ_H 3.89, δ_C 56.3) was placed on C-7 from its HMBC cross-peak to C-7. The singlet methyl proton (δ_H 2.35) showed HMBC correlations with C-2 and C-3, indicating the location of the methyl group at C-2. Additionally, observed HMBC correlations of 5-OH with C-4a, C-5 and C-6 verified the location of the hydroxyl group on C-5. This assignment was also supported by the appearance of the hydroxyl proton downfield due to a chelation effect. Thus, the structure of **1** was established as shown. The propose structure of **1** was further confirmed and its relative configuration were established by single-crystal X-ray diffraction analysis using Mo Kα radiation. Crystal data and structure refinement of **1** were described in Table 2.3, and a perspective ORTEP plot is depicted in Figure 2.19. Crystallographic data for **1** and its refinement structure are described in Table 2.11. Furthermore, compound **1** has been deposited with the Cambridge Crystallographic Data Centre under the deposition number CCDC 1406338.

To the best our knowledge, chromones possessing a γ-lactone ring as a side chain seem to be rare. The only precedents include lachnones C-D from a filamentous fungus *Lachnum* sp. [38]. These results strongly indicated that the structure of **1** was established as a novel derivative of chromone and it was named rhytidchromone A.

Table 2.3 NMR data of compound **1** in $CDCl_3$

Position	**1**	
	δ_C	δ_H (mult, *J* in Hz)
2	167.1	
3	108.7	6.04, s
4	182.5	
4a	104.9	
5	163.4	
6	95.2	6.36, s
7	162.9	
8	103.4	
8a	155.7	
1'	69.2	6.00, dd (7.2, 9.6)
2'	33.6	2.55, ddd (7.2, 10.0, 12.8) 2.86, ddd (7.2, 9.6, 12.8)
3'	76.1	4.29, t (10.0)
4'	174.9	
2-Me	20.4	2.35, s
5-OH		13.04, br s
7-OMe	56.3	3.89, s
1'-OMe		
3'-OMe	58.6	3.64, s
4'-OMe		

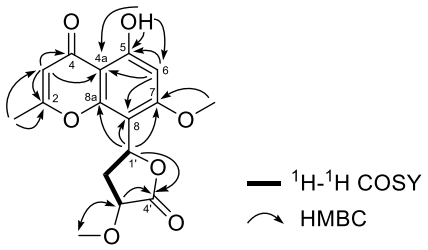

Figure 2.26 ^{1}H–^{1}H COSY and key HMBC correlations of **1**

Table 2.4 Crystal data and structure refinement for compound **1**

Identification code	Rhytidchromone A
Empirical formula	$C_{16}H_{16}O_7$
Formula weight	320.30
Temperature	298 K
Wavelength	0.71073 Å
Crystal system, space group	$P2_1$
Unit cell dimensions	a = 8.0040 (4) Å
	b = 8.6152 (4) Å
	c = 11.7898 (4) Å
Volume	766.45(6) Å^3
Z, Calculated density	2, 1.388 mg/m^3
Absorption coefficient	0.11 mm^{-1}
F(000)	336.2376
Crystal size	0.50 × 0.20 × 0.20 mm^3
Theta range for data collection	2.7 to 26.4 °
Limiting indices	-8<=h<=10, -7<=k<=10,-14<=l<=10
Reflections collected / unique	2347 (R_{int} = 0.016)
Completeness to theta	109.478 (1)°
Refinement method	Full-matrix least-squares on F^2
Data / restraints / parameters	2347 / 0 / 211
Goodness-of-fit on F^2	2.59
Final R indices [I>2sigma(I)]	R_1 = 0.030, *wR2* = 0.060
R indices (all data)	R_1 = 0.032, *wR2* = 0.060
Absolute structure parameter	-1.8 (3)
Largest diff. peak and hole	0.14 and -0.17 e.Å^3

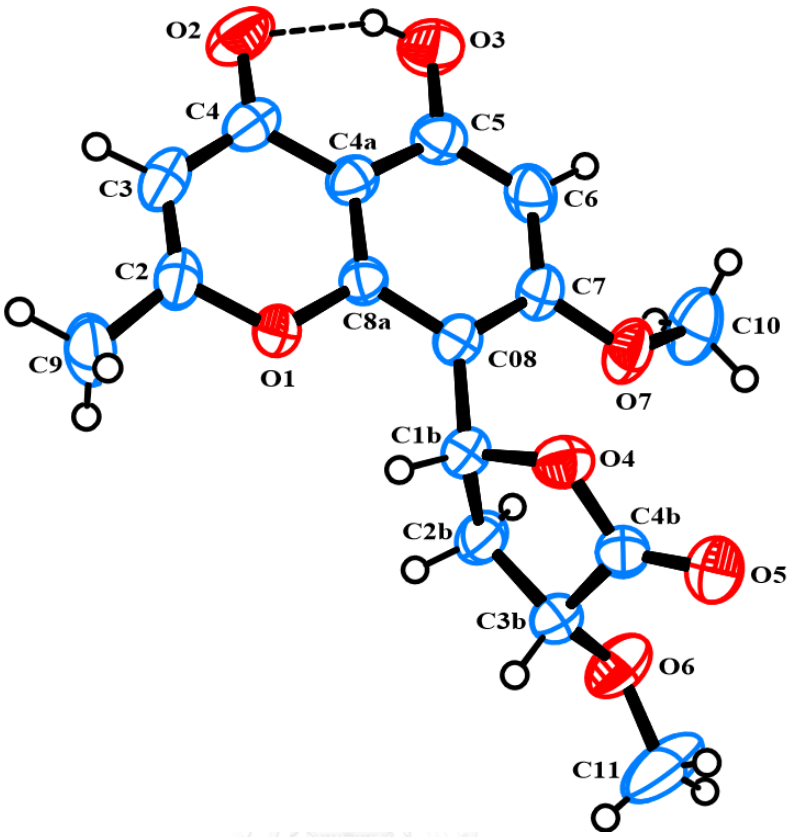

Figure 2.27 ORTEP drawing of compound **1**

Compound **2** was obtained as a pale yellow gum, $[\alpha]^{20}_{D}$ -24.8 (*c* 0.1, MeOH), UV (MeOH) λ_{max} (log ε) 246 (3.58) nm, 265 (3.64) nm and 291 (3.50) nm, IR (neat) υ_{max} 3346, 1743, 1638, 1539, 1404, 1242 cm^{-1}. Its molecular formula was established as $C_{18}H_{22}O_8$ by HRESIMS data (*m/z* 389.1207 $[M+Na]^+$, calcd 389.1212), implying eight units of unsaturation. Investigation of ^{13}C NMR and HSQC NMR data of **2** revealed the presence of one conjugated ketone carbonyl (δ_C182.9), one ester carbonyl (δ_C 172.8), six quaternary carbons (δ_C 166.9, 164.1, 162.5, 156.1, 105.3 and 104.8), four methines (δ_C 108.4, 95.3, 78.2 and 70.6), four methoxys (δ_C 58.1, 56.7, 56.2 and 51.8), one methylene (δ_C 36.9) and one methyl carbon (δ_C 20.5). The NMR data displayed signals for one phenolic proton boned to a carbonyl group (δ_H 13.01 s), one aromatic proton (δ_H 6.40 s) attributed to a pentasubstituted aromatic ring, one olefinic proton (δ_H 6.05 s) assigned to a trisubstituted olefin, four methoxy singlets (δ_H 3.90, 3.73,

3.29 and 3.17), and one methyl singlet (δ_H 2.38). The HMBC and ^1H–^1H COSY correlations were similar to those of compound **1**. However, compound **2** had no γ-lactone ring in the structure due to lack of the HMBC correlation from H-1' to an ester carbonyl at δ_C 172.8. This was correlated to its DBE, implying that the structure of **2** contained the oxygenated alkyl side chain in place of the γ–lactone ring in **1**. In addition, the addition proton signals of two methoxy groups were observed. The HMBC correlation of the methoxy protons at δ_H 3.17 with C-1' allowed the attachment of this methoxy on the C-1' carbon, while the methoxy protons at δ_H 3.73 displayed the HMBC cross-peak with the ester carbonyl carbon (δ_C 172.8), thus indicating the presence of the methyl ester at C-4'. The relative configurations of **1** were determined by on basic of the NOESY data. In the NOESY spectrum, the NOE correlation between 2-Me and 4'-OMe, in combination with the lack of correlation between 1'-OMe and 3'-OMe, indicated the difference orientation of the methoxy groups at C-1' and C-3'. Thus, **2** was determined as a new compound and given the name rhytidchromone B.

Table 2.5 NMR data of compound **2** in $CDCl_3$

Position	**2**	
	δ_C	δ_H (mult, *J* in Hz)
2	166.9	
3	108.4	6.05, s
4	182.9	
4a	105.3	
5	162.5	
6	95.3	6.40, s
7	164.1	
8	104.8	
8a	156.1	
1'	70.6	5.10, t (7.2)
2'	36.9	2.30, m 2.60, dt (7.2, 14.0)
3'	78.2	3.63, dd (4.8, 12.8)
4'	172.8	
2-Me	20.5	2.38, s
5-OH		13.01, br s
7-OMe	56.2	3.90, s
1'-OMe	56.7	3.17, s
3'-OMe	58.1	3.29, s
4'-OMe	51.8	3.73, s

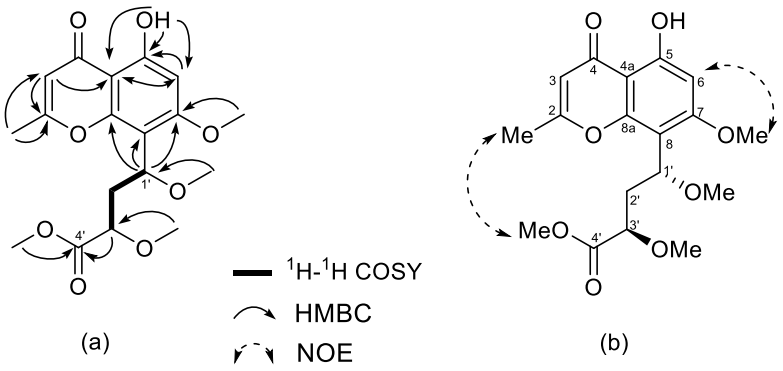

Figure 2.28 (a) ^{1}H–^{1}H COSY, key HMBC and (b) selected NOESY correlations of **2**

Compound **3** was obtained as a pale yellow gum, $[\alpha]^{20}_{D}$ +7.2 (*c* 0.1, MeOH), UV (MeOH) λ_{max} (log ε) 245 (3.62) nm, 266 (3.68) nm and 292 (3.58) nm, IR (neat) υ_{max} 3365, 1721, 1642, 1536, 1403, 1236 cm^{-1}. Its molecular formula was established as $C_{18}H_{22}O_8$ by HRESIMS data (*m/z* 389.1211 $[M+Na]^+$, calcd 389.1212), being the same as that of compound **2**. Compound **3** contained eight units of unsaturation. Investigation of ^{13}C NMR and HSQC NMR spectra of **2** implying one conjugated ketone carbonyl (δ_C182.9), one ester carbonyl (δ_C 173.3), six quaternary carbons (δ_C 166.9, 164.0, 162.3, 155.9, 105.8 and 104.7), four methines (δ_C 108.4, 95.3, 77.9 and 70.2), four methoxys (δ_C 58.4, 56.6, 56.2 and 51.8), one methylene (δ_C 37.4) and one methyl carbon (δ_C 20.5). The spectrum NMR contained signals for one phenolic proton boned to a carbonyl group (δ_H 13.01 s), one aromatic proton (δ_H 6.38 s) attributed to a pentasubstituted aromatic ring, one olefinic proton (δ_H 6.04 s) assigned to a trisubstituted olefin, four methoxy singlets (δ_H 4.06, 3.89, 3.71 and 3.19), and one methyl singlet (δ_H 2.38). The HMBC and ^{1}H–^{1}H COSY correlations were closely resembled those of compound **2**. Moreover, detailed 2D NMR analysis revealed that they shared the same planar structure. The obvious differences were the chemical shift of the proton signals for the side chain. This indicated compounds **2** and **3** differed in the configurations at C-1' and/or C-3'. The observed NOE correlation between 1'-OMe and 3'-OMe as well as between 2-Me and 4'-OMe supported the same orientation of the methoxy groups at C-1' and C-3'. This

assignment was supported by the opposite signs of their specific rotations ($[\alpha]^{20}_{D}$-24.8 for **2**vs +7.20 for **3**). Consequently, compound **3** was determined to be a new chromone, named rhytidchromone C.

Table 2.6 NMR data of compound **3** in $CDCl_3$

Position	**3**	
	δ_C	δ_H (mult, *J* in Hz)
2	166.9	
3	108.4	6.04, s
4	182.9	
4a	105.8	
5	162.3	
6	95.3	6.38, s
7	164.0	
8	104.7	
8a	155.9	
1'	70.2	5.09, dd (3.9, 9.9)
2'	37.4	1.97, ddd (3.9, 9.7, 14.1) 2.70, ddd (3.7, 9.9, 14.1)
3'	77.9	4.06, dd (3.7, 9.7)
4'	173.3	
2-Me	20.5	2.38, s
5-OH		13.03, s
7-OMe	56.2	3.89, s
1'-OMe	56.6	3.19, s
3'-OMe	58.4	3.43, s
4'-OMe	51.8	3.71, s

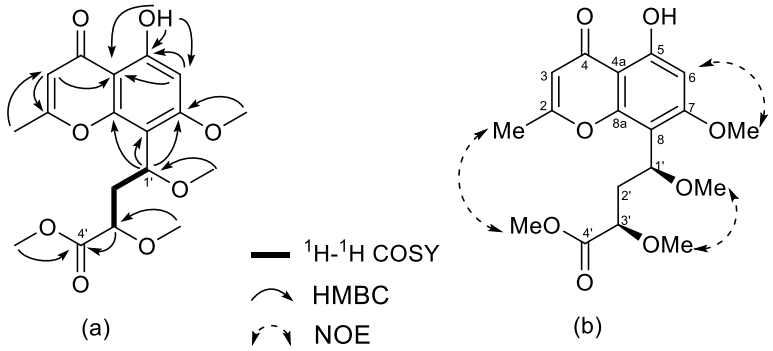

Figure 2.29 (a) ^{1}H–^{1}H COSY, key HMBC and (b) selected NOESY correlations of **3**

Compound **4** was obtained as a pale yellow gum, $[\alpha]^{20}_D$ -18.2 (*c* 0.1, MeOH), UV (MeOH) λ_{max} (log ε) 247 (3.59) nm, 265 (3.64) nm and 289 (3.52) nm, IR (neat) υ_{max} 3349, 1727, 1639, 1535, 1403, 1236 cm^{-1}. Its molecular formula was established as $C_{17}H_{28}O_8$ by HRESIMS data (*m/z* 375.1056 $[M+Na]^+$, calcd 375.1061). The NMR spectroscopic data of compound **4** closely related to those of compound **2**, except for the disappearance of signals for a methoxy group. The HMBC and ^{1}H–^{1}H COSY correlations were similar to those of compound **2**. The location of three methoxy group at C-7, C-1' and C-3' was confirmed by the HMBC experiment. Thus compound **4** was identified as a carboxylic acid derivative of **2** or **3** from its molecular formula, although the intensity of the carboxylic carbonyl in the ^{13}C NMR spectrum was quite low and no HMBC cross-peak from any proton to the carbonyl carbon was observed. Finally, the configurations at C-1' and C-3' in compound **4** was identified as same as those in **2** from the almost identical chemical shift, splitting and coupling patterns of H-1', H_2-2' and H-3', as well as the same sign of their specific rotations ($[\alpha]^{20}_D$ -18.2 for **4** vs -24.8 for **2**). Thus, the structure **4** was established as shown and it was found to be a new compound, given name as rhytidchromone D.

Table 2.7 NMR data of compound **4** in $CDCl_3$

Position	**4**	
	δ_C	δ_H (mult, *J* in Hz)
2	167.1	
3	108.4	6.05, s
4	182.8	
4a	105.1	
5	162.5	
6	95.3	6.39, s
7	164.0	
8	104.8	
8a	156.1	
1'	70.6	5.16, t (6.8)
2'	36.0	2.30, m 2.64, m br
3'	78.2	3.68, br s
4'[a]	175.0	
2-Me	20.5	2.38, s
5-OH		13.05, br s
7-OMe	56.2	3.89, s
1'-OMe	56.6	3.18, s
3'-OMe	58.1	3.34, s

[a]ambiguous signal was assigned.

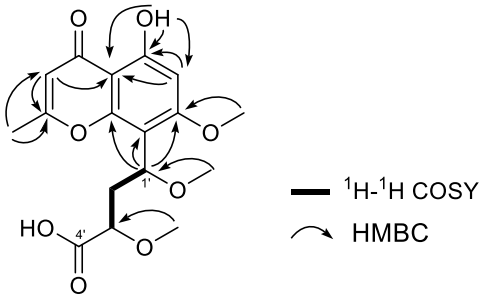

Figure 2.30 ^{1}H–^{1}H COSY and key HMBC correlations of **4**

Compound **5** was obtained as a pale yellow gum, $[\alpha]^{20}_{D}$ -13.2 (*c* 0.1, MeOH), UV (MeOH) λ_{max} (log ε) 244 (3.55) nm, 260 (3.61) nm and 289 (3.46) nm, IR (neat) υ_{max} 3359, 1725, 1635, 1540, 1405, 1235 cm^{-1}. Its molecular formula was established as $C_{17}H_{28}O_8$ by HRESIMS data (*m/z* 375.1050 $[M+Na]^+$, calcd 375.1061), being the same that of compound **4**. The NMR analysis data (Table 2.15) of compound **5** were very similar to those of compound **4**. The difference was the loss of signals for a methoxy group. Interpretation of 2D NMR spectroscopic data established the same planar structure as compound **4**. Similarity, the identical chemical shift, splitting and coupling patterns of H-1', H_2-2' and H-3' to those in compound **5** and the same sign of their specific rotation led to designation of the same configurations at C-1' and C-3'. Thus, the structure of **5** was established and it was name rhytidchromone E as shown.

Table 2.8 NMR data of compound **5** in $CDCl_3$

Position	**5**	
	δ_C	δ_H (mult, *J* in Hz)
2	167.0	
3	108.4	6.05, s
4	182.8	
4a	105.2	
5	162.5	
6	95.3	6.37, s
7	163.9	
8	104.8	
8a	156.0	
1'	70.6	5.10, dd (4.0, 10.0)
2'	37.0	2.00, ddd (4.0, 8.4, 14.0) 2.78, ddd (4.0, 10.0, 14.0)
3'	77.8	4.05, dd (4.0, 8.4)
4'[a]	175.0	
2-Me	20.5	2.38, s
5-OH		13.04, br s
7-OMe	56.2	3.88, s
1'-OMe	56.5,	3.20, s
3'-OMe	58.7	3.48, s

[a]ambiguous signal was assigned.

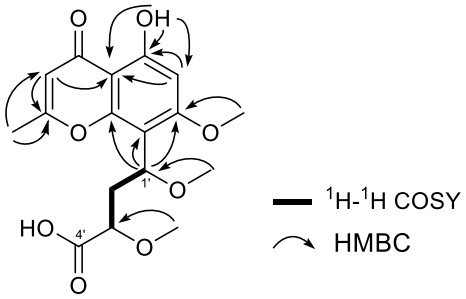

Figure 2.31 ^{1}H–^{1}H COSY and key HMBC correlations of **5**

The existence of the carboxylic acid functionality as C-4' in both **4** and **5** could be proved by an additional evidence. Both compounds **4** and **5** were gradually converted into the mixture between **1** and **1a** ratio nearly 1:1, a pair of C-1' epimer, in $CDCl_3$ over few days. The relative configuration of **1a** at C-1' and C-3' was determined by the NOE correlations. The NOESY spectrum (Figure 2.24) of **1** and **1a** mixture showed correlation of H-1' (δ_H 6.00)/H-2'β (δ_H 2.86) and H-2'β/H-3' (δ_H 4.29) for **1**, consistent with its ORTEP diagram. In the case of correlation for **1a**, the correlation of H-1' (δ_H 6.25)/H-2'β (δ_H 2.70) and H-2'β (δ_H 2.52)/H-3' (δ_H 4.29), with the lack of correlations between H-2'β/H-3' suggested the α-orientation of C-1' of the γ-lactone ring. Considering the **1/1a** ratio of the obtained mixture indicated, upon exposure to the acidity of $CDCl_3$, the benzylic carbocation might first be formed owing to its stability, and the lactone ring is subsequently formed by the attack of the hydroxyl lone pair of 4'**–**COOH on carbocation, which can occur from either side of the planar, *sp*^{2}**–**hybridized carbocation to afford compounds **1** and **1a** as shown in Scheme 2.5. Therefore, it seems reasonable to postulate that the biosynthetic origin of **1** would probably be compounds **4** and **5** as evident. This also supports the relative configurations of compounds **2** and **3**, the methyl ester derivatives of **4** and **5**, respectively.

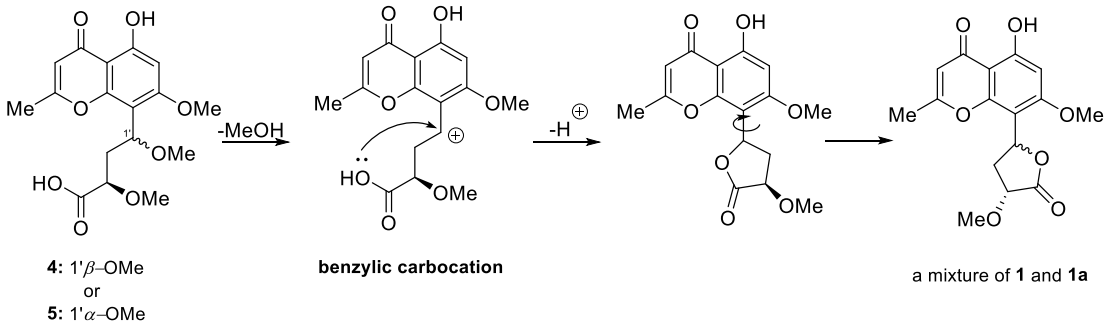

Scheme 2.5 Proposed mechanism for the formation of a mixture of compounds **1** and **1a** from **4** or **5**

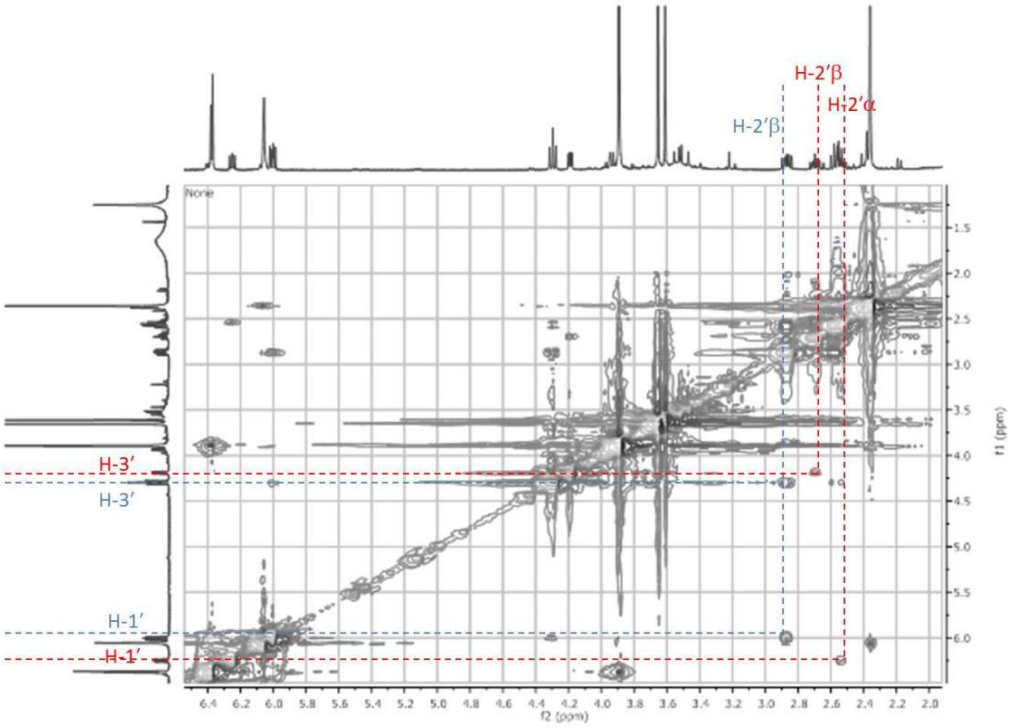

Figure 2.32 NOESY spectrum of **4** in $CDCl_3$ over 3 days (a mixture of **1** and **1a**)

Compound **6** was obtained as a yellow crystal, mp 189-191°C, $[\alpha]^{20}_{D}$ -92.2 (*c* 0.1, MeOH), UV (MeOH) λ_{max} (log ε) 213 (3.58) nm, 265 (3.72) nm, 313 (3.62), 343 (3.60), 357 (3.61) and 376 (3.45) nm. Its molecular formula was established as $C_{19}H_{18}O_7$ by HRESIMS data (*m/z* 357.0984 $[M- H]^-$, calcd 375.0980). The IR spectrum displayed absorption bands at 3431 and 1665 cm^{-1} for hydroxyl and conjugated lactone carbonyl groups, respectively. The ^{1}H NMR spectrum consisted of signals for six aromatic/double bond protons [δ_H 7.15 d (*J*=15.9 Hz), 6.48 d (*J*=2.0 Hz), 6.37 d (*J*=1.9 Hz), 6.31 s, 6.10 s and 5.89 d (*J*=15.9 Hz)], one tertiary methyl (δ_H 1.48 s), one methoxy (δ_H 3.87 s) and a chelated hydroxyl proton (δ_H 11.03 s). In addition, analysis of ^{13}C and HSQC NMR data revealed the presence of two ester carbonyls (δ_C 172.9 and 165.3), one aromatic ring, three carbon-carbon double bounds, two methylenes (one oxygenated), and one oxygenated quaternary carbon. These data indicated that compound **6** was an isocoumarin derivative. Observed HMBC correlations of 5–OH with C-5 and C-6 verified the location of the hydroxyl group on C-5 and the correlation of methoxy protons with C-7 confirmed the lacation of 7-OMe. The seven-membered lactone ring was corroborated by HMBC correlations of H-4'/C-3, H-9'/C-4', H-9'/C-8', H-7'/C-9' and H-7'/C-6'. The connection of a tertiary methyl group at C-8' was due to its HMBC correlation with C-8'. A carbon-carbon double bound was positioned between the isocoumarin nucleus at C-2 and the 7-membered lactone ring at C-3' owing to HMBC correlations of H-1'/C-2 and H-2'/C-4', respectively. A big coupling constant of 15.9 Hz between H-1' and H-2' suggested that the C-1'–C-2' double bond was an *E*-configuration. Thus, the structure of compound **6** was established as shown, and it was identified as a new isocoumarin derivative.

Table 2.9 NMR data of compound **6** in $CDCl_3$

Position	**6**	
	δ_C	δ_H (mult, *J* in Hz)
1	107.4	6.31, s
2	151.4	
4	165.3	
4a	100.3	
5	163.9	
6	101.1	6.48, d (2.0)
7	166.9	
8	102.5	6.37, d (1.9)
8a	138.8	
1'	122.1	5.89, d (15.9)
2'	125.0	7.15, d (15.9)
3'	136.8	
4'	73.0	4.86, s
6'	172.9	
7'	45.1	2.71, s
8'	88.6	
9'	134.9	6.10, s
8'-Me	25.9	1.48, s
5-OH		11.03, s
7-OMe	55.7	3.87, s

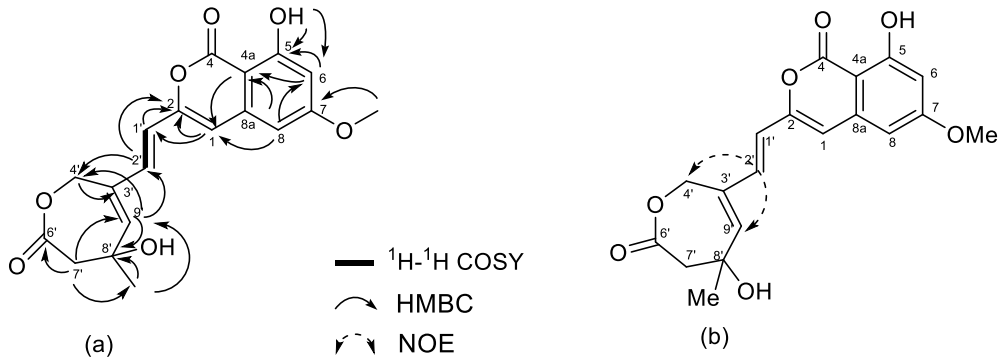

Figure 2.33 (a) ^{1}H–^{1}H COSY, key HMBC and (b) selected NOESY correlations of **6**

Compound **7** was obtained as a pale yellow gum, $[\alpha]^{20}_{D}$ -24.0 (*c* 0.1, MeOH), UV (MeOH) λ_{max} (log ε) 206 (2.70) nm and 267 (3.28) nm, molecular formula was established as $C_7H_{14}O_6$ by HRESIMS data (*m/z* 217.0684 $[M+Na]^+$, calcd 217.0688). Analysis of the ^{1}H, ^{13}C and HSQC NMR spectra of **7** showed the presence of one acetal methine (δ_H 4.15, δ_C 105.5), four methines (δ_C 78.1, 78.0, 75.1 and 71.7), one methoxy (δ_H 3.51, δ_C 57.4), one oxymethylene (δ_H 3.86, 3.65, δ_C 62.8). The ^{1}H–^{1}H COSY spectrum revealed the existence of one spin system, CH_2(7)–CH(2)–CH(3)–CH(4)–CH(5)–CH(6). By comparison of its NMR data (Table 2.10) with those reported in the literature [39, 40], it indicated that compound **7** was α-D-galacto pyranoside methyl.

Table 2.10 NMR data of compound **7** in MeOD

Position	**7**	
	δ_C	δ_H (mult, *J* in Hz)
2	78.0	3.25, d (0.8)
3	71.7	3.26, m
4	78.1	3.34, s
5	75.1	3.15, ddd (4.0, 4.4, 8.4)
6	105.5	4.15, d (3.8)
7	62.8	3.86, d (5.4) 3.65, m
6-OMe	57.4	3.51, s

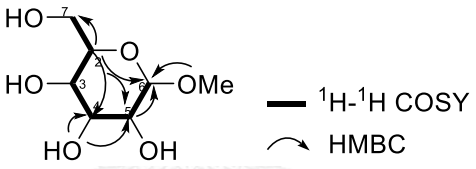

Figure 2.34 ^{1}H-^{1}H COSY and key HMBC correlations of **7**

2.11.5 Cytotoxic activities

Pure isolated compounds were evaluated for cytotoxic effect against four human tumor cell lines: hepato carcinoma (Hep-G2), gastric carcinoma (KATO-3), human breast cancer (MCF-7) and cervical carcinoma (CaSki) by MTT colorimetric method. Doxorubicin was used as a positive control. Results are presented in Table 2.11.

Rhytidchromones A (**1**) and E (**5**) showed weak cytotoxicity against Hep-G2, MCF-7 and KATO-3 with IC_{50} values ranging from 17.7 to 29.3 μM. Compound **5** showed weak activity on CaSki with an IC_{50} value of 25.3 μM, while compound **1** did not show activity against CaSki cells. Compounds **3**, **6** and **7** did not show any

significant activity against all tested cell lines, while compounds **2** and **4** were selectively active against KATO-3 with an IC_{50} 21.4 and 16.8 μM, respectively.

Table 2.11 Cytotoxic activity of pure compounds on Hep-G2, KATO-3, MCF-7 and CasKi cell lines

Compounds	IC_{50} (μM)			
	Hep-G2	KATO-3	MCF-7	CaSki
1	29.3	23.4	19.3	I
2	I	21.4	I	I
3	I	I	I	I
4	I	16.8	I	I
5	24.9	16.0	17.7	25.3
6	I	I	I	I
7	I	I	I	I
Doxorubicin	0.14	0.98	0.06	0.20

I=Inactive

2.12. Conclusion

A total of 64 pure isolates of endophytic fungi were isolated from *L. racemosa*, *T. spathacea*, *X. granatum*, *A. sarmentosa*, *B. gymnorrhiza*, *B. cylindrical* and *S. trilobatum*. Based on characteristic interesting ^{1}H NMR data, BG2Y fungus cultured on SDB was selected for large scale cultivation and isolation. This fungus was isolated from a Thai mangrove, *B. gymnorrhiza* and identified as *Rhytidhysteron rufulum*. Broth and mycelium EtOAc crude extracts isolated by chromatographic technique provided five new chromone derivatives, rhytidchromones A-E (**1-5**), one new isocoumarin derivative (**6**) and one known α-D-galacto pyranoside methyl (**7**).

All compounds were assessed for their toxicity against human cancer cell line. Rhytidchromone A (**1**) showed weak cytotoxicity against Hep-G2, KATO-3 and MCF-7, while rhytidchromone E (**5**) was weakly active against Hep-G2, KATO-3, MCF-7 and CaSki. Rhytidchromones B (**2**) and D (**4**) were active only for KATO-3 with IC_{50} values of 21.4 and 16.3 μM, respectively. However, rhytidchromone C (**3**), compounds **6** and **7** did not show any significant activity against all tested cell lines.

CHAPTER III

Sesquiterpenes from a mangrove-derived basidiomycetous fungus and their anti-angiogenic activity

3.1 Angiogenesis

Now the treatments are better able to treat cancer than ever. The improvement is the result of better methods to find cancer early and better methods to treat cancer once it is found, but the cancer treatment is difficult from perfect. However, many cancers cannot be treated, and some are still very hard to cure. The way of treatments for example, chemotherapy, maybe cause of severe side effects that can disturb a patient's daily life. Scientists have been trying to learn about cancer treatments. It has about what type's cancer cells different from normal cells in the body and it helped them find targeted drugs – drugs that focus on the cancer cells without having major effects on normal cells in the body. One promising of the cancer treatment to come from this research is called anti-angiogenesis treatment.

Angiogenesis, the formation of new blood vessels from the pre-existing vasculature, is not only required for the growth, but also for the transplantation and metastasis of tumors. The newly formed blood vessels promote the tumor progression by supplying oxygen and nutrient sufficiently and by, in turn, removing waste products from its own system. The cancers need blood vessels to get the nutrients and oxygen, since they need to survive and grow, so anti-angiogenesis drugs try to famish a cancer by preventing the development of new blood vessels[41].

The idea of anti-angiogenic therapy was the brainchild of Dr. Judah Folkman in the early 1970s. He proposed that by cutting off the blood supply, cancer cells would be deprived of nutrients and, hence, treated [42].

Angiogenesis needs the binding of signaling molecules, for example vascular endothelial growth factor (VEGF), to receptors on the surface of normal endothelial cells. When VEGF and other endothelial growth factors bind to their receptors on

endothelial cells, indicators within these cells are initiated and it can promote the growth and survival of new blood vessels (Figure 3.1).

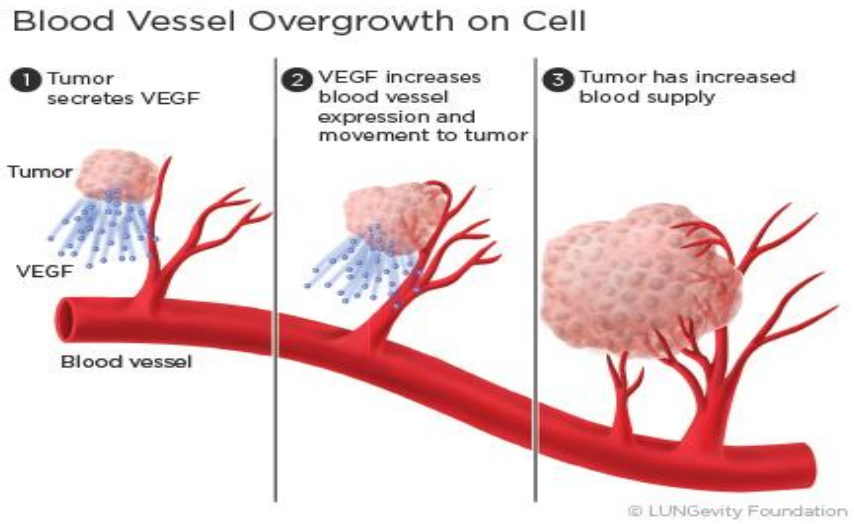

Figure 3.1 Cancer angiogenesis (http://www.lungevity.org/about-lung-cancer/lung-cancer-101/treatment-options/angiogenesis-inhibitors)

Since then, a display of anti-angiogenic, also as monotherapy or in combination with other cytotoxic and chemotherapy drugs, has been advanced, used in clinical trials, and accepted for the cure of cancer.

3.2 The anti-angiogenesis for cancer

Angiogenesis agents are unique cancer-fighting drugs because tumors cannot grow beyond a certain size or spread without a blood supply. Angiogenesis includes various mediators, but a worldwide agreement puts vascular endothelial growth factor (VEGF) (Figure 3.2) [43]. VEGF (also known as VEGF-A, but commonly referred to simply as VEGF) is a protein playing an important role in angiogenesis and lymphangiogenesis, because it is a highly specific mitogen for endothelial cells and

the signal transduction includes binding to tyrosine kinase receptors and results in endothelial cell proliferation, migration, and new vessel formation [44].

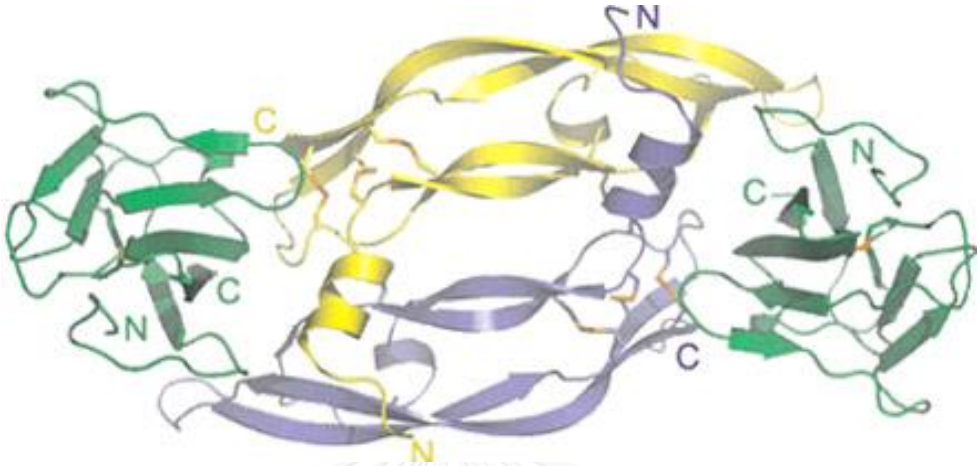

Figure 3.2 Structure of VEGF [This ribbon representation shows a dimerized VEGF/VEGF receptor complex, as observed by X-ray crystallography. Two monomers of VEGF (blue and yellow) are shown bound to domain 2 of the VEGFR-1 receptor (green)]

Researchers are trying to find ways to block tumor angiogenesis that are research about natural and synthetic angiogenesis inhibitors, similarly called antiangiogenic agents, with the idea that these molecules will prevent or slow the growth of cancer. However, this antiangiogenic agent is not much so it interested in the research to study these with from natural products.

3.2.1 Bevacizumab

Bevacizumab (trade name Avastin), is a recombinant humanized monoclonal IgG1 antibody, a man-made version of an immune system protein. It fits like a lock and key with a certain protein in the body. Bevacizumab attaches to a VEGF which is

required by the body to grow blood vessels. It is thought that by doing this, the drug stops tumors from being able to create new blood vessels capable of feeding and sustaining the tumor (Figure 3.3). This limits the tumor's supply of nutrients, which in turn may slow or stop their growth. Therefore, bevacizumab is sometimes referred to as an anti-angiogenic drug. There is another theory regarding avastin's mechanism of action that speaks to its ability to make tumor blood vessels (which are usually leaky) more stable, allowing chemotherapy to get into cancer cells more effectively. In colorectal cancer, avastin has been approved for use in metastatic disease and in combination with chemotherapeutic drugs such as 5FU, Xeloda, FOLFOX, and FOLFIRI [45].

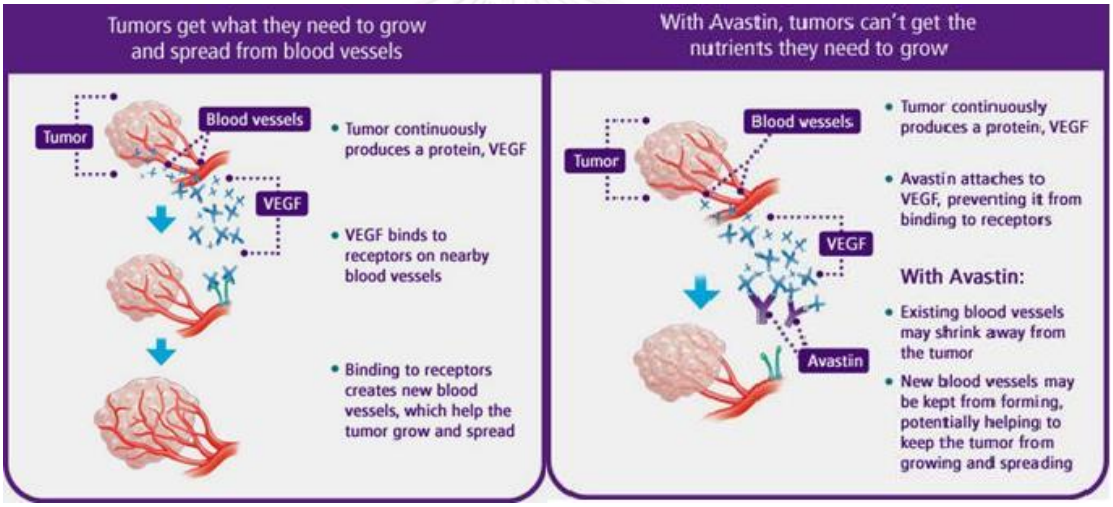

Figure 3.3 Mechanism of bevacizumab
(http://www.colorectal-cancer.ca/en/treating-cancer/treatment-cancer/)

Bevacizumab was approved by the U.S. Food and Drug Administration (FDA) in 2004 for certain metastatic cancers. It is combination use with standard chemotherapy for metastatic colon cancer and has since been approved for use in certain lung cancers, renal cancers, ovarian cancers, and glioblastoma multiforme of the brain.

3.2.2 Aflibercept

Aflibercept (Sanofi-aventis and Regeneron Pharmaceuticals Inc) approved in the United States and Europe under the trade name Eylea for the treatment of wet macular degeneration, and as Zaltrap for metastatic colorectal cancer. It is a new agent targeting the VEGF pathway and it has recently been shown to be well tolerated and effective in treating patients with metastatic colorectal cancer when combined with cytotoxic chemotherapy [46].

Aflibercept is binds to VEGF-A, VEGF-B, and PlGF subsequent in the inhibition of their interaction with specific receptors. Aflibercept has been advanced by employing the "trap technology" and it is a 97 kDA homodimeric glycoprotein developing from the combination of VEGFR-1 and VEGFR-2 extracellular domains to Fc portion of human IgG1. Thus, aflibercept stops interactions between VEGF and receptor showing on cellular surface, and then it does not cause as much hypoxia and so does not induce an angiogenic escape programme as strongly as VEGF-VEGFR inhibitors do. Figure 3.4 [46] shows the family of VEGF receptors, ligands and their functions. There are six VEGF ligands, VEGF-A, VEGF-B, VEGF-C, VEGF-D, VEGF-E, and PIGF and three main VEGF receptors, VEGFR-1, VEGFR-2, and VEGFR-3. Each VEGF ligand has specific affinity to different receptors as illustrated. Binding of ligands to the extramembrane domain of the receptors trigger dimerization of the receptor, autophosphorylation of the tyrosine kinase domain of the receptor, and initiate multiple downstream signal transduction pathways resulting in endothelial cell proliferation, migration, survival, and more.

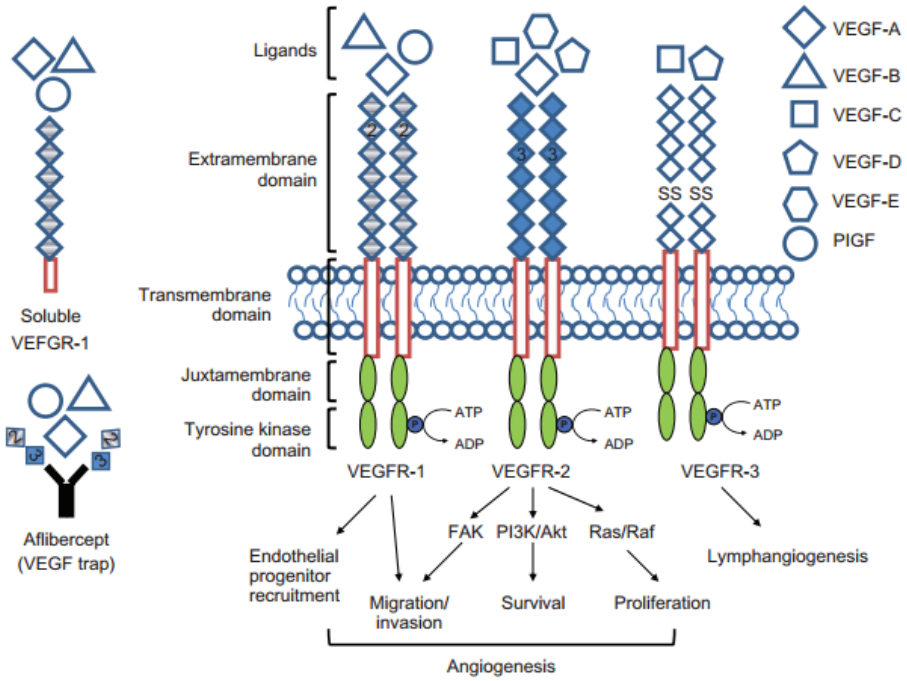

Figure 3.4 Mechanism of Aflibercept

(VEGF:vascular endothelial growth factor; PIGF: placenta growth factors; FAK:focal adhesion kinase; PI3K: phosphatidylinositol 3-kinase)

This strange mechanism of action might reduce the incidence of drug resistance. So, it is the suggestion of aflibercept as valid second-line therapeutic choice [47].

In some cancers, angiogenesis inhibitors are maximum active when joint with chemotherapy. It has been hypothesized that these drugs help normalize the blood vessels that supply the tumor, promote the delivery of other anticancer drug, but this probability is still being explored. Angiogenesis agent therapy does not necessarily kill tumors but instead may prevent tumors from growing. Furthermore, therapy with targeting angiogenesis can be applied for a broad spectrum of tumors because angiogenesis is required for all of them, and has the low potential for resistance due to the genetic stability of endothelial cells of which migration and proliferation involved in angiogenesis process [48].

3.3 Bioactive compounds from mangrove-derived basidiomycetous fungus

Recently, we have disclosed the isolation and identification of nor-chamigrane and chamigrane type sesquiterpene endoperoxides bearing unique chemical structures, namely, merulins A-C from the culture medium extract of a basidiomycetous fungus, the endophytic fungus of the Thai mangrove plant *Xylocarpus granatum*. Merulins A and C showed cytotoxicity against breast (BT474) and colon (SW620) cancer cell lines with IC_{50} values ranging from 1.57 to 4.98 μg/mL [49]. In this study, we interested in antiangiogenic activity of these chamigrane endoperoxides.

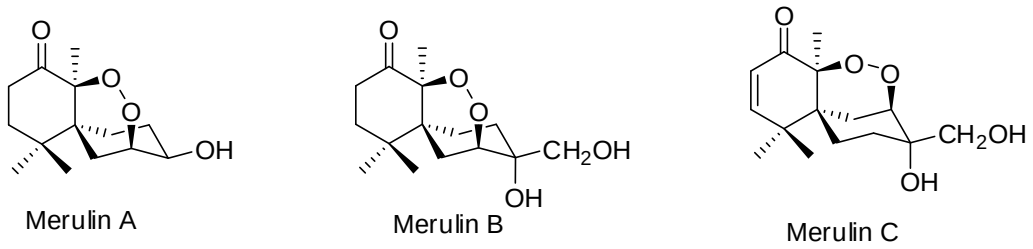

Figure 3.5 Structures of merulins A-C from a basidiomycetes

3.4 Large scale cultivation and extraction

The basidiomycete fungus strain XG8D [49], were grown-up on PDA plate at 30 °C for 7 days. Six pieces (6 x 6 mm^2) of the grown culture were cut and inoculated into 1,000 mL Erlenmeyer flasks (x 100) containing 200 mL of corn steep broth medium at 30 °C for 21 days under static conditions. The culture broth was subjected to filtration through five layers of sheet cloth which was comprehensively pressed. The filtrate was extracted with an equal volume of ethyl acetate (EtOAc) for 3 times. The organic layers were combined and the solvent was removed under reduced pressure to yield EtOAc crude extract 18.90 g.

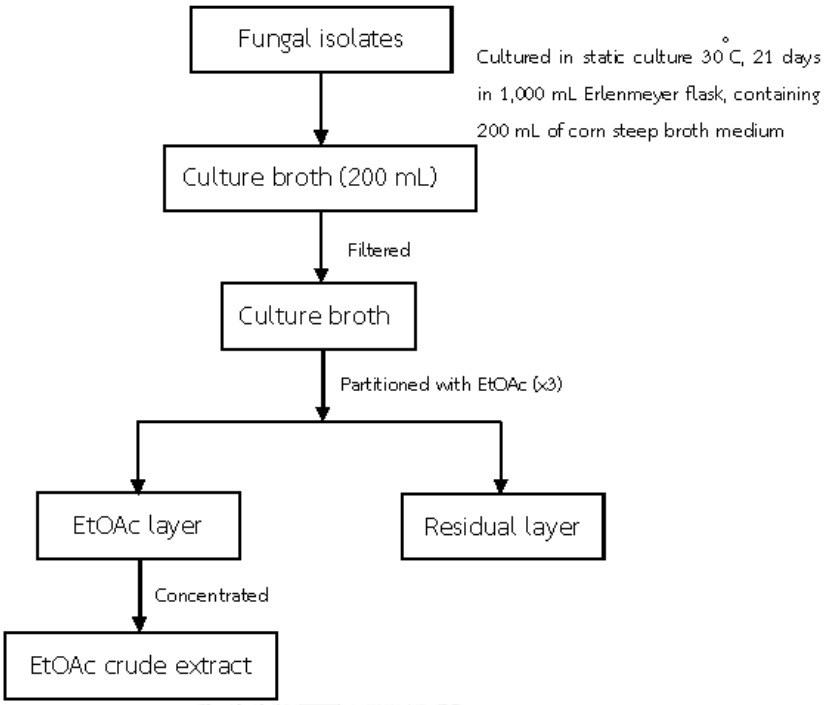

Scheme 3.1 Extraction of fungal culture broth

3.5 Isolation of sesquiterpene from of XG8D crude extract

The 18.90 g of EtOAc crude extract was subjected to Sephadex LH20 column chromatography and eluted with MeOH to yield seven fractions (A-G). Fraction E (3.06 g) was further purified by SiO_2 column chromatography (MeOH:CH_2Cl_2, 5:95) to yield 52 subfractions (E1-E52). Subfractions E33-E50 (1.38 g) were combined and recrystallized from MeOH to afford merulin A (**8**, 420.00 mg), while subfractions E15-E28 (0.86 g) were further purified by preparative HPLC (GL Science, ODS-3-A, 20 × 250 mm, flow rate 8.00 mL/min, MeCN:H_2O, 40:60) to yield merulin C (**10**, 130.00 mg). Fraction D (2.26 g) was subjected to flash column chromatography on silica gel (MeOH:CH_2Cl_2, 5:95), then purified further by a silica gel column (EtOAc:CH_2Cl_2, 4:1) to obtain merulin B (**9**, 45.00 mg). Fraction B (1.80 g) was fractionated by silica gel column chromatography (EtOAc:CH_2Cl_2, 4:1) to yield 30 subfractions (B1-B30). Subfraction B22-B24 (0.32 g) combined and purified further by silica gel column chromatography (EtOAc-CH_2Cl_2, 3:2) to afford steperoxide A (**12**, 32.0 mg). Fraction F

(1.76 g) was subjected to silica gel column chromatography (MeOH:CH_2Cl_2, 5:95), and then rechomatographed over silica gel (acetone:hexane, 3:2) to yield merulin D (**11**, 7.40 mg).

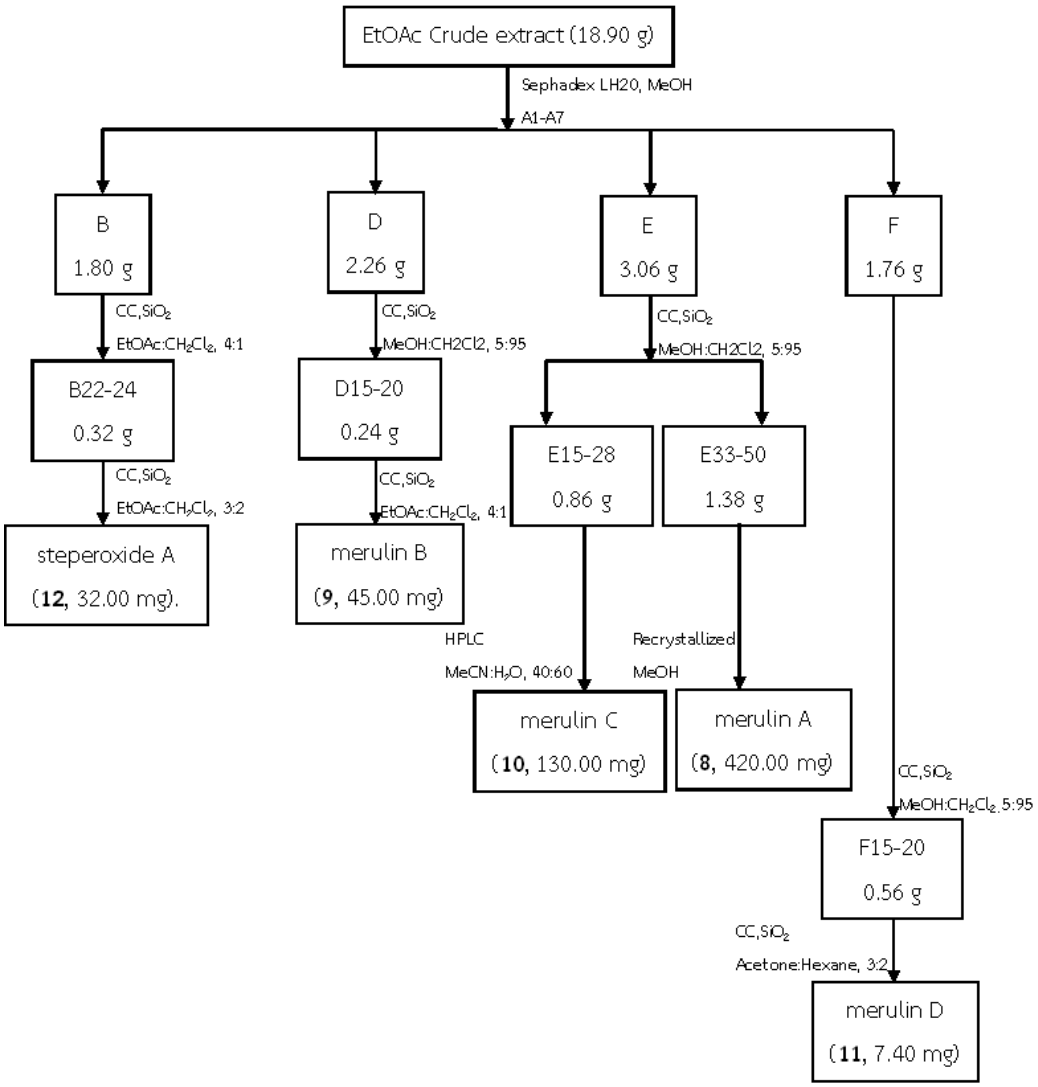

Scheme 3.2 Isolation of crude extracts (broth)

3.6 Anti-angiogenic assay

3.6.1 *Ex vivo* Angiogenesis Assay

The rat aortic ring assay is a more physiologically important assay with clear advantages over other *in vitro* methods because there are relatively low-cost and quick to operate. It many rings obtainable from few animals and associate cells are included in the creation of new blood vessels. The aortic ring assay model commonly excludes inflammatory mechanisms and tubule structures are clearly visible, advance over a time progression like to that *in vivo* and are lumenized [50].

Ex vivo Angiogenesis Assay used a male Wistar rat and it was sacrificed by bleeding from the right femoral artery under anesthesia with diethyl ether. The thoracic aorta was removed, washed with RPMI 1640 medium, turned inside out, and cut into 1-mm length. The aortic rings were then placed on 6-well culture plates and covered with 0.5 mL of gel matrix solution (8 volume of porcine tendon collagen solution, 1 volume of 10 × Eagle's MEM, and 1 volume of reconstitution buffer), then allowed to gel at 37°C for 30 min. Two mL of RPMI 1640 medium containing 1% of TIS+ with designated doses of compounds or vehicle (DMSO) were added to the wells. After incubation for 7 days at 37°C in 5% CO_2, capillary length was estimated by phase-contrast microscopy by measuring the distance from the cut end of the aortic segment to the approximate mid-point of the capillary.

3.6.2 *In vitro* Angiogenesis Assay

3.6.2.1 Proliferation Assay

HUVEC suspension in HuMedia EG2 (1.5×10^4 cells/mL) was seeded onto each well of a 96-well plate (100 μL) and incubated for 24 h at 37 $^{\circ}$C in 5% CO_2. The medium was removed and replaced with fresh HuMedia EG2 containing various doses of sample or vehicle (DMSO) and incubated for 72 h at 37 $^{\circ}$C in 5% CO_2. Cell proliferation was detected using WST-8 reagent, and the inhibition of proliferation was measured at 450 nm using a microplate reader.

3.6.2.2 Chemotactic Migration Assay

A microporous membrane (8 μm) of 24-well cell culture inserts was coated with 0.1% gelatin. A HUVEC suspension in Medium 199 with 0.1% bovine serum albumin (BSA) (2.5×10^5 cells/mL) was seeded in each chamber (400 μL). The well was filled with 400 μL of Medium 199 containing 0.1% BSA and 10 ng/mL of human recombinant VEGF with or without sample. The collected chamber was incubated for 6 h at 37 $^{\circ}$C in 5% CO_2. Non-migrated cells on the surface of the membrane were removed by scrubbing with a cotton swab. The migrated cells were fixed with methanol and stained with Diff-Quik stain (Sysmex, Kobe, Japan), then counted in three fields of each membrane under microscope at 200 × magnification. Lumenized [51].

3.6.2.3 Tube Formation Assay

HUVEC tube formation assay was performed according to the method using BD Matrigel. Solid gel was prepared on a 96-well tissue culture plate according to the manufacture's instruction. HUVECs (1×10^5 cells/mL) in HuMedia EG2 medium containing various doses of sample or vehicle (DMSO) were seeded onto the surface on sold BD Matrigel. After incubation for 12 h at 37 $^{\circ}$C in 5% CO_2, tube formation was observed under an inverted light microscope at 40 × magnification. Microscopic fields were photographed with a digital camera (OLYMPUS DSE330-A system).

3.6.3 *In vivo* Angiogenesis Assay

The Matrigel plug model was used in the present study, 0.5 mL of Matrigel (BD Biosciences) containing 10 μM of sample or vehicle, and bFGF (10 ng/mL) was injected subcutaneously into C57BL/6 mice. After injection, the Matrigel polymerized to form a plug. Three mice were used for each group. After 7 days, the animals were killed and the skin of each mouse were carefully pulled back to expose the Matrigel plug. The plugs were dissected out and fixed with 10% formaldehyde/phosphate-buffered saline and embedded in paraffin. The plugs were then sectioned and stained with hematoxylin-eosin stain. The amount of hemoglobin in the plugs was

measured using a QuantiChrom™ hemoglobin assay kit (BioAssay Systems, Hayward, CA, USA). The concentration of hemoglobin was calculated from a known amount of hemoglobin assayed in parallel.

3.6.4 Study on mechanism by Western Blotting

HUVECs were grown to confluent and starved for 16 h in RPMI 1640 containing 5% FBS. Cells were pretreated for 60 min with merulin C (2.5-10 μM) or vehicle and stimulated by the addition of VEGF (10 ng/mL) for 10 min. After stimulation, cells were washed with PBS twice and lysed with M-PER mammalian protein extraction reagent (Pierce, Rockford, IL, USA). Lysates were clarified by centrifugation for 15 min at 12000 rpm at 4 $^{\circ}$C. Protein concentration was determined using the microBCA protein assay kit (Pierce, Rockford, IL, USA) with BSA as standard. Fifty μg of protein were separated on SDS polyacrylamide gel under reducing conditions and transferred to nitrocellulose membrane. After blocking, the membranes were incubated with primary antibody for phopho-Erk1/2 or phospho-Akt (Cell Signaling Technology, Tokyo, Japan) at 4 $^{\circ}$C overnight and for Erk1/2 or Akt at room temperature, respectively. Immunoreactive bands were visualized by chemiluminescence using a WesternBreeze (Invitrogen) with a ChemiDoc XRS (BIO-RAD).

3.7 Results and Discussion

3.7.1 Isolation and identification of sesquiterpenes from XG8D fungus

The EtOAc crude extract of the fungus XG8D culture broth was subjected to fractionations using Sephadex LH-20 and silica gel column chromatography to obtain a new chamigrane endoperoxide, merulin D (**11**), and four known derivatives, merulins A-C (**8-10**) and steperoxide A (**12**) [49].

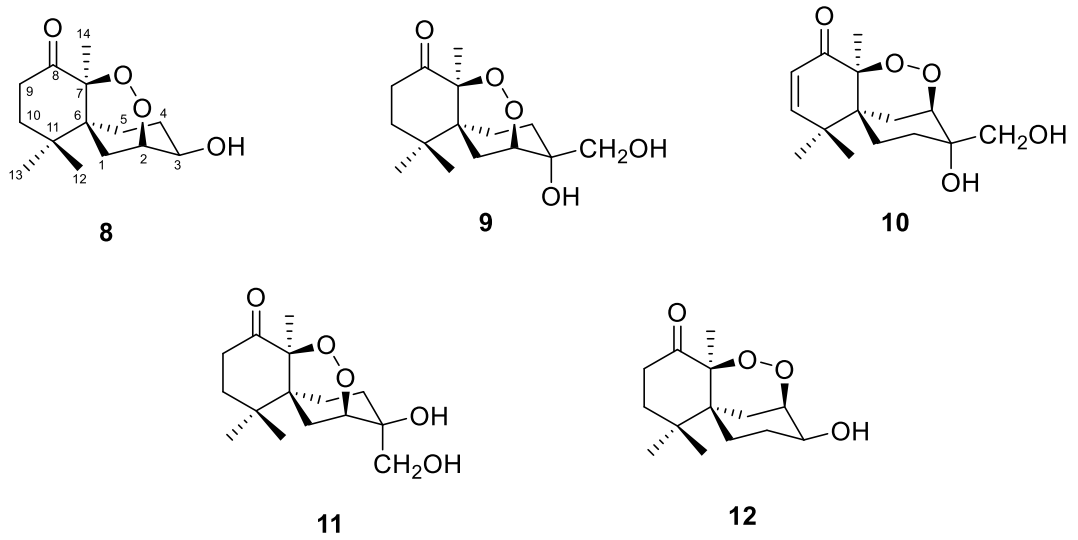

Figure 3.6 Structures of compounds **8**-**12**

Compound **8** was obtained as colorless crystals, Analysis of ^{13}C NMR spectra (Table 3.1) of **8** exposed three methyl carbons (δ_C 21.5, 24.7, and 26.2), five methylene carbons (δ_C 25.6, 30.5, 32.1, 35.6, and 35.8), two methine carbons (δ_C 69.4 and 79.1), three quaternary carbons (δ_C 37.3, 41.2, and 90.1), and one ketone carbonyl carbon (δ_C 208.4). Among them, two methines and one quaternary carbon (δ_C 90.1) were attributed as support oxygen atoms. As well as by comparison of ^{1}H and ^{13}C NMR (Table 3.1), compound **8** was identified as merulin A. The structure of this compound was finally confirmed by its ^{1}H–^{1}H COSY and HMBC correlations as shown in Figure 3.7 [49].

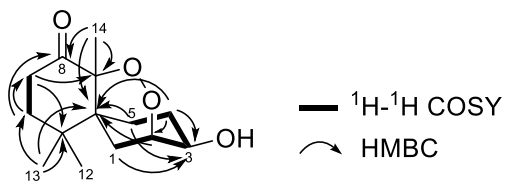

Figure 3.7 ^{1}H–^{1}H COSY and key HMBC correlations of **8**

Table 3.1 NMR data of compound **8** in $CDCl_3$

Position	**8**	
	δ_C	δ_H (mult, *J* in Hz)
1	30.5	2.05 (ddd, 13.5, 4.2, 3.9) 1.56 (dd, 13.5, 1.8)
2	79.1	4.14 (ddd, 4.2, 3.8, 1.8)
3	69.4	3.77 (ddd, 10.1, 7.9, 3.8)
4	32.1	2.17 (m)
5	25.6	2.11 (m) 1.59 (m)
6	41.2	-
7	90.1	-
8	208.4	-
9	35.6	2.69 (ddd, 15.4, 14.9, 6.7) 2.45 (ddd, 15.4, 4.7, 2.4)
10	35.8	2.01 (ddd, 14.9, 14.8, 4.7) 1.58 (m)
11	37.3	-
12	26.2	0.98 (s)
13	24.7	1.26 (s)
14	21.5	1.41 (s)
15	79.1	-

Compound **9** was obtained as a white powder. The ^{1}H and ^{13}C NMR data of **9** (Table 3.2) were similar to those of **8** with the only difference being the presence of a $–CH_2–OH$ unit instead of –H at C-3. This could be confirmed by $^{1}H–^{1}H$ COSY and HMBC correlations as shown in Figure 3.8. Comparison of NMR data of compound **9** with those published in the literature [49] indicated that compound **9** was merulin B.

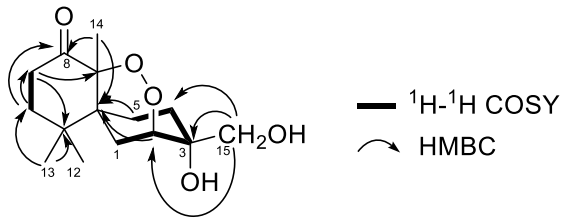

Figure 3.8 $^{1}H–^{1}H$ COSY and key HMBC correlations of **9**

Table 3.2 NMR data of compound **9** in $CDCl_3$

Position	**9**	
	δ_C	δ_H (mult, *J* in Hz)
1	27.2	2.05 (dd, 13.3, 1.8) 1.78 (ddd, 13.3, 4.1, 3.4)
2	78.5	4.03 (br s)
3	71.5	-
4	31.4	2.07 (13.9, 13.5, 6.5) 1.65 (dd, 13.9, 6.2)
5	22.8	1.96 (m) 1.81 (ddd, 13.5, 13.0, 6.2)
6	42.2	-
7	90.3	-
8	208.6	-

9	35.6	2.65 (ddd, 15.4, 14.8, 6.7) 2.41 (ddd, 15.4, 4.6, 2.3)
10	35.5	2.02 (ddd, 14.8, 14.4, 4.6) 1.55 (ddd, 14.4, 6.7, 2.3)
11	37.4	-
12	26.4	1.00 (s)
13	24.4	1.23 (s)
14	21.4	1.35 (s)
15	66.5	3.94 (d, 11.1) 3.43 (d, 11.1)

Compound **10** was isolated as a white powder. The ^{1}H and ^{13}C NMR spectra of **10** were closely analogous to those of **9**, except for the appearance of a new pair of doublet at δ_H 5.82 and 6.32 (J = 10.4 Hz) due to the olefinic protons, instead of two methylenes at C-9 and C-10 in **9**. All the NMR data implied that **10** is α,β-unsaturated ketone derivative of **9**, which was confirmed by 2D NMR (^{1}H-^{1}H COSY, and HMBC NMR data) (Figure 3.3). Finally, Based on the spectroscopic data in Table 3.3, compound **10** was identified to merulin C [49].

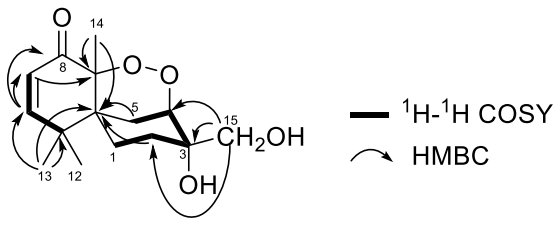

Figure 3.9 ^{1}H–^{1}H COSY and key HMBC correlations of **10**

Table 3.3 NMR data of compound **10** in $CDCl_3$

Positio	**10**	
n	δ_C	δ_H (mult, *J* in Hz)
1	27.0	1.97 (ddd, 14.5, 13.1, 7.0) 1.65 (m)
2	32.5	2.27 (ddd, 13.3, 13.1, 6.3) 1.54 (dd, 13.3, 7.0)
3	71.9	-
4	78.9	4.14 (d, 4.2)
5	23.0	2.29 (ddd, 13.1, 4.2, 3.6) 1.96 (dd, 13.1, 1.7)
6	40.6	-
7	87.8	-
8	197.6	-
9	123.6	5.82 (d, 10.4)
10	155.1	6.32 (d, 10.4)
11	40.2	-
12	27.0	1.09
13	23.8	1.26
14	23.9	1.82
15	66.3	3.99 (d, 11.0) 3.45 (d, 11.0)

Compound **11** was obtained as a colorless gum. $[\alpha]^{20}_{D}$ +160.7 (*c* 0.1, MeOH). The HRESIMS data showed a molecular formula identical to **9** of $C_{15}H_{24}O_5$ and the NMR data (Table 3.4) of **11** were also similar to those of **9**, and analysis of 2D NMR data revealed the same gross structure as **9**, suggesting that **11** and **9** were diastereomers. The major difference observed from their ^{1}H NMR spectra was the appearance of H_2-15 as a singlet at δ_H 3.56 in **11** that in place of a pair of doublets at δ_H 3.43 and 3.94 (*J* = 11.1 Hz) in **9**. It was thus possibly the consequence of the different configuration at the C-3 stereocenter. The ^{1}H and ^{13}C NMR data of **11** were strikingly similar to those of **9** with the only difference being the presence of a $-CH_2-$OH unit at C-15. This was confirmed by the HMBC correlations from H_2-15 to C-2, C-3, and C-4. NOESY correlations of H-1ax/H_2-15 and H-5ax/H_2-15 as well as absence of correlation between H-4ax and H_2-15 indicated an axial position for the $-CH_2-$OH fragment and the corresponding equatorial 3-OH group. Therefore, compound **11** was determined to be an epimer of **9** possessing the opposite configuration at C-3 as shown. Thus, **11** was determined as a new compound and given the name merulin D [49].

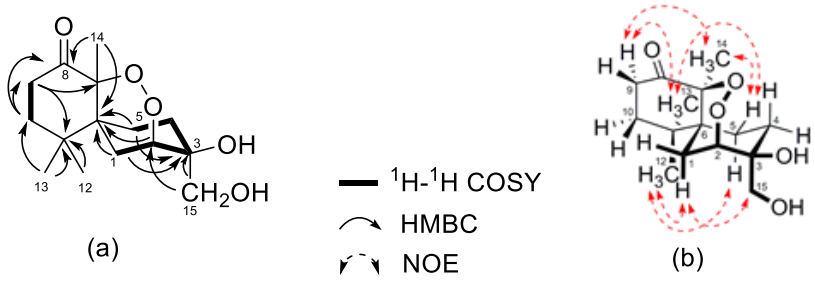

Figure 3.10 (a) ^{1}H–^{1}H COSY, key HMBC and (b) selected NOESY correlations of **11**

Table 3.4 NMR data of compound **11** in $CDCl_3$

Positio	**11**	
n	δ_C	δ_H (mult, *J* in Hz)
1	29.1	2.04 (m), H-1 eq 1.70 (dd, 13.8, 1.8), H-1ax
2	79.1	4.22 br (m)
3	72.7	-
4	34.0	2.25 (ddd, 14.0, 13.2, 6.4), H-4ax 1.84 (dd, 14.0, 6.4), H-4eq
5	25.0	2.06 (m), H-5eq 1.51 (ddd, 14.8, 14.0, 6.8), H-5ax
6	41.7	-
7	90.4	-
8	207.8	-
9	35.6	2.68 (ddd, 15.4, 14.8, 6.6) H-9α 2.44 (ddd, 15.4, 4.7, 2.3) H-9β
10	35.7	2.02 (m) H-10β 1.57 (ddd, 14.4, 6.7, 2.3) H-10α
11	37.3	-
12	26.2	0.98 (s)
13	24.6	1.25 (s)
14	21.4	1.41 (s)
15	66.7	3.56 br (s)

Compound **12** was obtained as yellowish paste, $[\alpha]^{20}_{D}$ +263.0 (*c* 0.1, MeOH), UV ($CHCl_3$) λ_{max} (log ε) 225 (3.85) nm. Its molecular formula was established as $C_{14}H_{22}O_4$ by HRESIMS data (*m/z* 217.1414 $[M+Na]^+$, calcd 277.1416), indicating four degrees of unsaturation. The ^1H and ^{13}C NMR data (Table 3.5) of **12** was similar to those of **8**, except for the downfield shift of Me-14 signals [δ_H 1.91 (s), δ_C 24.0]. Analysis 2D spectra (^1H-^1H COSY, HMQC, HMBC) indicated that **12** was a stereoisomer of **8**. The large coupling constant of 10.3 Hz between H-3 and H-2ax and strong NOESY correlation between H-3 and H-5ax suggested the axial position for H-3 and implied the equatorial position for 3-OH. NOESY correlations between H_{13}-13 and H_3-14 to H-9α, H_{13}-13 and H_3-14 to H-5eq, and H_3-12 to H-1ax supported the relative configuration of **12**, whose endoperoxide linkage was suggested to attach to C-4 and C-7 positions. Comparison of its NMR data with those reported in literature [52], revealed that **12** were steperoxide A, previously isolated from basidiomycete *Steccherinum ochraceum*.

Table 3.5 NMR data of compound **12** in $CDCl_3$

Position	**12**	
	δ_C	δ_H (mult, *J* in Hz)
1	28.2	1.83 (ddd, 15.0, 12.2, 7.0), H-1ax 1.70 (m), H-1eq
2	32.8	2.28 (13.0, 12.2, 10.3), H-2ax 2.11 (13.0, 7.0), H-2eq
3	70.3	3.75 (ddd, 10.3, 7.9, 3.4)
4	80.3	4.17 (dd, 3.7, 3.4)
5	26.1	2.52 (ddd, 13.5, 5.0, 3.7), H-5eq 1.34 (dd, 13.5, 1.2), H-5ax
6	42.8	-

7	89.7	-
8	208.1	-
9	35.3	2.81 (ddd, 15.5, 12.9, 7.5), H-9α 2.31 (ddd, 15.5, 5.7, 2.6), H-9β
10	36.8	2.03 (ddd, 14.2, 12.9, 5.7), H-10β 1.67 (ddd, 14.2, 7.5, 2.6), H-10α
11	35.9	-
12	27.3	0.98 (s)
13	25.1	1.24 (s)
14	24.0	1.91 (s)

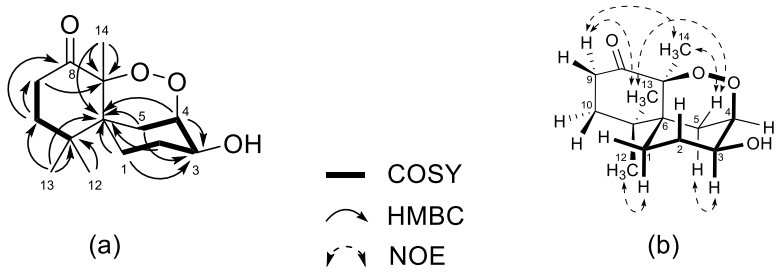

Figure 3.11 (a) ^{1}H–^{1}H COSY, key HMBC and (b) selected NOESY correlations of **12**

3.7.2 Anti-angiogenic activities

Angiogenesis contains many steps to achieve new blood vessel formation; endothelial cells must first escape from their stable position by breaking through the basement membrane. When this is realized, endothelial cells migrate to an angiogenic stimulus such as might be released from tumor cells or wound-associated macrophages. Furthermore, endothelial cells proliferate to provide the necessary number of cells for making a new vessel. Following to this proliferation, the new outgrowth of endothelial cells need to reorganize into a three-dimensionally tubular

structure. Each of these elements, basement membrane disturbance, cell migration, cell proliferation, and tube formation can be a target for interference.

Most studies of angiogenesis inducers and inhibitors rely on various models, *ex vivo*, *in vitro* and *in vivo*, as indicators of efficacy. In this research, experiments were separated into four steps as follows,

1. Screening by *Ex Vivo* angiogenesis assay

2. Investigation effect on human umbilical vein endothelial cells (HUVEC) by *in vitro* assay

3. Investigation of antiangiogenesis in *in vivo* model (mouse model)

4. Study on mechanism (Western Blotting)

3.7.2.1 *Ex vivo* angiogenesis assay

To evaluate *ex vivo* model of compounds **8**-**12**, they were first subjected to an *ex vivo* model, a rat aortic sprouting assay. As shown in Figure 3.12, merulin C (**10**) displayed strong activity with complete inhibition of microvessel sprouting from rings at a concentration of 2.5 μM, while steperoxide A (**12**) showed much weaker activity with complete inhibition was at 25 μM. Merulins A (**8**), B (**9**), and D (**11**) did not display any detectable activity at a screening dose (25 μM).

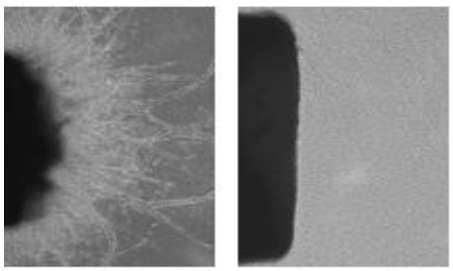

Figure 3.12 Suppressive effect of merulin C (**10**) in *ex vivo* angiogenesis model (rat aortic sprouting assay).

3.7.2.2 *In vitro* angiogenesis assay

In vitro models of angiogenesis have focused to date predominantly on proliferation, migration and tubule formation by endothelial cells in response to exogenous inhibitory or stimulatory agents. Most endothelial cell assays utilize HUVEC because they are relatively easy to harvest from large blood vessels. In vitro angiogenesis assay is composed of three steps including proliferation assay, chemotactic migration assay and tube formation assay.

3.7.2.2.1 Proliferation Assay

Proliferation of endothelial cells is needed for developing capillaries in the intact animal and it easy to implement and highly reproducible, giving themselves to accurate quantification. Endothelial cells recognized in culture are potent of cell division. Therefore, a number of markers of cell division can be used to evaluate their proliferation in culture. The activities of antiangiogenic molecules on proliferation can be assessed by direct cell counts.

The mechanism evaluate of merulin C (**10**) inhibited HUVEC proliferation in a dose-dependent manner with an IC_{50} value of 0.9 μM, and about 90% inhibition at 25 μM as shown.

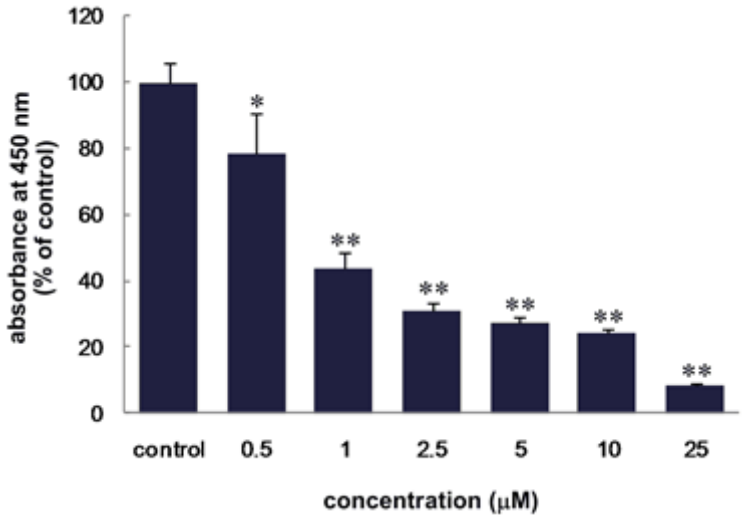

Figure 3.13 Effect of merulin C (**10**) on HUVEC proliferation

3.7.2.2.2 Chemotactic Migration Assay

HUVEC migration is important of angiogenesis because the movement process is directionally controlled by chemotactic, haptotactic, and mechanotactic stimuli and further involves degradation of the extracellular matrix to allow development of the migrating cells. The migration assay was achieved using a modified Boyden chamber. The Boyden chamber contains an upper chamber that is separated from a lower chamber by a porous membrane coated with an appropriate matrix. The cells are seeded on the upper of the membrane and the lower chamber is filled with medium having chemotactic proangiogenic agent and then the cells sense and migrates toward the source. After incubated, the cells that have traversed the membrane are stained and counted under the microscope[53].

The effect of merulin C (**10**) on VEGF-induced HUVEC migration was studied by using a modified Boyden chamber assay, the VEGF is known as a specific and critical growth factor involved in endothelial proliferation, migration, and survival during blood vessel formation. As shown in Figure 3.14, while VEGF strongly stimulated endothelial migration, merulin C (**10**) could suppress VEGF-induced migration of HUVEC in a dose-dependent manner. However, the significant inhibition was observed at concentrations higher than 5 μM.

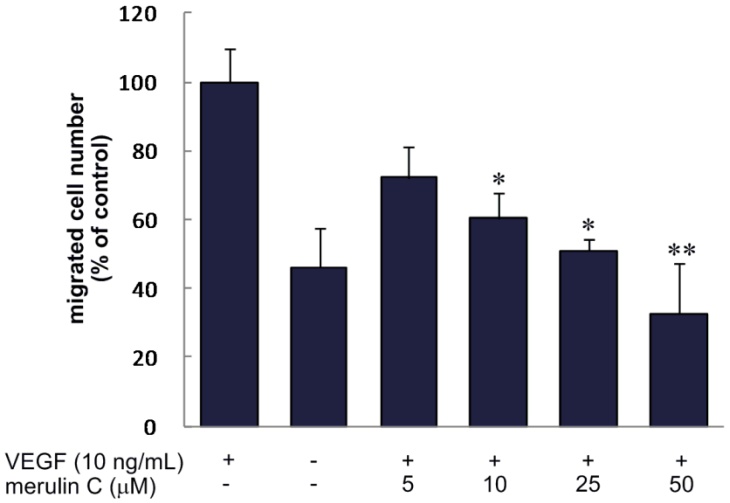

Figure 3.14 Effect of merulin C (**10**) on HUVEC migration

3.7.2.2.3 Tube Formation Assay

The tube formation of capillary-like tubes by endothelial cells on a basement membrane matrix is a powerful *in vitro* method to screen for various factors that promote or inhibit angiogenesis. This assay has massive litheness for the approach to testing angiogenic regulators and the factors can be added outside to the medium, transfected into the endothelial cells or breaked down in the endothelial cells to control their effects of role in angiogenesis. Tube formation assay is based on the differentiation of endothelial cells and the creation of tube-like structures on an extracellular matrix Matrigel [54].

Merulin C (**10**) could suppress VEGF-induced migration of HUVEC in a dose-dependent manner. However, the significant inhibition was observed at concentrations higher than 5 μM. Finally, the effect on HUVEC tube formation on Matrigel was investigated. Merulin C did not exhibit significant inhibitory effect on the tubular formation of HUVECs at concentrations ranging from 2.5 to 10 μM, 50% inhibition was observed at 25 μM, and complete inhibition was detected at 50 μM. It might be thought that inhibition of tubular formation is caused by the cytotoxic activity. According to the results, it is indicated the anti-angiogenic activity of merulin C (**10**) is mainly related to the suppression of endothelial cell proliferation and migration.

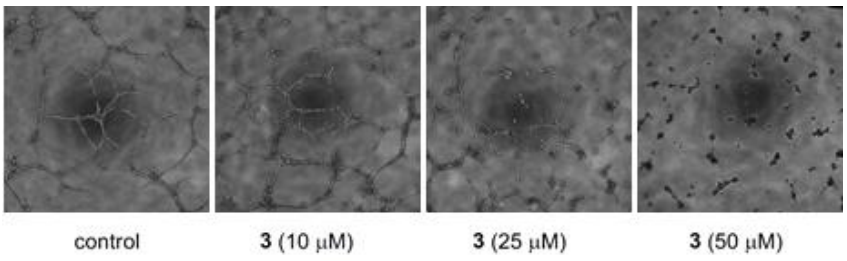

Figure 3.15 Effect of merulin C (**10**) on HUVEC tube formation (cells were plated on reconstituted gel)

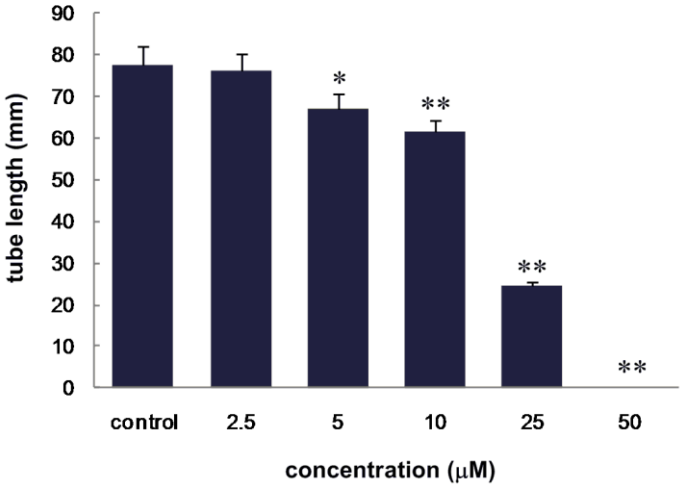

Figure 3.16 Effect of merulin C (**10**) on HUVEC tube formation (capillary length was measured. Significantly different from control: $^{*}p < 0.05$ and $^{**}p < 0.01$)

3.7.2.3 *In vivo* angiogenesis assay

The matrigel plug angiogenesis assay is a simple *in vivo* technique to identify the newly formed blood vessels in the transplanted gel plugs in mice. Finally, to examine whether merulin C (**10**) inhibits *in vivo* angiogenesis, a Matrigel plug assay was carried out. FGF-containing Matrigel, with 10 μM of merulin C (**10**) or vehicle (DMSO) was subcutaneously implanted into male C57BL/6 mice for seven days. As shown in Figure 3.17, suppression of neovascularization in mice implanted with Matrigel containing merulin C (**10**) was clearly observed, while analysis of the Matrigel plug of control mice obviously indicated an angiogenic response. Furthermore the level of hemoglobin in the Matrigel plug was determined by a QuantiChrom™ hemoglobin assay kit. The results were in agreement with those of the histological analysis, with the hemoglobin content of the merulin C (**10**) containing gel being about one third of that of controls one.

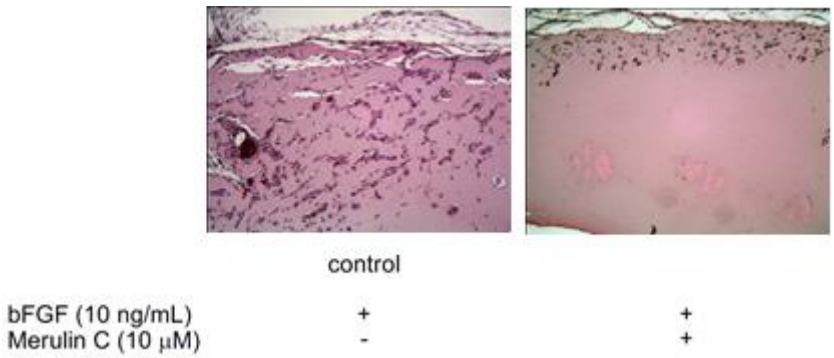

Figure 3.17 Effect of merulin C (**10**) on bFGF-induced vessel formation in the Matrigel plug assay

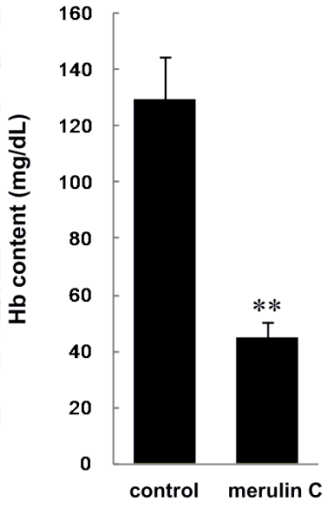

Figure 3.18 Effect of merulin C (**10**) measured hemoglobin content in the Matrigel plug. Significantly different from control: $^{**}p < 0.01$.

3.7.2.4 Study on mechanism by Western Blotting

The mechanism by which merulin C (**10**) regulates angiogenic inhibition was investigated by western blot analysis. It has two important pathways, phosphoinositide 3-kinase/Akt and extracellular signal-regulated kinase (Erk1/2), responsible for VEGF stimulus of endothelial cells. These pathways are involved in

endothelial cell proliferation, migration, and survival. Results showed that treatment of HUVECs with merulin C (**10**) suppressed the phosphorylation of Erk1/2 in both dose- and time-dependent manner (Figure 3.19, 3.20), but did not affect the expression of phosphorylated Akt. This suggested that anti-angiogenic property of merulin (**10**) is mediated by Erk1/2 signaling pathway. The strong suppressive effect of merulin C (**10**) on the phosphorylation of Erk1/2 is in line with a previous report in which inhibitors for Erk1/2 signaling pathway suppress endothelial cell proliferation. Furthermore not potent inhibitory effect of merulin C (**10**) on migration is consistent with its no effect on the phosphorylation of Akt, which plays an important role in endothelial cell migration.

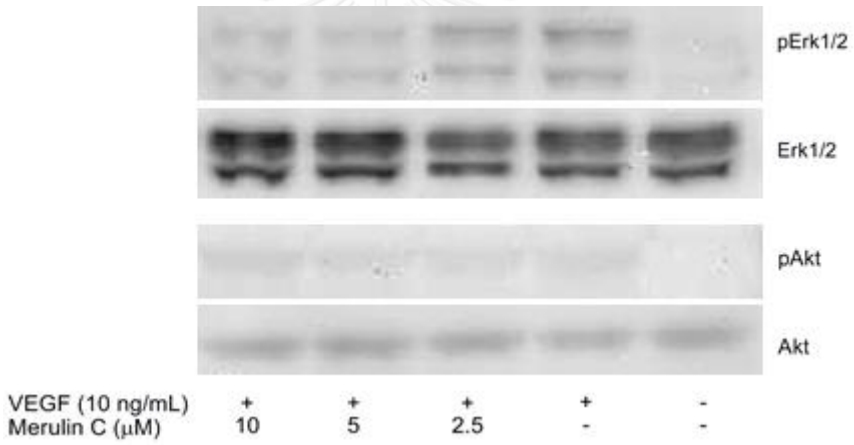

Figure 3.19 Effect of merulin C (**10**) on the phosphorylation of Erk1/2 and Akt in HUVECs (HUVECs were pretreated with vehical and merulin C (**10**) at doses ranging from 2.5 to 10 μM for 1 h)

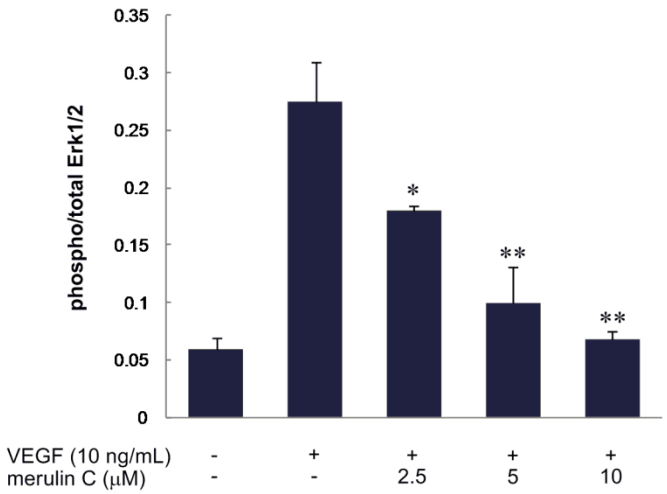

Figure 3.20 Effect of merulin C (**10**) on the phosphorylation of Erk1/2 and Akt in HUVECs (The level of phosphorylated and total Erk1/2 protein were determined by western blot analysis. Significantly different from control: $^{*}p < 0.05$ and $^{**}p < 0.01$)

3.8 Conclusion

Purification of EtOAc crude extract of XG8D fungus by chromatographic technique led to the isolation of one new chamigrane endoperoxide, merulin D (**11**), and four known derivatives, merulins A-C (**8-10**) and steperoxide A (**12**).

All compounds were screened for their anti-angiogenic activity by screening *ex vivo* model, only merulin C (**10**) displayed strong activity with complete inhibition of microvessel sprouting from rings at a concentration of 2.5 μM, while steperoxide A (**12**) showed much weaker activity, with complete inhibition at 25 μM. Merulins A (**8**), B (**9**), and D (**11**) did not display any detectable activity at a screening dose (25 μM). Among isolated nor-chamigrane and chamigrane endoperoxides, merulinC (**10**) and steperoxide A (**12**), possessing a C-4–C-7 endoperoxide linkage, exhibited anti-angiogenic activity, while derivatives sharing a C-2–C-7 endoperoxide linkage unit showed no activity. This implied that the C-4–C-7 endoperoxide might play a crucial role in the activity. Merulin C (**10**) is 10 times more potent than steperoxide A (**12**),

thus an α,β-unsaturated ketone and/or the hydroxymethyl functionality might be partially responsible for the bioacitivity.

Merulin C (**10**) exhibited potent anti-angiogenic activity mainly by suppression of endothelial cell proliferation and migration in a dose dependent manner, and its effect is mediated by reduction in the phosphorylation of Erk1/2. Merulin C (**10**) also displayed promising activity in a rat aortic ring sprouting (*ex vivo*) and a mouse Matrigel (*in vivo*) assay.

CHAPTER IV

Metabolites from a marine-derived fungus *Astrosphaeriella nypae*

4.1 Introduction

4.1.1 Marine natural products

Natural products have been recognized as very important sources of biologically active substances for the development of new drugs. Enormous effort has been conducted on isolation and characterization of bioactive compounds from natural resources; however it has become more and more difficult to find new valuable compounds. Bioactive metabolites from fungi have played an important role in drug development since the discovery of penicillin by Alexander Fleming in 1928. Since then, fungi have been recognized as potential sources of anticancer, antibacterial, antimalarial, and other therapeutic agents.

Variety of organisms from marine environment has motivated scientists for many years. Various structures and significant number of secondary metabolites have been reported from different type of marine organisms, for example, algae, corals, mollusks, tunicates, and sponges. Some metabolites could eventually be developed into therapeutics such as trabectedin (trade name Yondelis®) and plitidepsin (trade name Aplidin®).

Trabectedin (trade name Yondelis®, Figure 4.1) is a novel marine anticancer drug isolated from the Caribbean and Mediterranean Sea squirt, *Ecteinascidia turbinate*. It is a tetrahydroisoquinoline alkaloid, and the first marine anticancer agent approved in the European Union for patients with soft tissue sarcoma (STS) and patients with relapsed platinum-sensitive ovarian cancer [55].

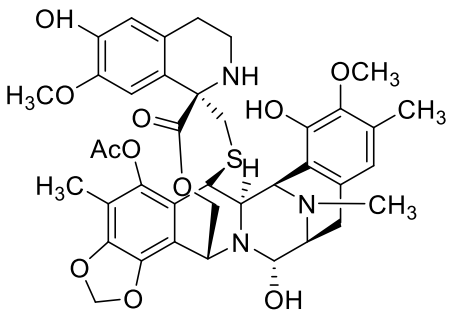

Figure 4.1 Structure of trabectedin

Plitidepsin (trade name Aplidin®, Figure 4.2) is a marine natural depsipeptide isolated from *Aplidium albicans*, a tunicate found in the Mediterranean Sea. It is a cyclic depsipeptide or a class of cyclic peptide in which some amino acids are replaced by hydroxyl acid units. Plitidepsin antitumor exhibits, antiviral exhibits, antiviral and immunosuppressive activities, and also shows promise in shrinking tumors in pancreatic, stomach, bladder, and prostate cancers [56].

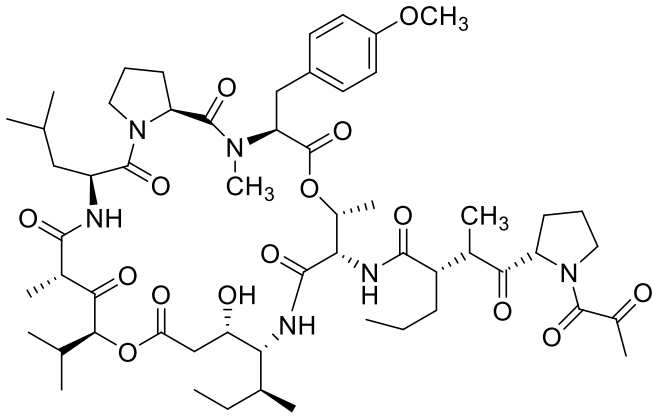

Figure 4.2 Structure of plitidepsin

4.1.2 Bioactive metabolites from marine fungi

Marine fungi can live or live in marine or estuarine environments. They differ from terrestrial and freshwater fungi in the taxonomy, morphology, and adaptations to a marine environment. Marine fungi are classified based on an ecological rather than taxonomic grouping, and can be separated into two groups. Obligate marine fungi can grow and sporulate only in a marine or estuarine habitat. Facultative marine fungi are primarily from terrestrial or freshwater origin, but after physiological adaptations, they are able to grow and possible to sporulate in the marine environment [26].

Marine-derived fungi are known as a rich source of bioactive metabolites with interesting structural properties and biological activities, for example, antifungal, antimalarial, antifouling and cytotoxic activities [57].

In 1997, phenylahistin is bioactive metabolites produced by *Aspergillus ustus* NSC-F038. It belongs to a class of naturally occurring 2, 5-diketopiperazines containing a dehydrohistidine residue. Phenylahistin was explored during the screening for cell cycle inhibitors. It displays important biological activities, such as anti-cancer or neurotoxic effects [58].

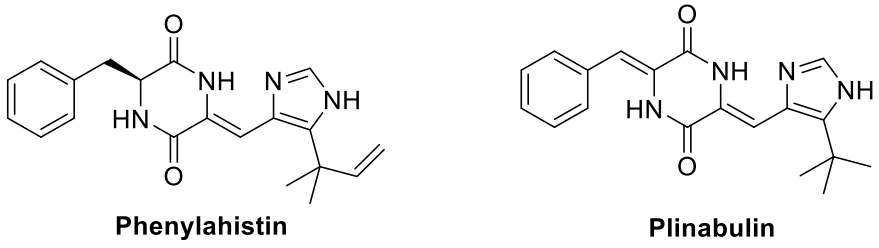

Figure 4.3 Structure of phenylahistin and plinabulin

In 2010, Ohkawa and co-workers reported a known SC2051 and two new hypochromins A and B from marine fungus *Hypocrea Vinosa*, isolated from the beach sand collected at the coast of Okinawa Prefecture, Japan. All compounds with bis(naphtho-γ-pyrone) skeleton showed tyrosine kinase inhibitory activity, with IC_{50} values of 42.1, 58.7, and 18.0 μM, respectively [59].

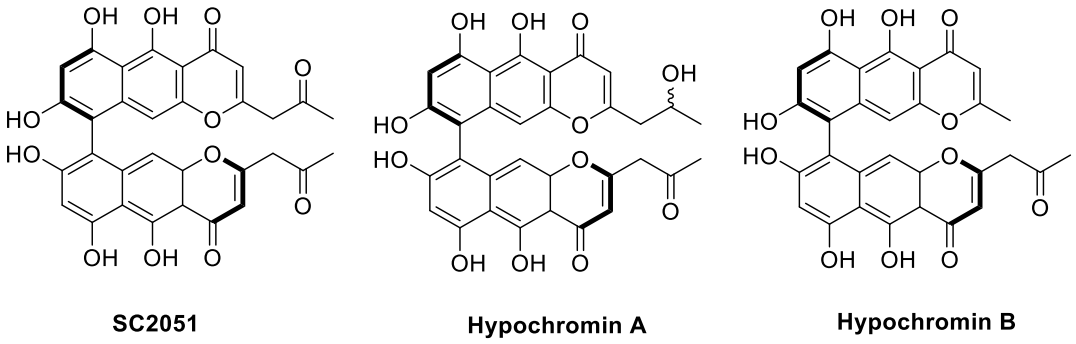

Figure 4.4 Structures of SC2051, hypochromin A and B.

In 2011, Li and co-workers found that a novel triazole carboxylic acid (penipanoid A), two new quinazolinone alkaloids (penipanoids B and C) and a very recently reported quinazolinone derivative were isolated from the marine sedimentderived fungus *Penicillium paneum* SD-44. Penipanoid A exhibited cytotoxicity against SMMC-7721 cell line (hepatocellular cancer *cell line)* with an IC_{50} value of 54.2 μM, while quinazolinone displayed significant cytotoxic activity against the A-549 and BEL-7402 cell lines with IC_{50} values of 17.5 and 19.8 μM, respectively. Penipanoids B and C were found to be inactive [60].

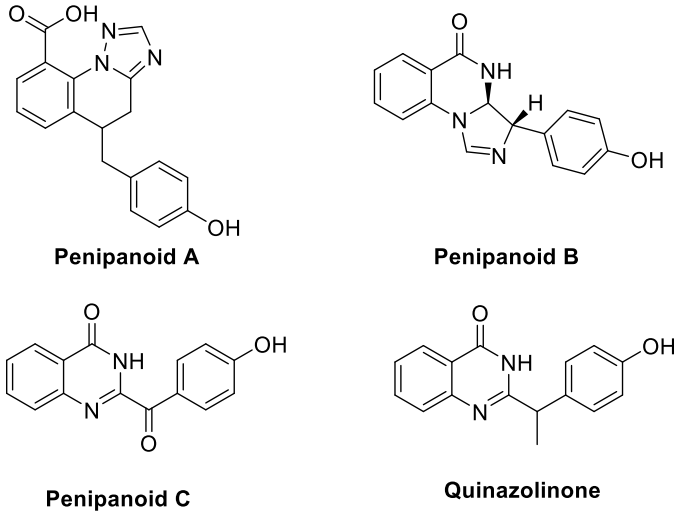

Figure 4.5 Structures of penipanoids A-C and quinzolinine

In 2012, Sun and co-workers reported that three new phenolic bisabolane sesquiterpenoid dimers (disydonols A–C) and a known (S)-(+)-sydonol were isolated from a marine-derived fungus *Aspergillus* sp., which was isolated from the sponge *Xestospongia testudinaria* collected from the South China Sea. All compounds were evaluated for cytotoxic activity. Disydonol A exhibited cytotoxicity against HepG-2 and Caski human tumor cell lines with IC_{50} of 9.3 and 12.4 μg/mL and disydonol C showed selective activity against these two cell lines with IC_{50} of 2.9 and 10.2 μg/mL, respectively. However, Disydonol C was found to be relatively non-cytotoxic against these two tumour cell lines [61].

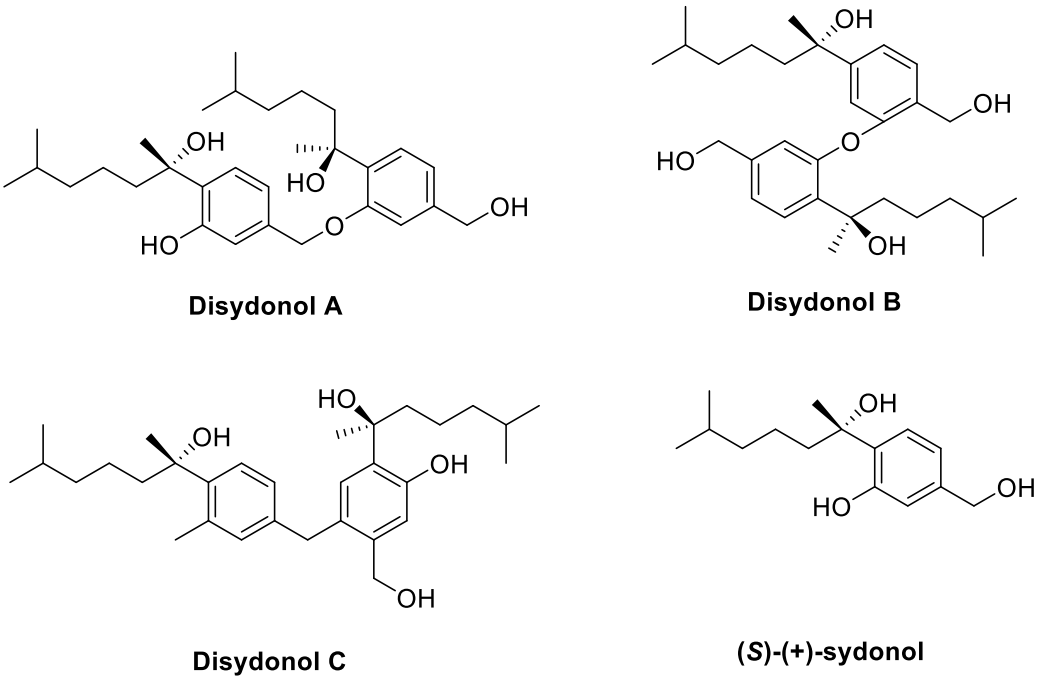

Figure 4.6 Structures of disydonols A-C and (*s*)-(+)-sydonol

In 2012, Sun and co-workers discovered five new oxygenated pimarane diterpenes (scopararanes C–G) and six known pimarane diterpenes (libertellenone A, scopararane B, diaporthein A, diaporthein B, 11-deoxydiaporthein A , and isopimara-8(14),15-diene) from the culture of a marine sediment-derived fungus *Eutypella scoparia* FS26 obtained from the South China Sea. Diaporthein B exhibited strong

cytotoxicities against SF-268 (human glioma cell line), MCF-7 (human breast adenocarcinoma cell line) and NCI-H460 (human non-small cell lung cancer cell line) cell growth with IC_{50} values of 9.2, 4.4, 9.9 μM, respectively. Libertellenone A displayed varying cytotoxic activities against the three cell lines with IC_{50} values of 20.5, 12.0, 40.2 μM. Scopararanes C and D showed moderate cytotoxic activities against the tumor cell line MCF-7 with IC_{50} values of 35.9 μM and 25.6 μM, respectively. The other compounds displayed no appreciable activity, except that scopararane E, scopararane G, and scopararane B showed weak cytotoxic activities against the MCF-7 cell line with IC_{50} values of 74.1 μM, 85.5 μM, and 60.1 μM, respectively [62].

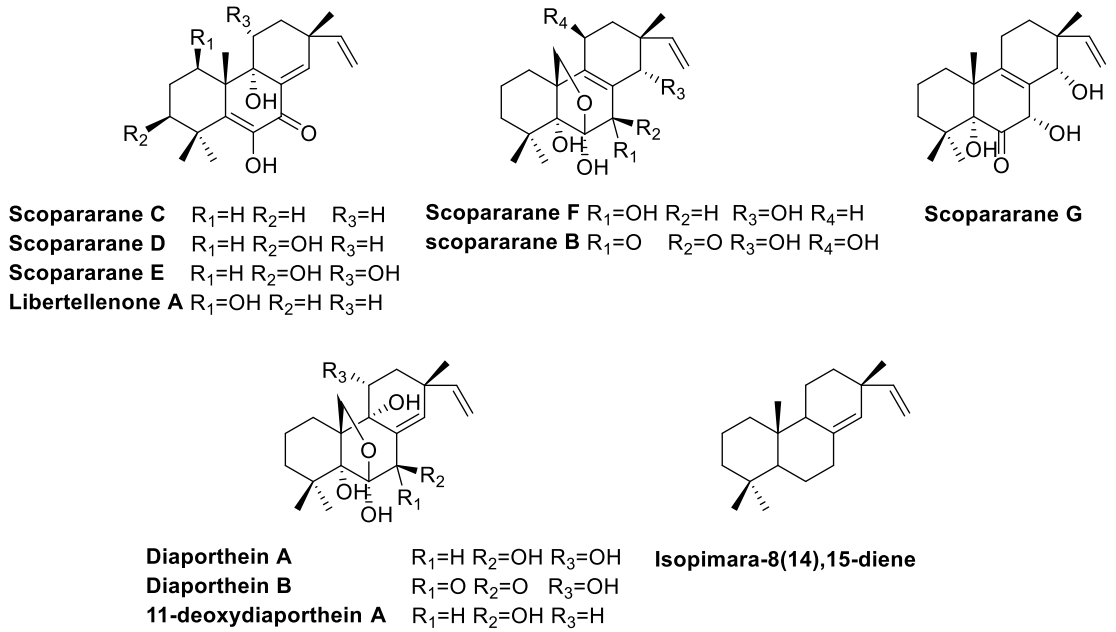

Figure 4.7 Structures of oxygenated pimarane diterpenes and pimarane diterpenes from *E. scoparia* FS26

In 2013, Shen and co-workers reported two new prenylated indole alkaloids (17-epinotoamides Q and M) and two new phenyl ether derivatives (cordyols D and E) together with 10 known compounds from the marine fungal strain *Aspergillus* sp. XS-20090066, isolated from the gorgonian *Dichotella gemmacea*. All compounds were tested for their cytotoxic activity against human erythroleukemia K562 cell

lines. 4- methoxycarbonyldiorcinol showed cytotoxic activity against the K562 cell lines with an IC_{50} value of 5.94 μM, while the other compounds were found to be inactive[63].

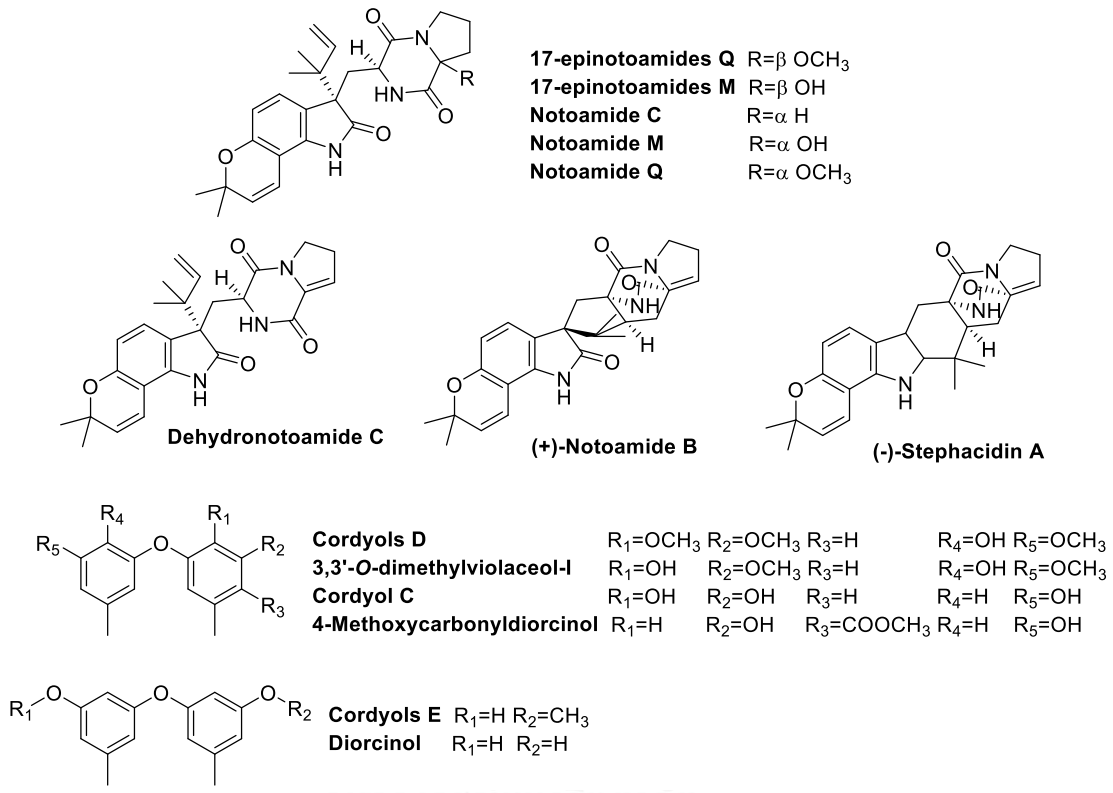

Figure 4.8 Structures of prenylated indole alkaloids and phenyl ether derivatives from *Aspergillus* sp. XS-20090066

In 2014, Wang and co-workers found that three new thiodiketopiperazines, named phomazines A–C, and 10 known analogues, were isolated from the fermentation broth of a marine-derived fungus, *Phoma* sp. OUCMDZ-1847, associated with the mangrove plant *Kandelia candel*. Phomazine A, epicorazine A, epicorazine B, epicorazine C, and exserohilone A showed cytotoxicities against the HL-60 (human promyelocytic leukemia *cell line*), HCT-116 (human colon *cancer cell* line), K562 (human erythroleukemic *cell line*), MGC-803 (human gastric *cancer cell line)*, and

A549 (human lung adenocarcinoma epithelial *cell line*) cell lines with IC_{50} values in the range between 0.05 and 8.5 μM [64].

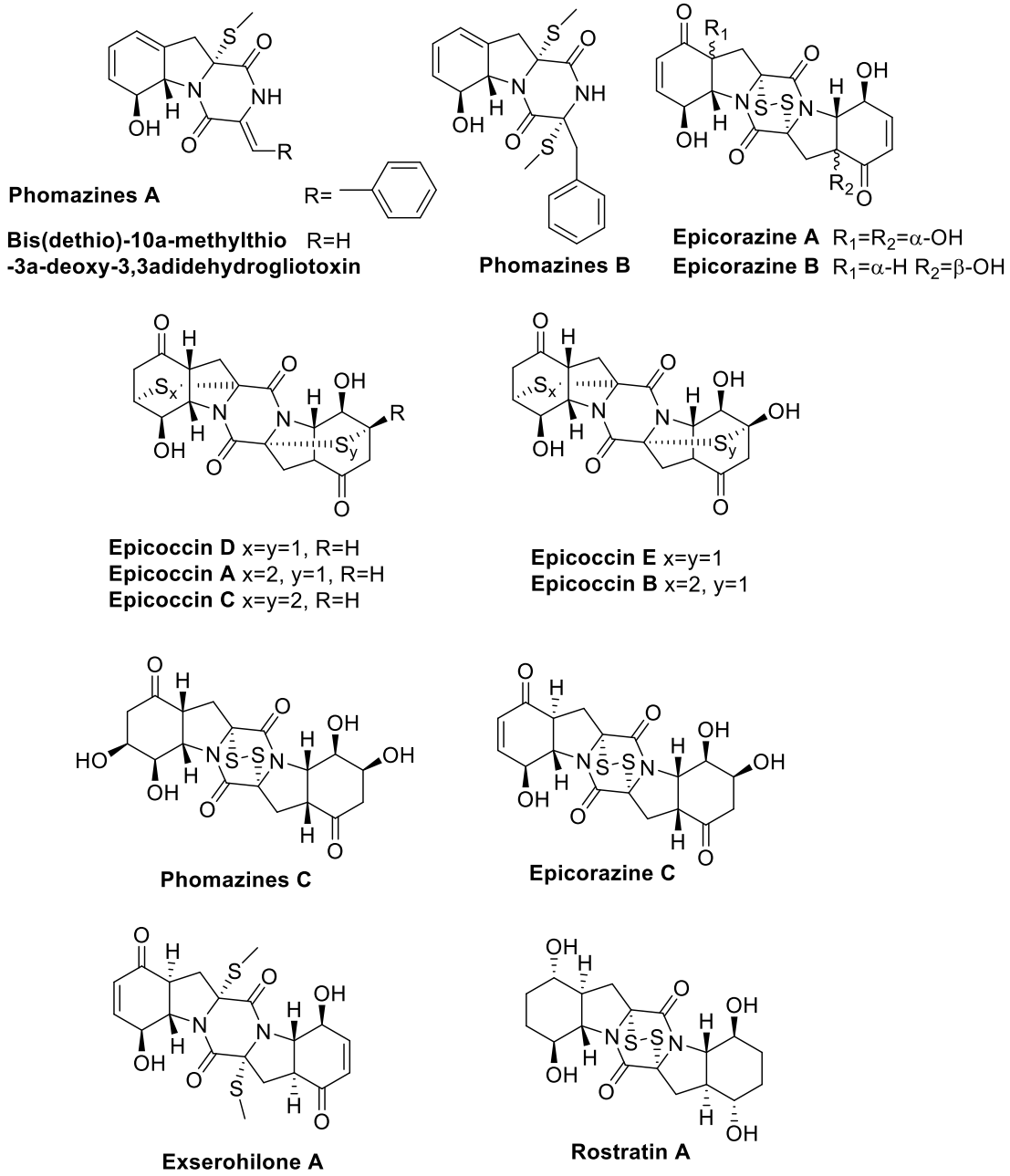

Figure 4.9 Structures of thiodiketopiperazines from marine-derived fungus, *Phoma* sp. OUCMDZ-1847

In 2015, Liu and co-workers reported that two new bisthiodiketopiperazine derivatives (adametizines A and B) and two new acorane sesquiterpenes (adametacorenols A and B) were produced from a fungal strain, *Penicillium adametzioides* AS-53, which was isolated from an unidentified sponge collected at Hainan Island in the South China Sea. All compounds were evaluated for brine shrimp lethality, antimicrobial potency, and cytotoxic activity. Adametacorenols B, which showed selective activity against the NCI-H446 cell line with an IC_{50} value of 5.0 μM. Adametizines A exhibited lethality against brine shrimp (*Artemia salina*) with an LD_{50} value of 4.8 μM and was found to be active against *Staphyloccocus aureus*, *Aeromonas hydrophilia*, *Vibrio harveyi*, *Vibrio parahaemolyticus*, and *Gaeumannomyces graminis* with minimum inhibitory concentration (MIC) values of 8.0, 8.0, 32.0, 8.0, and 16.0 μg/mL, respectively [65].

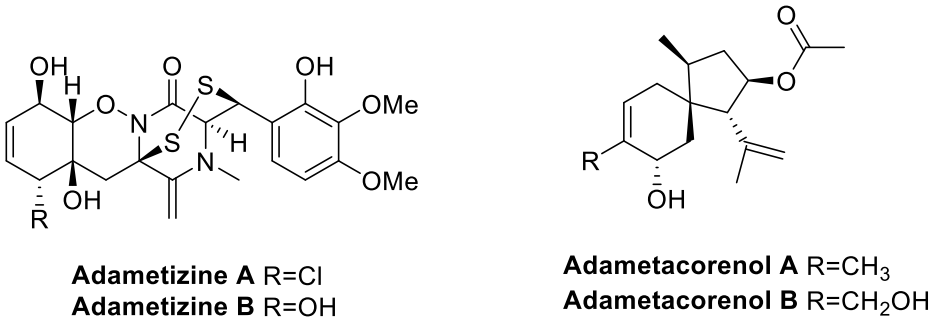

Adametizine A R=Cl
Adametizine B R=OH

Adametacorenol A R=CH_3
Adametacorenol B R=CH_2OH

Figure 4.10 Structures of adametizines A-B and adametacorrenols A-B

4.2 Fungal collection and isolation of the marine fungal isolate BCC 3553

The fungus was isolated from *Nypa fruticans* was collected at Samut Prakan province, Thailand, and deposited at the BIOTEC Culture Collection as BCC 5335 on March, 1999 by Assit. Prof. Dr. Apiradee Pilantanapak, Department of Microbiology, Faculty of Science, Burapha University, Bangsaen, Chonburi, Thailand.

Woody materials were randomly collected from different coastal locations of Thailand. They were washed by sea water to remove mud and sediments and

returned to the laboratory in sterile plastic bags. Fungal specimens (woody samples) were kept and incubated in plastic boxes spraying with sterilized distilled water. Single spore ascospore was isolated on seawater agar corn meal (SCMA) supplemented with two antibiotics (streptomycin sulfate 0.5 g/L, penicillin G 0.5 g/L). Germinated spores were directly transferred to a fresh agar plate and incubated for 14 days at 25ºC or at room temperature for further growth. Microscopic features of studied marine fungi were identified based on their morphological characteristics on SCMA and seawater agar potato dextrose agar (SPDA). Slides were mounted in seawater or lactophenol cotton blue, observed under microscope and sealed with polyvinyl alcohol. Measurements of ascoma, asci and ascospores to define the exact range of their sizes were made. Selected strains were used for the molecular identification.

4.3 Fungal identification of the marine fungal isolate BCC 3553

The isolate BCC 3553 was taxonomically (molecular method) identified by Miss. Satinee Suetrong and Mr. Anupong Klaysuban, Fungal Biodiversity Laboratory, Bioresouces Technology Unit, National Center for Genetic Engineering and Biotechnology (BIOTEC), Pathum Thani, Thailand.

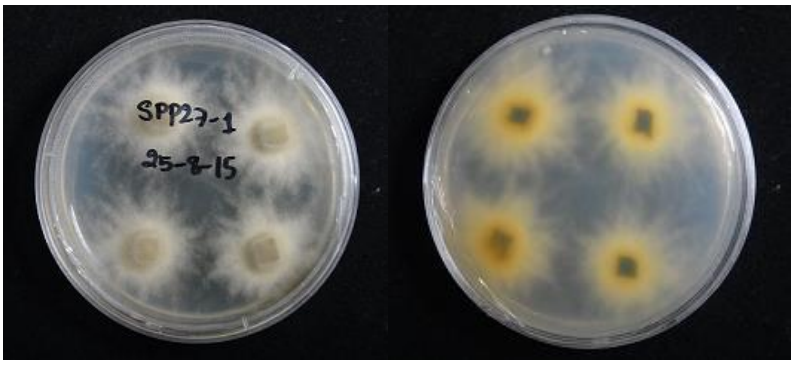

Figure 4.11 Colony morphology of the marine fungus isolate BCC 3553 on PDA

The fungus BCC 5335 was identified as *Astrophaeriella nypae* on the basis of morphology and host affiliation. Its total genomic DNA was extracted from lyophilized mycelia. The large subunit (LSU) and small subunit (SSU) regions were PCR amplified, and sequenced by Macrogen Inc., Korea. Its sequence with 904 nucleotides showed 94% identity with the 20 closest fungal matches at NCBI as shown in Fig. 4.12. Phylogenetic analysis of the sequence data using BioEdit 7.0.5.3 and Paup 4.0b10 programs indicated that the fungus BCC 5335 was a member of order Pleosporales (class Dothideomycetes and subclass Pleosporomycetidae,). According to limitation of the exiting phylogenetic database, uncertain taxonomic position, and polyphyletic relationship in this order, therefore, it is not possible to classify the family level of BCC 5335 at present. The sequences were submitted to GenBank with accession numbers KU258054 (SSU rDNA) and KU258055 (LSU rDNA).

Table 4.1 Thirty-nine fungal names with closest BLAST match based on 28S large subunit ribosomal RNA gene, partial sequence.

Fungal name and original code	%Identity	Accession
Pleurophoma ossicola CPC:24985	94%	KR476770.1
Paraconiothyrium brasiliense CBS:254.88	94%	JX496171.1
Paraconiothyrium brasiliense CBS:122851	94%	JX496149.1
Paraconiothyrium brasiliense CBS 115.92	94%	JX496135.1
Keissieriella qenistae CBS:113798	94%	GU205222.1
Didymosphaeria sp. HA-2014 strain MFLUCC 14-0023	94%	KJ436586.1

Fungal name and original code	%Identity	Accession
Didymosphaeria sp. HA-2014 strain MFLUCC 14-0024	94%	KJ436586.1
Paraconiothyrium fungicola strain CBS:113269	94%	JX496133.1
Keissieriella cladophila strain CBS:104.55	94%	JX681090.1
Keissieriella cladophila strain CBS:104.55	94%	GU205221.1
Paraconiothyrium sp. HA-2014 strain MFLUCC 10-0278	94%	KJ939283.1
Montaqnulaceae sp. NW-2014	94%	KJ803030.1
Coniothyrium juniper strain CBS:610.72	94%	JX681081.1
Paraconiothyrium vanabile strain CBS:461.90	94%	JX496206.1
Paraconiothyrium vanabile strain CBS:433.71	94%	JX496202.1
Paraconiothyrium vanabile strain CBS:122322	94%	JX496148.1
Paraconiothyrium vanabile strain CBS:121164	94%	JX496141.1
Paraconiothyrium vanabile strain CBS:112.72	94%	JX496132.1
Paraconiothyrium brasiliense strain CBS:100299	94%	JX496124.1
Microdipiodia hawailensis strain CBS:120025	94%	DQ885897.1
Microdipiodia hawailensis strain CBS:12268	94%	DQ885896.1
Dendrothyrium longisporum strain CBS:824.84	94%	JX496228.1
Dendrothyrium longisporum strain CBS:121517	94%	JX496143.1

Fungal name and original code	%Identity	Accession
Paraconiothyrium vanabile strain CBS:121754	94%	JX496144.1
Paraconiothyrium vanabile strain CBS:121166	94%	JX496142.1
Uncultured Ascomycota clone 4M1	94%	EU489931.1
Curreya pityophila strain CBS:149.32	94%	JX681087.1
Paraconiothyrium vanabile strain CBS:638.93	94%	JX496215.1
Paraphaeosphaeria sporulosa strain CBS:317.81	94%	JX496187.1
Paraphaeosphaeria sporulosa strain CBS:281.81	94%	JX496175.1
Paraphaeosphaeria sporulosa strain CBS:245.76	94%	JX496169.1
Paraphaeosphaeria sporulosa strain CBS:221.78	94%	JX496168.1
Paraphaeosphaeria sporulosa strain CBS:177.59	94%	JX496163.1
Paraphaeosphaeria sporulosa strain CBS:163.69	94%	JX496159.1
Paraphaeosphaeria brasiliense strain CBS:122319	94%	JX496145.1
Paraphaeosphaena sporulosa strain CBS:109.72	94%	JX496128.1
Paraphaeosphaena sp. CBS:101464	94%	JX496125.1
Curreya pityophila strain CBS:149.32	94%	DQ384102.1
Kalmusia italic MFLUCC 13-0068	94%	KP325441.1

4.4 Large scale cultivation and extraction

The BCC 5335 was cultivated to large scale on November, 2012 by Miss Supawadee Deelai. Marine fungal strain BCC 5335 was culture on potato dextrose agar (PDA) at 25 °C. The PDA agar six fragments (6x6 mm^2) were transferred into Erlenmeyer flasks (4 × 250 mL), each containing of potato dextrose broth (PDB) 25 mL. After incubation on a rotary shaker (200 rpm) for 7 days, the primary seed culture (4 × 25 mL) was transferred into Erlenmeyer flasks (4 × 1 L), each containing 250 mL of PDB, and then fermented on a rotary shaker (200 rpm) for 7 days. The secondary seed culture (40 × 25 mL) was subsequently transferred into Erlenmeyer flasks (40 × 1 L), each containing 250 mL of LCN medium comprising of mannitol 10 g, glucose 10 g, yeast extract 5 g, and soytone 5.0 g in 1 L of distilled H_2O, then cultured at 25 ºC for 21 days on static condition. The culture was filtered to separated broth and mycelia. The filtrate was extracted with an equal volume of ethyl acetate (EtOAc) for 3 times. The organic layers were combined and evaporated under reduced pressure to yield EtOAc crude extract broth.

After filtration to separate between broth and mycelia, the mycelia were soaked in MeOH for 2 days, and then the MeOH soluble fraction was collected by filtering through sheet cloth (five layers). The filtrate was extracted with an equal volume of hexane for 3 times. The MeOH layers were combined and evaporated under vacuum and the residue was partitioned between EtOAc and H_2O, and then extracted with an equal volume of EtOAc for 3 times. The EtOAc soluble fraction was evaporated under reduced pressure to yield the mycelial EtOAc crude extract (Scheme 4.1).

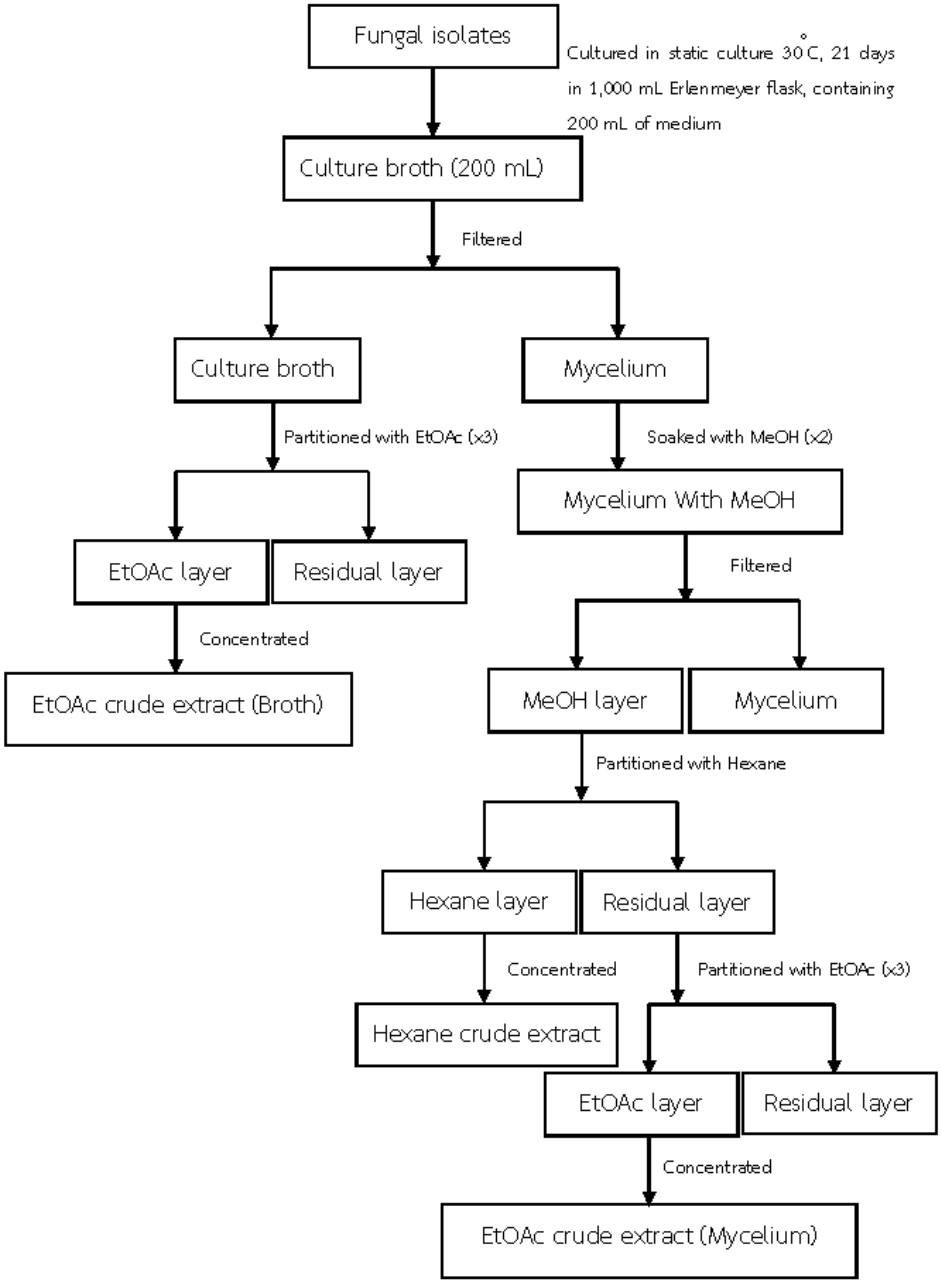

Scheme 4.1 Extraction of fungal culture broth and mycelium

4.5 Isolation of bioactive compounds from crude extracts of BCC 3553

The broth was extracted with an equal amount of EtOAc for 3 times. The EtOAc solution was evaporated under reduced pressure to afford a brown gum (4.73 g). The crude extract was subjected to a Sephadex LH-20 column (elution with MeOH) to provide 11 fractions (B1-B11). Fraction B2 (989.30 mg) was fractionated by silica gel (SiO_2) column chromatography elution with acetone 20%:80% CH_2Cl_2 to give 15 fractions (B1-B15). The fraction B4 (74.70 mg) was purified by semi-preparative HPLC using a reversed-phase column (SunFire C18, 5 μm, 19x150 mm; flow rate 10mL/min; a linear gradient of MeCN: H_2O, 30% to 70%--->90% to 100% over 25 min) to give **13** (13.50 mg). The fraction D (650.30 mg) was rechomatographed by a Sephadex LH-20 column (elution with MeOH) to provide 7 fractions (D1-D7). The fraction D3 (0.10g) was purified by semi-preparative HPLC using a reversed-phase column (sunfire C18, 5 μm, 19x150 mm; gradient MeCN : H_2O, 30% to 70%--->90% to 100%) to afford **18** (7.90 mg) and the fraction C4 (0.18g) was rechomatographed by preparative HPLC using a reversed-phase column (sunfire C18, 10 μm, 19x250 mm; gradient MeCN : H_2O, 30% to 70%--->90% to 100%) to give **17** (4.40 mg), **16** (4.20 mg), **14** (16.80 mg) and **15** (2.30 mg).

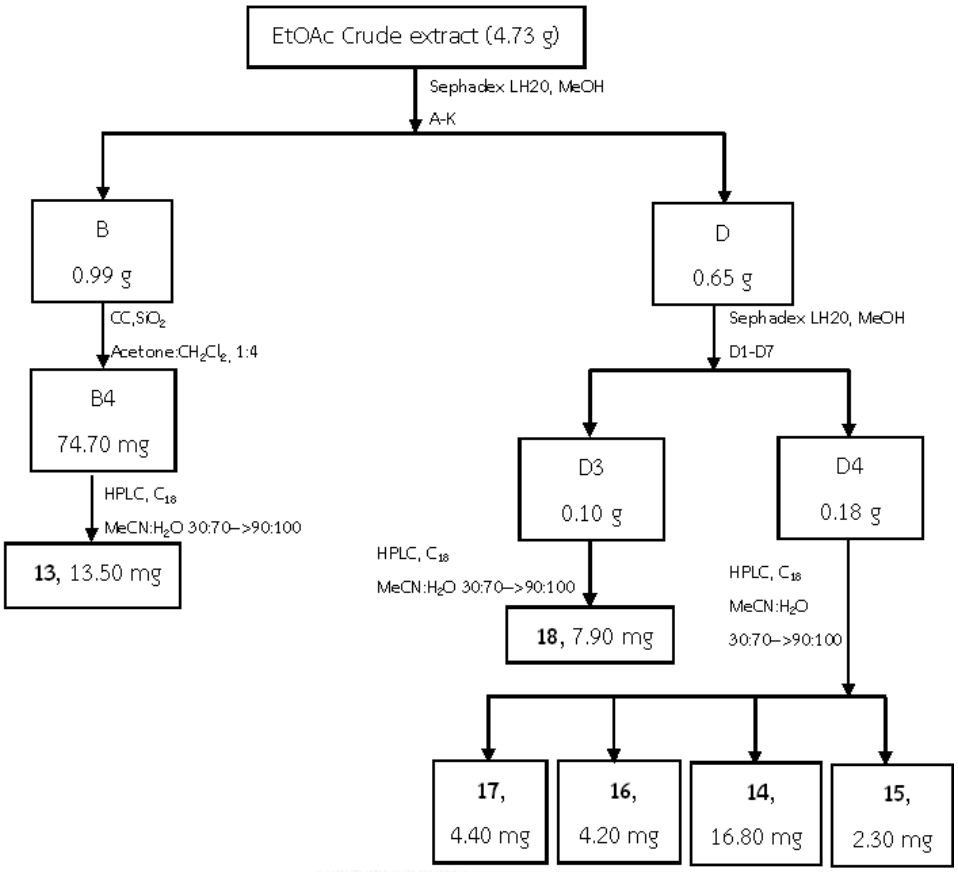

Scheme 4.2 Isolation of broth crude extract of fungus *A.nypae*

The mycelia were separated from the broth by filtration and macerated in MeOH (500 mL, 2 days), and filtered. The filtrate was diluted with H_2O (50 mL) and extracted with hexane (2 x 300 mL). The aqueous MeOH layer was concentrated under reduced pressure and the residue was extracted with EtOAc (400mL), and dissolved with H_2O (150 mL). The organic layer was concentrated under vacuum to provide a brown gum (1.43 g). The crude mycelial extract was fractionated using a Sephadex LH-20 column (eluted with MeOH) to provide 5 fractions (A-E). Fraction D (34.30 mg) was purified by semi-preparative HPLC using a reversed-phase column (sunfire C18, 5 μm, 19x150mm; gradient MeCN: H_2O, 30% to 90%) to furnish **19** (11.60 mg).

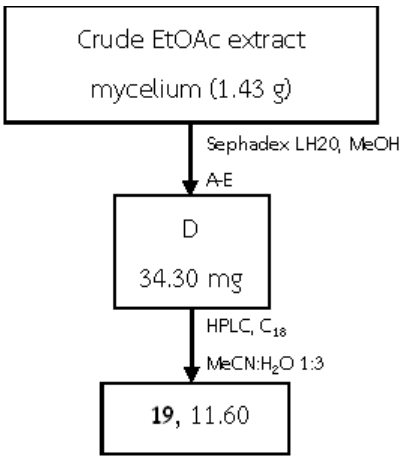

Scheme 4.3 Isolation of mycelium crude extract *A.nypae*

4.6 Biological assays

Testing for biological assay was conducted by Bioassay Laboratory, National Center for Genetic Engineering and Biotechnology (BIOTEC), Thailand.

4.6.1 Antimalarial activity

Plasmodium falciparum (K1, multidrug resistant strain) was cultured continuously according to the method of Tragen and Jensen. The quantitative assessment of the anti-malarial activity *in vitro* was performed in accordance with the microculture radioisotope technique based upon the method described by Desjardins, *et al*. A standard anti-malarial compound, dihydroartemisinin (IC_{50} value of 0.002 μM), was used as the positive control for the assay.

4.6.2 Cytotoxic activity

Bioassay of cytotoxicity activity was performed *in vitro* by MTT (3-(4,5-dimethylthiazol-2-yl)-2,5-diphynyltrazolium bromide) calorimetric method against African green monkey kidney fibroblast (Vero) cells. In Principle, the viable cell number/well was directly proportional to the production of formazan, followed by

solubilization, and could be measured spectrophotometrically. A positive control for cytotoxic activity used by ellipticine (IC_{50} value of 0.003 μM).

4.7 Results and Discussion

4.7.1 Structures of secondary metabolites produced by BCC 3553

The crude extracts from culture broth and mycelia of marine fungus strain BCC 3553 were subjected to fractionations using Sephadex LH-20, silica gel column chromatography and HPLC to obtain three new (**13-15**), and four known compound (**16-19**).

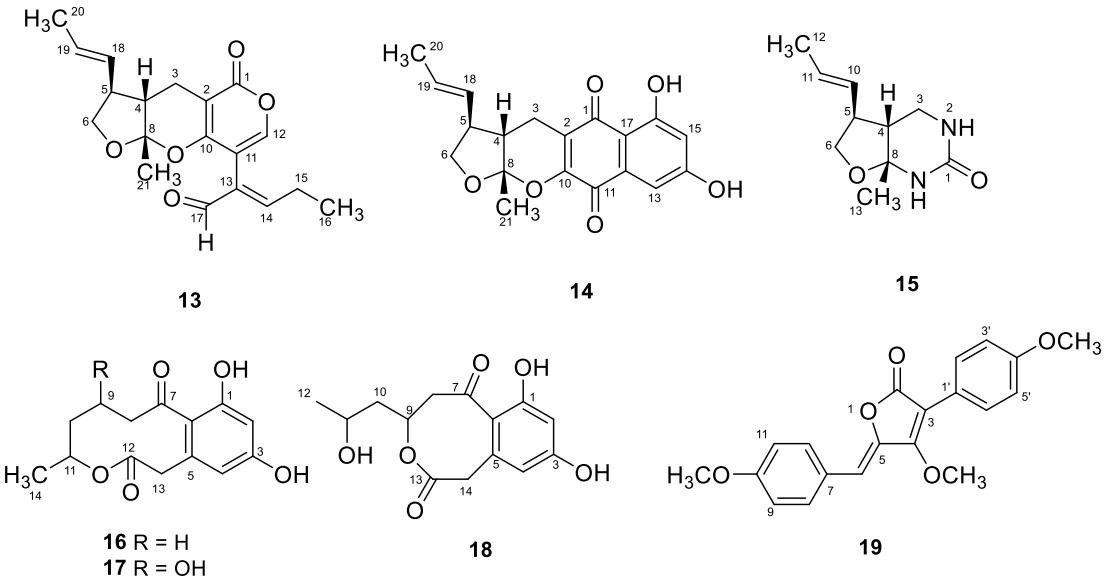

Figure 4.12 Structures of compounds 13-19

Compound **13** was isolated as a yellow brown solid. mp 196-198 °C, $[\alpha]^{20}_{D}$ -42.80 (*c* 0.1, MeOH), UV (MeOH) λ_{max} (log ε) 216 (3.33) nm and 289 (3.17) nm, IR (neat) υ_{max} 2938, 1708, 1648, 1380, 1052 cm^{-1}, Its molecular formula was established as $C_{19}H_{22}O_5$ by HRESIMS data (*m/z* 353.1352 $[M+Na]^+$, calcd 353.1359). The ^{13}C NMR spectrum showed signals for an aldehyde carbonyl (δ_C 192.3), an ester carbonyl (δ_C

163.2), four olefinic/aromatic methine (δ_C 159.9, 149.3, 129.8 and 128.8), four quarternary sp^2 carbons (δ_C 160.4, 134.4, 108.9, and 96.8), a hemiacetal carbon (δ_C 109.8), an oxymethylene (δ_C 72.1), two methines (δ_C 45.8 and 44.8), two methylenes (δ_C 23.4 and 18.5), and three methyl groups (δ_C 21.7, 17.4, and 12.4). The ^{1}H NMR spectrum displayed resonances corresponding to a *trans*-propenyl moiety [δ_H 5.56, (1H, dq, *J* = 15.1, 6.4 Hz), 5.35 (1H, ddq, *J* = 15.1, 8.7, 1.5 Hz), and 1.67 (3H, dd, *J* 6.4, 1.5 Hz), *trans*-2-pentenal unit 2-pentenal unit (δ_H 9.54 (1H, s), 7.03 (1H, t, *J* = 7.6 Hz), 2.37 (2H, quin, *J* = 7.6 Hz), 1.11 (3H, t, *J* = 7.6 Hz)], one olefinic proton [δ_H 7.35 (1H, s)], two oxymethylene protons [δ_H 4.01 (1H, dd, *J* = 8.7, 8.6 Hz) and 3.65 (1H, dd, *J* = 8.7, 8.6 Hz)], two methylene protons [δ_H 2.53 (2H, m)], two methines [δ_H 2.25 (1H, ddd, *J* = 11.4, 5.2, 2.6 Hz) and 2.60 (1H, dq, *J* = 11.4, 8.7 Hz)], and one methyl singlet [δ_H 1.44 (3H, s)]. Two partial stuctures of the molecule, CH_3-CH-CH-CH(CH_2)-CH-CH_2 and CH_3-CH_2-CH, were deduced from COSY spectroscopic data as shown in Figure 4.12. Key HMBC correlations were observed from H_2-3 to C-1 and C-10; H-4 to C-2; H_2-6 to C-8; H-12 to C-1, C-10, C-11, and C-13; H-14 to C-11 and C-17; H-17 to C-11; and H_3-21 to C-4 and C-8. NOESY cross peaks observed between H-4/H_3-21 and H-4/H-18 suggested a *cis*-ring junction between tetrahydrofuran and dihydropyran moieties and the same orientations for *trans*-propenyl unit, proton H-4, and the methyl group (CH_3-21). This compound has similar core structure to that of known penicipyrone, previously described from the marine-derived fungus *Penicillium* sp. PSU-F44[66] with only the exception that its *trans*-2-pentenal at C-11 was replaced by a methyl group for penicipyrone.

Table 4.2 NMR data of compound **13** in acetone-d_6

Position	**13**	
	δ_C	δ_H (mult, *J* in Hz)
1	163.2	
2	96.8	
3	18.5	2.53, m
4	45.8	2.25, ddd (11.4, 5.2, 2.6)
5	44.8	2.60, dq (11.4, 8.7)
6	72.1	α 4.01, dd (8.7, 8.6) β 3.65, dd (8.7, 8.6)
8	109.8	
10	160.4	
11	108.9	
12	149.3	7.35, s
13	133.4	
14	159.9	7.03, t (7.6)
15	23.4	2.37, quin (7.6)
16	12.4	1.11, t (7.6)
17	193.2	9.54, s
18	129.8	5.35, ddq (15.1, 8.7, 1.5)
19	128.8	5.56, dq (15.1, 6.4)
20	17.4	1.67, dd (6.4, 1.5)
21	21.7	1.44, s

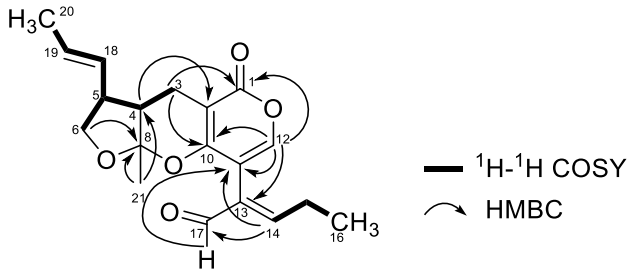

Figure 4.13 ^{1}H–^{1}H COSY and key HMBC correlations of **13**

Compound **14** was obtained as an orange solid. mp 194-196 °C, $[\alpha]^{20}_{D}$ -54.4 (*c* 0.1, MeOH), UV (MeOH) λ_{max} (log ε) 214 (4.52) nm, 265 (4.29) nm, 305 (4.03) nm and 441 (3.43) nm, IR (neat) υ_{max} 3327, 2922, 1671, 1635, 1615, 1404, 1323, 1092, 982, 856, 779 cm^{-1}, Its molecular formula was established as $C_{19}H_{18}O_6$ by HRESIMS data (m/z 365.0997 $[M+Na]^+$, calcd 365.0996). Analysis of ^{13}C NMR, DEPT and HMQC spectra indicated the presence of two conjugated ketone carbonyl (δ_C 189.1 and 178.1), four olefinic/aromatic methine (δ_C 129.4, 128.8, 107.6, and 107.5), six quarternary sp^2 carbons (δ_C 163.6, 163.3, 153.4, 133.4, 116.7 and 107.9), a hemiacetal carbon (δ_C 109.8), an oxymethylene (δ_C 72.0), two methines (δ_C 45.2 and 44.8), one methylene (δ_C 17.6), and two methyl groups (δ_C 21.7 and 17.1). The ^{1}H NMR spectrum displayed resonances corresponding to a *trans*-propenyl moiety [δ_H 5.58, (1H, dq, *J* = 15.1, 6.5 Hz), 5.36q, *J* = 15.1, 8.8, 1.5 Hz), and 1.66 (3H, dd, *J* 6.5, 1.5 Hz)], one chelated hydroxyl proton [δ_H 12.51 (1H, s)], two *meta*-coupled aromatic protons (δ_H 7.03 (1H, d, *J* = 2.4 Hz) and 6.58 (1H, d, *J* = 2.4 Hz)], two oxymethylene protons [δ_H 4.10 (1H, dd, *J* = 8.8, 8.8 Hz) and 3.69 (1H, dd, *J* = 8.8, 8.8 Hz)], two methylene protons [δ_H 2.74 (1H, dd, *J* = 19.3, 0.9 Hz) and 2.61(1H, dd, *J* = 19.3, 6.7 Hz)], two methines [δ_H 2.30 (1H, ddd, *J* = 11.6, 6.7, 0.9 Hz) and 2.70 (1H, dq, *J* = 11.6, 8.8 Hz)], and one methyl singlet [δ_H 1.54 (3H, s)]. The presence of a 5,7-dihydroxy-1,4-naphthoquinone moiety was assigned based on IR spectrum, absorption maxima at 441 nm in the UV spectrum, and NMR spectroscopic dat. The ^{1}H NMR spectrum of **14** showed resonances of two *meta*-coupled aromatic protons (H-13 and H-15), and one

chelated hydroxyl proton (16-OH). HMBC correlations observed from the chelated hydroxyl proton (16-OH) to three aromatic carbons (C-15, C-16, and C-17); from the upfield aromatic proton H-13 to C-14, C-15, C-17 and the quinone carbonyl at δ_C 178.1 (C-11) supported the partial structure of 5,7-dihydroxy-1,4-naphthoquinone moiety. The tetrahydrofuran-dihydropyran subunit was assigned in the same manner as compound **13**. HMBC correaltion from H_2-3 to C-10 and the other quinone carbonyl at δ_C 189.1 (C-1); and from H-4 to C-2 indicated the attachment of nathoquinone to tetrahydrofuran ring and the planar structure of **14**. Based on NOESY experiment and $^3J_{H-H}$ coupling constants in the same manner as described for **13,** the relative configuration of **14** was assigned as depicted. Therefore, **14** was determined as a new compound and given the name astronyquinone.

Table 4.3 NMR data of compound **14** in acetone-d_6

Position	**14**	
	δ_C	δ_H (mult, *J* in Hz)
1	189.1	
2	116.7	
3	17.6	2.74, dd (19.3, 0.9) 2.61, dd (19.3, 6.7)
4	45.2	2.30, ddd (11.6, 6.7, 0.9)
5	44.8	2.70, dq (11.6, 8.8)
6	72.1	4.10, dd (8.8, 8.8) 3.69, dd (8.8, 8.8)
8	109.8	
10	153.4	
11	178.1	
12	133.4	
13	107.5[a]	7.03, d (2.4)

14	163.6[b]	
15	107.6[a]	6.58, d (2.4)
16	163.6[b]	1.11, t (7.6)
17	107.9	9.54, s
18	129.4	5.36, ddq (15.1, 8.8, 1.5)
19	128.8	5.58, dq (15.1, 6.5)
20	17.1	1.66, dd (6.5, 1.5)
21	21.7	1.54, s
16-OH		12.51, s

[a,b] Interchangeable signals.

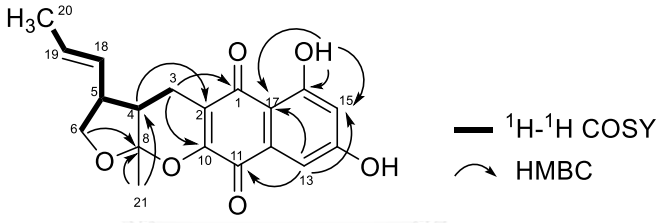

Figure 4.14 ^{1}H–^{1}H COSY and key HMBC correlations of **14**

Compound **15** was obtained as a yellow-brown amorphous solid. $[\alpha]^{20}_{D}$ -69.0 (*c* 0.1, MeOH), UV (MeOH) λ_{max} (log ε) 285 (2.60) nm, IR (neat) υ_{max} 3250, 2936, 1698, 1644, 1509, 1384, 1154, 1024, 778 cm^{-1}, Its molecular formula was established as $C_{10}H_{16}O_2$ by HRESIMS data (m/z 219.1101 $[M+Na]^+$, calcd 219.1104), Analysis of 2D NMR data indicated the presence of a urea carbonyl (δ_C 155.6), two olefinic methines (δ_C 131.0 and 127.2), a quaternary carbon (δ_C 91.3), an oxymethylene (δ_C 70.3), two methines (δ_C 48.5 and 45.0), one methylene carbon (δ_C 37.3), and two methyl groups (δ_C 27.0 and 17.1). The ^{1}H NMR spectrum displayed resonances corresponding to two CO(N*H*)$_2$ [δ_H 5.69 (1H, br s) and 5.66 (1H, br s)], a *trans*-propenyl moiety [δ_H 5.57, (1H, ddq, *J* = 15.1, 0.6, 6.4 Hz), 5.39 (1H, ddq, *J* = 15.1, 8.8, 1.5 Hz), and 1.66 (3H, dd, *J* 6.4,

1.5 Hz)], two oxymethylene protons [δ_H 3.93 (1H, dd, *J* = 8.4, 8.3 Hz) and 3.47 (1H, dd, *J* = 8.5, 8.4 Hz)], two methylene protons [δ_H 3.31 (1H, ddd, *J* = 12.6, 3.4, 2.9 Hz) and 3.07 (1H, ddd, *J* = 12.6, 5.0, 1.9 Hz)], two methines [δ_H 2.99 (1H, dddd, *J* = 9.5, 8.8, 8.5, 8.4 Hz) and 1.98 (1H, ddd, *J* = 9.5, 3.4, 1.9 Hz)], and one methyl singlet [δ_H 1.46 (3H, s)]. The presence of a urea functionality was suggested by IR absorption bands at 3250, 1698 cm^{-1}, and ^1H NMR observation of an upfield carbonyl signal (δ_C 155.6, C-1) and two labile protons (δ_H 5.69 and 5.66, NH) suggested. The partial structure, CH_3-CH-CH-CH(CH_2)-CH-CH_2, was deduced from COSY spectroscopic data. Key HMBC correlations from H_2-3 to C-1; H_3-13 to C-4 and C-8; from H-6 to C-8 supported the planar structure of **15**. The large coupling constant between H-4 and H-5 (*J* = 9.5 Hz) and NOESY correlation from H-4 to H_3-21, and from H-4 to H-18 suggested the relative configuration of **15**. Thus, compound **15** was determined to be a new cyclic urea, astronyurea.

Table 4.4 NMR data of compound **15** in acetone-d_6

Position	**15**	
	δ_C	δ_H (mult, *J* in Hz)
1	155.6	
3	37.3	3.31, ddd (12.6, 3.4, 2.9) 3.07, ddd (12.6, 5.0, 1.9)
4	48.5	1.98, ddd (9.5, 3.4, 1.9)
5	45.0	2.99, dddd (9.5, 8.8, 8.5. 8.4)
6	70.3	3.93, dd (8.4, 8.3) 3.47, dd (8.5, 8.4)
8	91.3	
10	131.04	5.39, ddq (15.1, 8.8, 1.5)
11	127.2	5.57, ddq (15.1, 0.6, 6.4)

12	17.1	1.66, dd (6.4, 1.5)
13	27.0	1.46, s
NH		5.69, br s
		5.66, br s

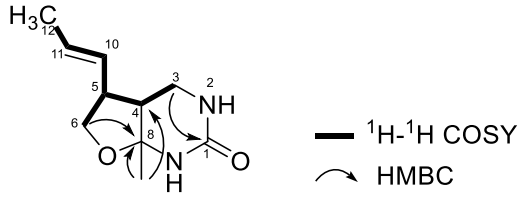

Figure 4.15 ^{1}H– ^{1}H COSY and key HMBC correlations of **15**

Compound **16** was obtained as a yellow-brown solid, mp 184-186 °C,$[\alpha]^{20}_{D}$ +58.8 (*c* 0.1, MeOH). Its molecular formula was established as $C_{14}H_{16}O_5$ by HRESIMS data (*m/z* 287.0883 $[M+Na]^+$, calcd 287.0890). Analysis of ^{13}C NMR and HMQC spectra of **16** revealed the presence of one conjugated ketone carbonyl (δ_C 207.2), one ester carbonyl (δ_C 169.1), four quaternary carbons (δ_C 159.2, 156.9, 135.3 and 122.4), three methines (δ_C 109.8, 101.6 and 73.8), four methylenes (δ_C 45.7, 40.0, 36.8 and 22.6) and one methyl carbon (δ_C 20.4). The ^{1}H NMR spectrum displayed signals for phenolic proton(s) (δ_H 8.97), two *meta*-coupled aromatic protons (δ_H 6.38 (d, *J* = 2.1 Hz) and 6.24 (d, *J* = 1.6 Hz)], one methine (δ_H 4.70) bearing an oxygen atom of the lactone ring, eight methylene protons (δ_H 3.98-1.43), and one methyl doublet (δ_H 1.10). The upfield signals of two *meta*-coupled aromatic methines (δ_H 6.24/δ_C 109.8 and δ_H 6.38/δ_C 101.6) suggested the existence of 1,3-dihydroxy substituents. The partial structure of -CH_2-CH_2-CH_2-$CH(CH_3)$- was supported by COSY spectroscopic data. HMBC correlations from methylene protons, H_2-8 and H_2-9, to ketone carbonyl at δ_C 207.2 (C-7); from methylene H_2-13 to ester carbonyl C-12 (δ_C 169.1); and from aromatic proton H-4 to methylene carbon C-13 supported the remaining lactone

cyclic and the attachment to 1,3-dihydroxybenzene ring (Fig. 4.15). These results strongly indicated that compound **16** was identical to xestodecalactone A [67].

Table 4.5 NMR data of compound **16** in acetone-d_6

Position	**16**	
	δ_C	δ_H (mult, *J* in Hz)
1	156.9	
2	101.6	6.38, d (2.1)
3	159.2	
4	109.8	6.24, d (1.6)
5	135.3	
6	122.4	
7	207.2	
8	45.7	2.96, m 2.69, ddd (15.7, 8.5, 1.6)
9	22.6	1.96-1.74, m[a]
10	36.8	1.96-1.74, m[a] 1.43, m
11	73.8	4.70, d sex (2.1. 6.3)
12	169.1	
13	40.0	3.98, d (18.3) 3.44, d (18.4)
14	20.4	1.10, d (6.2)
Ar-OH		8.97, br

[a] Overlapping signal.

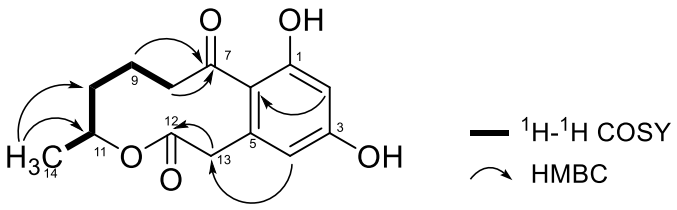

Figure 4.16 ^{1}H–^{1}H COSY and key HMBC correlations of **16**

Compound **17** was obtained as pale yellow brown gum, $[\alpha]^{20}_{D}$ +196.4 (*c* 0.1, MeOH). Its molecular formula was established as $C_{14}H_{16}O_6$ by HRESIMS data (*m/z* 303.0841 $[M+Na]^+$, calcd 303.0839), indicating one additional oxygen when compared to **16**. Analysis of ^{13}C NMR and HMQC NMR spectra of **17** exposed at one conjugated ketone carbonyl (δ_C 207.9), one ester carbonyl (δ_C 168.9), four quaternary carbons (δ_C 159.7, 157.4, 136.2 and 120.9), four methines (δ_C 110.2, 101.5, 67.8 and 65.9), three methylene (δ_C 49.9, 42.4 and 40.3) and one methyl carbon (δ_C 19.7). The NMR spectrum contained signals for two aromatic protons (δ_H 6.28 and 6.41), one methine (δ_H 5.03) bearing an oxygen atom of the lactone ring, one hydroxymethine (δ_H 4.17), six methylene protons (δ_H 3.90-1.78) and one methyl doublet (δ_H 1.18). The partial structure of -CH_2-CH-CH_2-CH(CH_3)- was supported by COSY spectroscopic data. Analysis of its 2D NMR data suggested similar chemical structures between **17** and **16** with the exception that a methylene (δ_H 1.96-1.74/δ_C 22.6, CH_2-9) of **16** was replaced by a hydroxymethine [δ_H 4.17/δ_C 65.9, CH-9] in **17**. The planar structure of compound **16** was identical to the two diastereomers, xestodecalactone B (9,11-*cis*) and xestodecalactone C (9,11-*trans*). However, comparison of NMR data of compound **16** with those published in the literature [67] (Table 4.5) supported that compound **16** was most likely to be assigned as xestodecalactone B.

Table 4.6 NMR data of compound **17** in acetone-d_6

Position	**17**	
	δ_C	δ_H (mult, *J* in Hz)
1	157.4	
2	101.5	6.41, d (2.0)
3	159.7	
4	110.2	6.28, d (1.3)
5	136.2	
6	120.9	
7	207.9	
8	49.9	3.40, dd (15.3, 2.1) 2.89, ddd (15.7, 8.5, 1.6)
9	65.9, CH	4.17, tt
10	42.4	1.98, ddd (14.8, 7.3, 3.2) 1.78, ddd (14.8, 9.3, 2.1)
11	67.8	4.70, ddd (1.18, 1.78, 2.89)
12	168.9	
13	40.3	3.90, d (18.1) 3.52, d (18.1)
14	19.7	1.18, d (6.4)

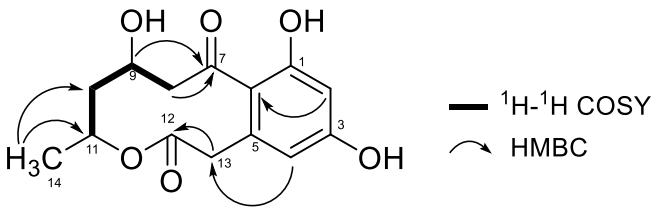

Figure 4.17 ^{1}H–^{1}H COSY and key HMBC correlations of **17**

Compound **18** was obtained as a pale yellow brown gum, $[\alpha]^{20}_{D}$ +50.40 (*c* 0.1, MeOH). Its molecular formula was established as $C_{14}H_{18}O_5$ by ESIMS data (*m/z* 281.10 $[M+H]^+$, calcd 281.10) with seven degrees of unsaturation. Investigation of ^{13}C NMR and HSQC spectra of **18** indicated the presence of a conjugated ketone carbonyl (δ_C 191.4), an ester carbonyl (δ_C 171.1), four quaternary carbons (δ_C 164.7, 162.6, 139.6 and 113.1), four methines (δ_C 114.0, 102.1, 75.5 and 63.2), three methylenes (δ_C 43.8, 43.3 and 40.1), and one methyl carbon (δ_C 23.2). The ^1H NMR spectrum revealed signals for two aromatic protons (δ_H 6.41, 6.36), one methine (δ_H 4.60) bearing an oxygen atom of the lactone ring, one hydroxymethine (δ_H 4.01), six methylene protons (δ_H 3.93-1.78) and one methyl doublet (δ_H 1.22). The partial structure of $-CH_2-CH-CH_2-CH(CH_3)-$ was supported by COSY spectroscopic data. HMBC correlations were observed from methylene protons, H_2-8, and a methine H-9, to ketone carbonyl at δ_C 191.4 (C-7); from methylene H_2-14 to ester carbonyl C-13 (δ_C 171.1); and from aromatic proton H-4 to methylene carbon C-14. These data supported the same partial structures as those of **17**, which possessed the same molecular formula. However, the downfield chemical shifts of CH-9 (δ_H 4.60/δ_C 75.5) comparing to chemical shift of CH-11 (δ_H 4.01/δ_C 63.2) suggested that the methine proton H-9 was attached to oxygen of the lactone ring instead of the hydroxy group. Therefore, the 8-membered cylic lactone was proposed as the partial structure of **18**, instead of 10-membered lactone as described for **16** and **17**. The planar structure of compound **18** was identical to the two diastereomers, coryoctalactones A and B. However, NMR data of compound **16** were consitent with those published in the literature for coryoctalactone B [68] (Table 4.6).

Table 4.7 NMR data of compound **18** in acetone-d_6

Position	**18**	
	δ_C	δ_H (mult, *J* in Hz)
1	164.7, qC[a]	
2	102.1	6.36, d (2.2)
3	162.6, qC[a]	
4	114.0	6.41, d (2.4)
5	139.6	
6	113.1	
7	191.4	
8	43.3	2.62
9	75.5	4.60, dq (8.8, 6.5)
10	43.8	2.01, ddd (14.8, 7.3, 3.2) 1.78, ddd (14.8, 9.3, 2.1)
11	63.2	4.01, m
12	23.2	1.22, d (6.2)
13	171.1	
14	40.1	3.93, d (4.6)

[a] Interchangeable signal

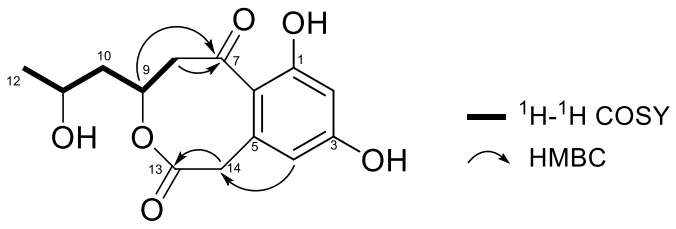

Figure 4.18 ^{1}H–^{1}H COSY and key HMBC correlations of **18**

Compound **19** was obtained as a green solid, mp 140-144 °C Its molecular formula was established as $C_{20}H_{18}O_5$ by HRESIMS data (*m/z* 361.1047 $[M+Na]^+$, calcd 361.1046), indicating twelve degrees of unsaturation. The ^{13}C NMR and HMQC spectra of **17** indicated the presence of one ester carbonyl (δ_C 168.1), seven quaternary sp^2 carbons (δ_C 163.2, 160.3, 159.8, 141.2, 125.8, 121.7 and 105.1), nine sp^2 aromatic/olefinic methines (δ_C 2 x 131.9, 2 x 131.2, 2 x 114.3, 2 x 113.6 and 106.9), and three methoxy carbons (δ_C 60.5, 54.8 and 54.7). Its ^1H NMR spectrum displayed signals of eight *ortho*-coupled aromatic protons, an olefinic proton, and three methoxy groups. Two methoxyphenyl groups in the molecule were assigned based on COSY cross peaks (between H-8/H-9, H-11/H-12, H-2'/H-3', and H-5'/H-6'), and HMBC correlations from 10-OCH_3 to C-10; H-8 and H-12 to C-10; H-9 and H-11 to C-7; 4'-OCH_3 to C-4'; H-2' and H-6' to C-4'; H-3' and H-5' to C-1'. HMBC correlations from 4-OCH_3 to C-4; H-6 to C-4, C-5, C-8, and C-12; H-8 and H-12 to C-6; H-2' to C-3; and H-6' to C-3 supported a remaining of furanone ring and its attachment to a methoxybenzylidene and a methoxyphenyl group. Spectroscopic data comparison between compound **19** with those published in the literature [69] indicated that compound **19** was dimethoxy-*O*-methylpulvinone.

Table 4.8 NMR data of compound **19** in acetone-d_6

Position	**19**	
	δ_C	δ_H (mult, *J* in Hz)
2	168.1	
3	105.1	
4	163.2	
5	141.2	
6	106.9	6.36, s
7	125.8	
8	131.9	7.79, td (1.8, 8.8)

9	114.3	7.03, dd (8.9, 2.9)
10	160.3	
11	114.3	7.03, dd (8.9, 2.9)
12	131.9	7.79, td (1.8, 8.8)
1’	121.7	
2’	131.2	7.55, td (2.1, 8.8)
3’	113.6	7.03, dd (8.9, 2.9)
4’	159.8	
5’	113.6	7.03, dd (8.9, 2.9)
6’	131.2	7.55, td (2.1, 8.8)
4-OMe	60.5, CH_3[a]	3.92, s[b]
10-OMe	54.8, CH_3	3.86, s
4’-OMe	54.7, CH_3[a]	3.85, s[b]

[a,b] Interchangeable signals.

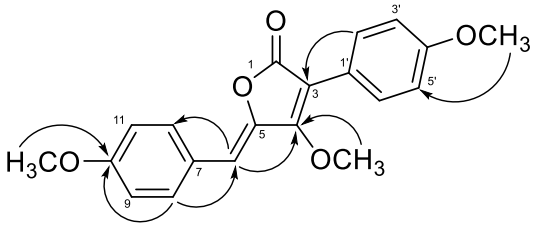

Figure 4.19 Key HMBC correlations of 19

4.7.2 Antimalarial activity and cytotoxic activity

Pure isolated compounds (**14**, **16** and **19**) were evaluated for antimalarial activity against *Plasmodium falciparum* K1 and cytotoxicity against African green monkey kidney fibroblast (Vero) cells. Compound **19** exhibited antimalarial activity against *Plasmodium falciparum* K1 with IC_{50} of 16.9 μM and **14** exhibited cytotoxic activity against Vero cell lines with an IC_{50} of 50.9 μM. Dihydroartemisinin (IC_{50} value

of 0.002 μM) and ellipticine (IC_{50} value of 0.003 μM) were used as positive controls, respitively.

4.8 Conclusion

The aims of this study are to investigate and structural elucidate bioactive compounds from marine-derived fungus *A. nypae*, BCC 3553 isolated from *N. fruticans*. Purification of EtOAc crude extract (broth and mycelium) of *A. nypae* cultured on LCN medium broth by chromatographic technique led to the isolation of three new; astronypyrone(**13**)**,** astronyquinone (**14**) and astronyurea (**15**), along with four known compound; xestodecalactones A,B (**16-17**), coryoctalactone B (**18**) and dimethoxy-*O*-methylpulvinone (**19**). Three metabolites (**14, 16** and **19**) were evaluated for their biological activities including antimalarial activity against *Plasmodium falciparum* K1 and toxicity against Vero cell lines (*African green monkey* kidney *cell line*). Only **19** exhibited antimalarial activity K1 with an IC_{50} value of 16.9 μM, while **14** exhibited toxicity against Vero cell lines with an IC_{50} value of 50.9 μM.

CHAPTER V

CONCLUSION

The objectives of this research are to investigate and structural elucidate bioactive compounds from endophytic fungi isolated from Thai mangrove plants and marine fungi. A total of 64 pure isolates of endophytic fungi were isolated from seven species of Thai mangroves, *L. racemosa*, *T. spathacea*, *X. granatum*, *A. sarmentosa*, *B. gymnorrhiza*, *B. cylindrical* and *S. trilobatum*. Based on characteristic ^{1}H NMR data for its metabolites, the fungus *Rhytidhysteron rufulum* was selected for large scale cultivation and isolation. This fungus was isolated from *B. gymnorrhiza*. Purification of the EtOAc extracts led to the isolation of five new chromone derivatives, rhytidchromones A-E (**1-5**), one new isocoumarin derivative (**6**) and one known α-D-galacto pyranoside methyl (**7**).

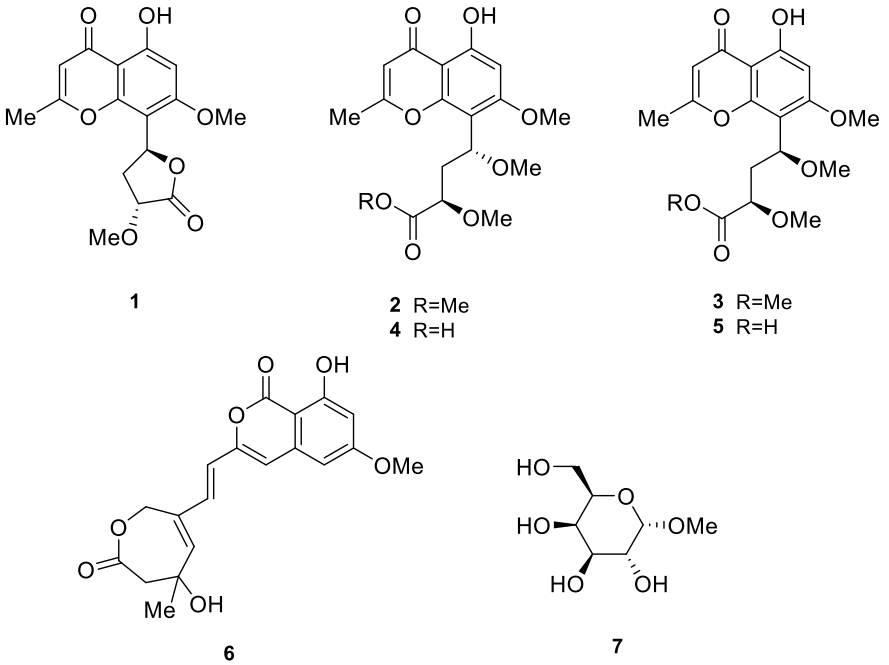

Figure 5.1 Metabolites of an endophytic fungus *R.rufulum*

Rhytidchromone A (**1**) showed weak cytotoxicity against Hep-G2, KATO-3 and MCF-7 with IC_{50} values of 29.3, 23.4 and 19.3 μM, respectively. Rhytidchromones B (**2**) and D (**4**) were active only for KATO-3 with IC_{50} values of 21.4 and 16.3 μM, respectively. Rhytidchromone E (**5**) showed weak cytotoxicity against Hep-G2, KATO-3, MCF-7 and CaSki with IC_{50} values of 24.9, 16.0, 17.7 and 25.3 μM, respectively. However, rhytidchromone C (**3**), compounds **6** and **7** did not show any significant activity against all tested cell lines.

In order to study anti-angiogenic activity of sesquiterpene endoperoxides from a basidiomycetous XG8D fungus of the Thai mangrove plant *X.granatum*. Purification of its EtOAc extract by chromatographic technique led to the isolation of one new chamigrane endoperoxide, merulin D (**11**), and four known derivatives, merulins A-C (**8-10**) and steperoxide A (**12**).

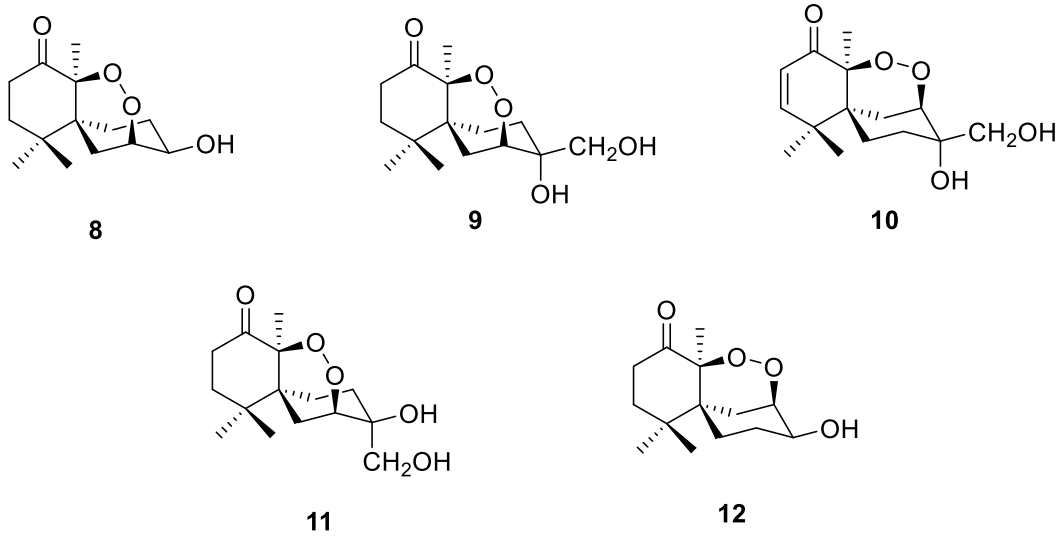

Figure 5.2 Metabolites of a basidiomycetous endophytic fungus XG8D

Only merulin C (**10**) displayed strong activity with complete inhibition of microvessel sprouting from rings at a concentration of 2.5 μM and its potent activity was mainly provided by suppression of endothelial cell proliferation and migration. Its effect is mediated by reduction in the phosphorylation of Erk1/2 which is the result of proliferation.

In addition, investigation of chemical components of a marine-derived fungus *Astrophaeriella nypae*, BCC 3553 isolated from *Nypa fruticans* was performed. Purification of EtOAc crude extract (broth and mycelium) of the fungus cultured on LCN medium broth led to the isolation of three new, astronypyrone(**13**), astronyquinone (**14**) and astronyurea (**15**), along with four known compounds, xestodecalactones A and B (**16-17**), coryoctalactone B (**18**) and dimethoxy-*O*-methylpulvinone (**19**).

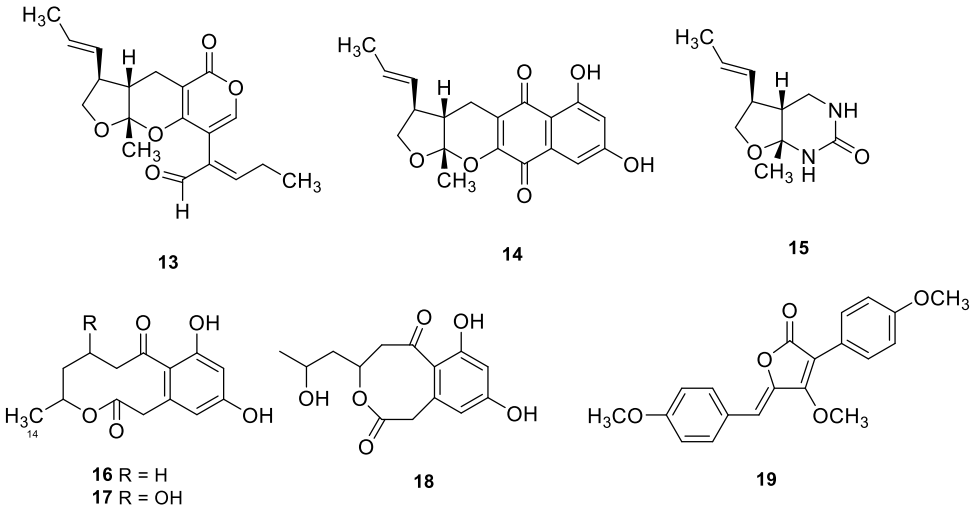

Figure 5.3 Metabolites from a marine fungus *A.nypae*

Compounds **14, 16** and **19** were evaluated for their antimalarial activity against *Plasmodium falciparum* K1 and toxicity against Vero cell lines (*African green monkey* kidney *cell line*). Only **19** exhibited antimalarial activity with an IC_{50} value of 16.9 μM and **14** exhibited cytotoxic activity against Vero cell lines with an IC_{50} value of 50.9 μM.

REFERENCES

[1] Organization, W.H. World cancer report, 2014. WHO Report. Geneva: WHO (2014).

[2] Kumar, R., et al. CancerDR: Cancer Drug Resistance Database. Sci. Rep. 3 (2013).

[3] Faltas, B. Cornering metastases: therapeutic targeting of circulating tumor cells and stem cells. Frontiers in Oncology 2 (2012).

[4] K S Jagadish, A.R.P., V.N.Sutariya, S T Shukla, P V Habbu, V H Kulkarni. Need to study of endophytes to obtain bioactive compounds and their pharmacological relevance. 2014. Vol. 2, 2014.

[5] Shweta, S., et al. Endophytic fungal strains of Fusarium solani, from Apodytes dimidiata E. Mey. ex Arn (Icacinaceae) produce camptothecin, 10-hydroxycamptothecin and 9-methoxycamptothecin. Phytochemistry 71(1) (2010): 117-122.

[6] Farquhar, D., Cherif, A., Bakina, E., and Nelson, J.A. Intensely Potent Doxorubicin Analogues: Structure–Activity Relationship. Journal of Medicinal Chemistry 41(6) (1998): 965-972.

[7] Owellen, R.J. and Donigian, D.W. [3H]-Vincristine. Preparation and preliminary pharmacology. Journal of Medicinal Chemistry 15(9) (1972): 894-898.

[8] Johnson, T.A., et al. Natural Product Libraries to Accelerate the High-Throughput Discovery of Therapeutic Leads. Journal of Natural Products 74(12) (2011): 2545-2555.

[9] Cragg, G.M. and Newman, D.J. Natural products: A continuing source of novel drug leads. Biochimica et Biophysica Acta - General Subjects 1830(6) (2013): 3670-3695.

[10] Knapp, C.W., Dolfing, J., Ehlert, P.A.I., and Graham, D.W. Evidence of Increasing Antibiotic Resistance Gene Abundances in Archived Soils since 1940. Environmental Science & Technology 44(2) (2009): 580-587.

[11] Wang, J., Zhang, Z., and Tan, R. Stimulation of artemisinin production in Artemisia annua hairy roots by the elicitor from the endophytic Colletotrichum sp. Biotechnology Letters 23(11) (2001): 857-860.

[12] Aly, A., Debbab, A., and Proksch, P. Fifty years of drug discovery from fungi. Fungal Diversity 50(1) (2011): 3-19.

[13] Faseleh Jahromi, M., Liang, J.B., Ho, Y.W., Mohamad, R., Goh, Y.M., and Shokryazdan, P. Lovastatin Production by Aspergillus terreus Using Agro-Biomass as Substrate in Solid State Fermentation. Journal of Biomedicine and Biotechnology 2012 (2012): 11.

[14] Ahn, E.Y., Shrestha, A., Hoang, N.H., Huong, N.L., Yoon, Y.J., and Park, J.W. Structural characterization of cyclosporin A, C and microbial bio-transformed cyclosporin A analog AM6 using HPLC–ESI–ion trap-mass spectrometry. Talanta 123 (2014): 89-94.

[15] Liu, D., et al. Nigerapyrones A–H, α-Pyrone Derivatives from the Marine Mangrove-Derived Endophytic Fungus Aspergillus niger MA-132. Journal of Natural Products 74(8) (2011): 1787-1791.

[16] Ding, L., Dahse, H.-M., and Hertweck, C. Cytotoxic Alkaloids from Fusarium incarnatum Associated with the Mangrove Tree Aegiceras corniculatum. Journal of Natural Products 75(4) (2012): 617-621.

[17] Meng, L.-H., Li, X.-M., Lv, C.-T., Huang, C.-G., and Wang, B.-G. Brocazines A–F, Cytotoxic Bisthiodiketopiperazine Derivatives from Penicillium brocae MA-231, an Endophytic Fungus Derived from the Marine Mangrove Plant Avicennia marina. Journal of Natural Products 77(8) (2014): 1921-1927.

[18] Pudhom, K., Teerawatananond, T., and Chookpaiboon, S. Spirobisnaphthalenes from the Mangrove-Derived Fungus Rhytidhysteron sp. AS21B. Marine Drugs 12(3) (2014): 1271-1280.

[19] Fukai, M., et al. Hypoxylonols C–F, Benzo[j]fluoranthenes from Hypoxylon truncatum. Journal of Natural Products 75(1) (2012): 22-25.

[20] Kang, H., Seo, C., and Park, Y. Marine Peptides and Their Anti-Infective Activities. Marine Drugs 13(1) (2015): 618.

[21] Sirirak, T., Kittiwisut, S., Janma, C., Yuenyongsawad, S., Suwanborirux, K., and Plubrukarn, A. Kabiramides J and K, Trisoxazole Macrolides from the Sponge Pachastrissa nux. Journal of Natural Products 74(5) (2011): 1288-1292.

[22] Mishra, B.B. and Tiwari, V.K. Natural products: An evolving role in future drug discovery. European Journal of Medicinal Chemistry 46(10) (2011): 4769-4807.

[23] Aly, A.H., Debbab, A., and Proksch, P. Fungal endophytes – secret producers of bioactive plant metabolites. Die Pharmazie - An International Journal of Pharmaceutical Sciences 68(7) (2013): 499-505.

[24] Kaul, S., Gupta, S., Ahmed, M., and Dhar, M. Endophytic fungi from medicinal plants: a treasure hunt for bioactive metabolites. Phytochemistry Reviews 11(4) (2012): 487-505.

[25] Strobel, G. and Daisy, B. Bioprospecting for Microbial Endophytes and Their Natural Products. Microbiology and Molecular Biology Reviews 67(4) (2003): 491-502.

[26] Sithranga Boopathy, N. and Kathiresan, K. Anticancer Drugs from Marine Flora: An Overview. Journal of Oncology 2010 (2010).

[27] Soliman, S.S.M., Tsao, R., and Raizada, M.N. Chemical Inhibitors Suggest Endophytic Fungal Paclitaxel Is Derived from Both Mevalonate and Non-mevalonate-like Pathways. Journal of Natural Products 74(12) (2011): 2497-2504.

[28] Chandra, S. Endophytic fungi: Novel sources of anticancer lead molecules. Applied Microbiology and Biotechnology 95(1) (2012): 47-59.

[29] Deshmukh, S.K., Verekar, S., and Bhave, S.V. Endophytic Fungi: A Reservoir of Antibacterials. Frontiers in Microbiology 5 (2015).

[30] Eyberger, A.L., Dondapati, R., and Porter, J.R. Endophyte Fungal Isolates from Podophyllum peltatum Produce Podophyllotoxin. Journal of Natural Products 69(8) (2006): 1121-1124.

[31] Strobel, G.A. Rainforest endophytes and bioactive products. Critical Reviews in Biotechnology 22(4) (2002): 315-333.

[32] Xu, J., et al. Chromones from the Endophytic Fungus Pestalotiopsis sp. Isolated from the Chinese Mangrove Plant Rhizophora mucronata. Journal of Natural Products 72(4) (2009): 662-665.

[33] Huang, H., et al. Azaphilones and p-Terphenyls from the Mangrove Endophytic Fungus Penicillium chermesinum (ZH4-E2) Isolated from the South China Sea. Journal of Natural Products 74(5) (2011): 997-1002.

[34] Xiao, Z.e., et al. Asperterpenols A and B, New Sesterterpenoids Isolated from a Mangrove Endophytic Fungus Aspergillus sp. 085242. Organic Letters 15(10) (2013): 2522-2525.

[35] An, C.-Y., et al. 4-Phenyl-3,4-dihydroquinolone Derivatives from Aspergillus nidulans MA-143, an Endophytic Fungus Isolated from the Mangrove Plant Rhizophora stylosa. Journal of Natural Products 76(10) (2013): 1896-1901.

[36] Zhou, Z.-F., et al. Penibruguieramine A, a Novel Pyrrolizidine Alkaloid from the Endophytic Fungus Penicillium sp. GD6 Associated with Chinese Mangrove Bruguiera gymnorrhiza. Organic Letters 16(5) (2014): 1390-1393.

[37] Liu, Y., et al. Polyketides with α-Glucosidase Inhibitory Activity from a Mangrove Endophytic Fungus, Penicillium sp. HN29-3B1. Journal of Natural Products 78(8) (2015): 1816-1822.

[38] Rukachaisirikul, V., Chantaruk, S., Pongcharoen, W., Isaka, M., and Lapanun, S. Chromone Derivatives from the Filamentous Fungus Lachnum sp. BCC 2424. Journal of Natural Products 69(6) (2006): 980-982.

[39] König, W.A., Lutz, S., Mischnick-Lübbecke, P., Brassat, B., and Wenz, G. Cyclodextrins as chiral stationary phases in capillary gas chromatography I. Pentylated α-cyclodextrin. Journal of Chromatography A 447(0) (1988): 193-197.

[40] Albert, R., Dax, K., Pleschko, R., and Stütz, A.E. Tetrafluoroboric acid, an efficient catalyst in carbohydrate protection and deprotection reactions. Carbohydrate Research 137(0) (1985): 282-290.

[41] Folkman, J. and Shing, Y. Angiogenesis. Journal of Biological Chemistry 267(16) (1992): 10931-10934.

[42] Al-Husein, B., Abdalla, M., Trepte, M., DeRemer, D.L., and Somanath, P.R. Anti-angiogenic therapy for cancer: An update. Pharmacotherapy 32(12) (2012): 1095-1111.

[43] Ferrara, N. Vascular Endothelial Growth Factor: Basic Science and Clinical Progress. Endocrine Reviews 25(4) (2004): 581-611.

[44] Hoeben, A., Landuyt, B., Highley, M.S., Wildiers, H., Van Oosterom, A.T., and De Bruijn, E.A. Vascular Endothelial Growth Factor and Angiogenesis. Pharmacological Reviews 56(4) (2004): 549-580.

[45] Hurwitz, H., et al. Bevacizumab plus Irinotecan, Fluorouracil, and Leucovorin for Metastatic Colorectal Cancer. New England Journal of Medicine 350(23) (2004): 2335-2342.

[46] Wang, T.-F. and Lockhart, A.C. Aflibercept in the Treatment of Metastatic Colorectal Cancer. Clinical Medicine Insights. Oncology 6 (2012): 19-30.

[47] Giordano, G., et al. Targeting Angiogenesis and Tumor Microenvironment in Metastatic Colorectal Cancer: Role of Aflibercept. Gastroenterology Research and Practice 2014 (2014): 13.

[48] Wentink, M.Q., Huijbers, E.J.M., de Gruijl, T.D., Verheul, H.M.W., Olsson, A.-K., and Griffioen, A.W. Vaccination approach to anti-angiogenic treatment of cancer. Biochimica et Biophysica Acta (BBA) - Reviews on Cancer 1855(2) (2015): 155-171.

[49] Chokpaiboon, S., Sommit, D., Teerawatananond, T., Muangsin, N., Bunyapaiboonsri, T., and Pudhom, K. Cytotoxic Nor-chamigrane and Chamigrane Endoperoxides from a Basidiomycetous Fungus. Journal of Natural Products 73(5) (2010): 1005-1007.

[50] Baker, M., et al. Use of the mouse aortic ring assay to study angiogenesis. Nat. Protocols 7(1) (2012): 89-104.

[51] Kim, K.S., et al. Anti-angiogenic Activity of the Recombinant Kringle Domain of Urokinase and Its Specific Entry into Endothelial Cells. Journal of Biological Chemistry 278(13) (2003): 11449-11456.

[52] Liu, D.-Z., Dong, Z.-J., Wang, F., and Liu, J.-K. Two novel norsesquiterpene peroxides from basidiomycete Steccherinum ochraceum. Tetrahedron Letters 51(23) (2010): 3152-3153.

[53] Lamalice, L., Le Boeuf, F., and Huot, J. Endothelial Cell Migration During Angiogenesis. Circulation Research 100(6) (2007): 782-794.

[54] Arnaoutova, I. and Kleinman, H.K. In vitro angiogenesis: endothelial cell tube formation on gelled basement membrane extract. Nat. Protocols 5(4) (2010): 628-635.

[55] Marco, E., David-Cordonnier, M.-H., Bailly, C., Cuevas, C., and Gago, F. Further Insight into the DNA Recognition Mechanism of Trabectedin from the Differential Affinity of Its Demethylated Analogue Ecteinascidin ET729 for the Triplet DNA Binding Site CGA. Journal of Medicinal Chemistry 49(23) (2006): 6925-6929.

[56] González-Santiago, L., et al. Proteomic Analysis of the Resistance to Aplidin in Human Cancer Cells. Journal of Proteome Research 6(4) (2007): 1286-1294.

[57] Liu, Q.-A., Zheng, J.-J., Gu, Y.-C., Wang, C.-Y., and Shao, C.-L. Chapter 7 - The Chemistry and Bioactivity of Macrolides from Marine Microorganisms. in Atta ur, R. (ed.)Studies in Natural Products Chemistry, pp. 353-401: Elsevier, 2015.

[58] Kanoh, K., et al. (−)-Phenylahistin: A new mammalian cell cycle inhibitor produced by aspergillus ustus. Bioorganic & Medicinal Chemistry Letters 7(22) (1997): 2847-2852.

[59] Ohkawa, Y., et al. Antiangiogenic Metabolites from a Marine-Derived Fungus, Hypocrea vinosa. Journal of Natural Products 73(4) (2010): 579-582.

[60] Li, C.-S., et al. Triazole and Dihydroimidazole Alkaloids from the Marine Sediment-Derived Fungus Penicillium paneum SD-44. Journal of Natural Products 74(5) (2011): 1331-1334.

[61] Sun, L.-L., et al. New bisabolane sesquiterpenoids from a marine-derived fungus Aspergillus sp. isolated from the sponge Xestospongia testudinaria. Bioorganic & Medicinal Chemistry Letters 22(3) (2012): 1326-1329.

[62] Sun, L., Li, D., Tao, M., Chen, Y., Dan, F., and Zhang, W. Scopararanes C–G: New Oxygenated Pimarane Diterpenes from the Marine Sediment-Derived Fungus Eutypella scoparia FS26. Marine Drugs 10(3) (2012): 539-550.

[63] Chen, M., et al. Bioactive Indole Alkaloids and Phenyl Ether Derivatives from a Marine-Derived Aspergillus sp. Fungus. Journal of Natural Products 76(4) (2013): 547-553.

[64] Kong, F., Wang, Y., Liu, P., Dong, T., and Zhu, W. Thiodiketopiperazines from the Marine-Derived Fungus Phoma sp. OUCMDZ-1847. Journal of Natural Products 77(1) (2014): 132-137.

[65] Liu, Y., et al. Bisthiodiketopiperazines and Acorane Sesquiterpenes Produced by the Marine-Derived Fungus Penicillium adametzioides AS-53 on Different Culture Media. Journal of Natural Products 78(6) (2015): 1294-1299.

[66] Trisuwan, K., Rukachaisirikul, V., Sukpondma, Y., Phongpaichit, S., Preedanon, S., and Sakayaroj, J. Lactone Derivatives from the Marine-Derived Fungus Penicillium sp. PSU-F44. Chemical and Pharmaceutical Bulletin 57(10) (2009): 1100-1102.

[67] Edrada, R.A., et al. Online Analysis of Xestodecalactones A–C, Novel Bioactive Metabolites from the Fungus Penicillium cf. montanense and Their Subsequent Isolation from the Sponge Xestospongia exigua#. Journal of Natural Products 65(11) (2002): 1598-1604.

[68] Ebrahim, W., Aly, A.H., Wray, V., Proksch, P., and Debbab, A. Unusual octalactones from Corynespora cassiicola, an endophyte of Laguncularia racemosa. Tetrahedron Letters 54(48) (2013): 6611-6614.

[69] Ojima, N., Takenaka, S., and Seto, S. New butenolides from Aspergillus terreus. Phytochemistry 12(10) (1973): 2527-2529.

APPENDIX

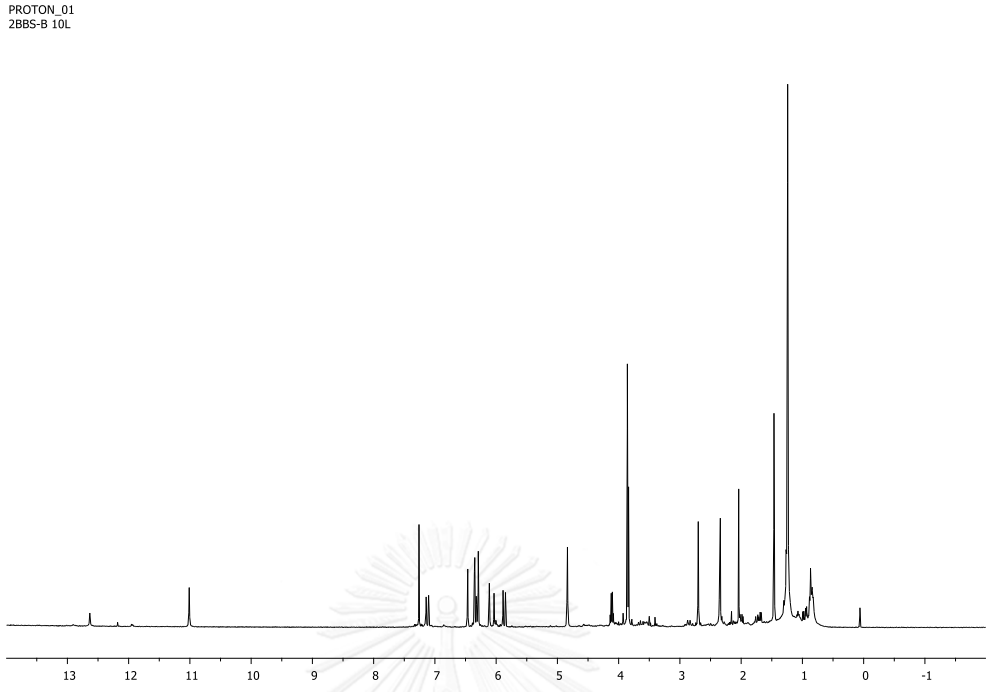

Figure A.1 ^{1}H NMR (400 MHz, $CDCl_3$) spectrum of crude broth (BG2Y cultured on SDB medium)

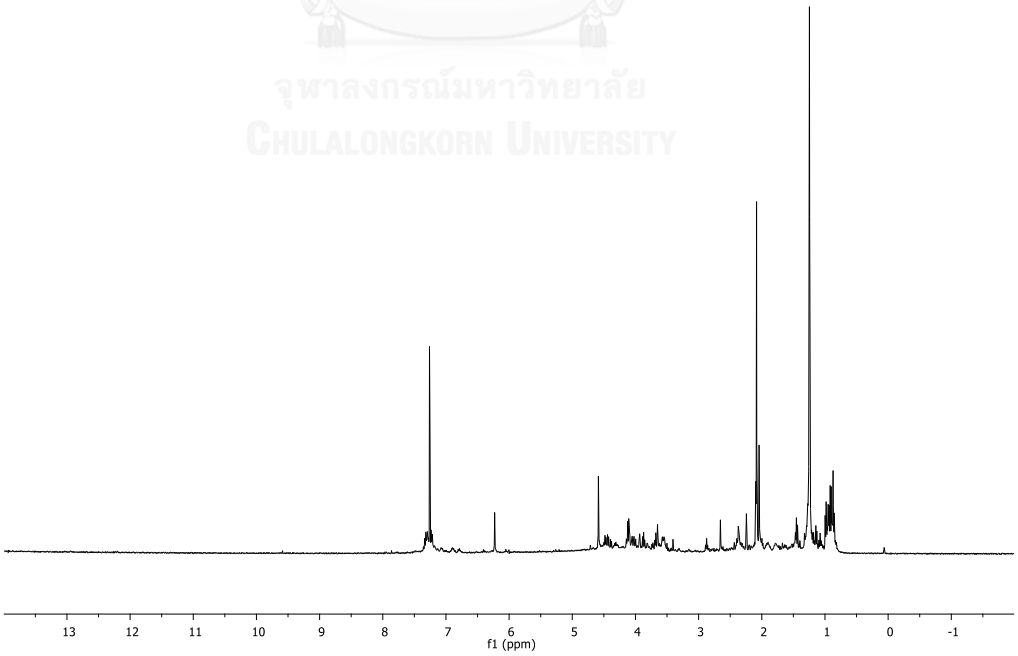

Figure A.2 ^{1}H NMR (400 MHz, $CDCl_3$) spectrum of crude mycelium (BG2Y cultured on SDB medium)

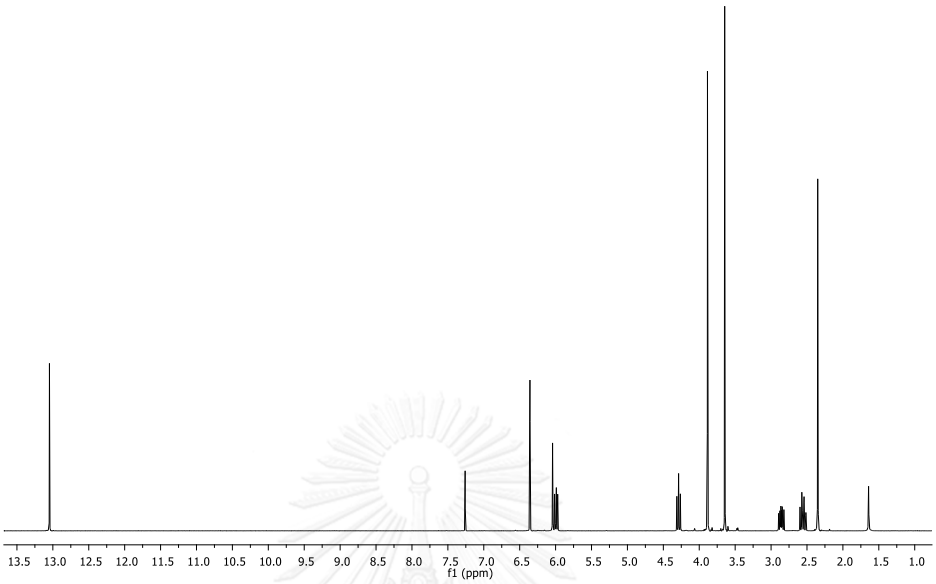

Figure A.3 ^{1}H NMR (400 MHz, $CDCl_3$) spectrum of compound **1**

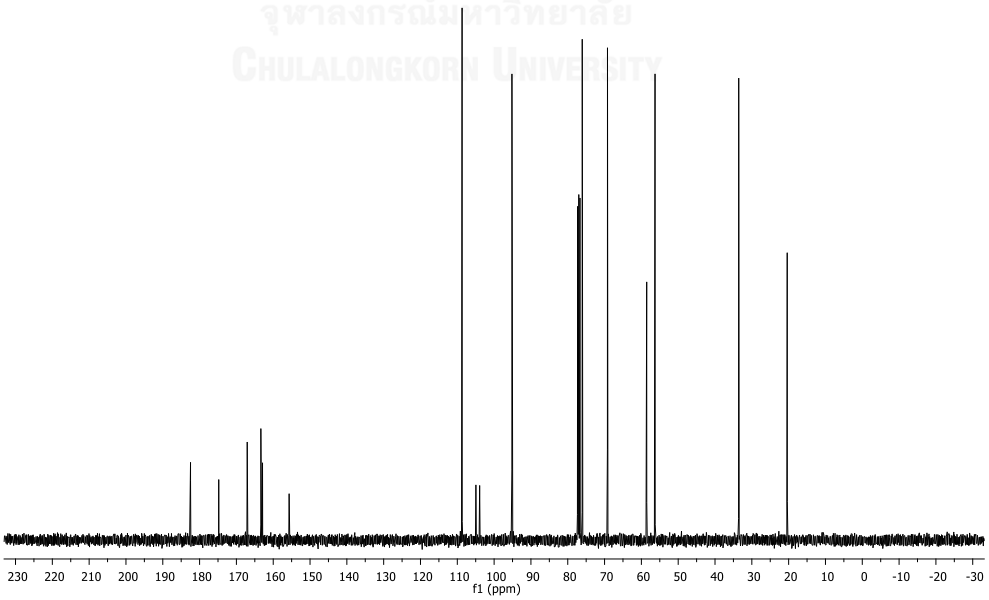

Figure A.4 ^{13}C NMR (100 MHz, $CDCl_3$) spectrum of compound **1**

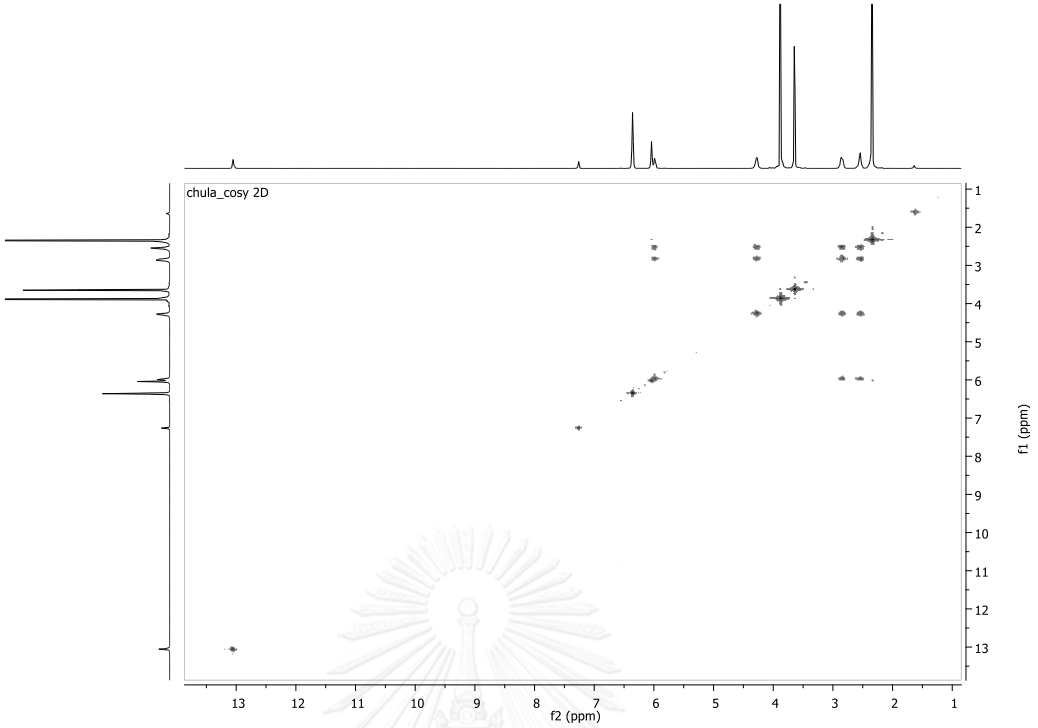

Figure A.5 ^{1}H-^{1}H COSY spectrum ($CDCl_3$) of compound **1**

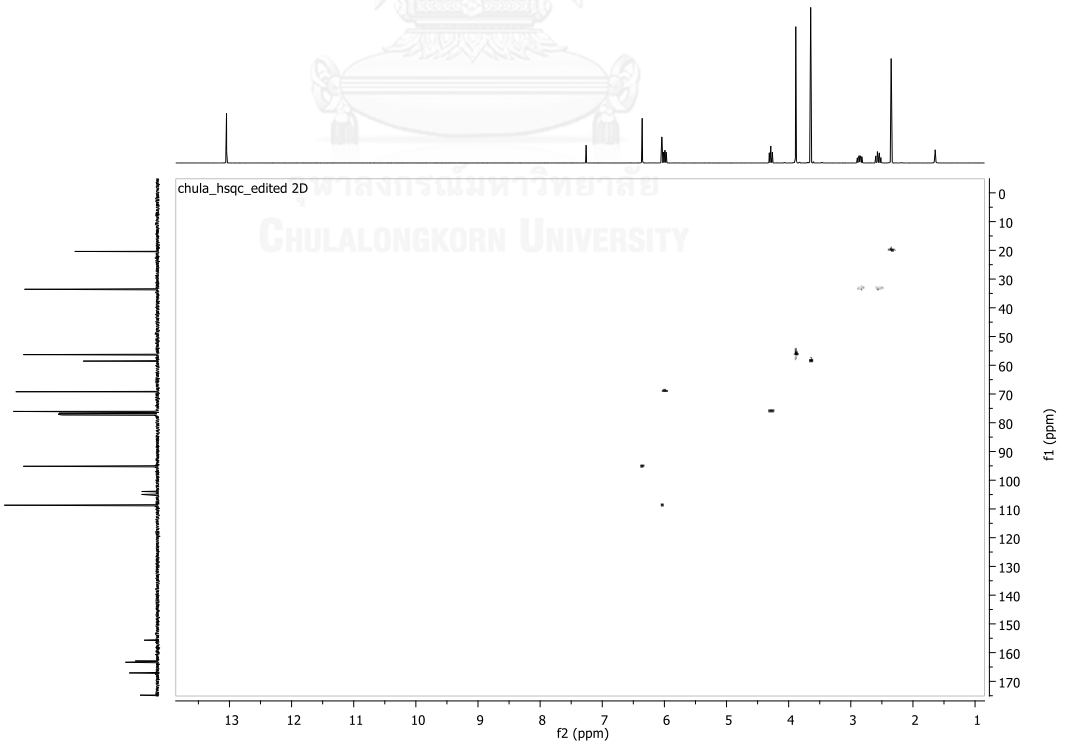

Figure A.6 HSQC spectrum ($CDCl_3$) of compound **1**

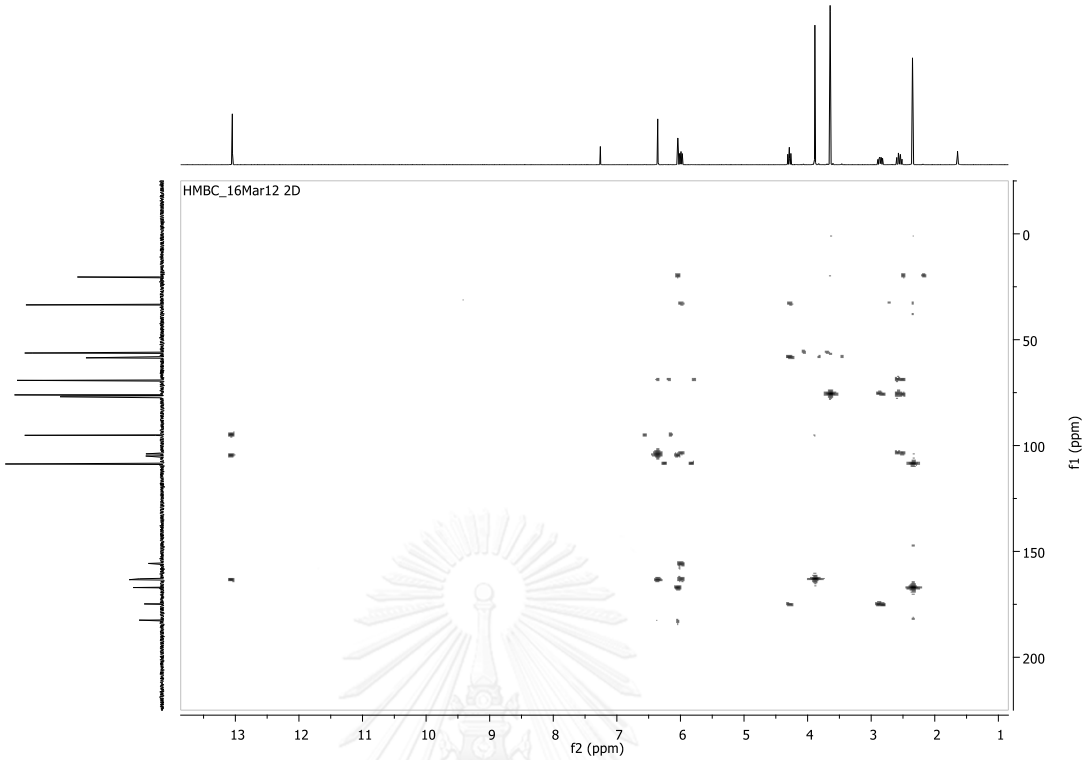

Figure A.7 HMBC spectrum ($CDCl_3$) of compound **1**

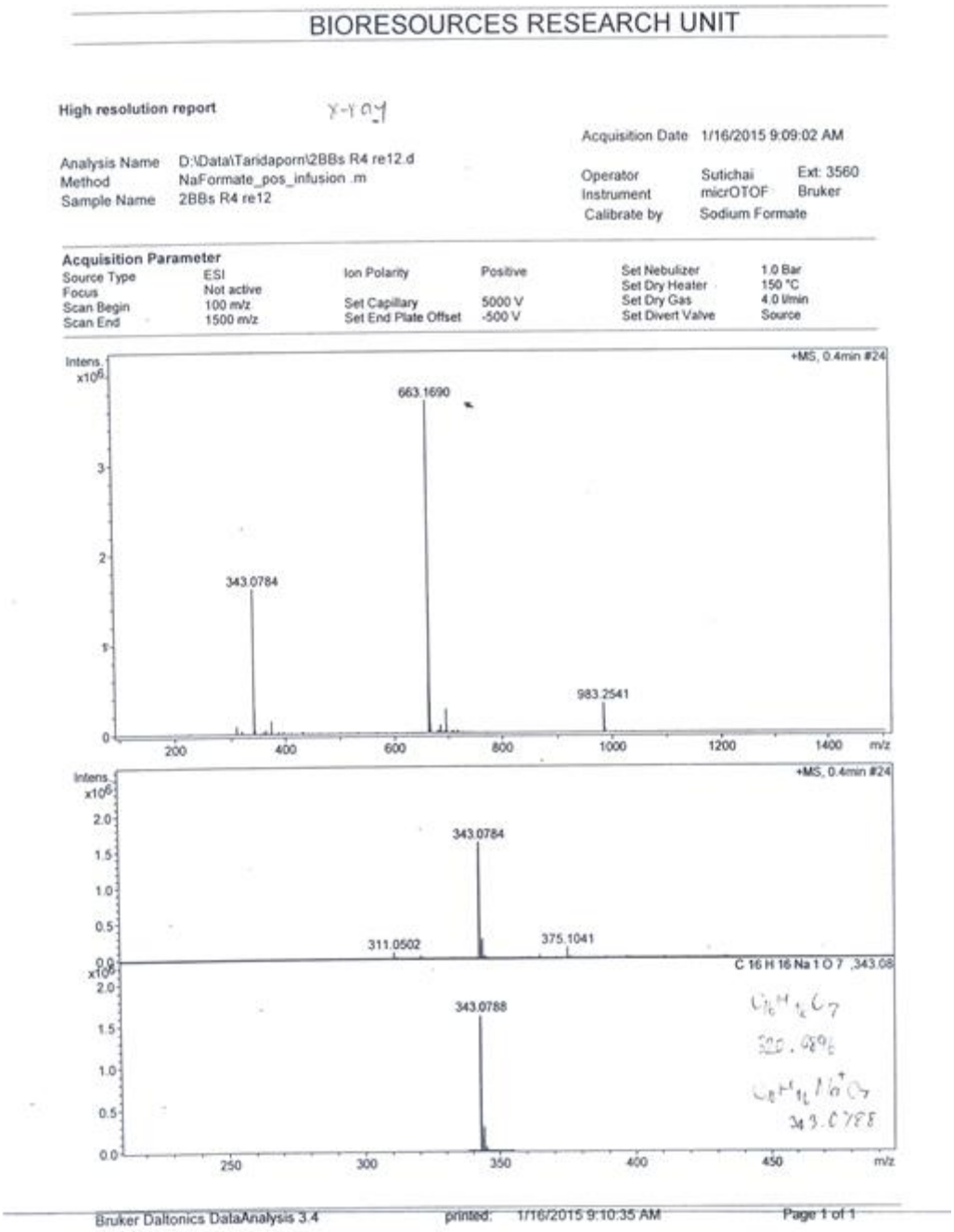

Figure A.8 HRESIMS Mass spectrum of compound **1**

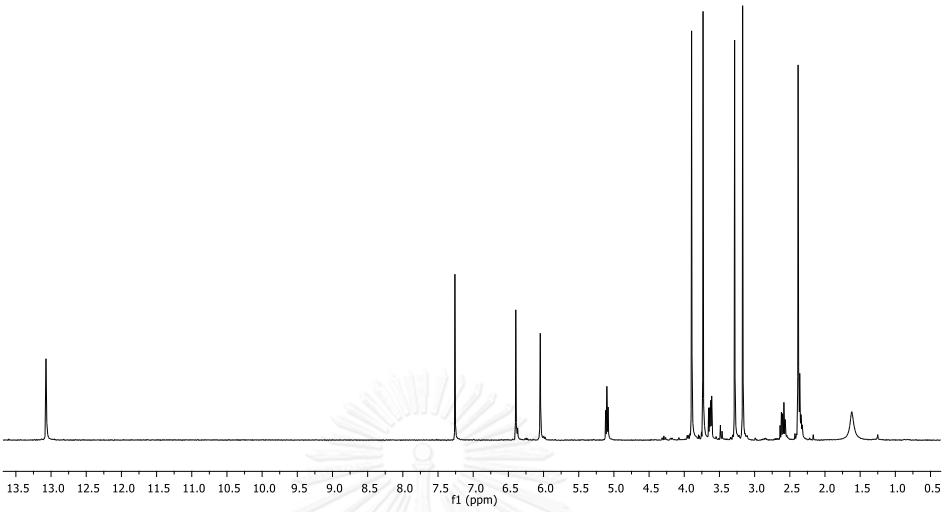

Figure A.9 ^{1}H NMR (400 MHz, $CDCl_3$) spectrum of compound **2**

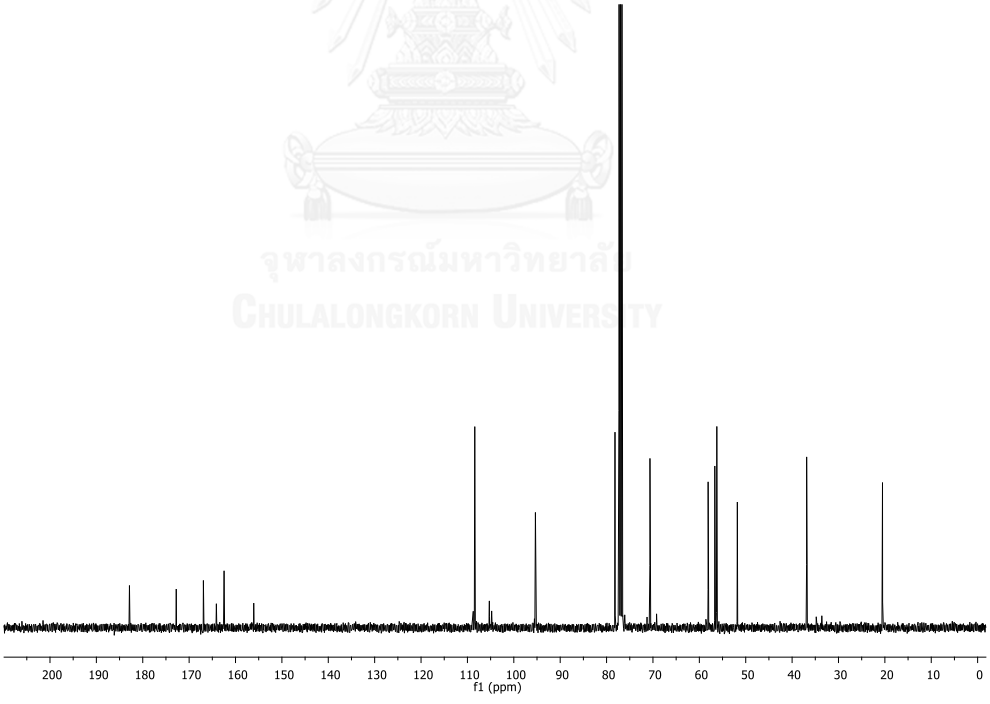

Figure A.10 ^{13}C NMR (100 MHz, $CDCl_3$) spectrum of compound **2**

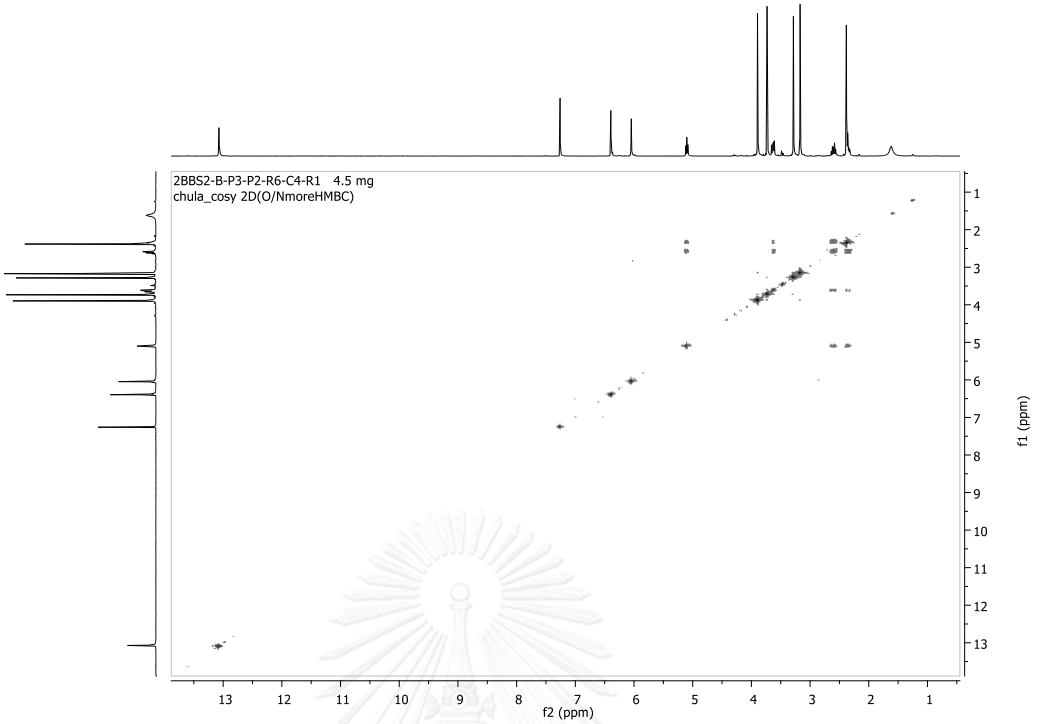

Figure A.11 ^{1}H-^{1}H COSY spectrum ($CDCl_3$) of compound **2**

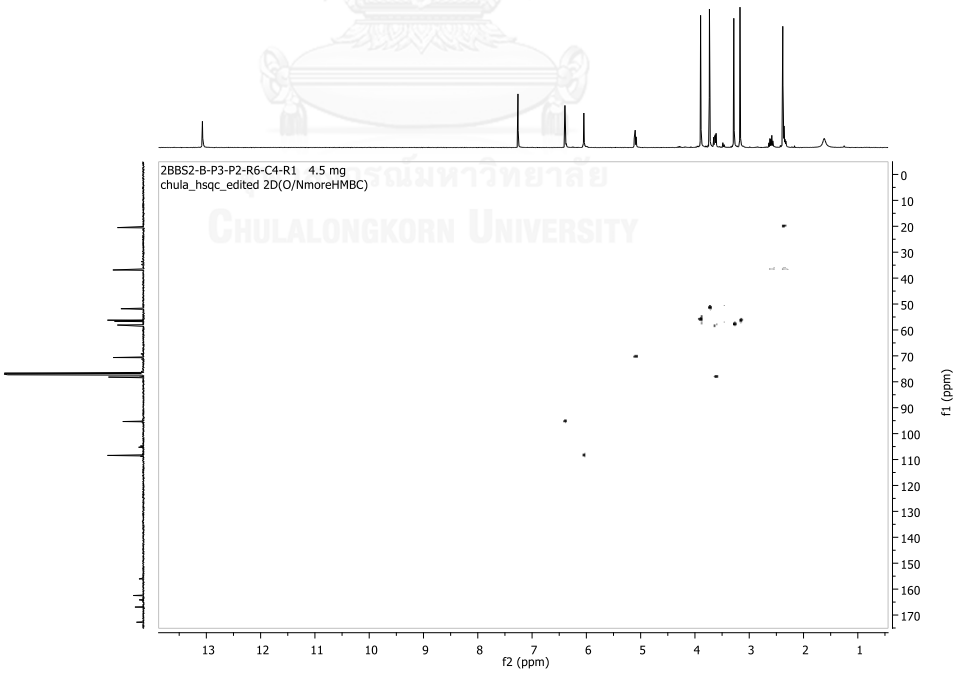

Figure A.12 HSQC spectrum ($CDCl_3$) of compound **2**

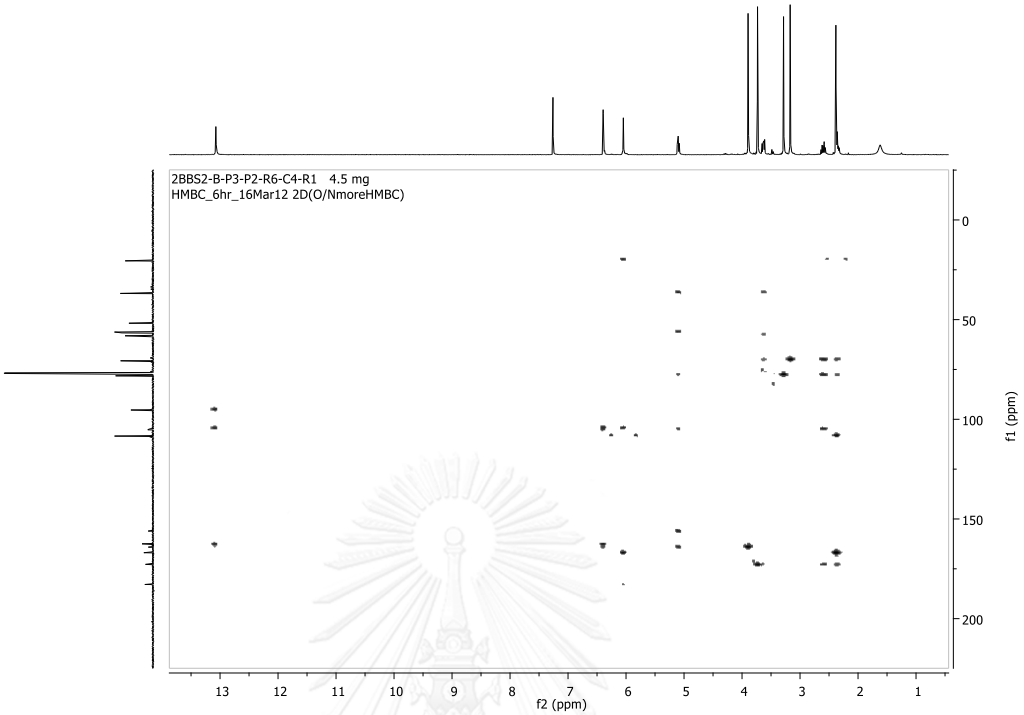

Figure A.13 HMBC spectrum ($CDCl_3$) of compound **2**

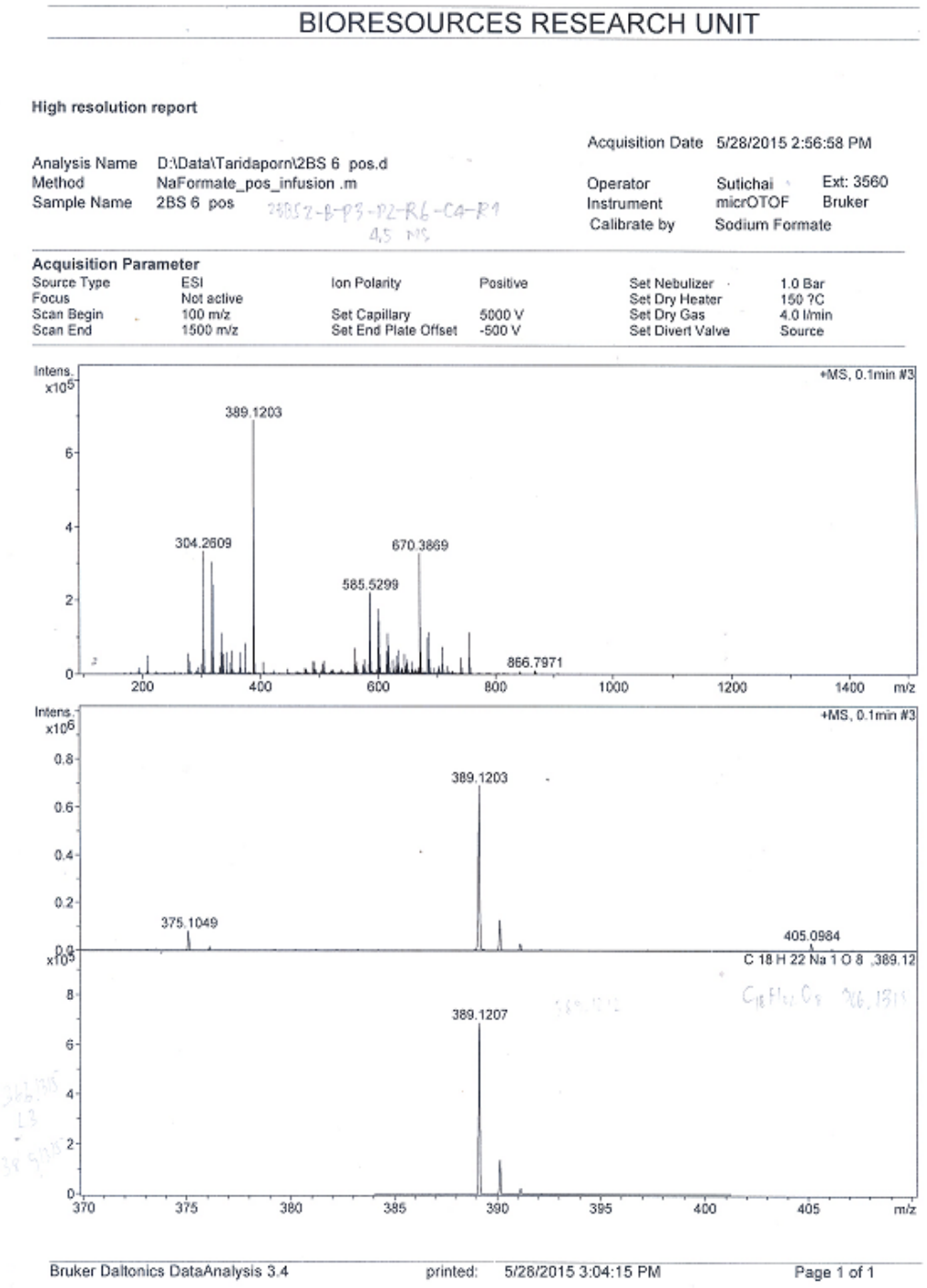

Figure A.14 HRESIMS Mass spectrum of compound **2**

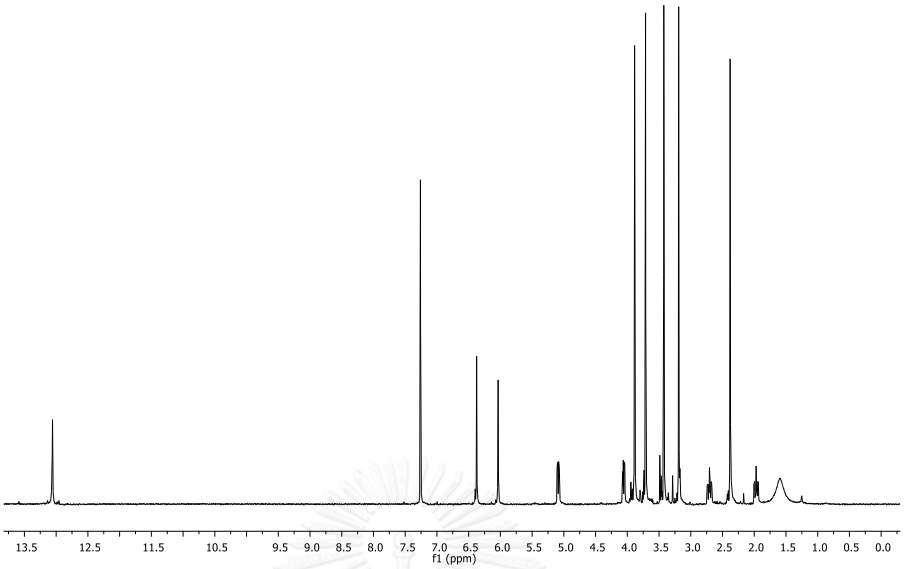

Figure A.15 ^{1}H NMR (400 MHz, $CDCl_3$) spectrum of compound **3**

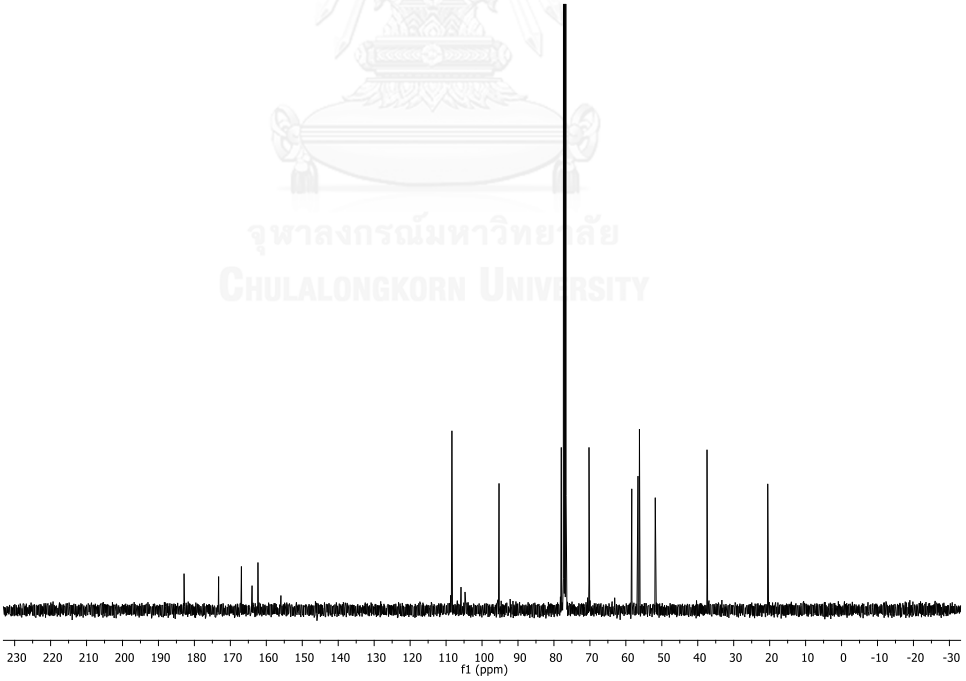

Figure A.16 ^{13}C NMR (100 MHz, $CDCl_3$) spectrum of compound **3**

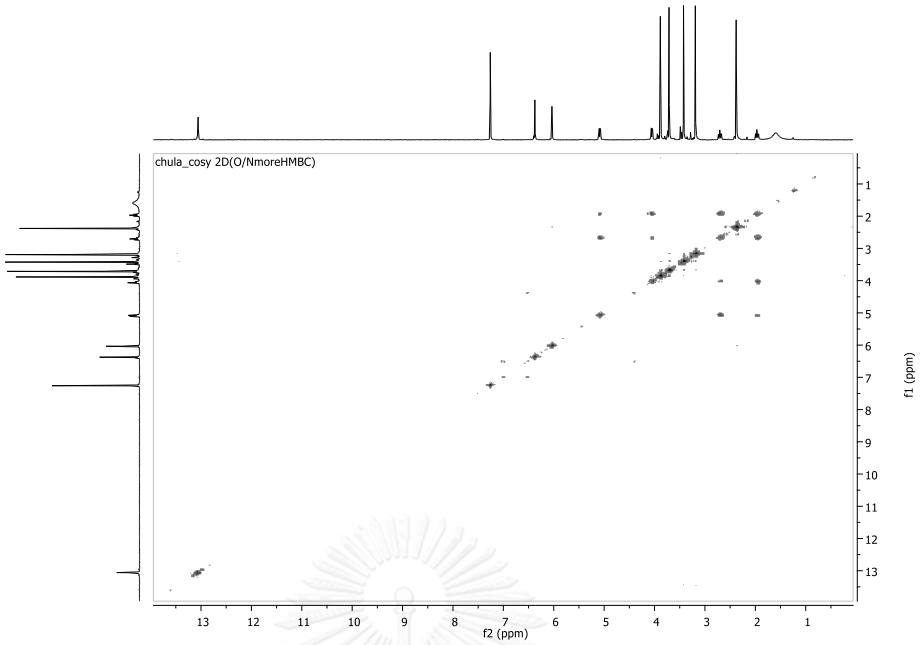

Figure A.17 ^{1}H-^{1}H COSY spectrum ($CDCl_3$) of compound **3**

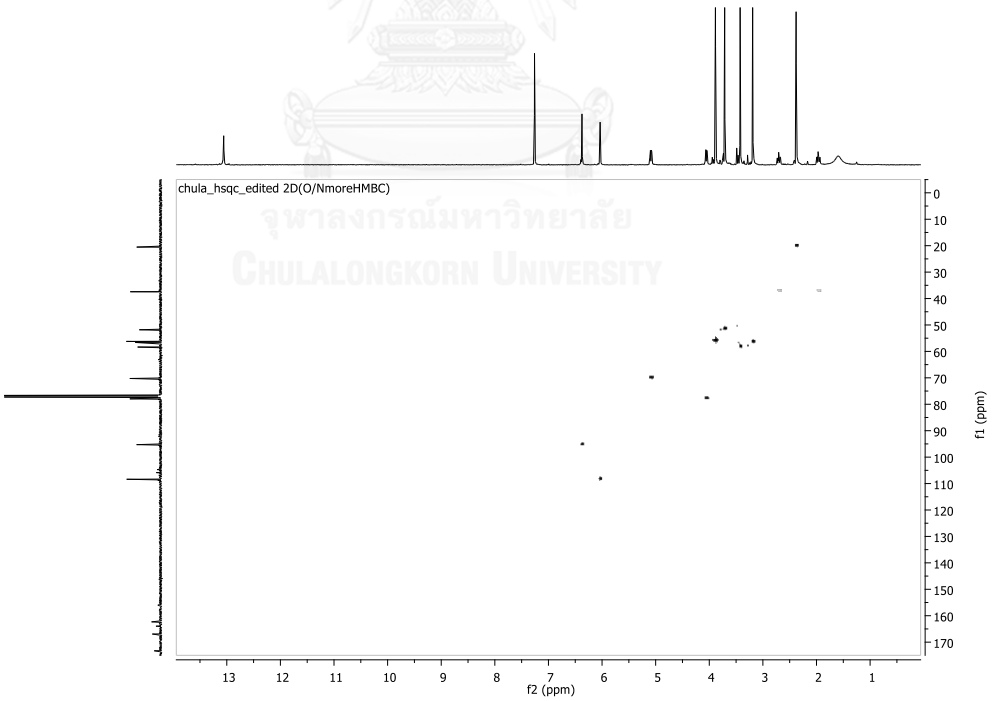

Figure A.18 HSQC spectrum ($CDCl_3$) of compound **3**

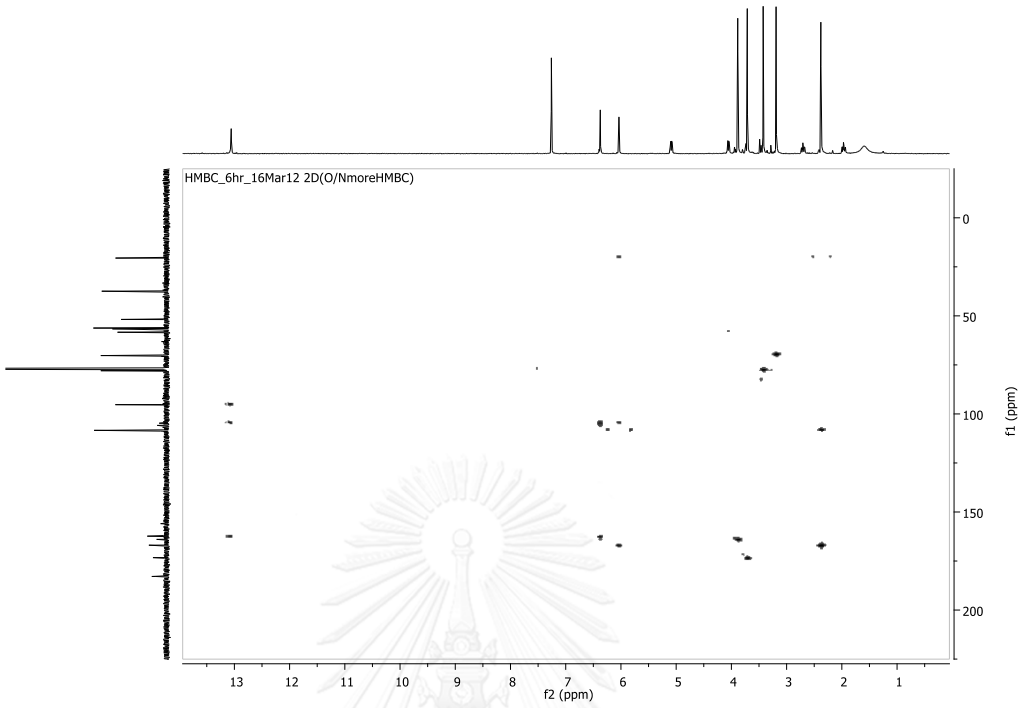

Figure A.19 HMBC spectrum ($CDCl_3$) of compound **3**

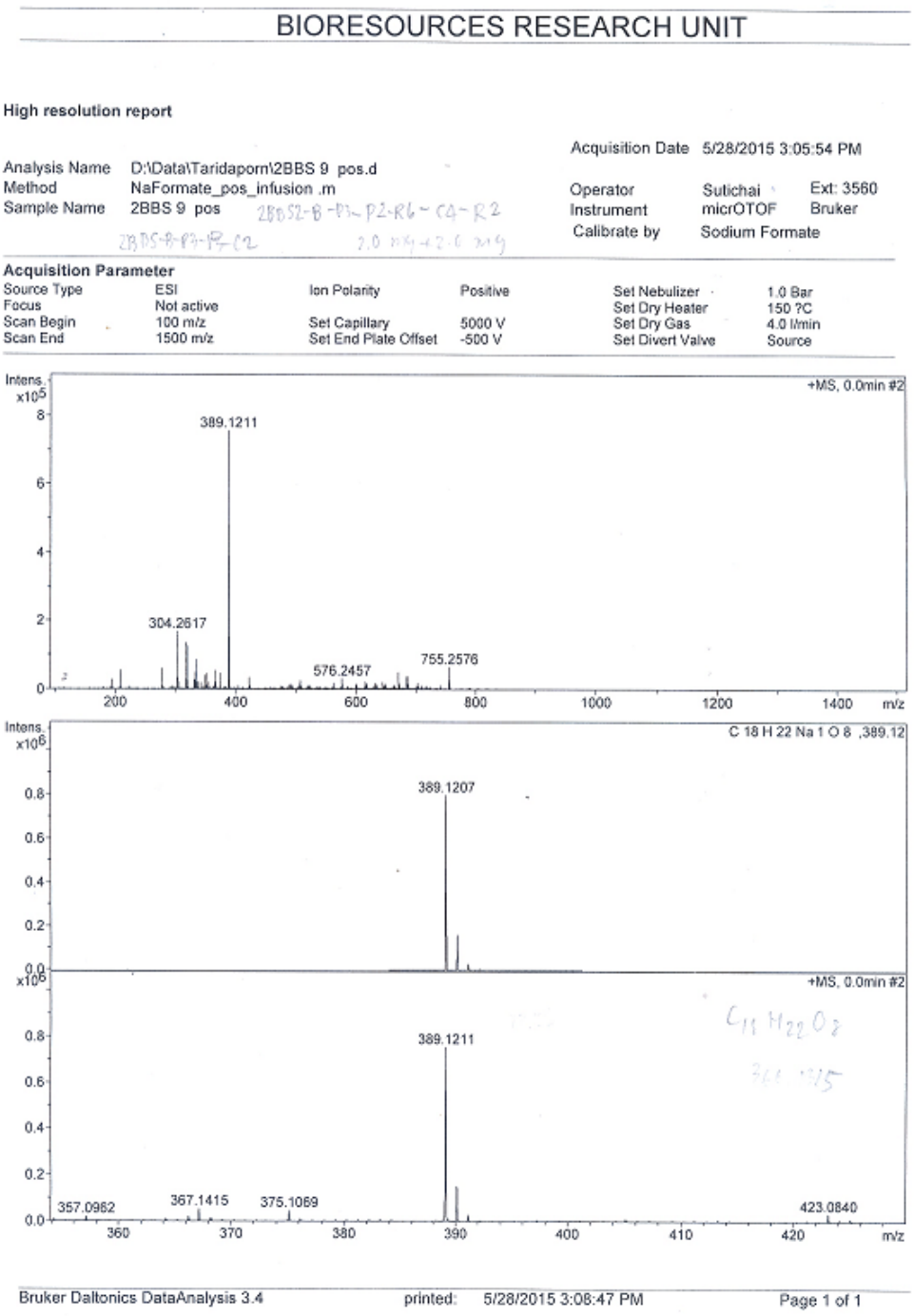

Figure A.20 HRESIMS Mass spectrum of compound **3**

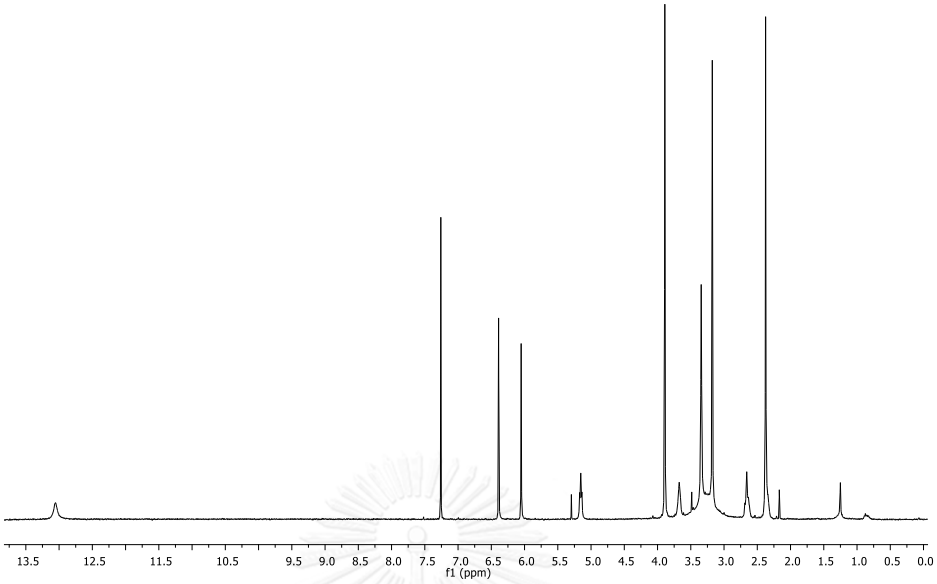

Figure A.21 ^{1}H NMR (400 MHz, $CDCl_3$) spectrum of compound **4**

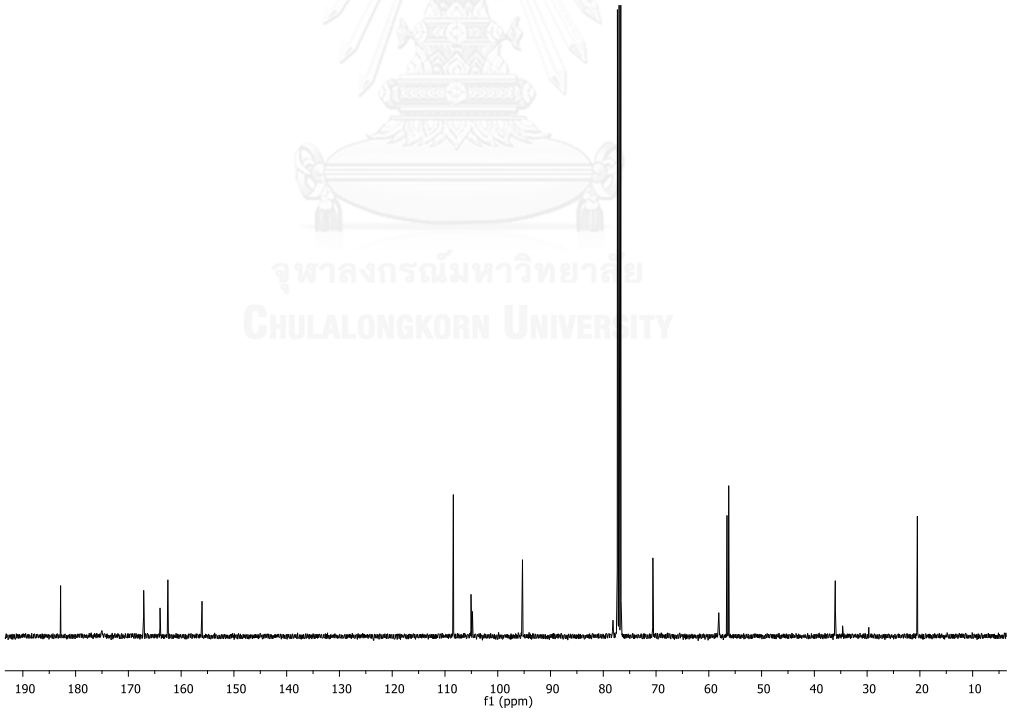

Figure A.22 ^{13}C NMR (100 MHz, $CDCl_3$) spectrum of compound **4**

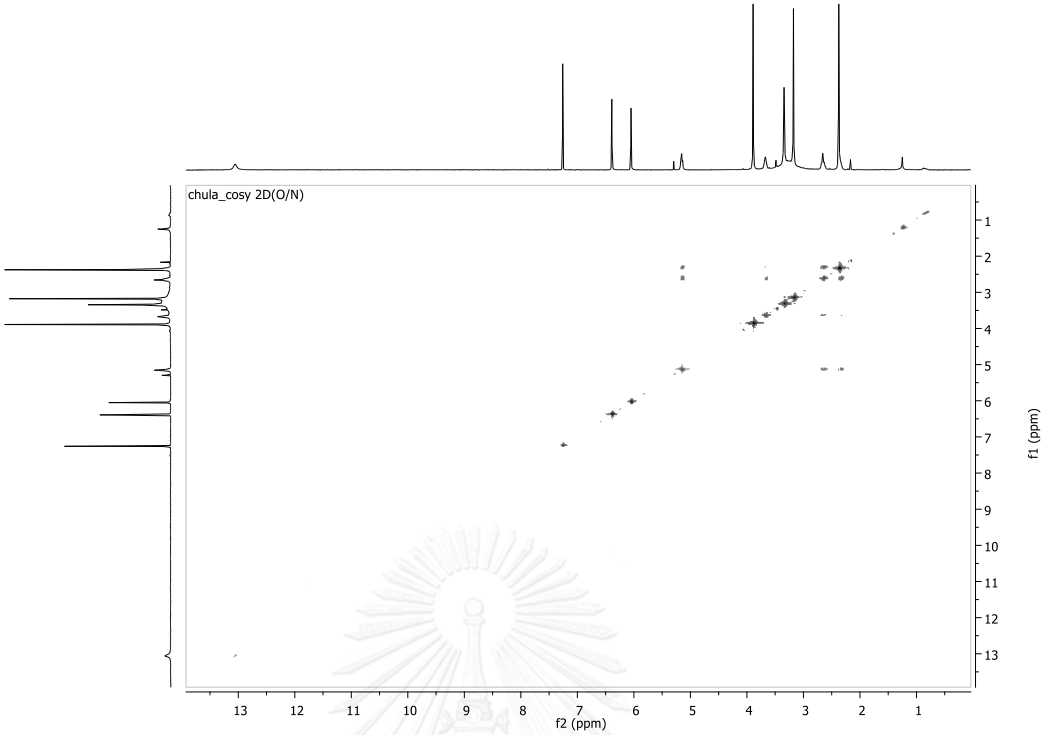

Figure A.23 ^{1}H-^{1}H COSY spectrum ($CDCl_3$) of compound **4**

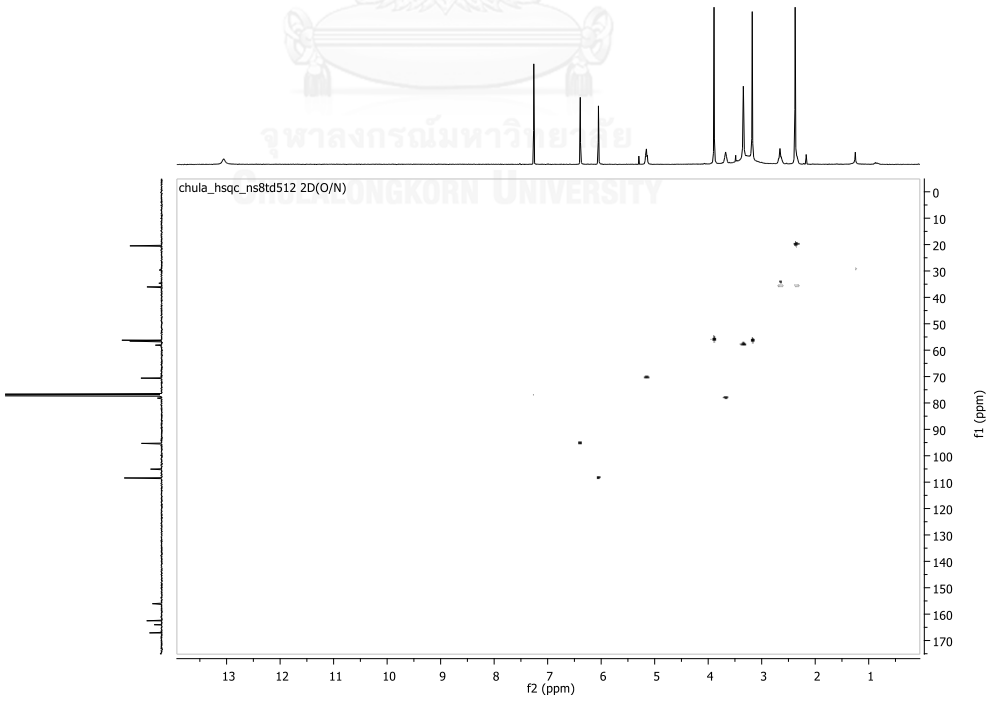

Figure A.24 HSQC spectrum ($CDCl_3$) of compound **4**

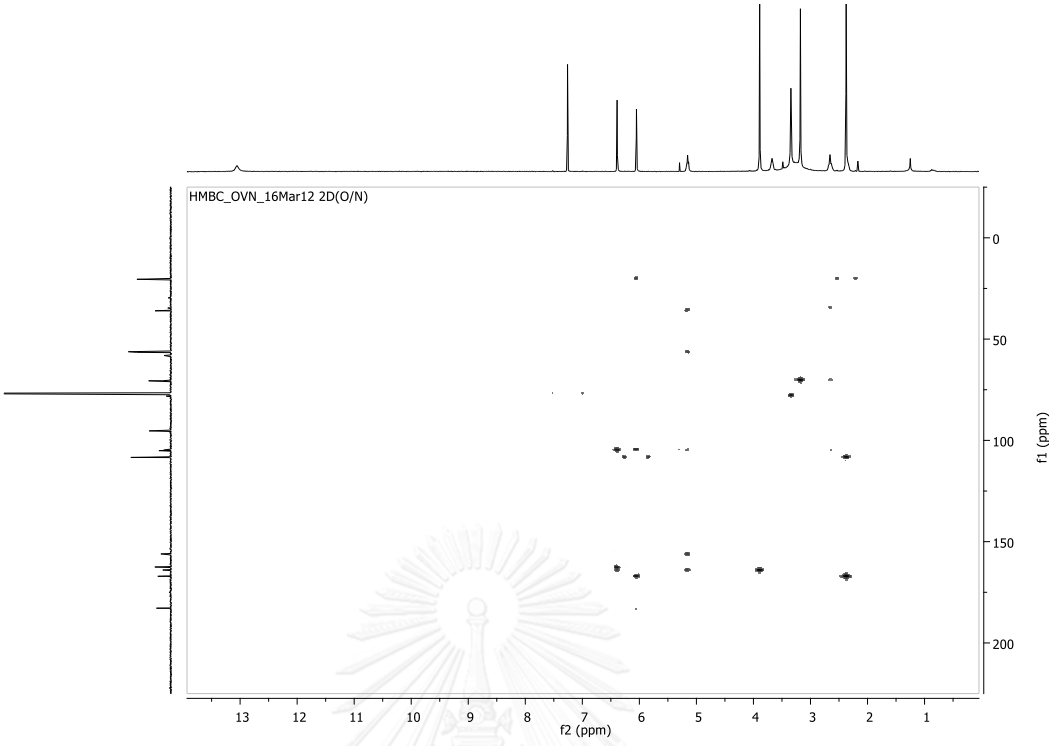

Figure A.25 HMBC spectrum ($CDCl_3$) of compound **4**

BIORESOURCES RESEARCH UNIT

High resolution report

Acquisition Date 4/3/2015 3:02:02 PM

Analysis Name D:\Data\Dua\2BBS C E D3 R7 C5.d
Method NaFormate_pos_infusion .m
Sample Name 2BBS C E D3 R7 C5

Operator Sutichai Ext: 3560
Instrument micrOTOF Bruker
Calibrate by Sodium Formate

Acquisition Parameter

Source Type	ESI	Ion Polarity	Positive	Set Nebulizer	1.0 Bar
Focus	Not active			Set Dry Heater	150 ?C
Scan Begin	100 m/z	Set Capillary	5000 V	Set Dry Gas	4.0 l/min
Scan End	1500 m/z	Set End Plate Offset	-500 V	Set Divert Valve	Source

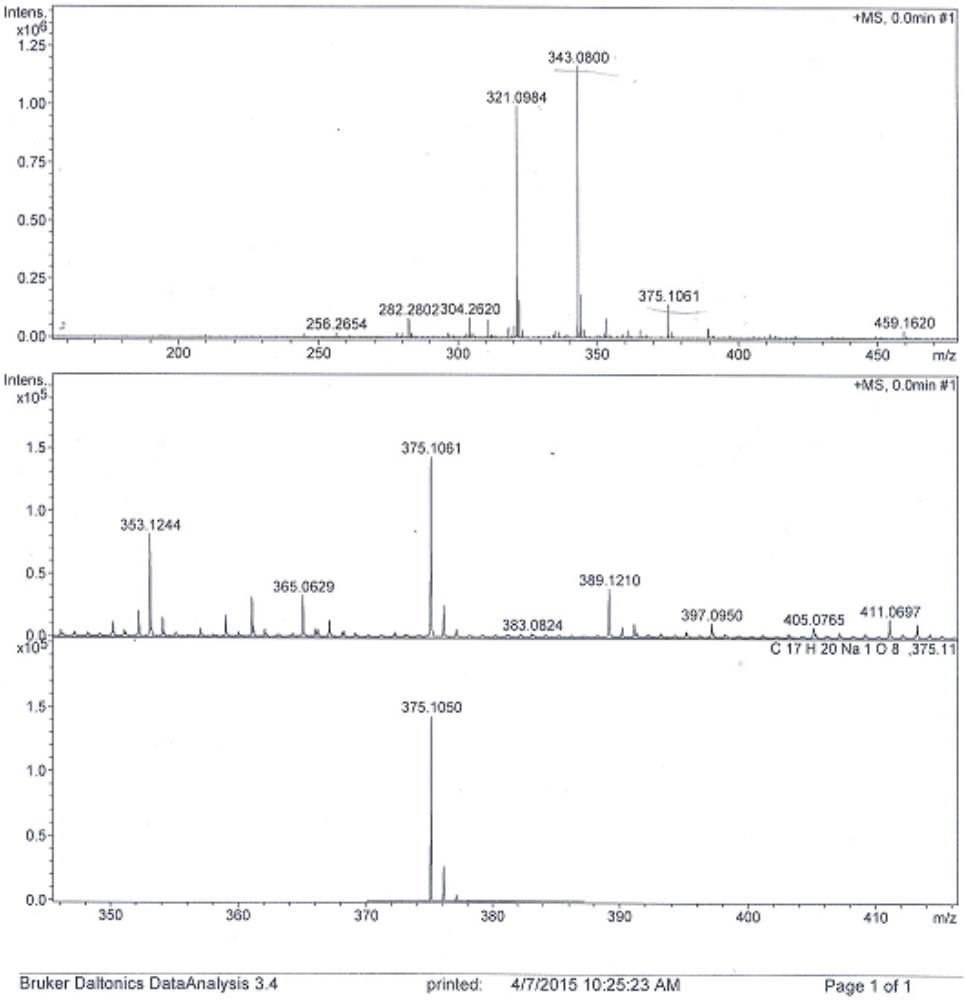

Bruker Daltonics DataAnalysis 3.4 printed: 4/7/2015 10:25:23 AM Page 1 of 1

Figure A.26 HRESIMS Mass spectrum of compound **4**

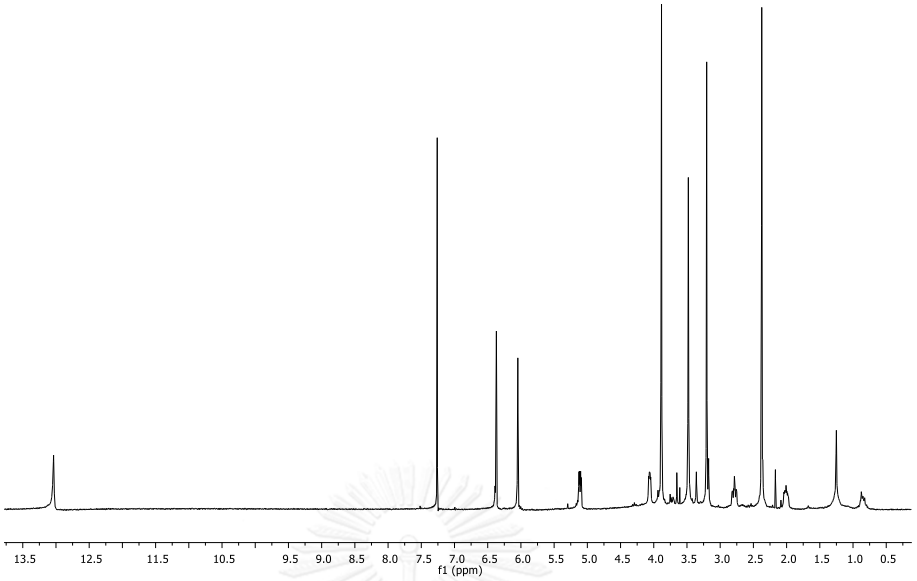

Figure A.27 ^{1}H (400 MHz, $CDCl_3$) NMR spectrum of compound **5**

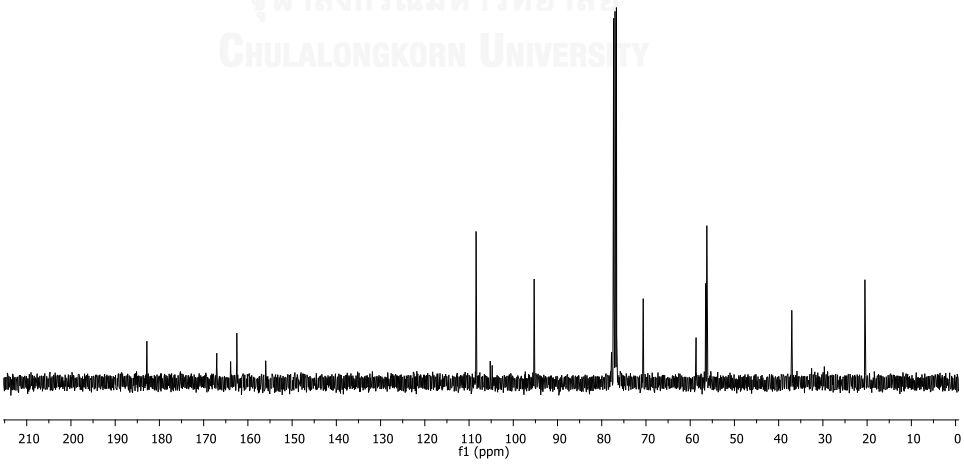

Figure A.28 ^{13}C NMR (100 MHz, $CDCl_3$) NMR spectrum of compound **5**

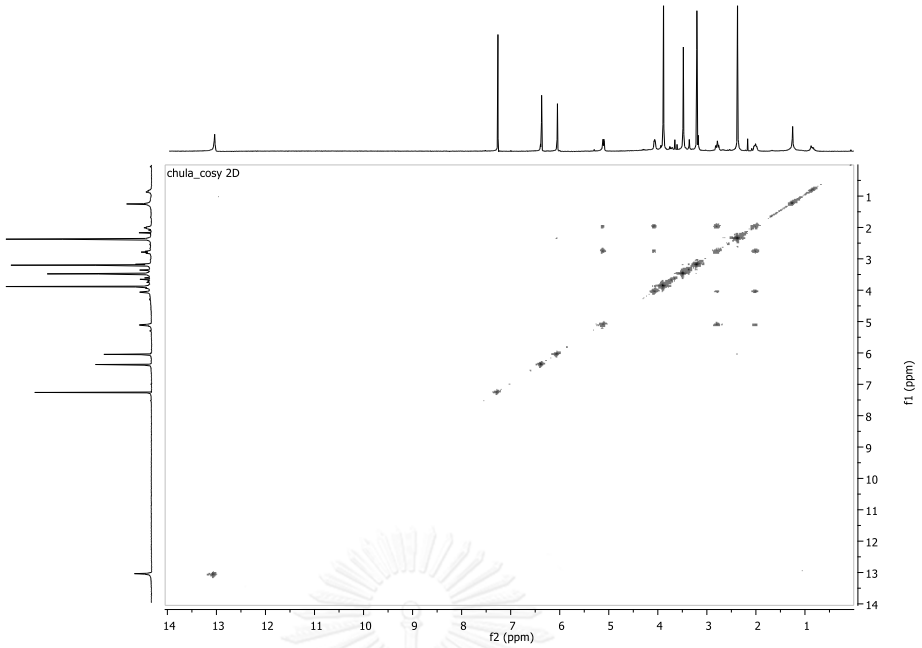

Figure A.29 ^{1}H-^{1}H COSY spectrum ($CDCl_3$) of compound **5**

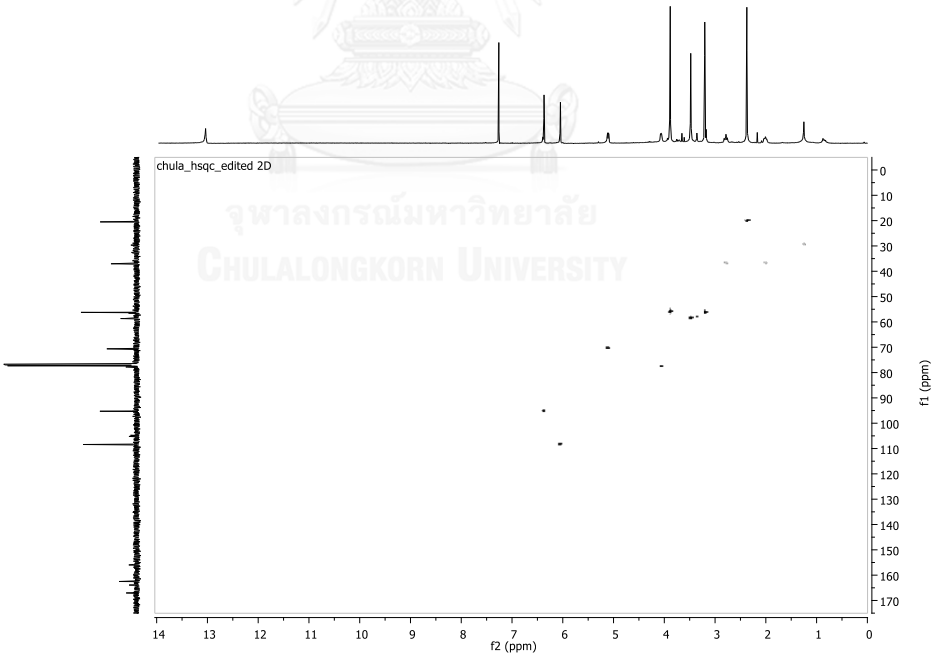

Figure A.30 HSQC spectrum ($CDCl_3$) of compound **5**

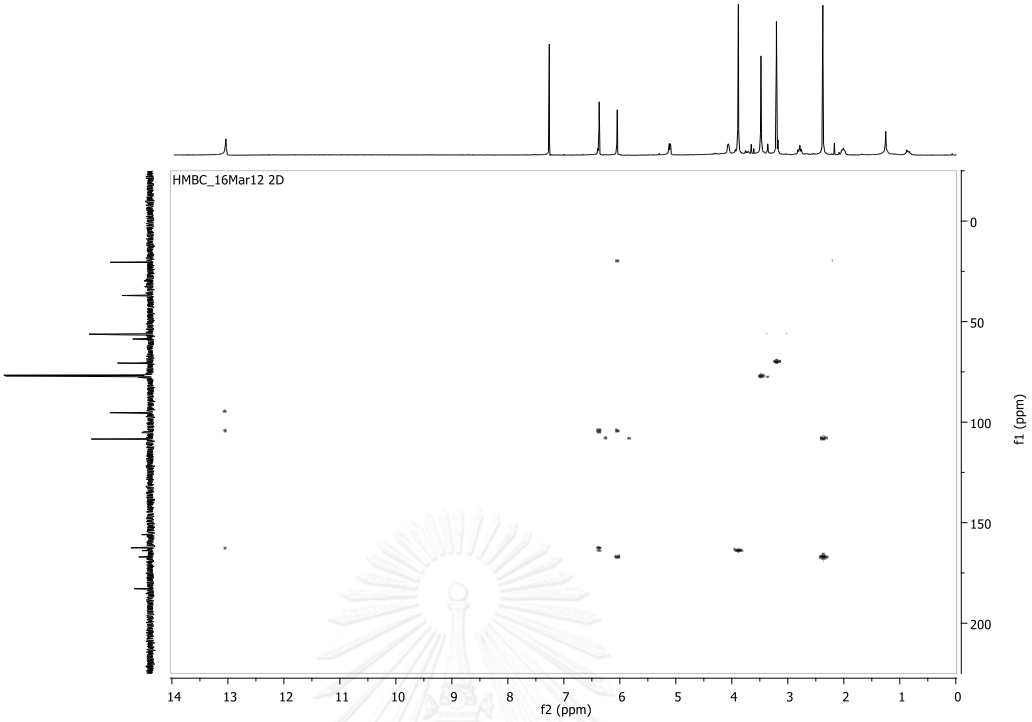

Figure A.31 HMBC spectrum ($CDCl_3$) of compound **5**

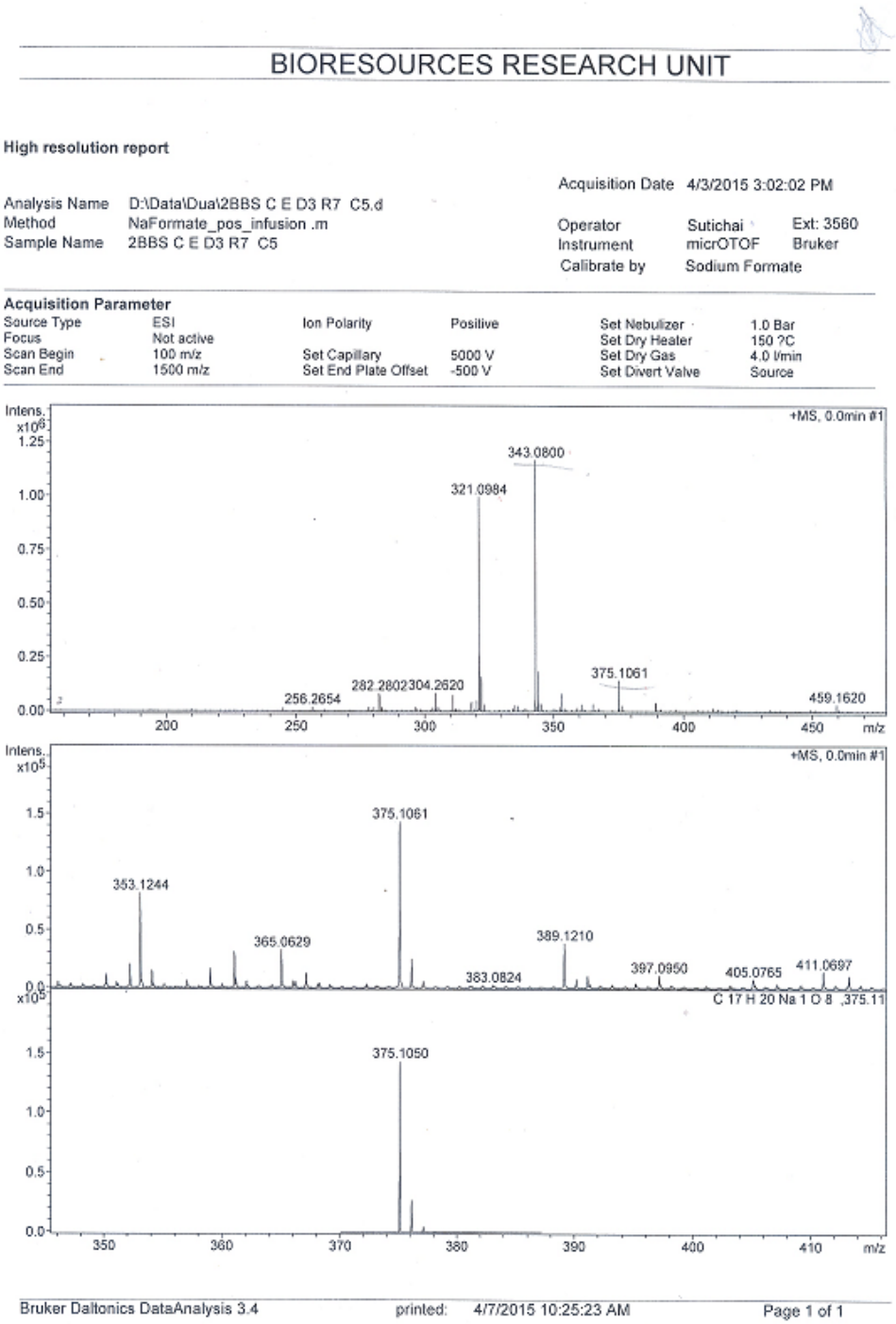

Figure A.32 HRESIMS Mass spectrum of compound **5**

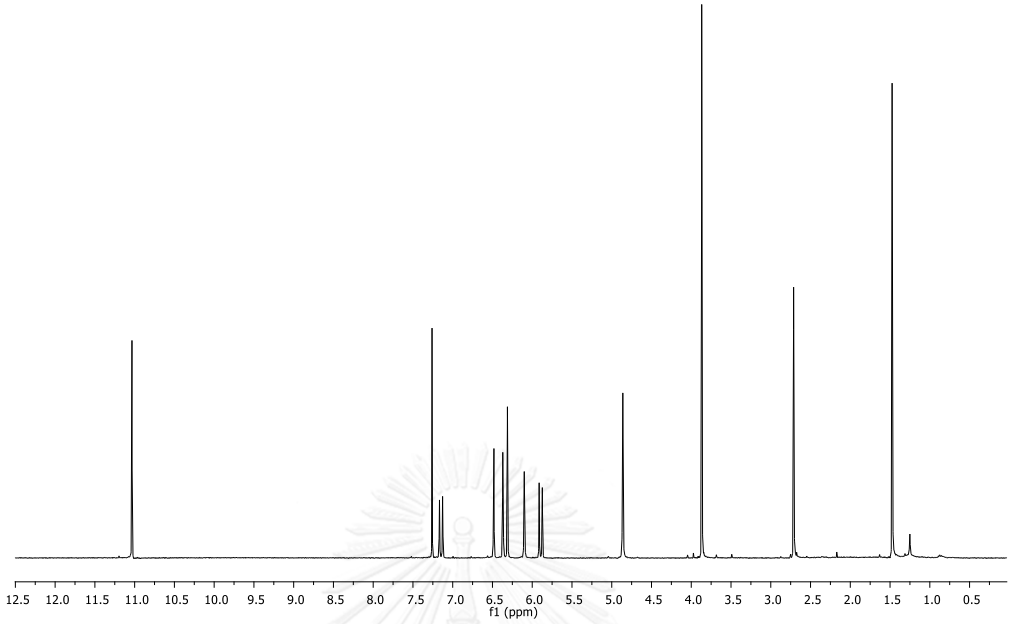

Figure A.33 ^{1}H NMR (400 MHz, $CDCl_3$) spectrum of compound **6**

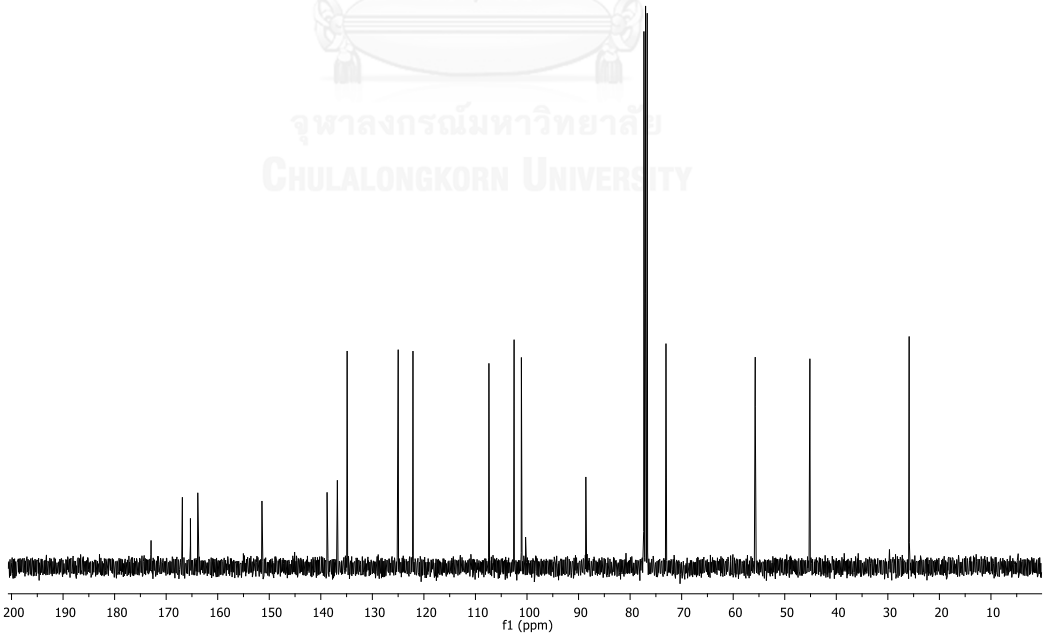

Figure A.34 ^{13}C NMR (100 MHz, $CDCl_3$) spectrum of compound **6**

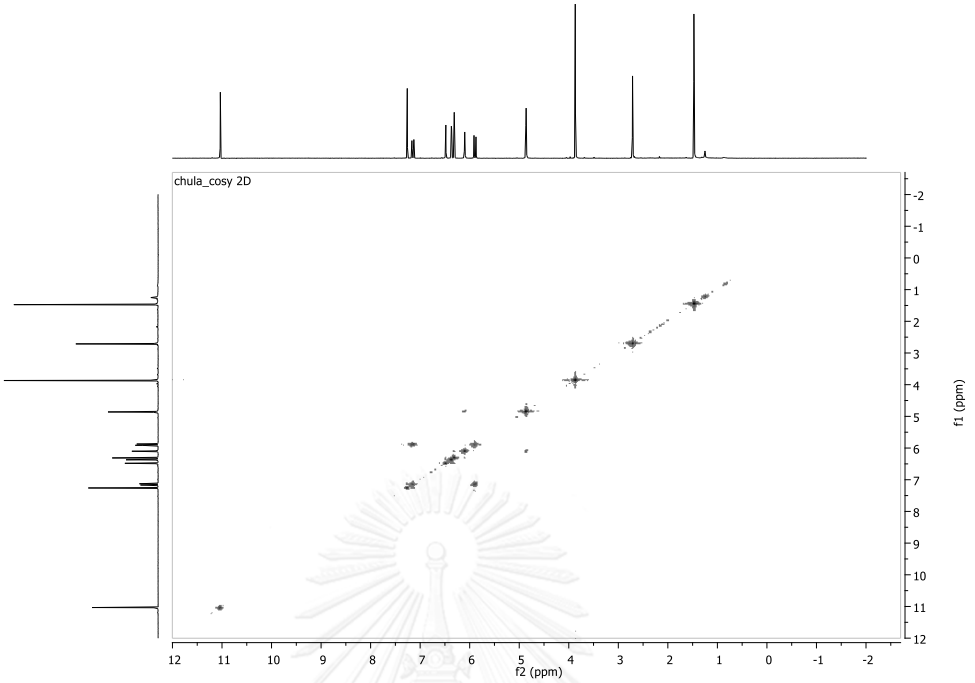

Figure A.35 ^{1}H-^{1}H COSY spectrum ($CDCl_3$) of compound **6**

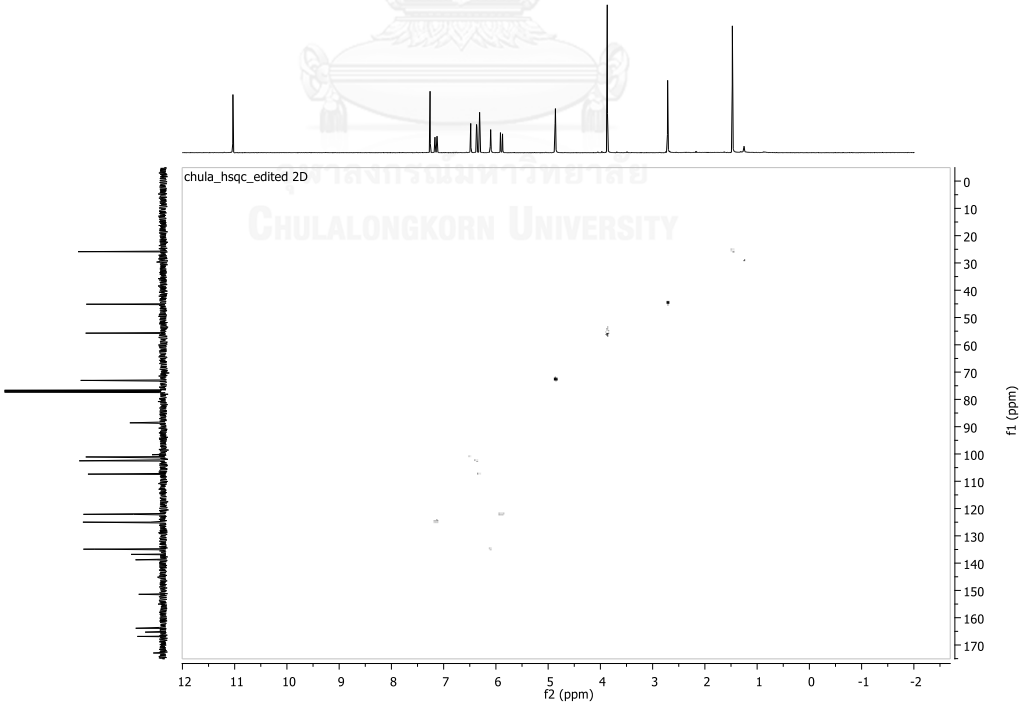

Figure A.36 HSQC spectrum ($CDCl_3$) of compound **6**

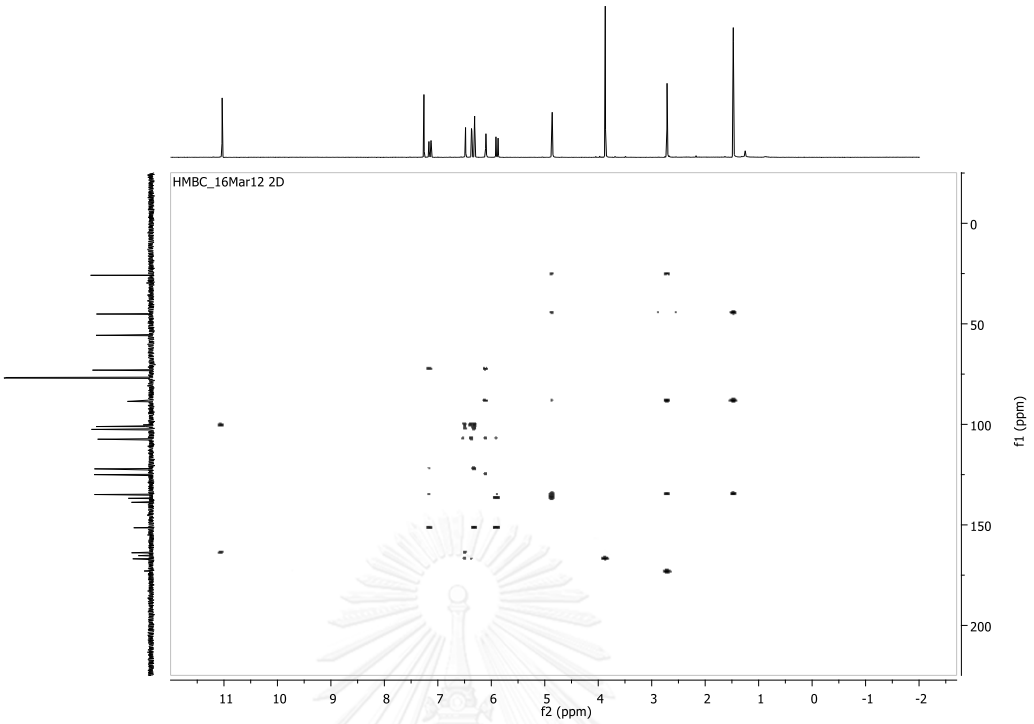

Figure A.37 HMBC spectrum ($CDCl_3$) of compound **6**

BIORESOURCES RESEARCH UNIT

High resolution report

		Acquisition Date	5/28/2015 2:47:21 PM
Analysis Name	D:\Data\Taridaporn\2BBS 3 neg.d		
Method	NaFormate_neg_infusion.m	Operator	Sutichai Ext: 3560
Sample Name	2BBS 3 neg	Instrument	micrOTOF Bruker
		Calibrate by	Sodium Formate

Acquisition Parameter

Source Type	ESI	Ion Polarity	Negative	Set Nebulizer	0.4 Bar
Focus	Not active			Set Dry Heater	200 ?C
Scan Begin	50 m/z	Set Capillary	4500 V	Set Dry Gas	5.0 l/min
Scan End	1500 m/z	Set End Plate Offset	-500 V	Set Divert Valve	Source

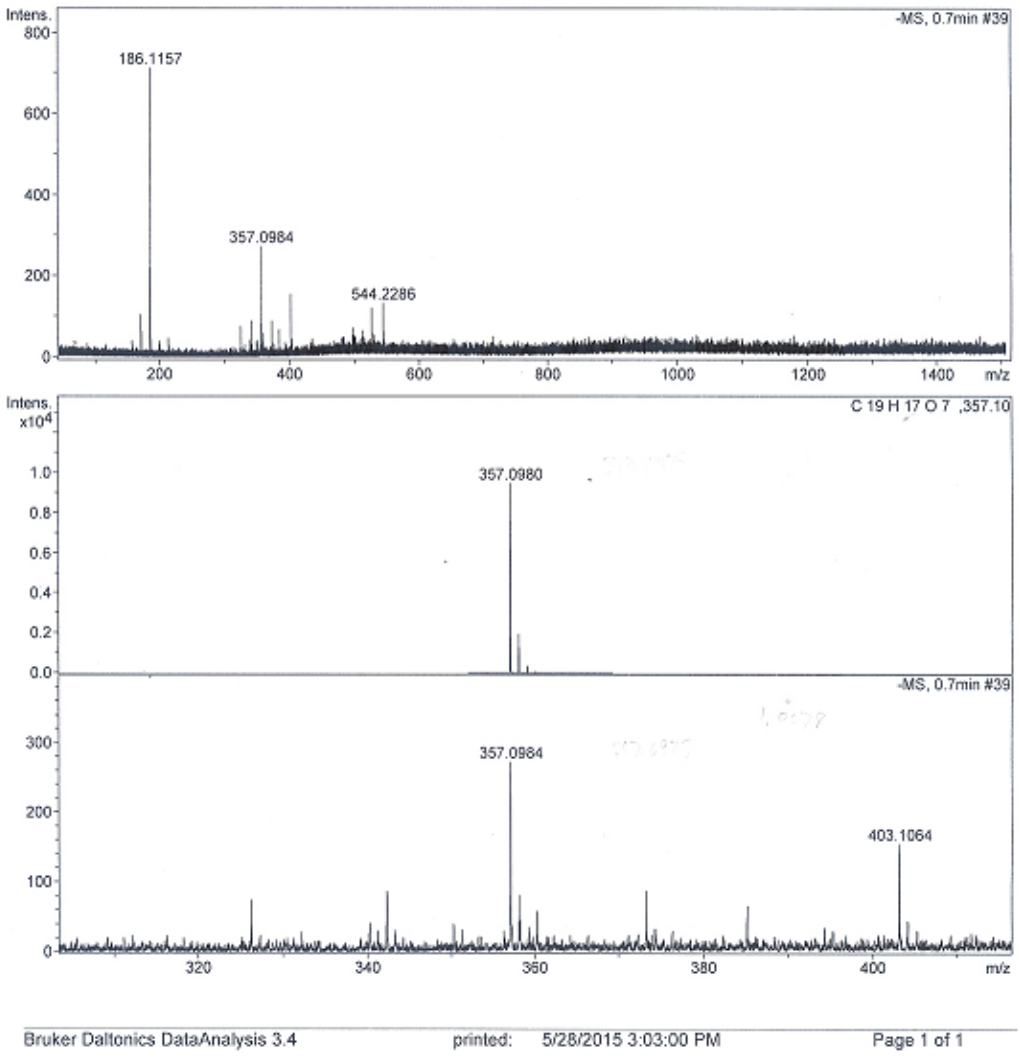

Bruker Daltonics DataAnalysis 3.4 printed: 5/28/2015 3:03:00 PM Page 1 of 1

Figure A.38 HRESIMS Mass spectrum of compound **6**

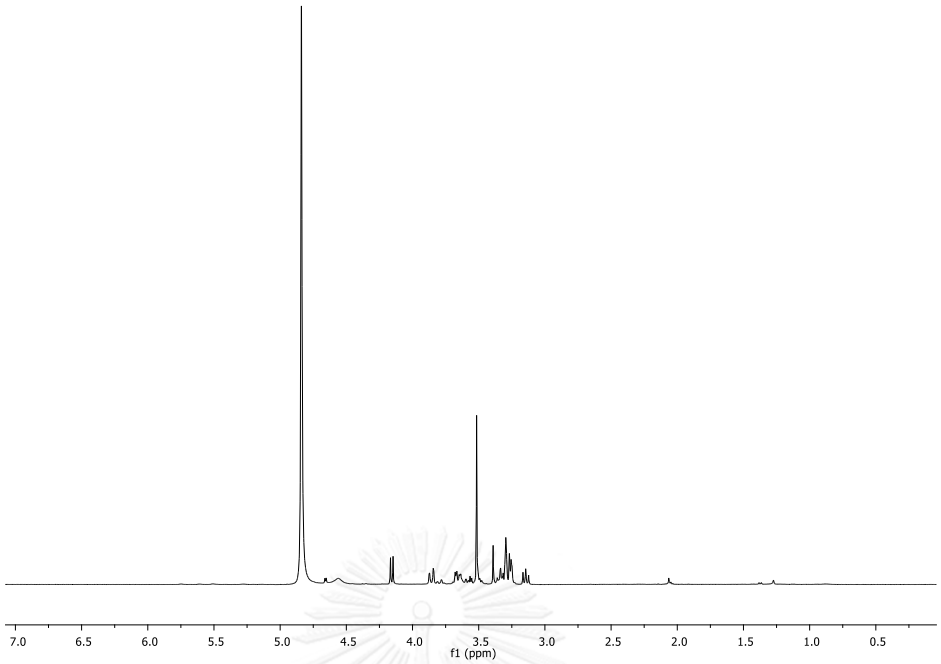

Figure A.39 ^{1}H NMR (400 MHz, Methanol-d4) spectrum of compound **7**

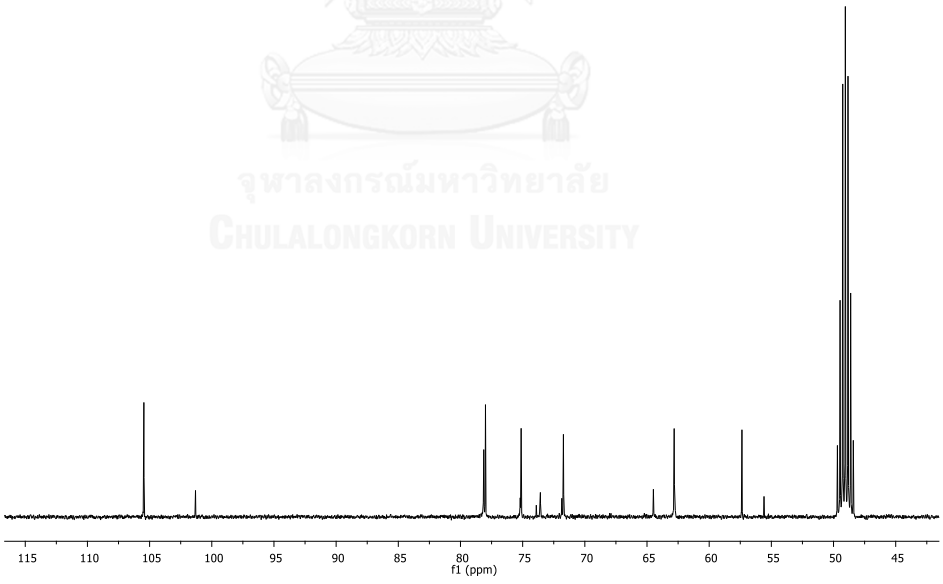

Figure A.40 ^{13}C NMR (100 MHz, Methanol-d4) spectrum of compound **7**

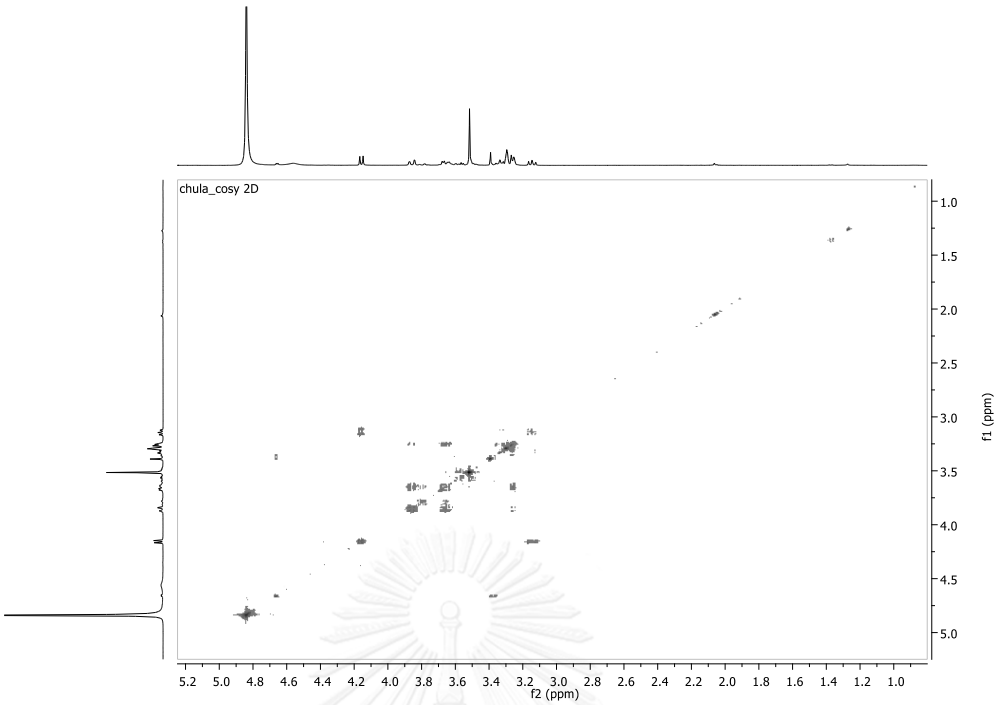

Figure A.41 ^{1}H-^{1}H COSY spectrum (Methanol-d4) of compound **7**

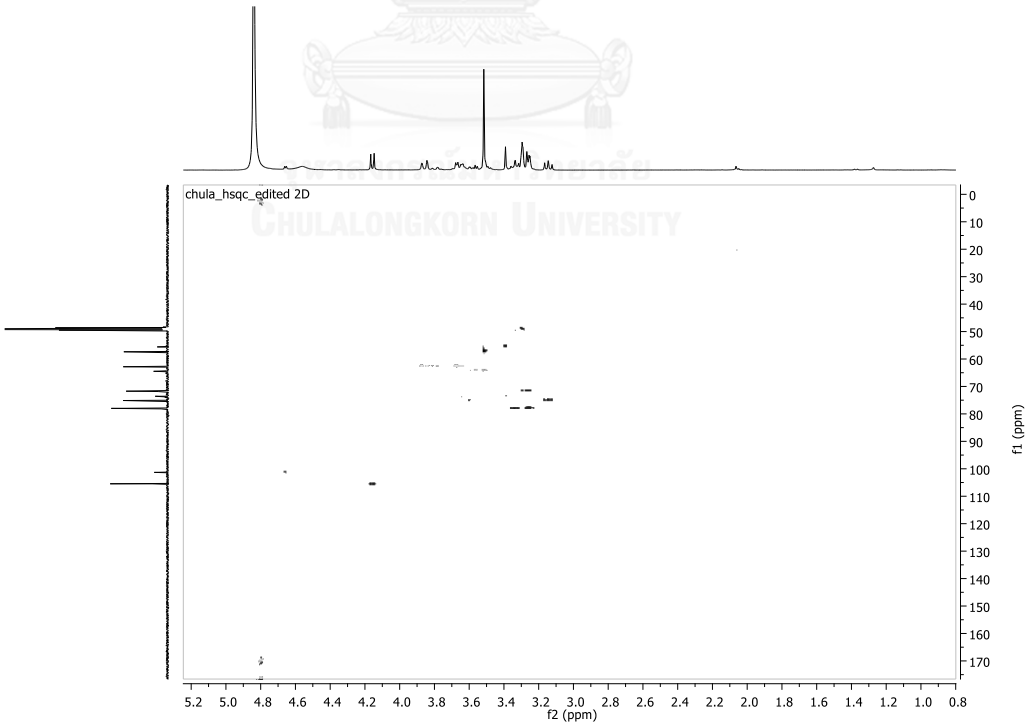

Figure A.42 HSQC spectrum (Methanol-d4) of compound **7**

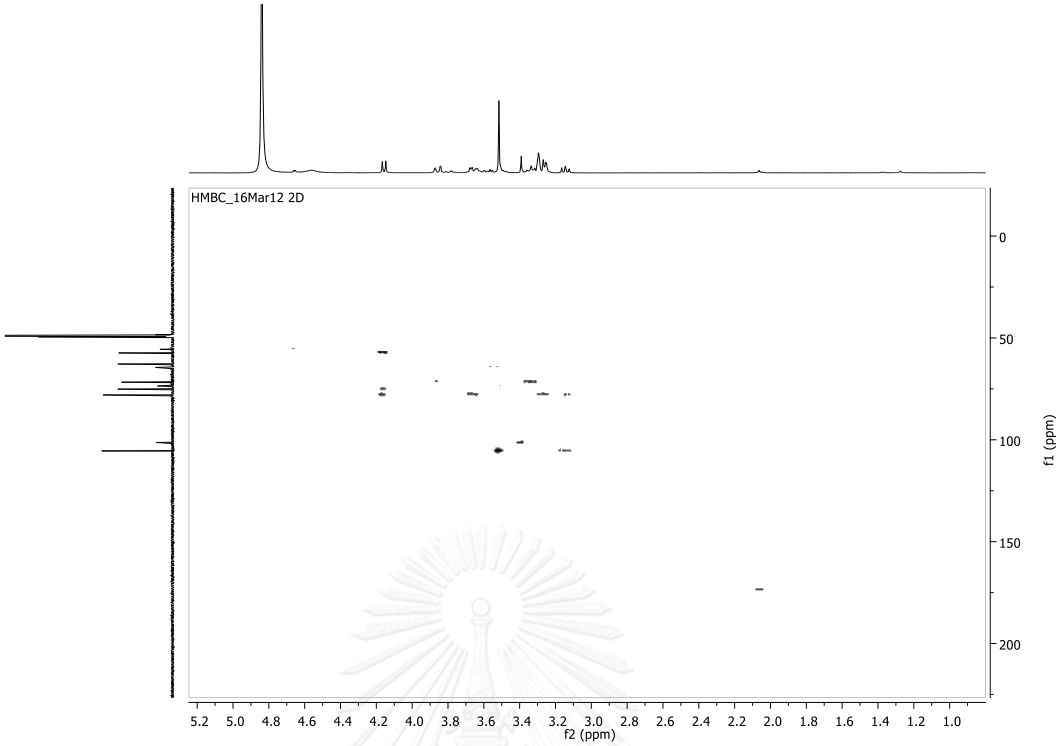

Figure A.43 HMBC spectrum (Methanol-d4) of compound **8**

BIORESOURCES RESEARCH UNIT

High resolution report

		Acquisition Date	1/28/2015 9:40:00 AM
Analysis Name	D:\Data\Taridaporn\2BS2 E C7 11 4.d		
Method	NaFormate_pos_infusion .m	Operator	Sutichai Ext: 3560
Sample Name	2BS2 E C7 11 4	Instrument	micrOTOF Bruker
		Calibrate by	Sodium Formate

Acquisition Parameter

Source Type	ESI	Ion Polarity	Positive	Set Nebulizer	1.0 Bar
Focus	Not active			Set Dry Heater	150 °C
Scan Begin	100 m/z	Set Capillary	5000 V	Set Dry Gas	4.0 l/min
Scan End	1500 m/z	Set End Plate Offset	-500 V	Set Divert Valve	Source

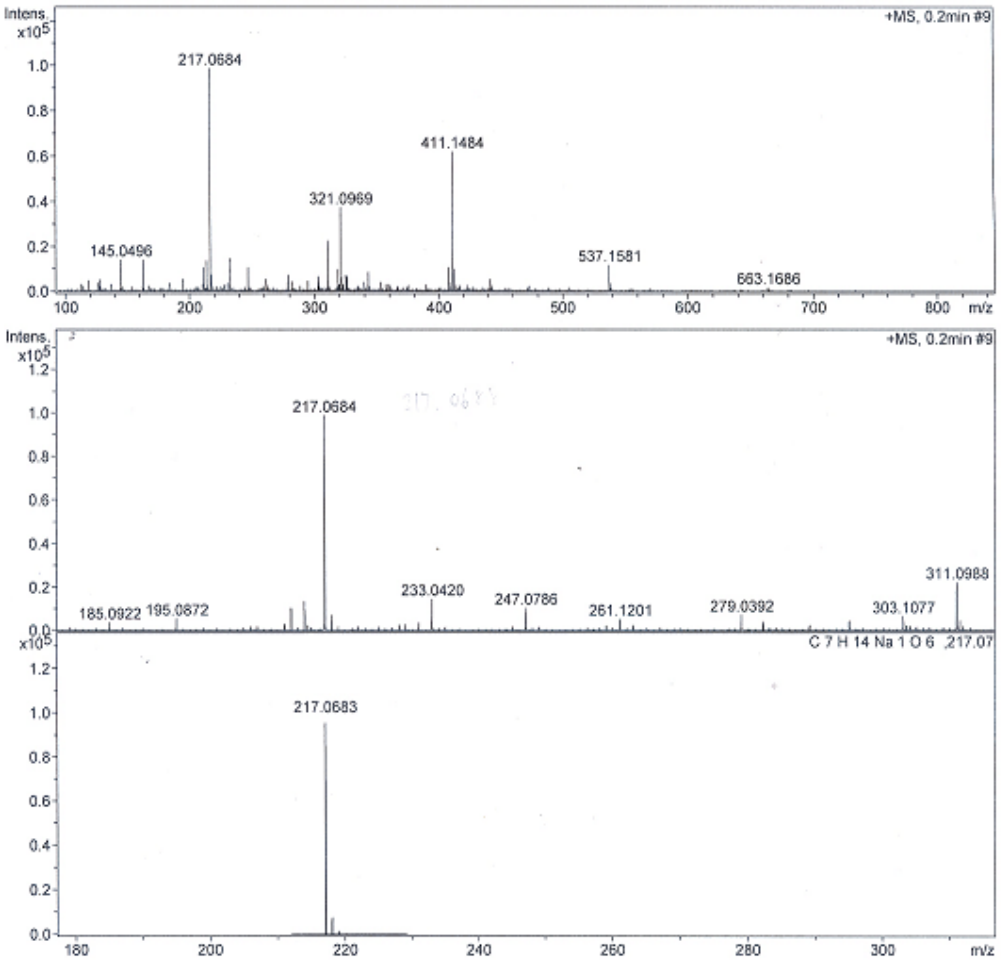

Bruker Daltonics DataAnalysis 3.4 printed: 1/28/2015 9:46:07 AM Page 1 of 1

Figure A.44 HRESIMS Mass spectrum of compound **7**

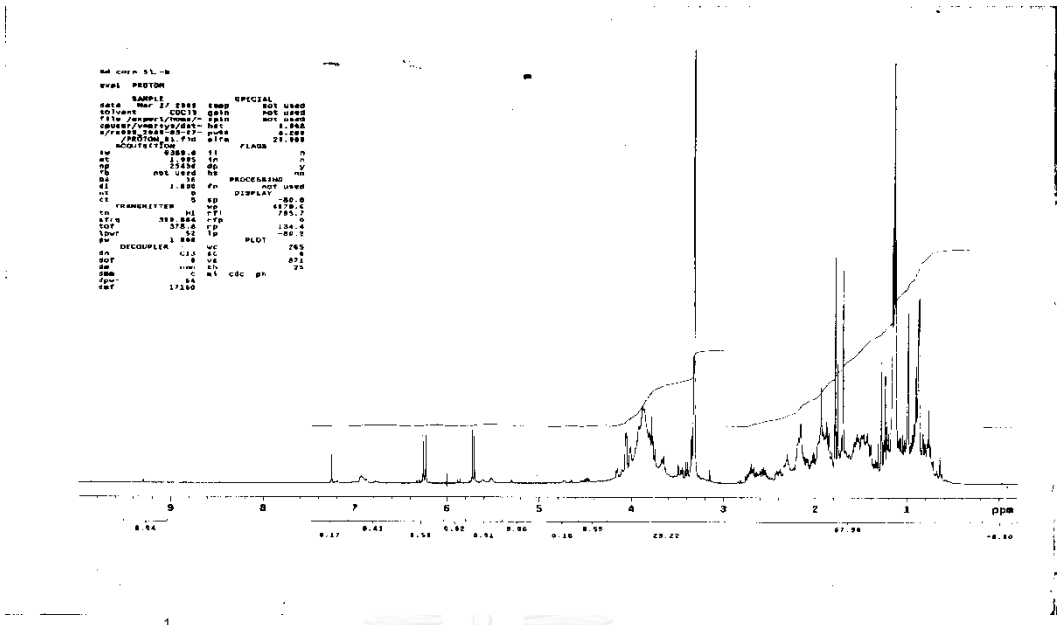

Figure A.45 ^{1}H NMR (400 MHz, $CDCl_3$) spectrum of crude broth (XG8D cultured on corn steep liquor)

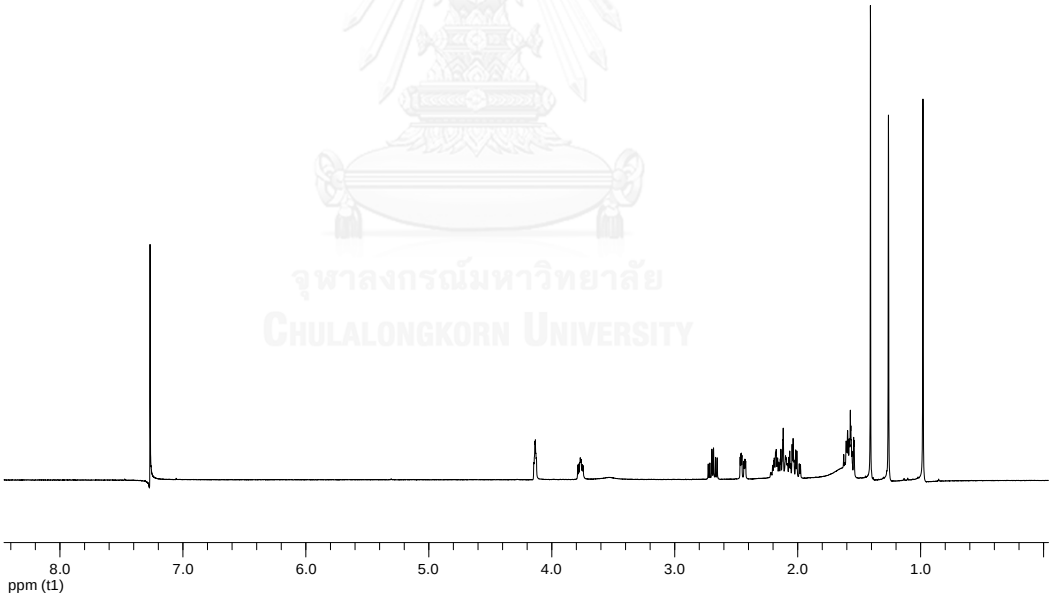

Figure A.46 ^{1}H NMR (400 MHz, $CDCl_3$) spectrum of compound **8**

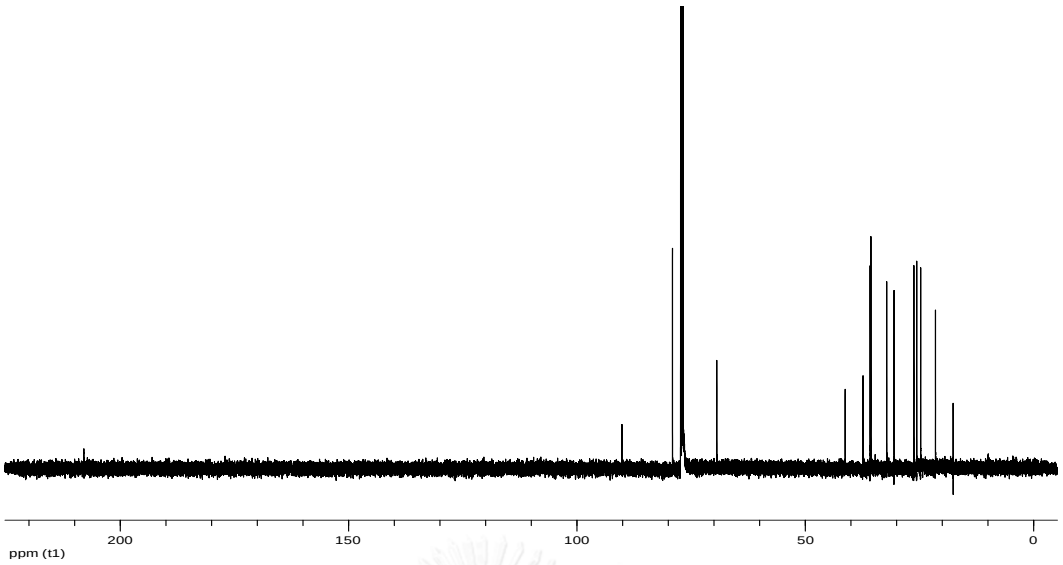

Figure A.47 ^{13}C NMR (100 MHz, $CDCl_3$) spectrum of compound **8**

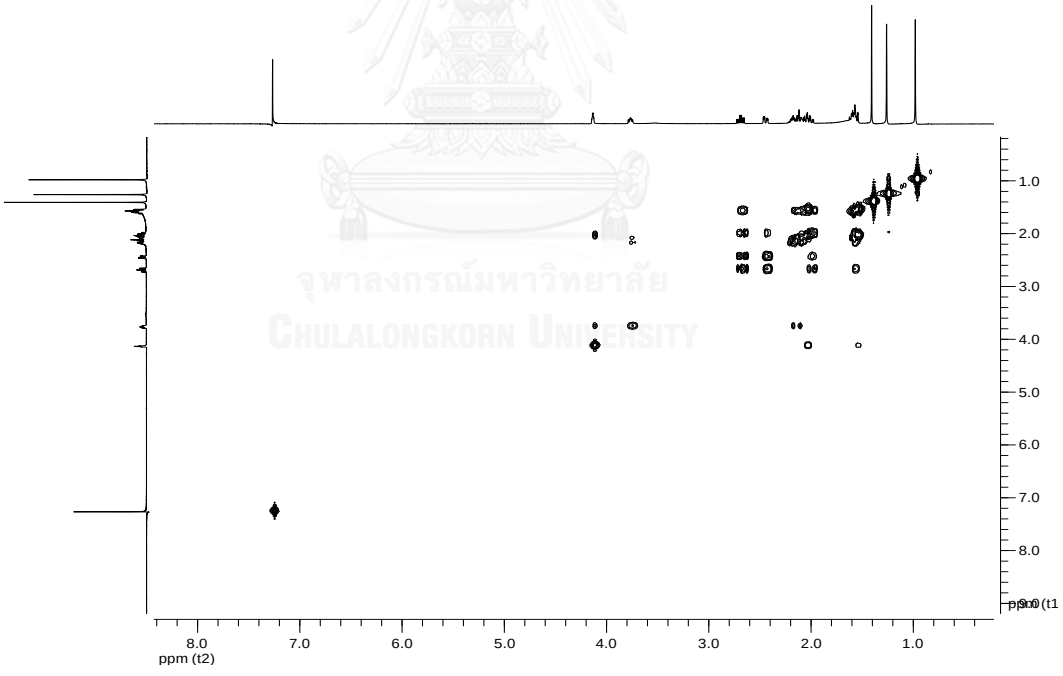

Figure A.48 ^{1}H-^{1}H COSY spectrum ($CDCl_3$) of compound **8**

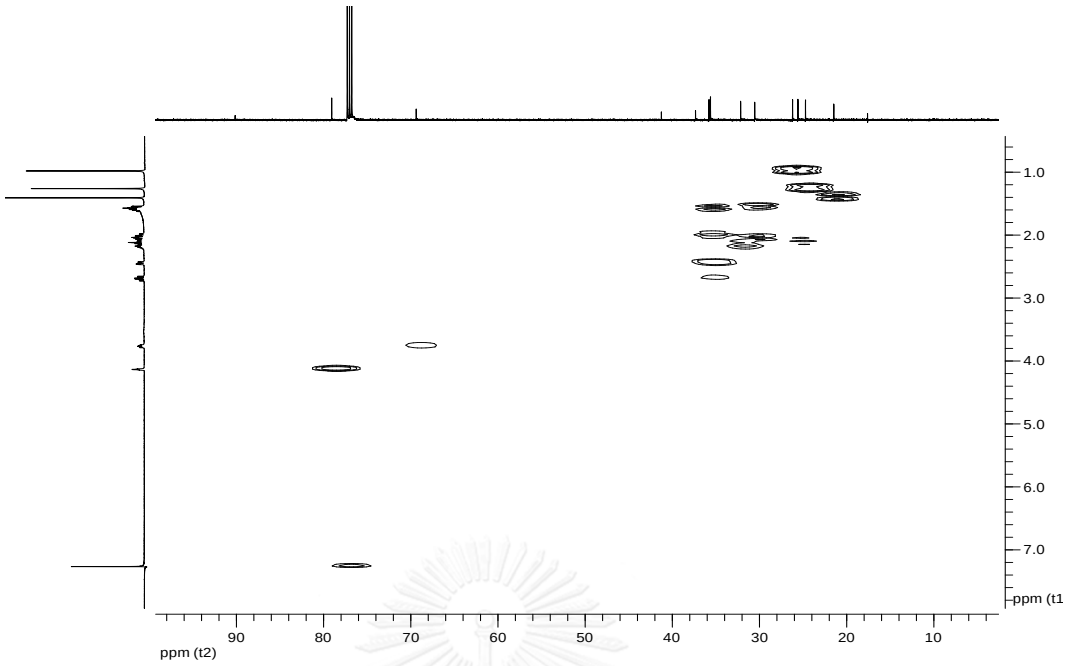

Figure A.49 HSQC spectrum ($CDCl_3$) of compound **8**

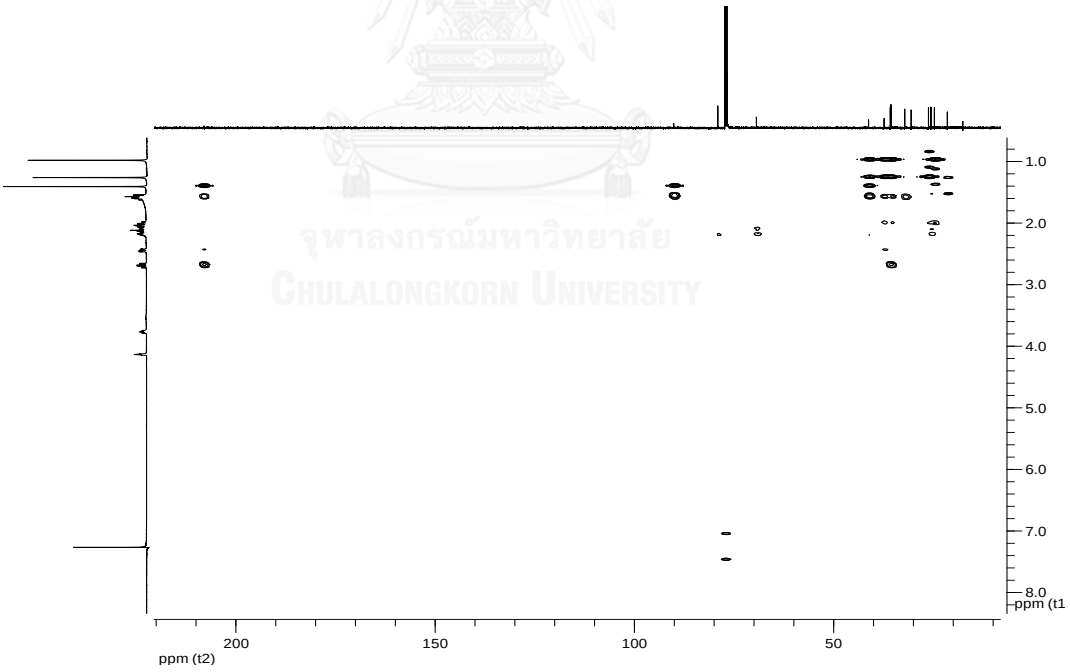

Figure A.50 HMBC spectrum ($CDCl_3$) of compound **8**

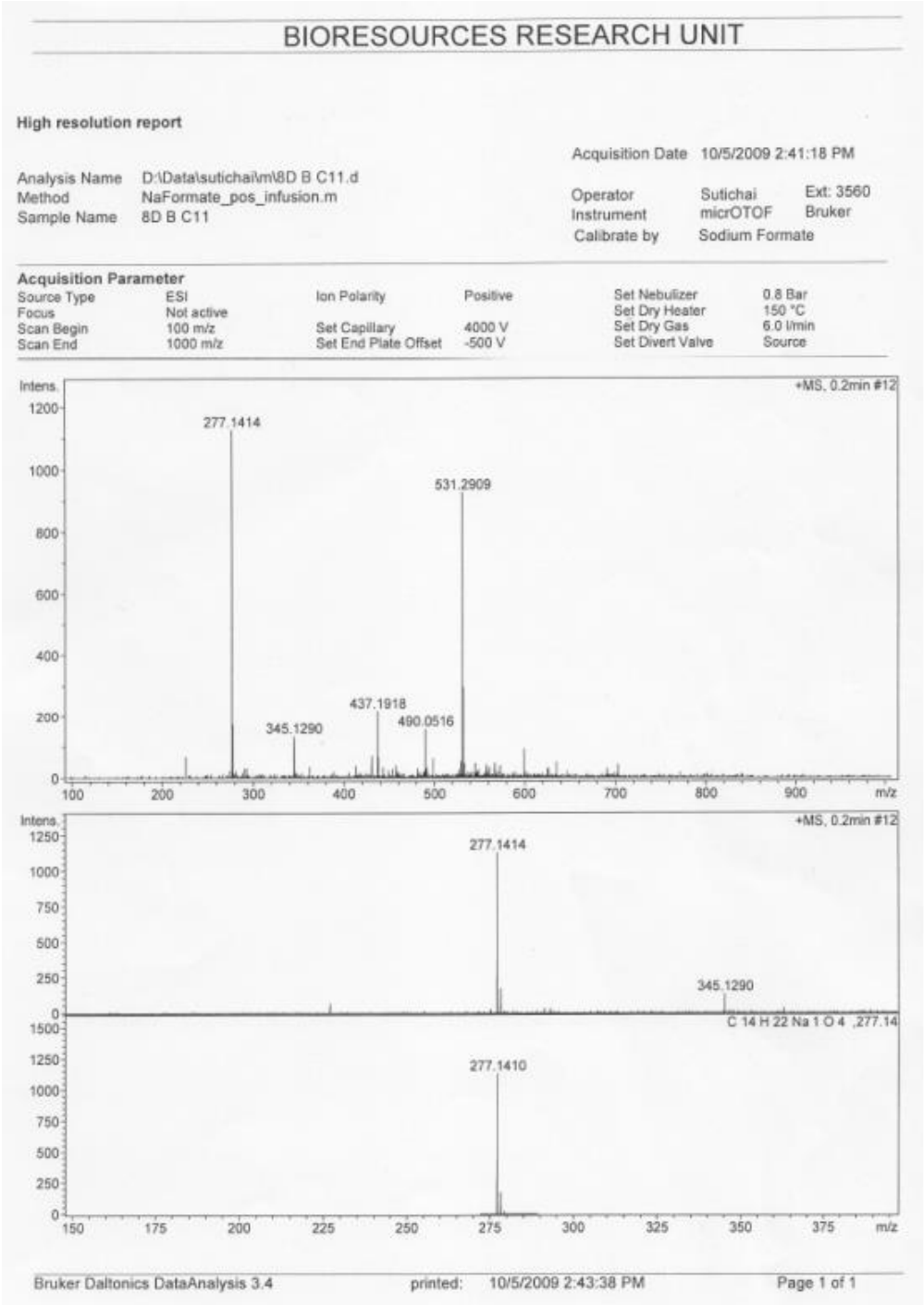

Figure A.51 HRESIMS Mass spectrum of compound **8**

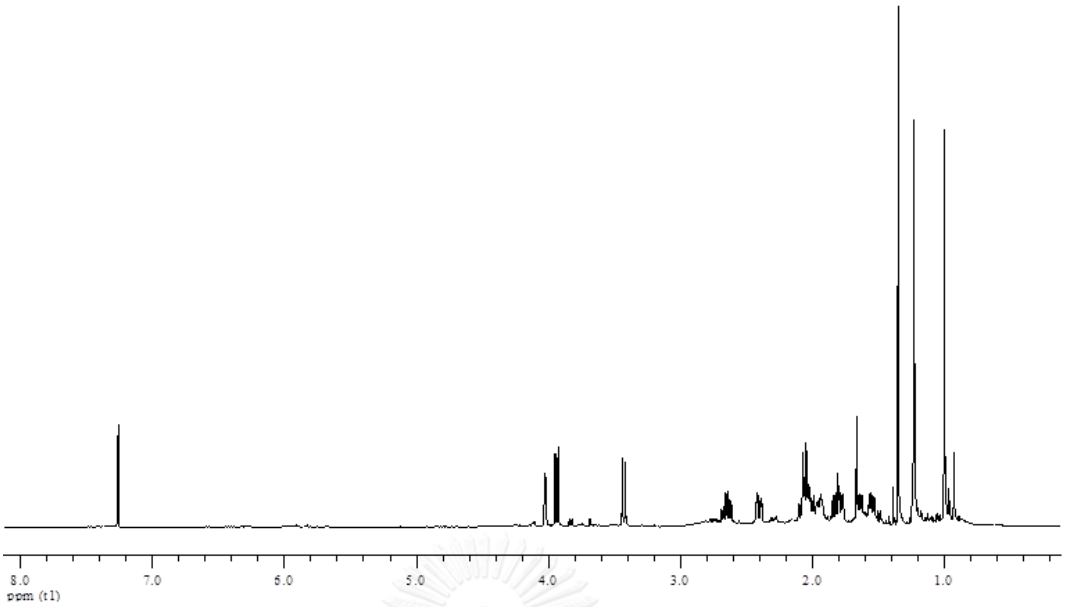

Figure A.52 ^{1}H NMR (400 MHz, $CDCl_3$) spectrum of compound **9**

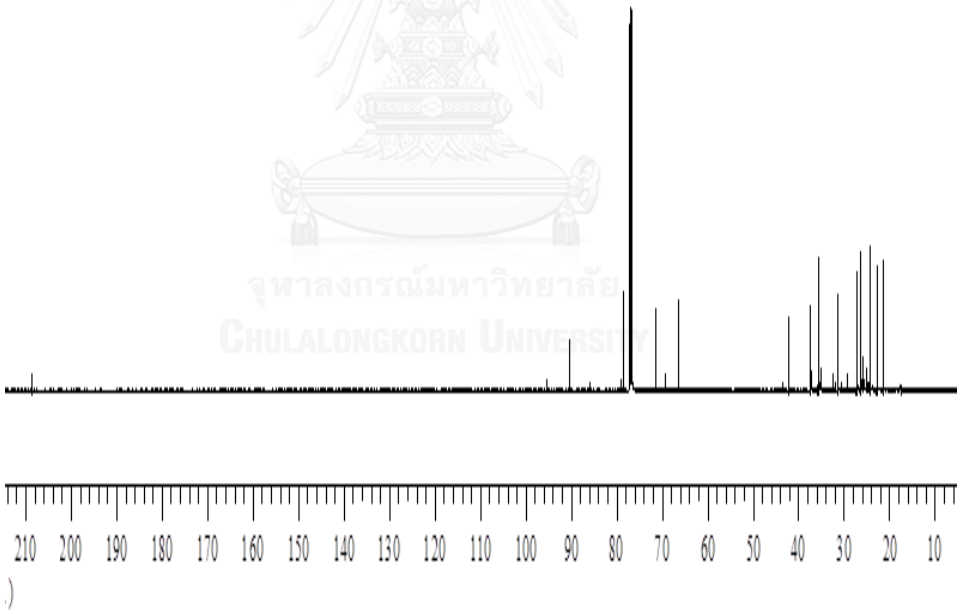

Figure A.53 ^{13}C NMR (100 MHz, $CDCl_3$) spectrum of compound **9**

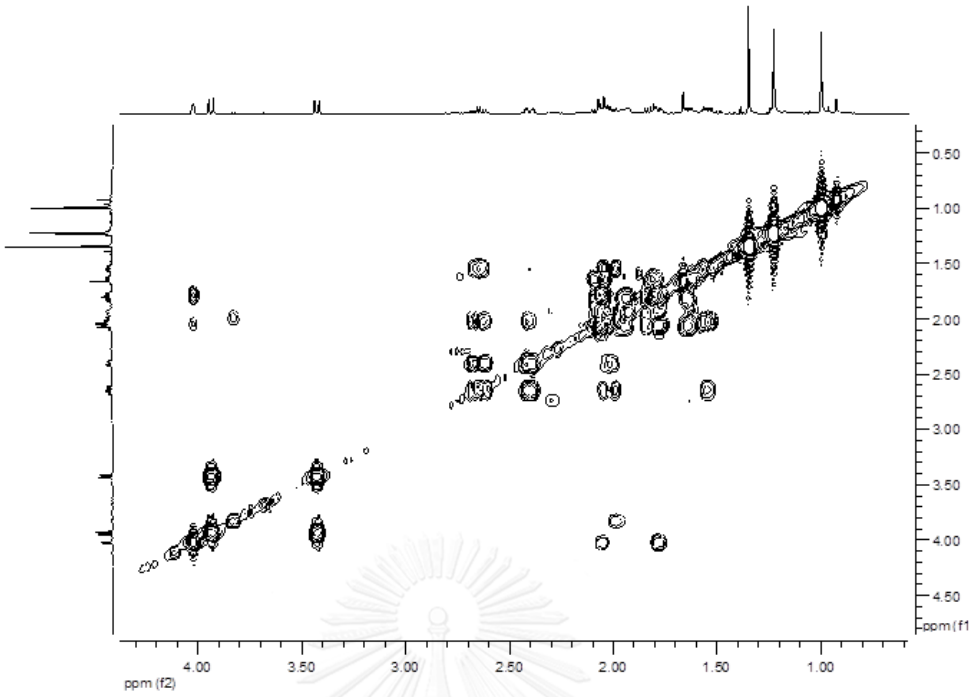

Figure A.54 ^{1}H-^{1}H COSY spectrum ($CDCl_3$) of compound **9**

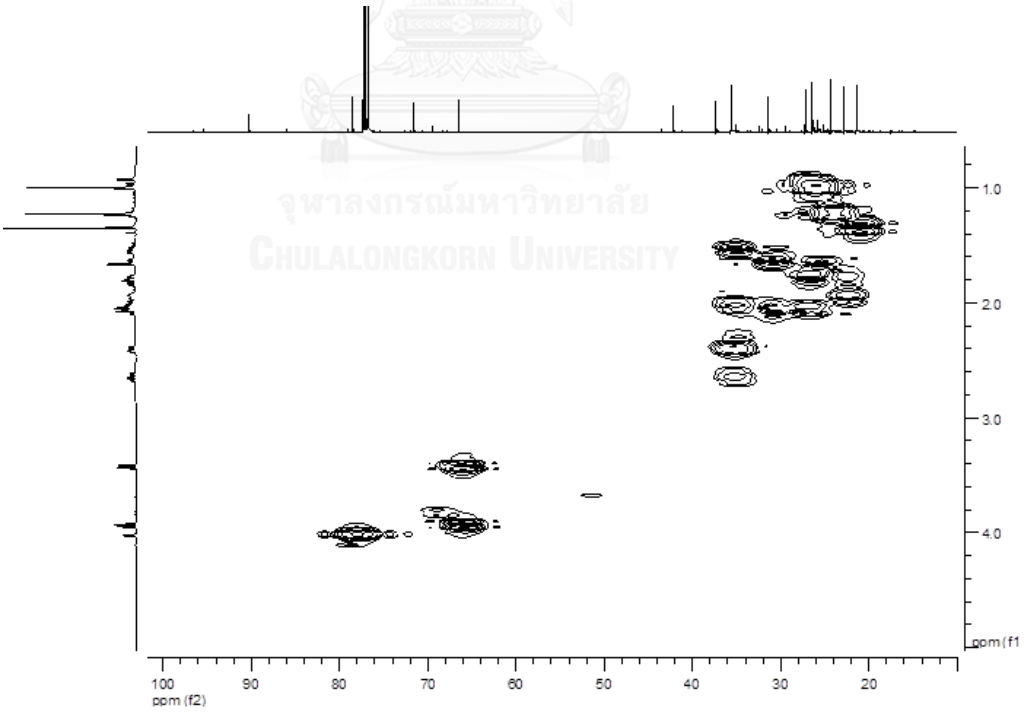

Figure A.55 HSQC spectrum of compound **9**

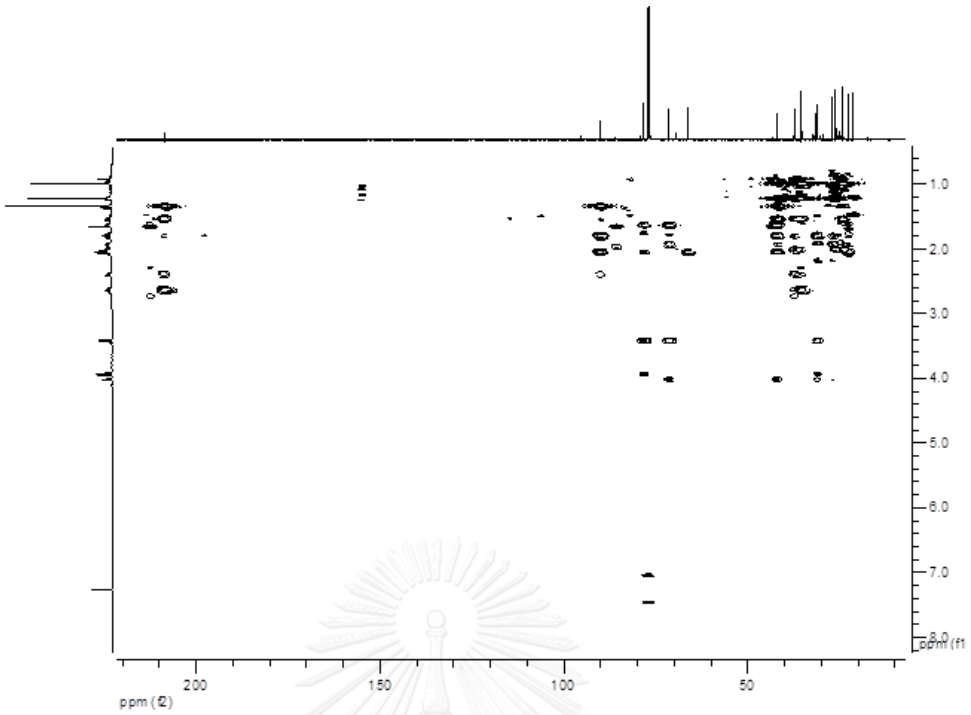

Figure A.56 HMBC spectrum ($CDCl_3$) of compound **9**

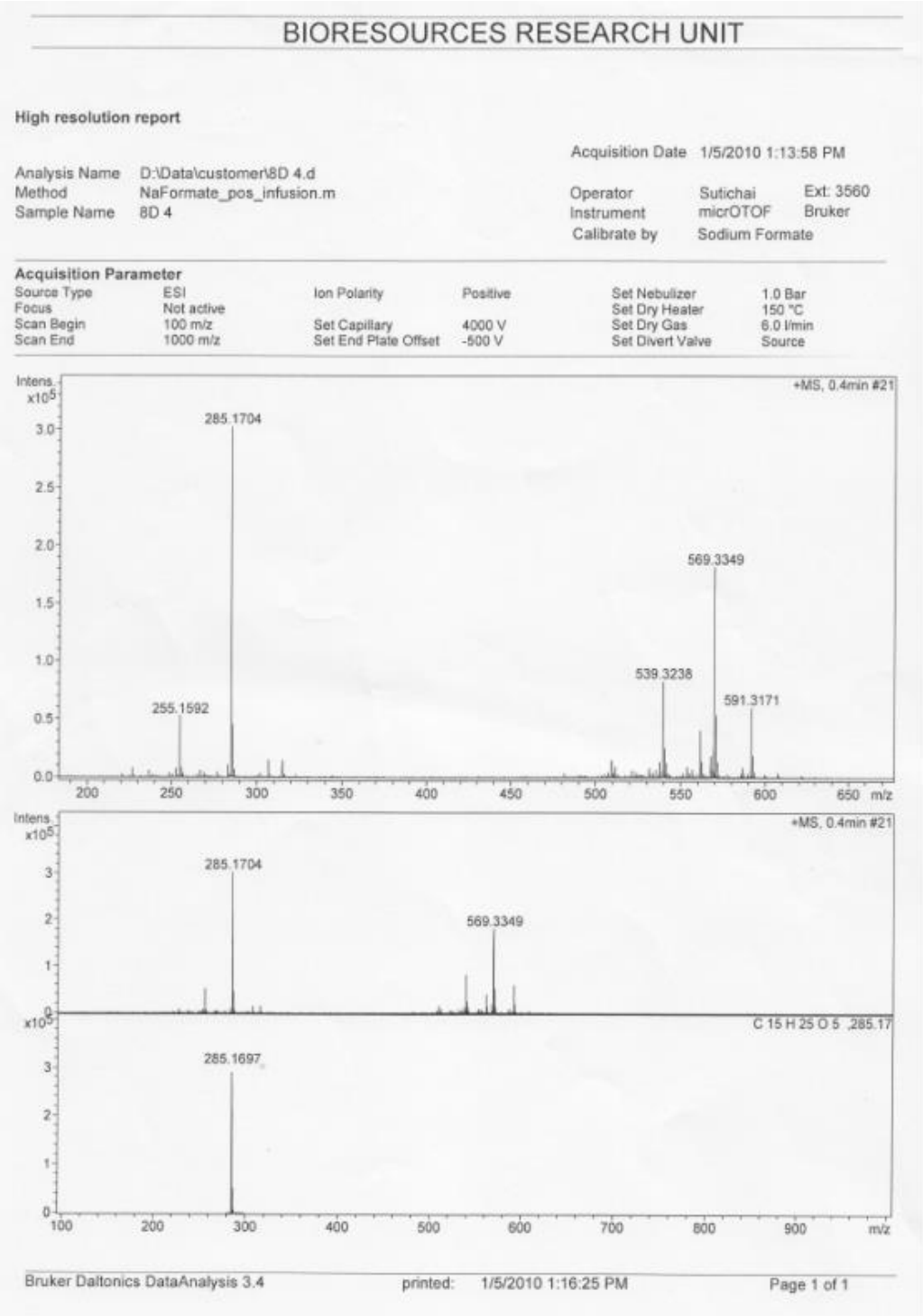

Figure A.57 HRESIMS Mass spectrum of compound **9**

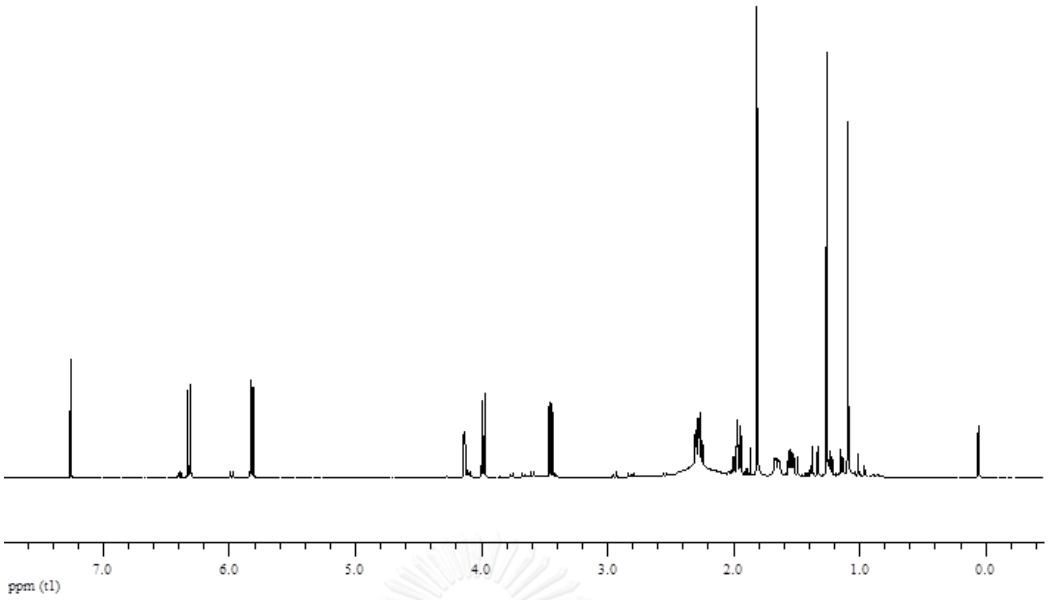

Figure A.58 ^{1}H NMR (500 MHz, $CDCl_3$) spectrum of compound **10**

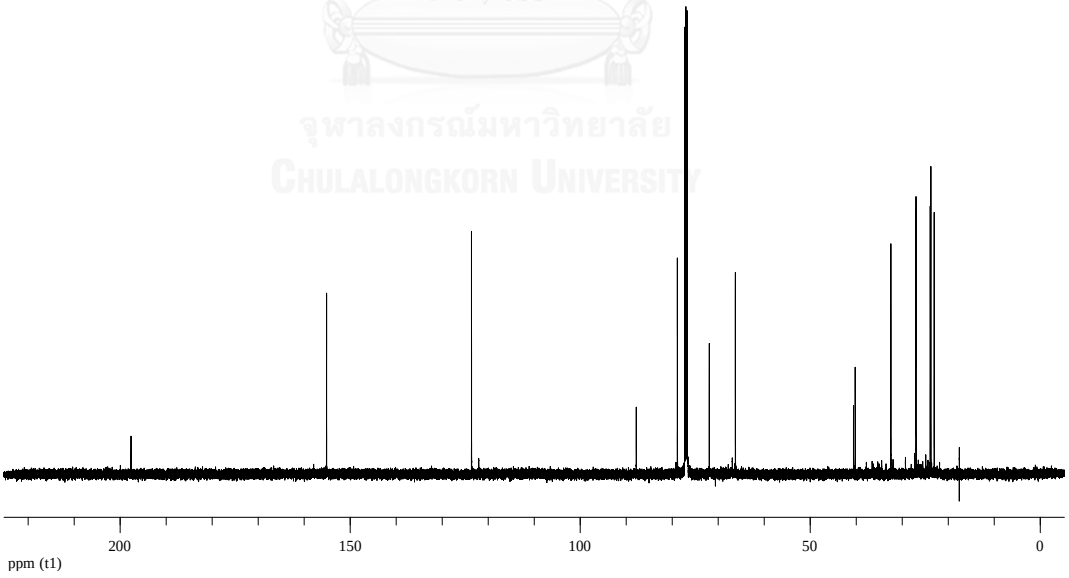

Figure A.59 ^{13}C NMR (100 MHz, $CDCl_3$) spectrum of compound **10**

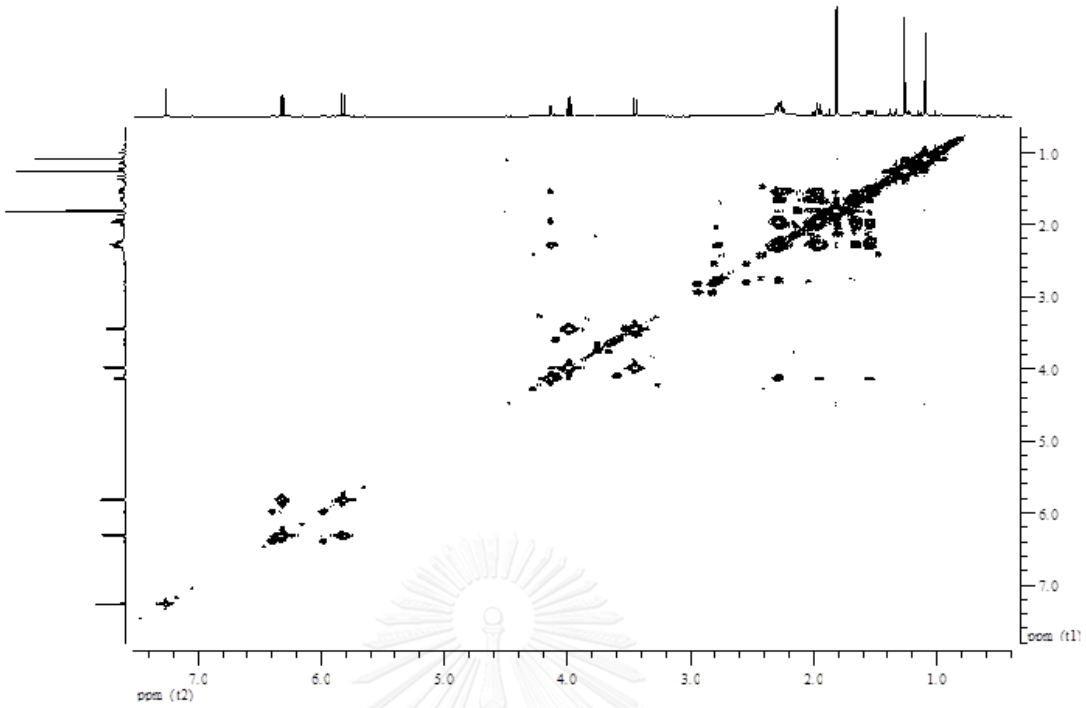

Figure A.60 ^{1}H-^{1}H COSY spectrum ($CDCl_3$) of compound **10**

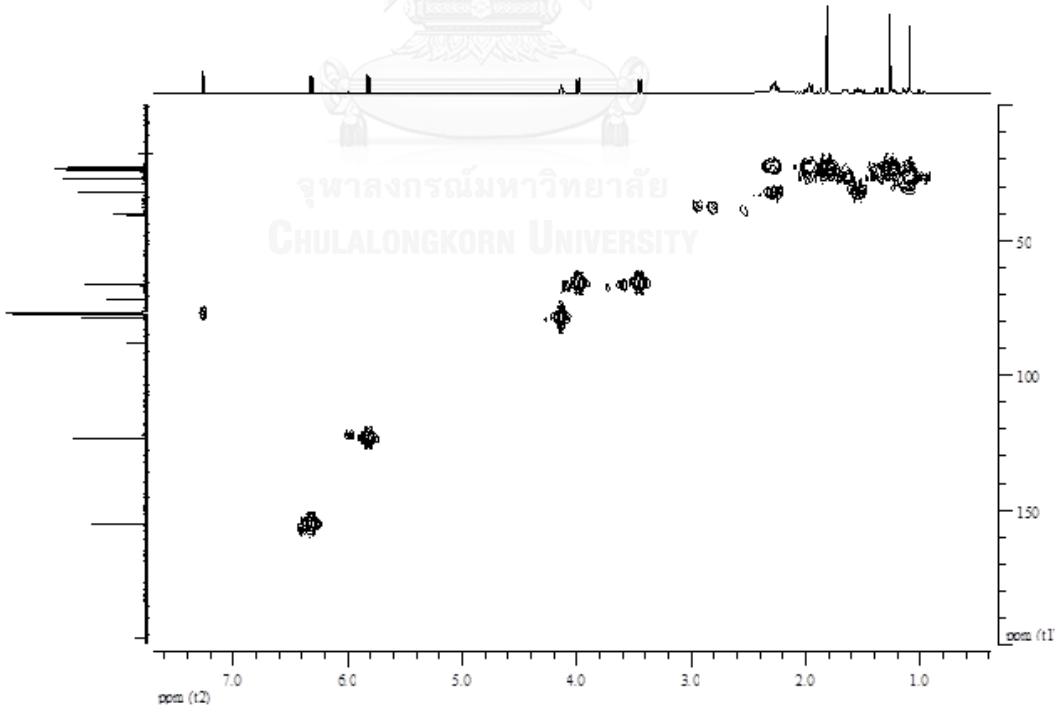

Figure A.61 HSQC spectrum of compound **10**

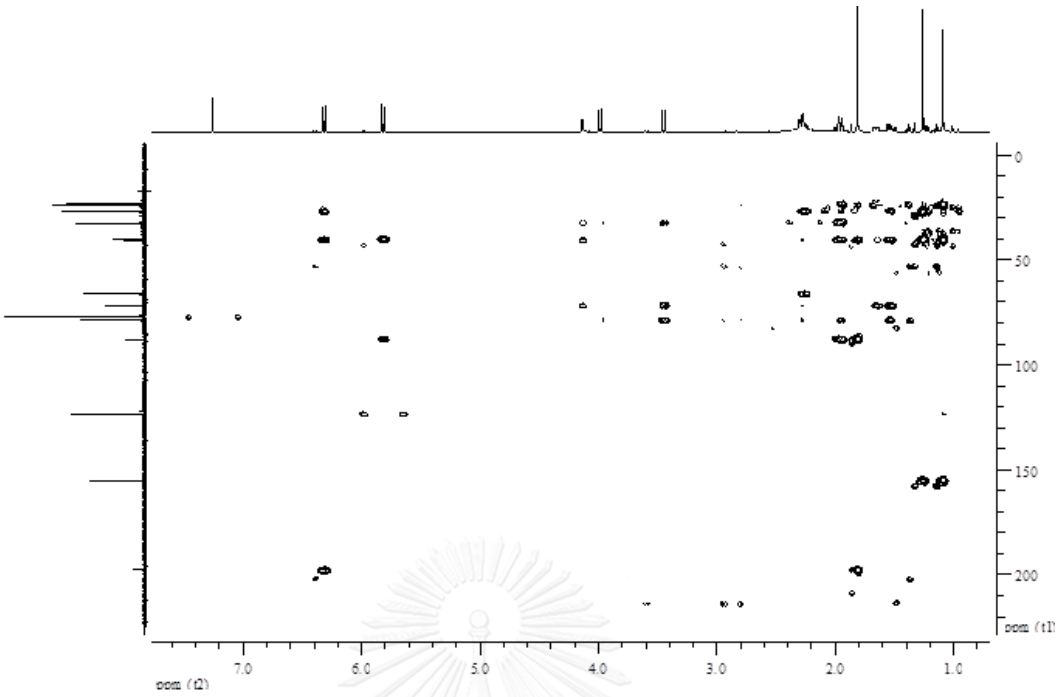

Figure A.62 HMBC spectrum ($CDCl_3$) of compound **10**

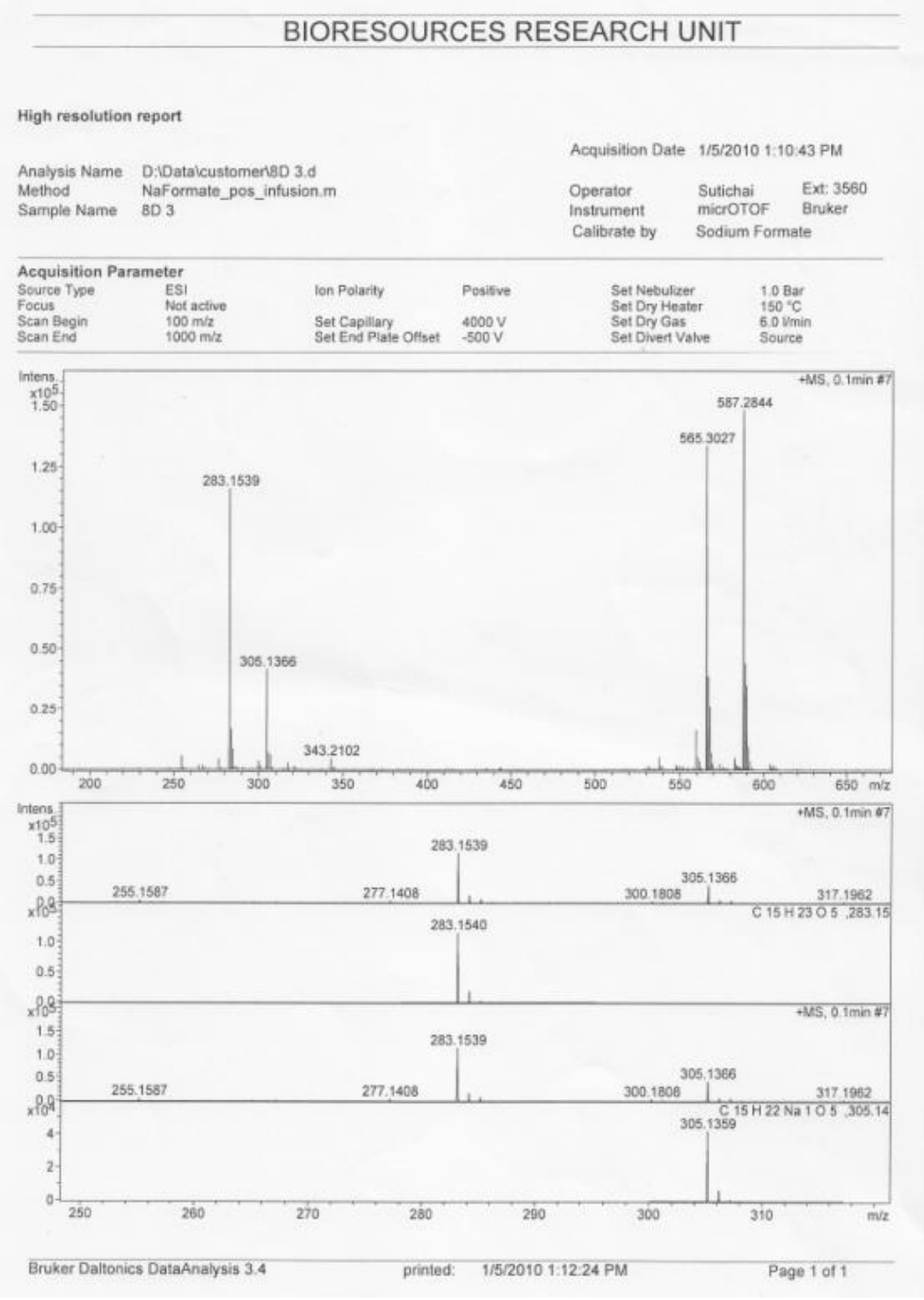

Figure A.63 HRESIMS Mass spectrum of compound **10**

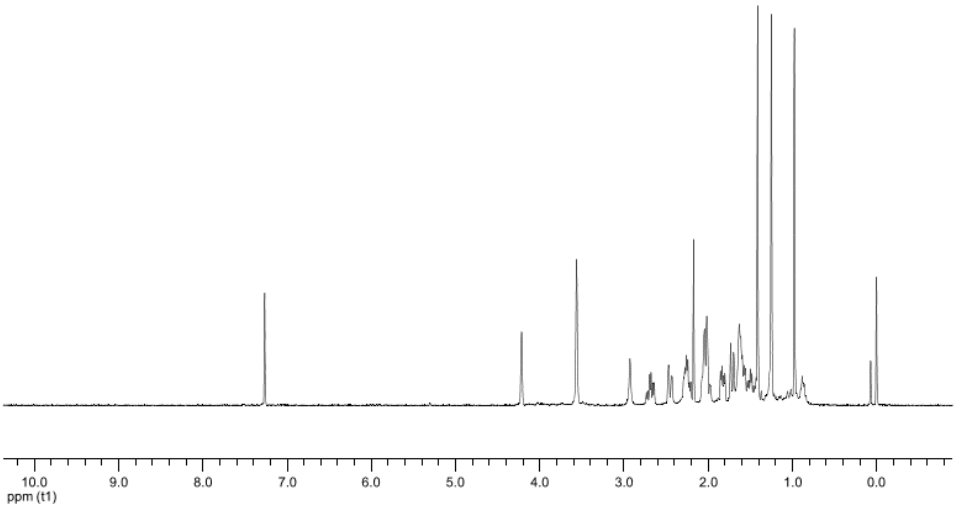

Figure A.64 ^{1}H NMR (400 MHz, $CDCl_3$) spectrum of compound **11**

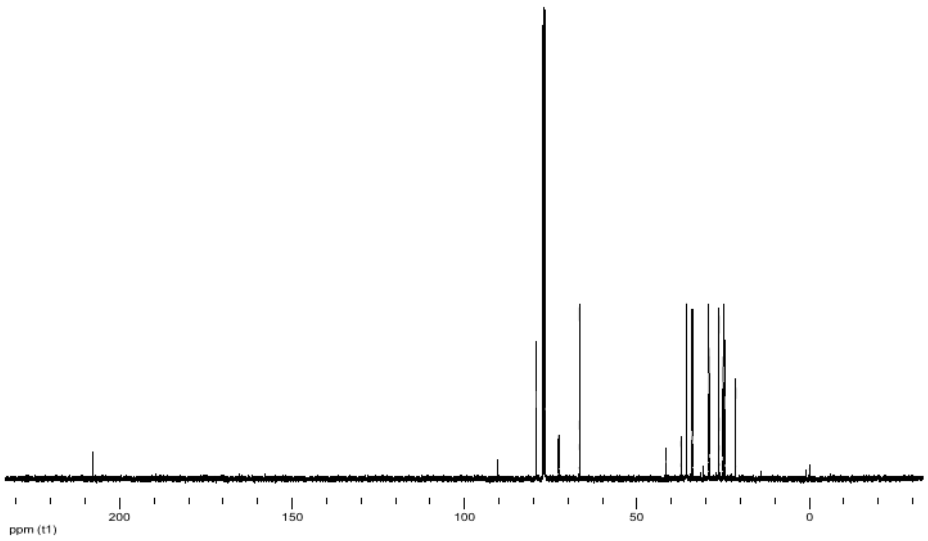

Figure A.65 ^{13}C NMR (100 MHz, $CDCl_3$) spectrum of compound **11**

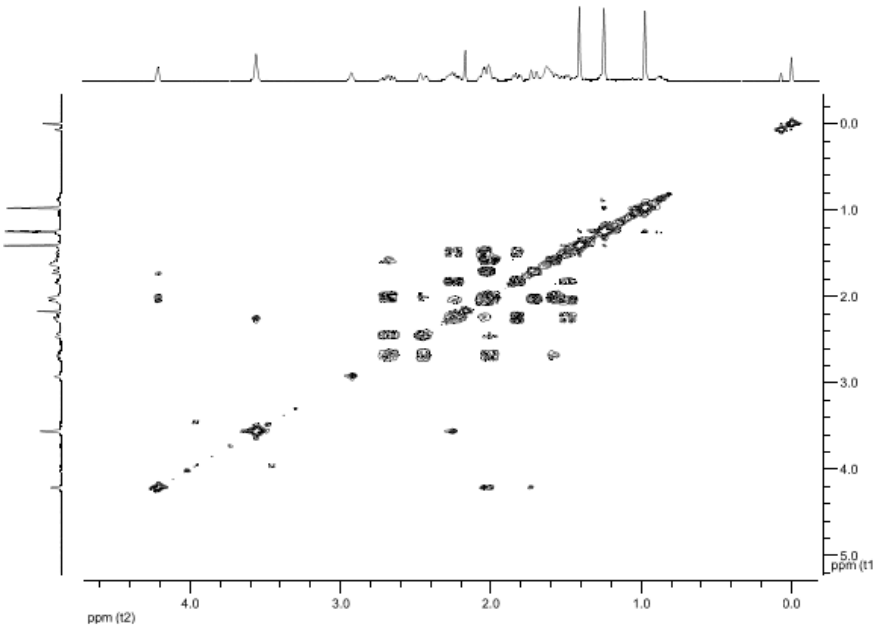

Figure A.66 ^{1}H-^{1}H COSY spectrum ($CDCl_3$) of compound **11**

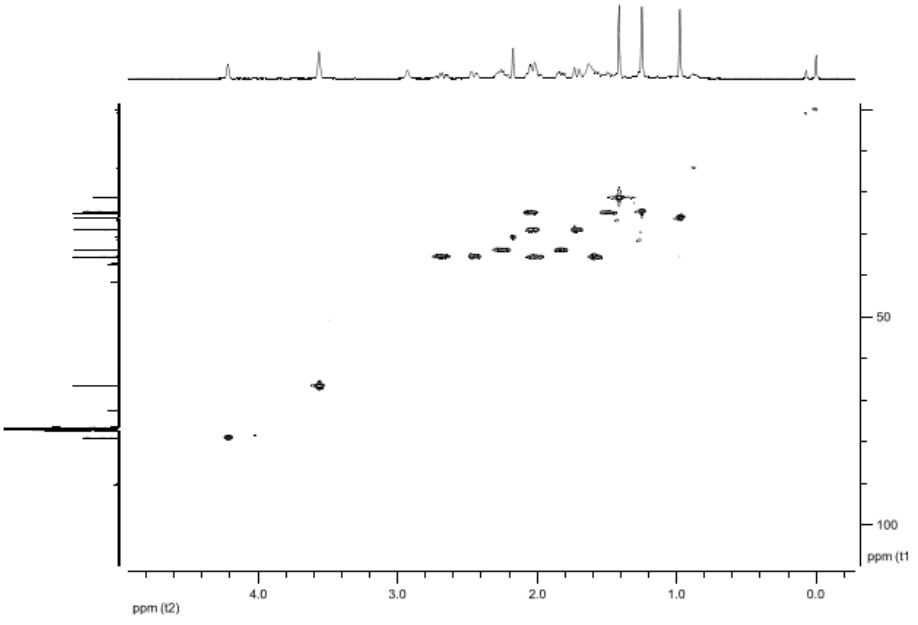

Figure A.67 HSQC spectrum of compound **11**

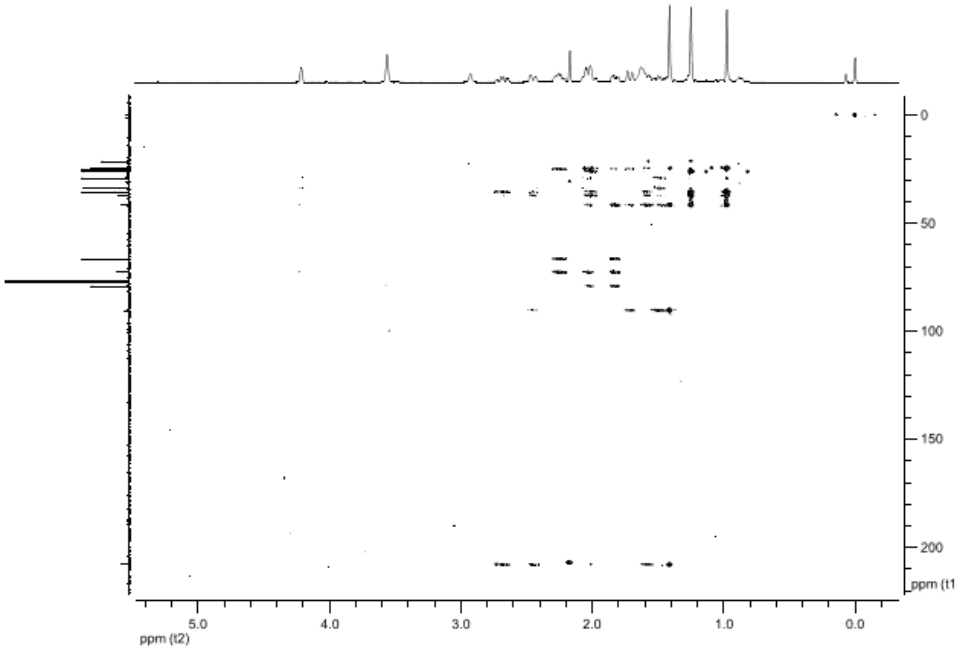

Figure A.68 HMBC spectrum ($CDCl_3$) of compound **11**

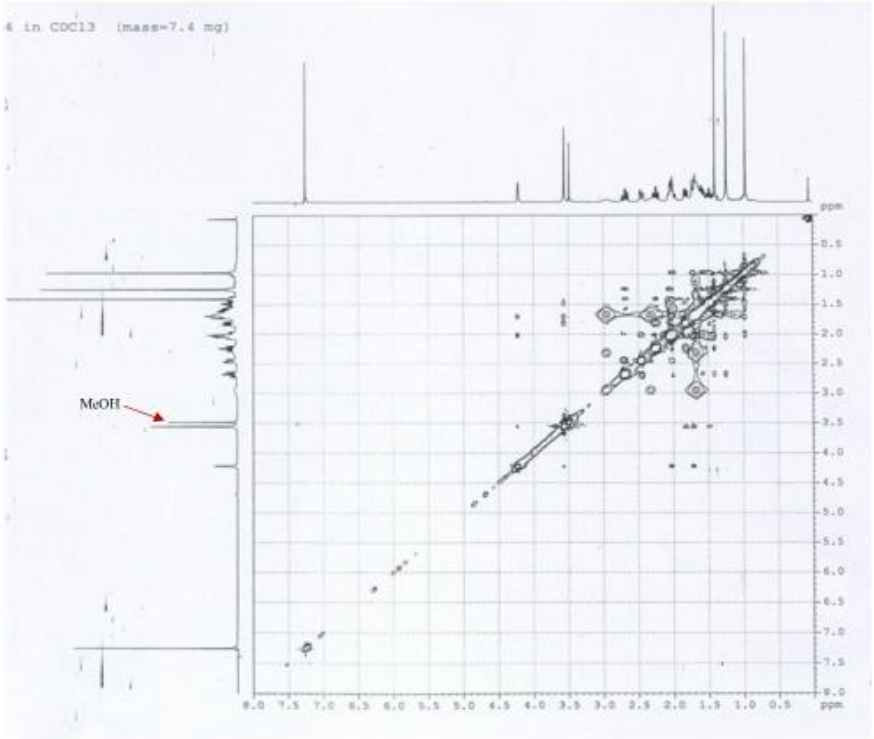

Figure A.69 NOESY spectrum ($CDCl_3$) of compound **11**

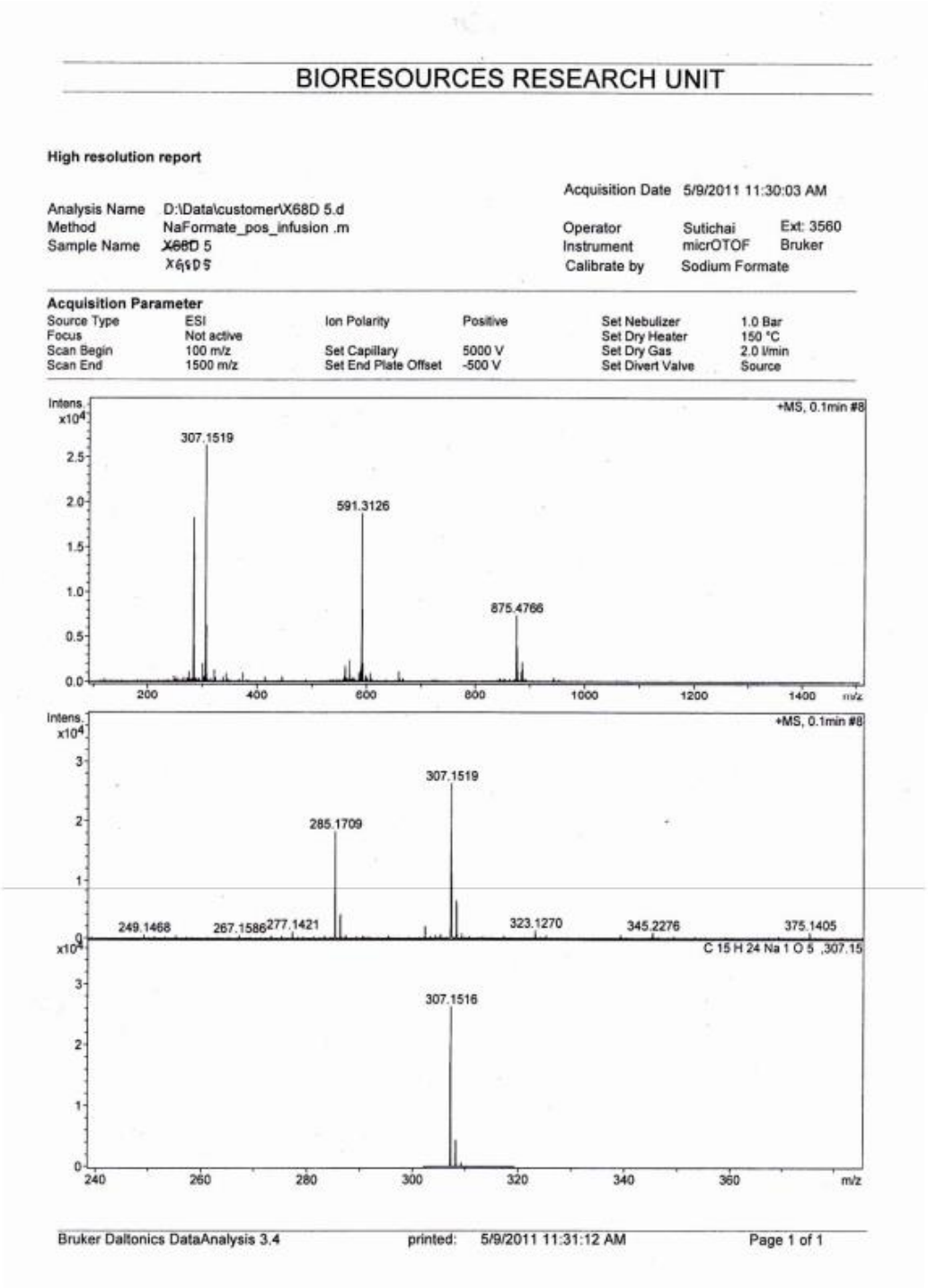

Figure A.70 HRESIMS Mass spectrum of compound **11**

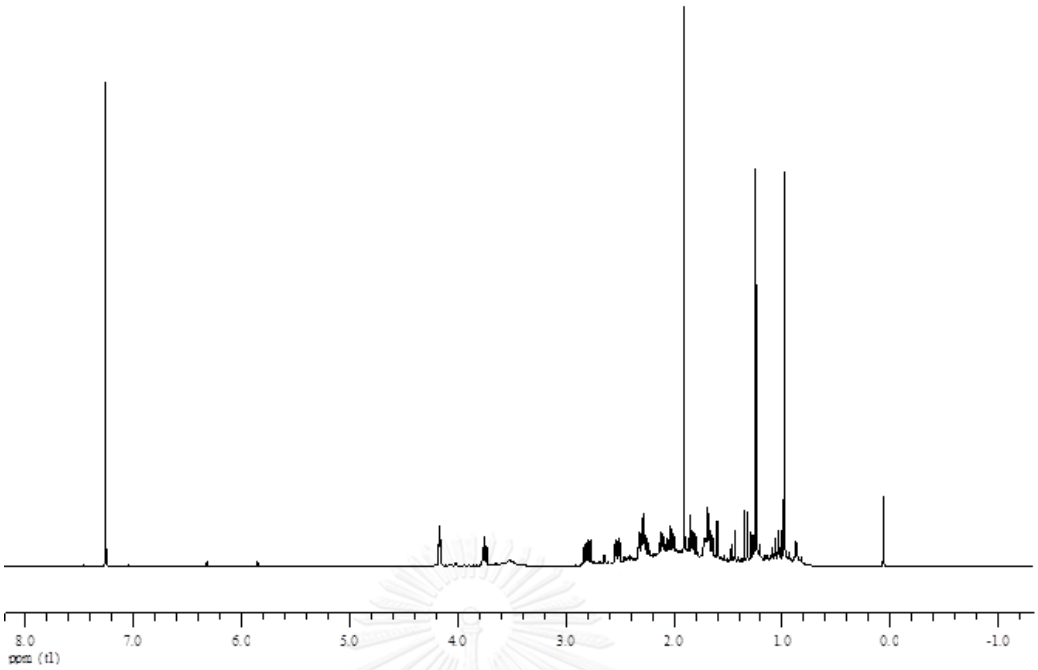

Figure A.71 ^{1}H NMR (400 MHz, $CDCl_3$) spectrum of compound **12**

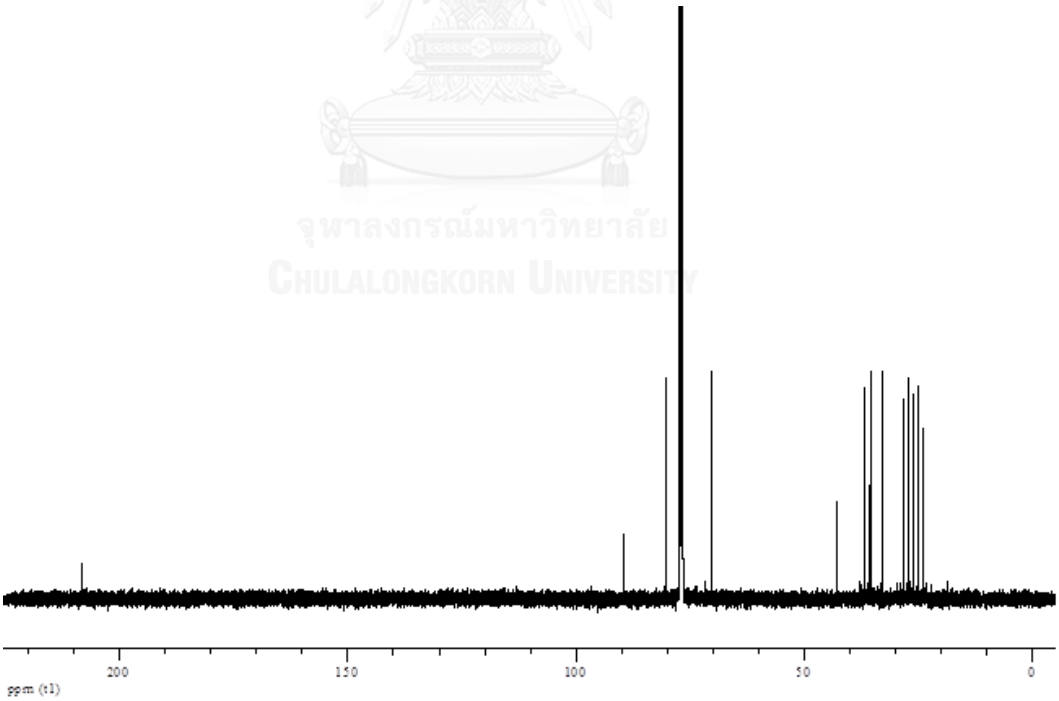

Figure A.72 ^{13}C NMR (100 MHz, $CDCl_3$) spectrum of compound **12**

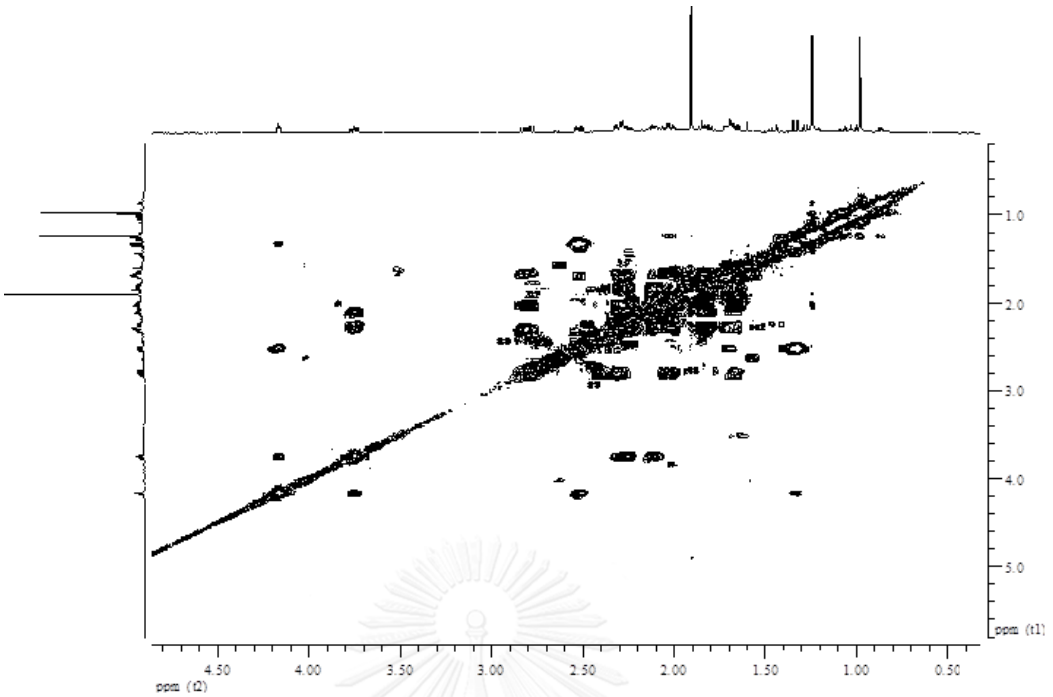

Figure A.73 ^{1}H-^{1}H COSY spectrum ($CDCl_3$) of compound **12**

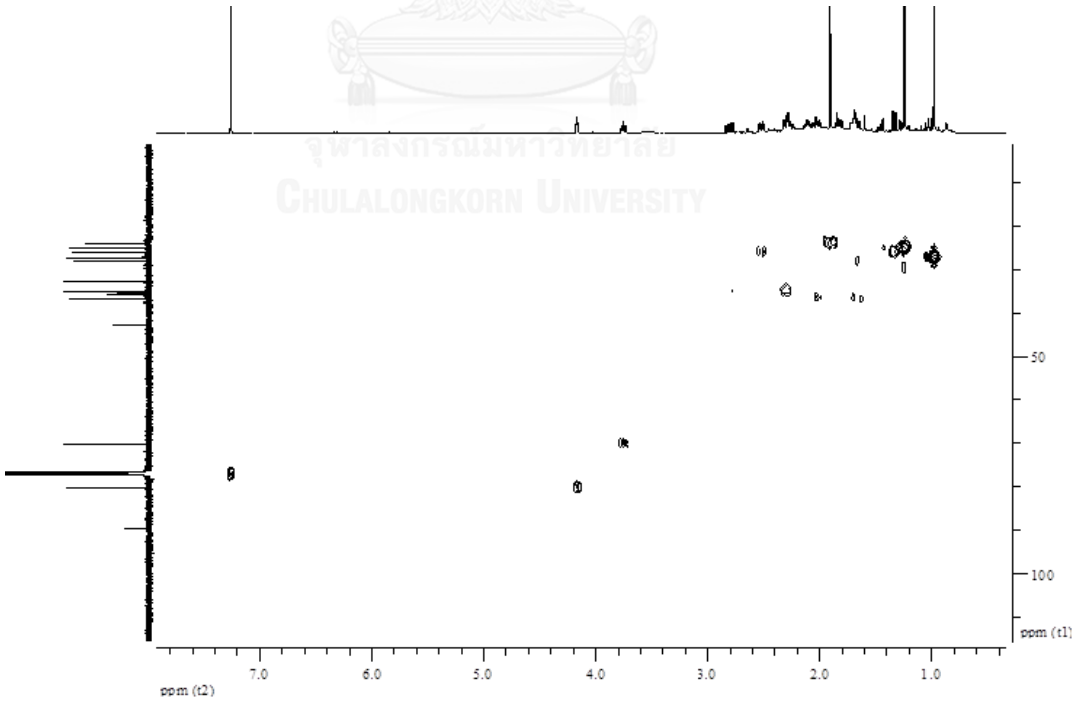

Figure A.74 HSQC spectrum ($CDCl_3$) of compound **12**

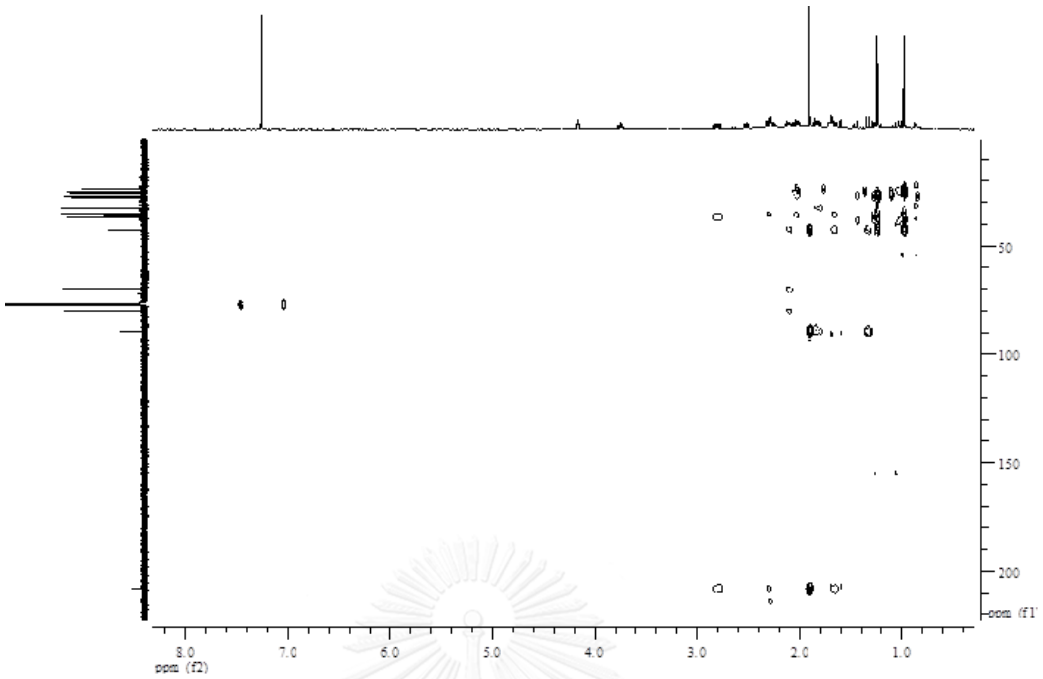

Figure A.75 HMBC spectrum ($CDCl_3$) of compound **12**

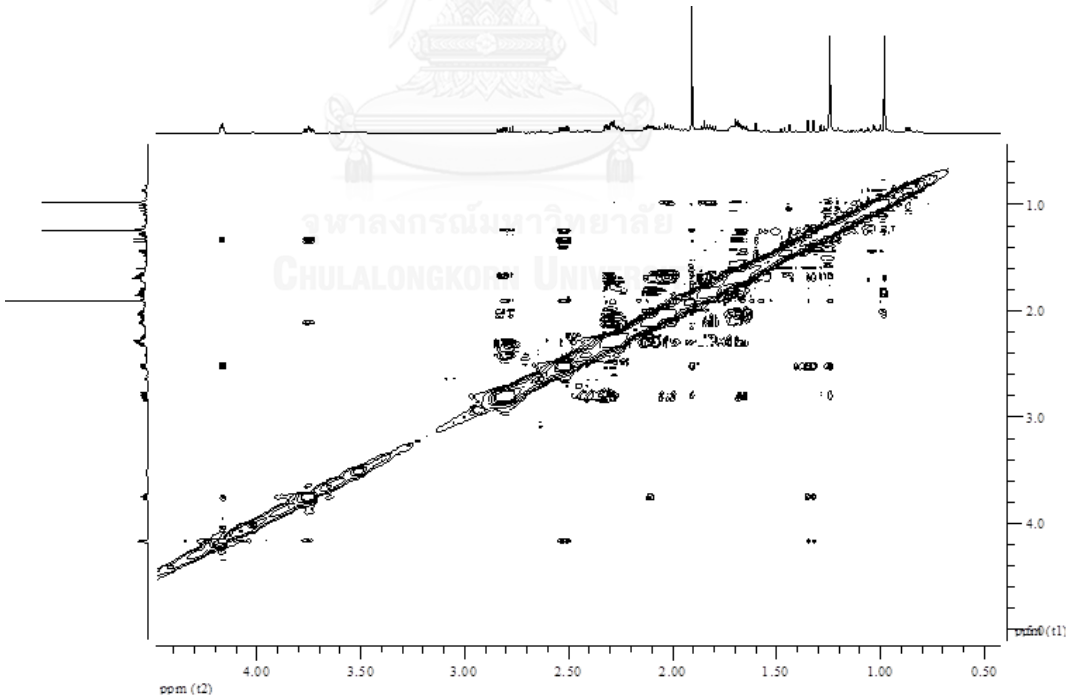

Figure A.76 NOESY spectrum ($CDCl_3$) of compound **12**

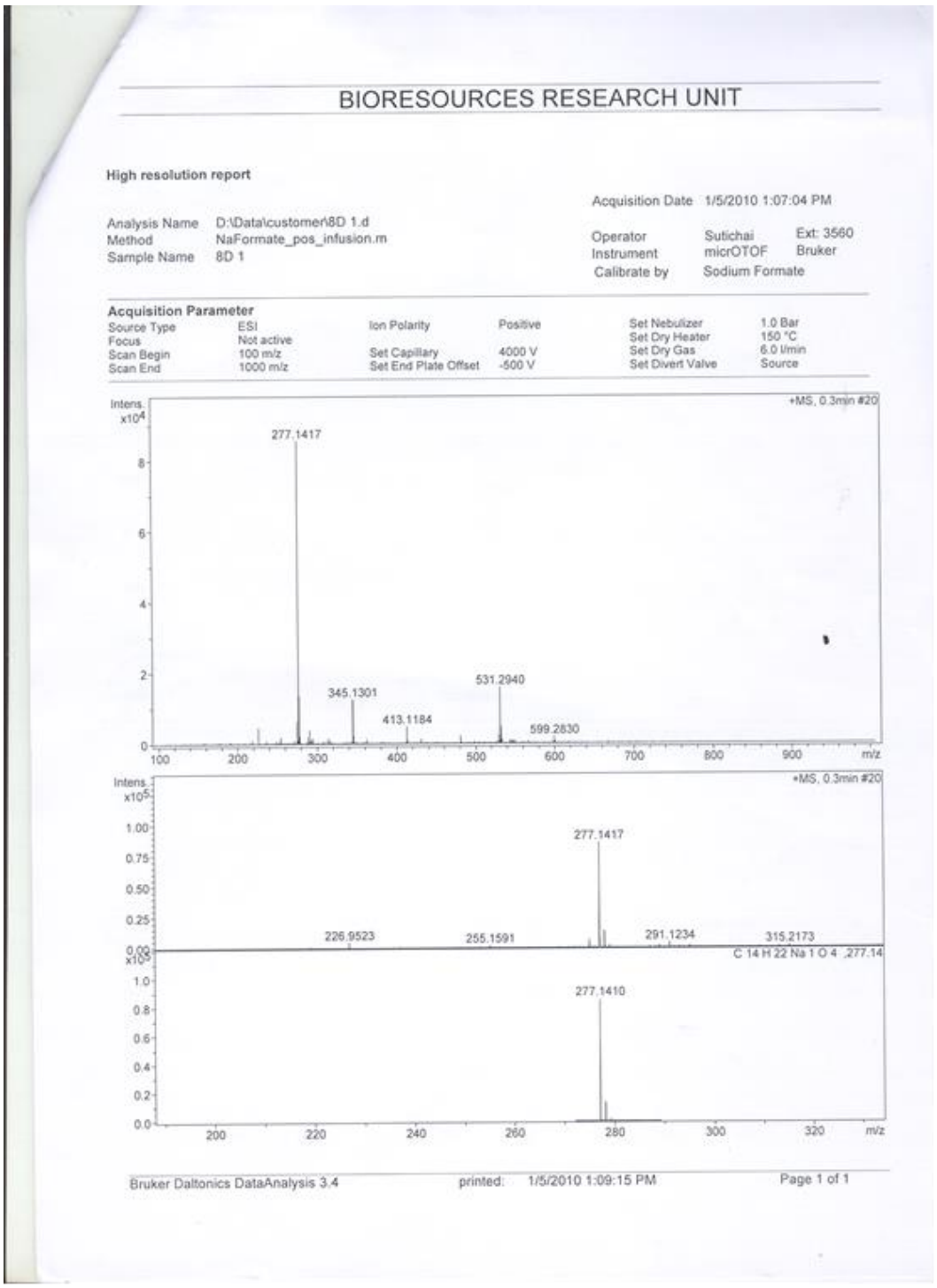

Figure A.77 HRESIMS Mass spectrum of compound **12**

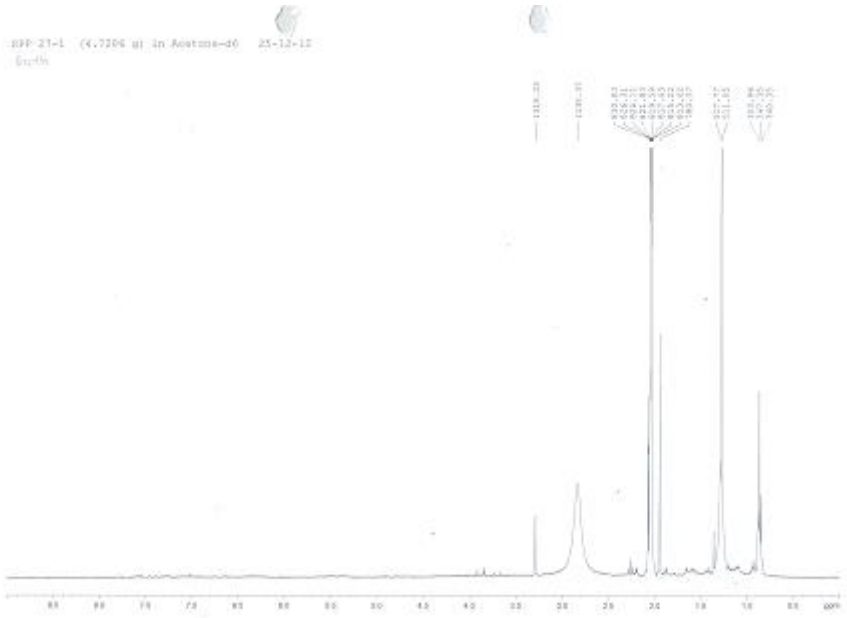

Figure A.78 ^{1}H (400 MHz, acetone-d_6) NMR spectrum of crude broth (BCC3553 cultured on LCN medium)

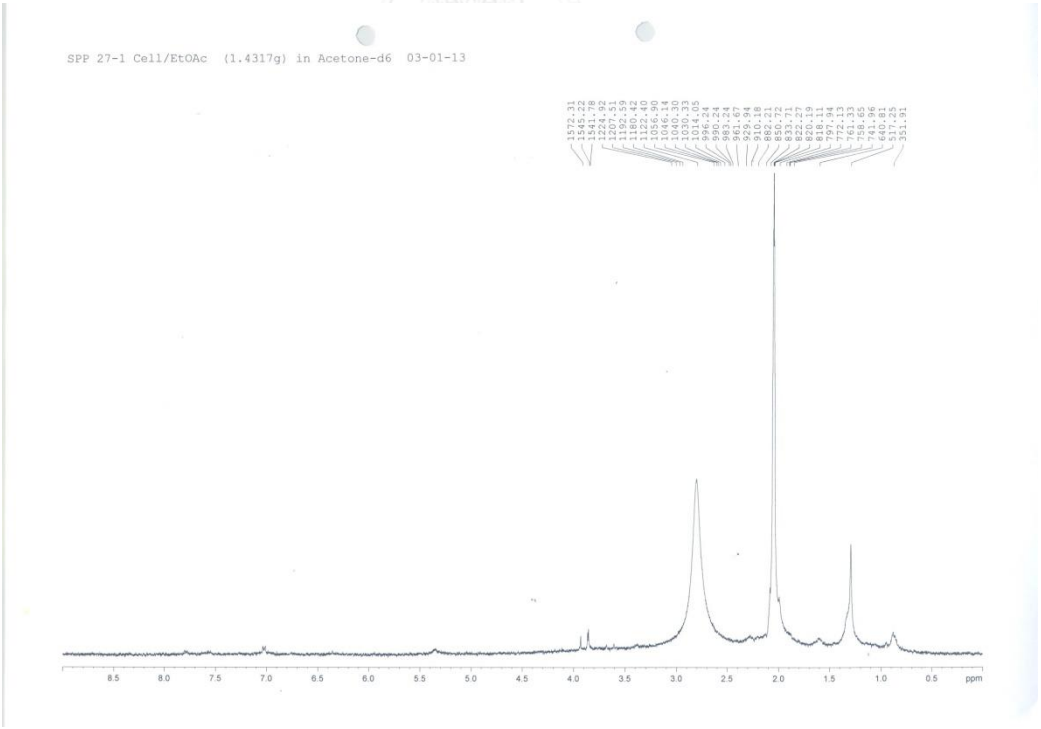

Figure A.79 ^{1}H (400 MHz, acetone-d_6) NMR spectrum of crude mycelium (BCC3553 cultured on LCN medium)

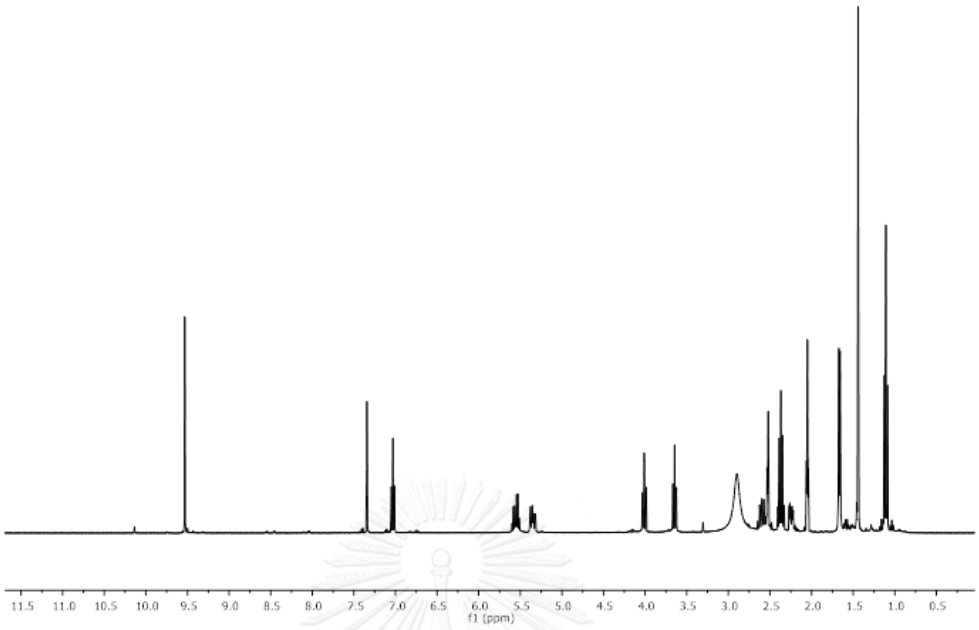

Figure A.80 ^{1}H (500 MHz, acetone-d_6) NMR spectrum of compound **13**

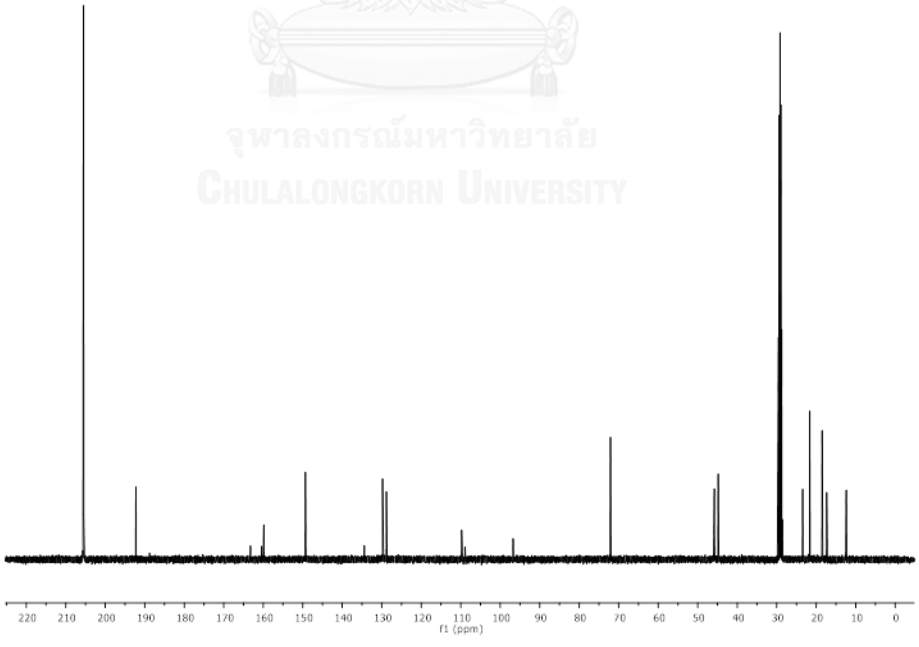

Figure A.81 ^{13}C NMR (acetone-d_6) NMR spectrum of compound **13**

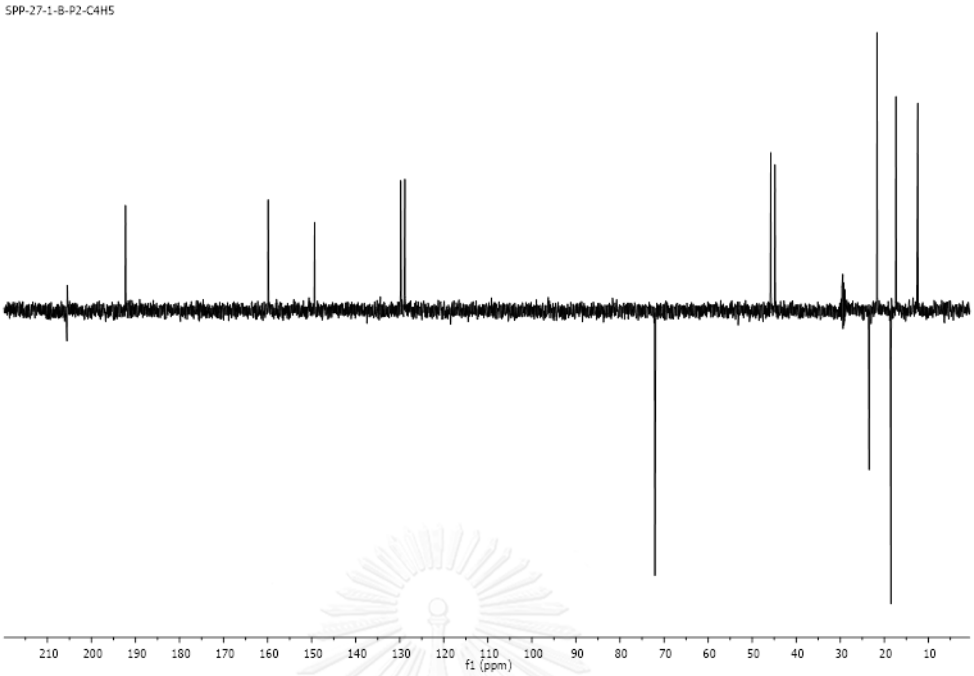

Figure A.82 DEPT spectrum (acetone-d_6) of compound **13**

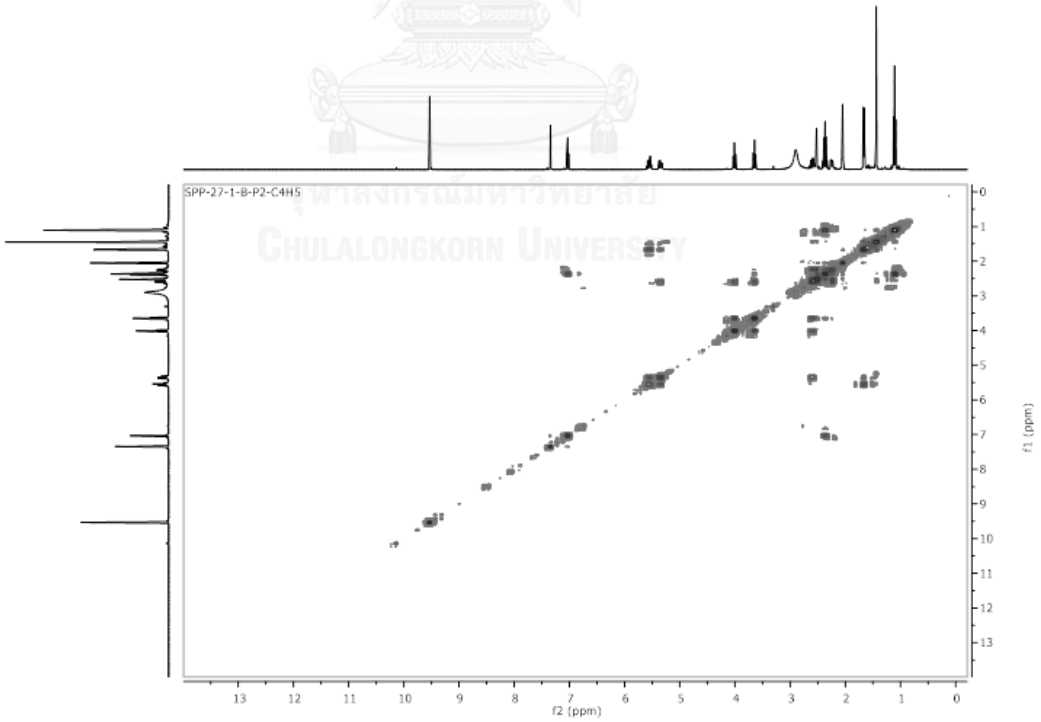

Figure A.83 ^{1}H-^{1}H COSY spectrum (acetone-d_6) of compound **13**

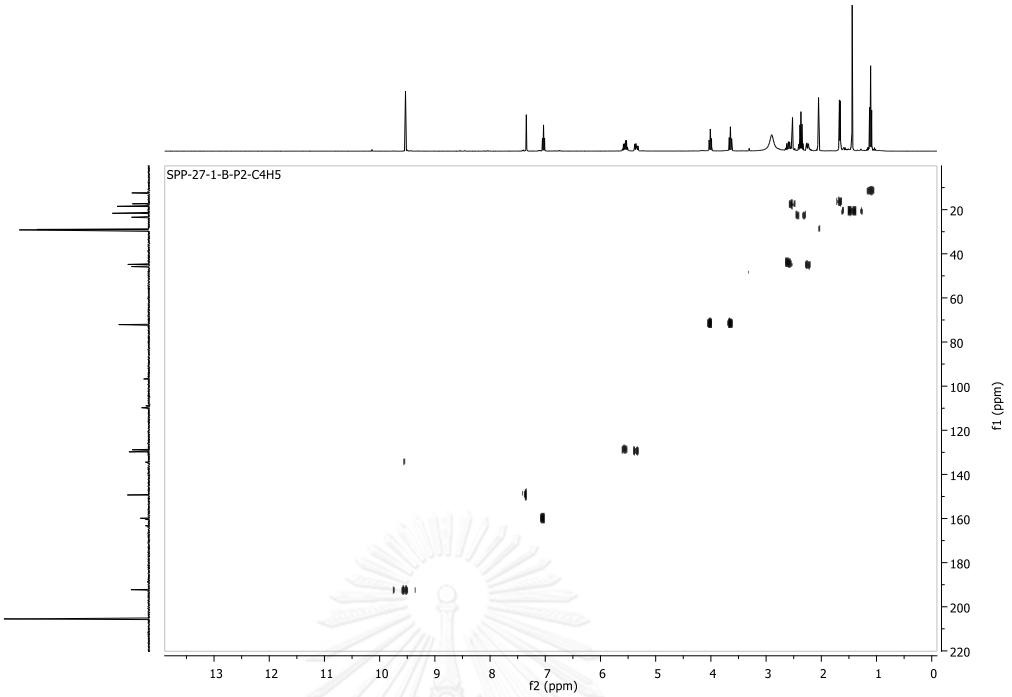

Figure A.84 HMQC spectrum (acetone-d_6) of compound **13**

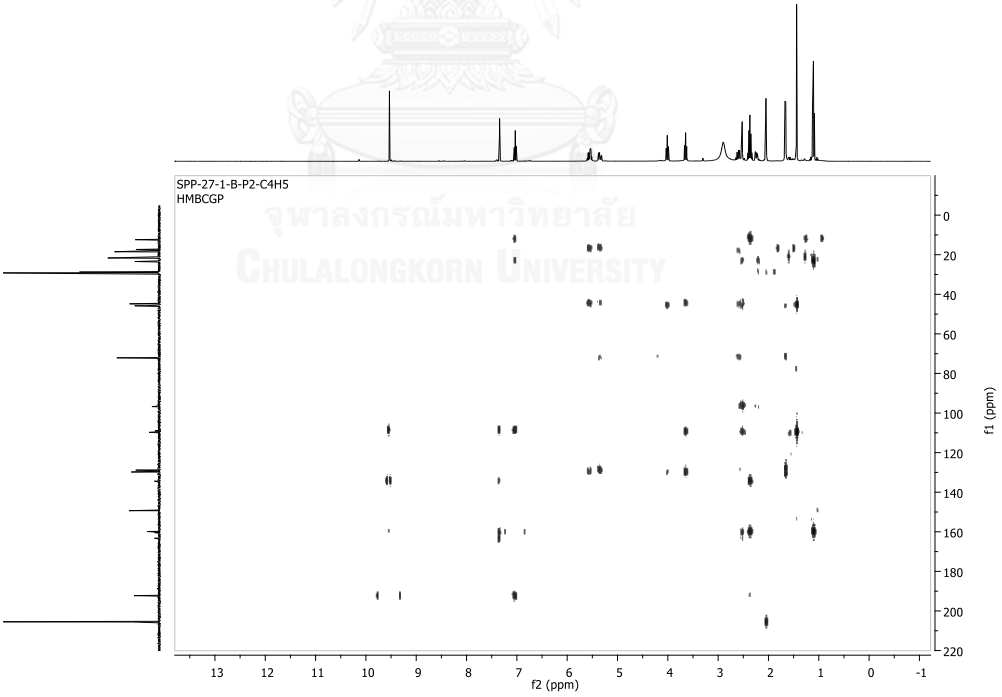

Figure A.85 HMBC spectrum (acetone-d_6) of compound **13**

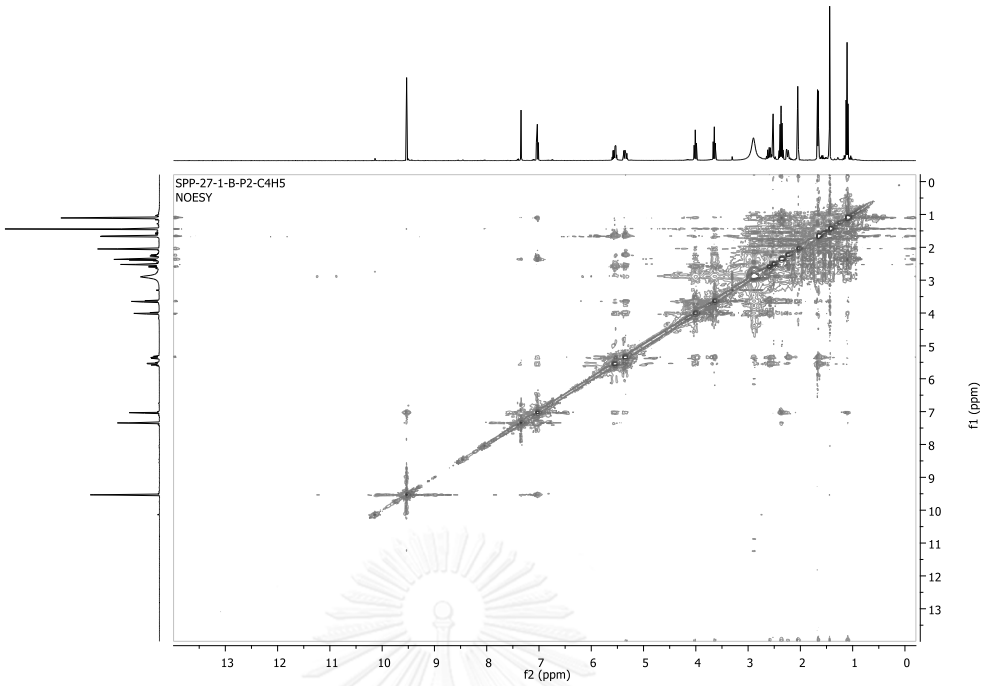

Figure A.86 NOESY spectrum (acetone-d_6) of compound **13**

BIORESOURCES RESEARCH UNIT

High resolution report

		Acquisition Date	10/18/2013 3:03:17 PM
Analysis Name	D:\Data\Taridaporn\SPP27 1 B P2 C4 H5.d		
Method	NaFormate_pos_infusion .m	Operator	Sutichai Ext: 3560
Sample Name	SPP27 1 B P2 C4 H5	Instrument	micrOTOF Bruker
		Calibrate by	Sodium Formate

Acquisition Parameter

Source Type	ESI	Ion Polarity	Positive	Set Nebulizer	1.0 Bar
Focus	Not active			Set Dry Heater	150 °C
Scan Begin	80 m/z	Set Capillary	5000 V	Set Dry Gas	2.0 l/min
Scan End	1500 m/z	Set End Plate Offset	-500 V	Set Divert Valve	Source

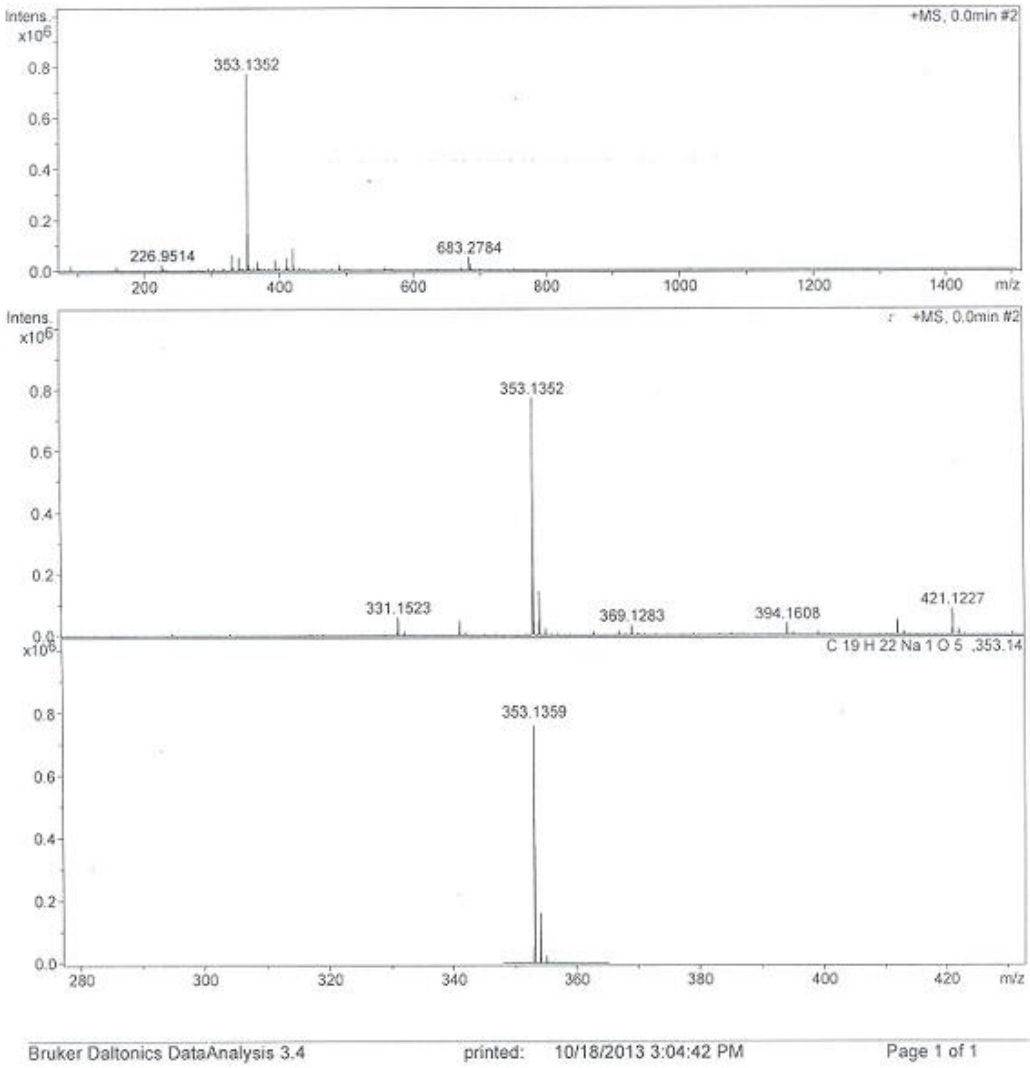

Bruker Daltonics DataAnalysis 3.4 printed: 10/18/2013 3:04:42 PM Page 1 of 1

Figure A.87 HRESIMS Mass spectrum of compound **13**

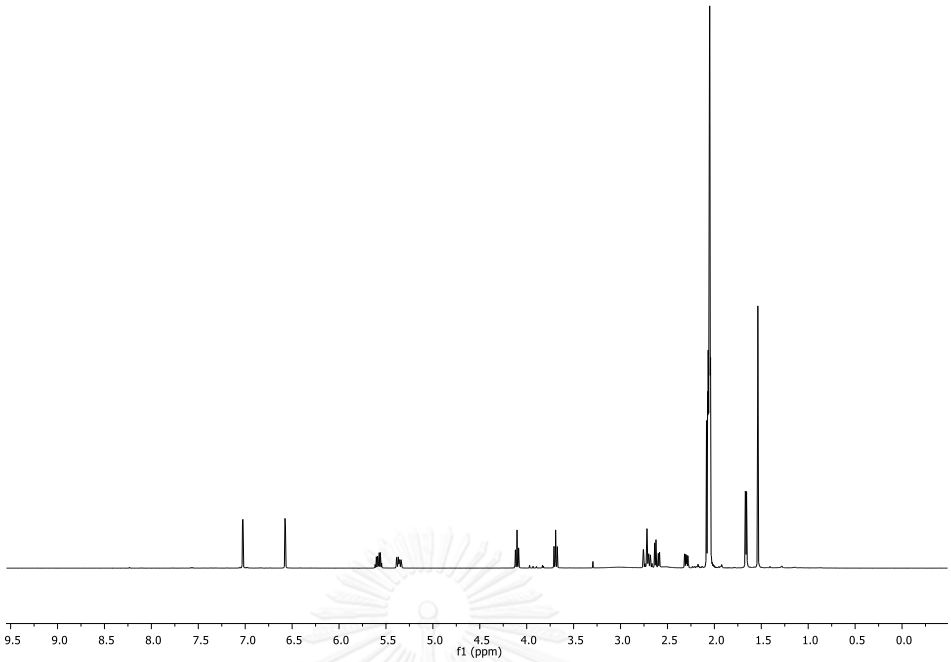

Figure A.88 ^{1}H (500 MHz, acetone-d_6) NMR spectrum of compound **14**

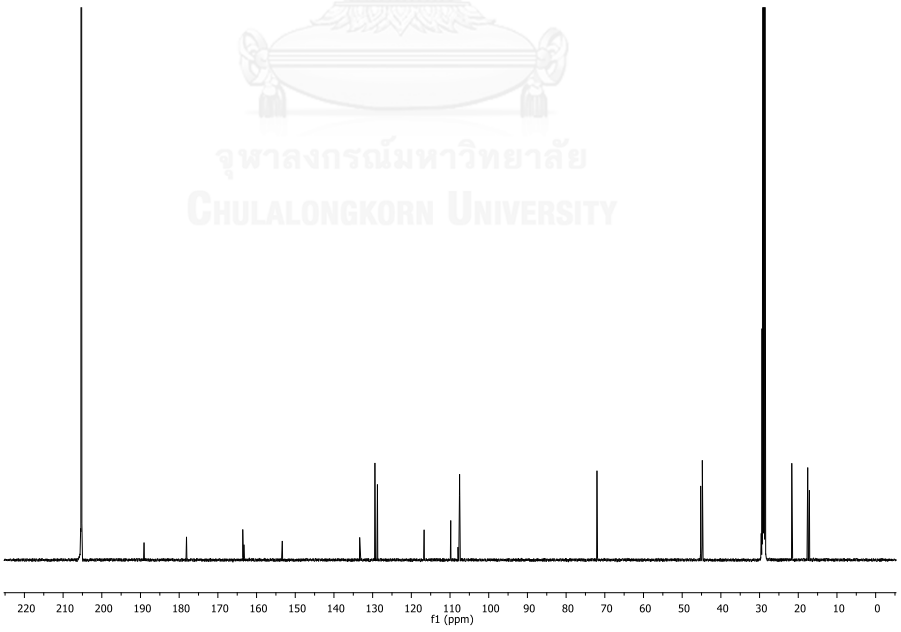

Figure A.89 ^{13}C NMR (acetone-d_6) NMR spectrum of compound **14**

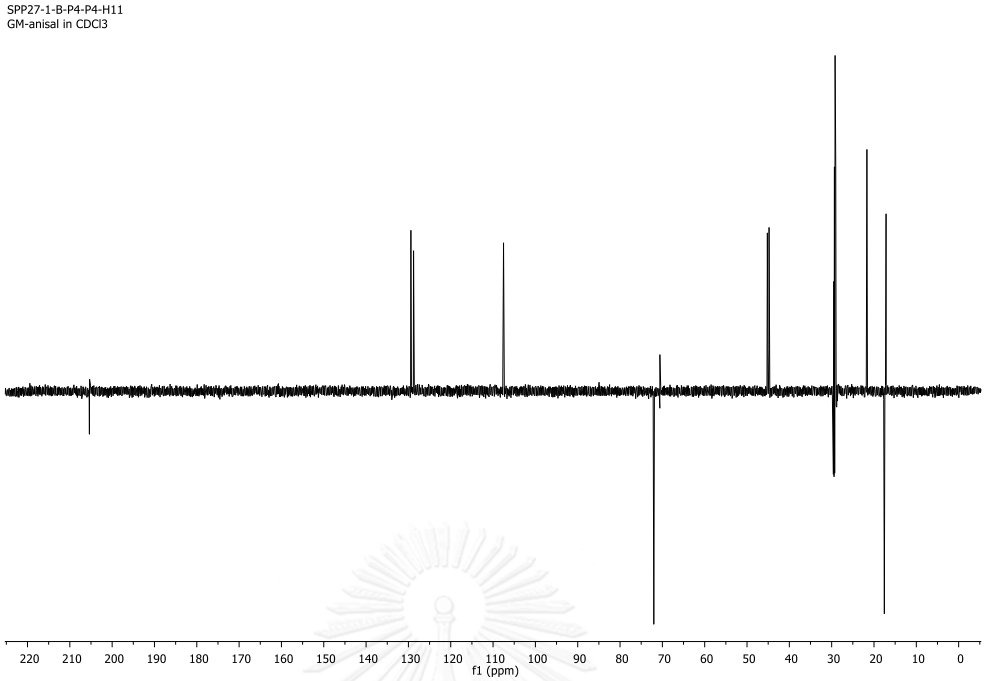

Figure A.90 DEPT spectrum (acetone-d_6) of compound **14**

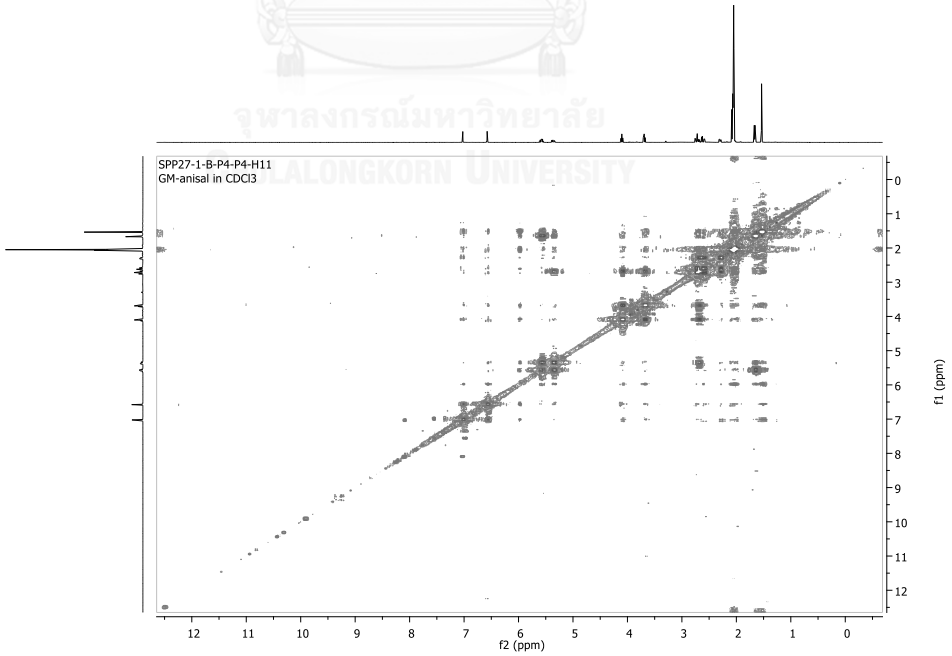

Figure A.91 ^{1}H-^{1}H COSY spectrum (acetone-d_6) of compound **14**

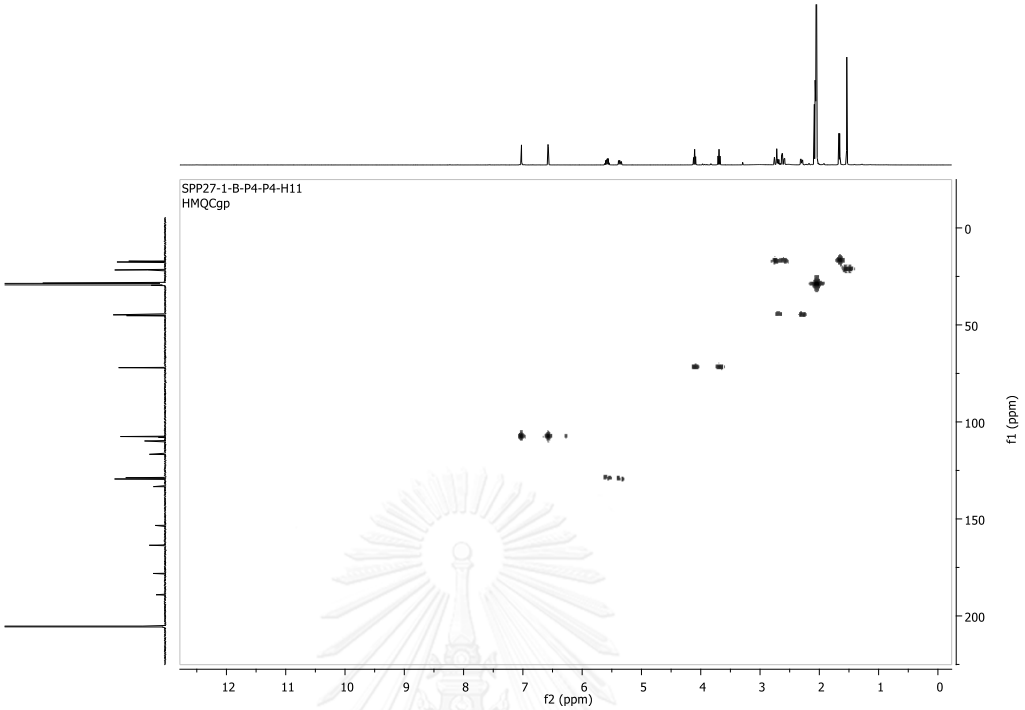

Figure A.92 HMQC spectrum (acetone-d_6) of compound **14**

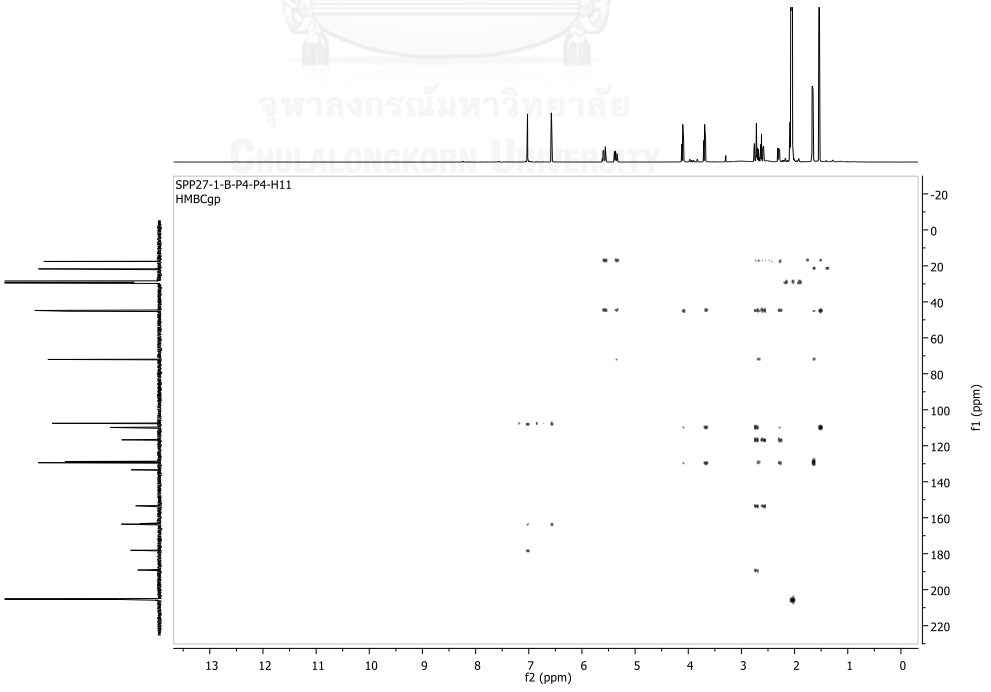

Figure A.93 HMBC spectrum (acetone-d_6) of compound **14**

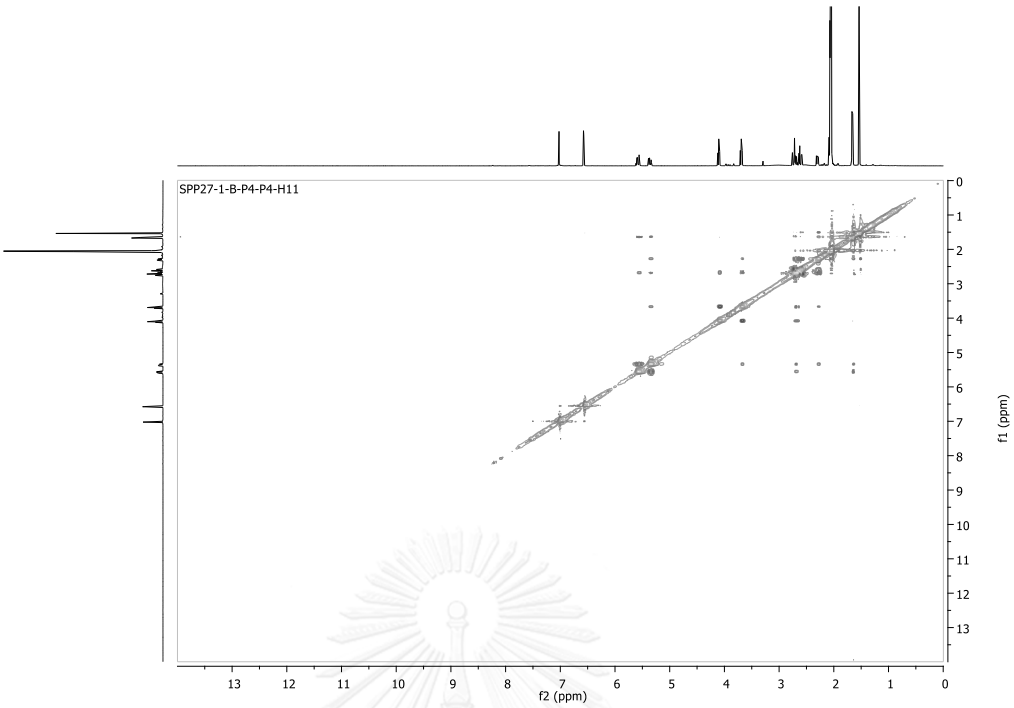

Figure A.94 NOESY spectrum (acetone-d_6) of compound **14**

BIORESOURCES RESEARCH UNIT

High resolution report

Acquisition Date 4/2/2014 10:26:42 AM

Analysis Name	D:\Data\Dua\SPP H11.d				
Method	NaFormate_pos_infusion .m	Operator	Sutichai	Ext: 3560	
Sample Name	SPP H11	Instrument	micrOTOF	Bruker	
		Calibrate by	Sodium Formate		

Acquisition Parameter

Source Type	ESI	Ion Polarity	Positive	Set Nebulizer	1.0 Bar
Focus	Not active			Set Dry Heater	150 °C
Scan Begin	100 m/z	Set Capillary	5000 V	Set Dry Gas	4.0 l/min
Scan End	1500 m/z	Set End Plate Offset	-500 V	Set Divert Valve	Source

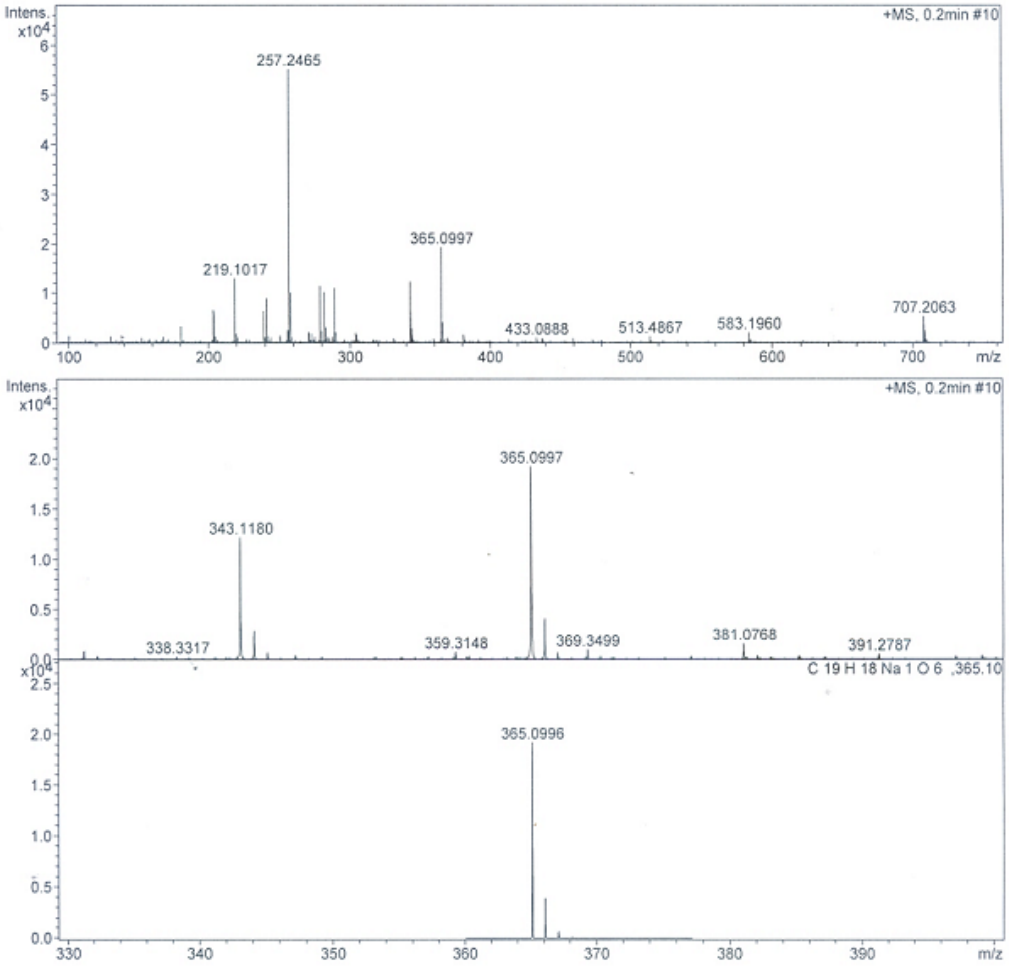

Bruker Daltonics DataAnalysis 3.4 printed: 4/2/2014 10:31:15 AM Page 1 of 1

Figure A.95 HRESIMS Mass spectrum of compound **14**

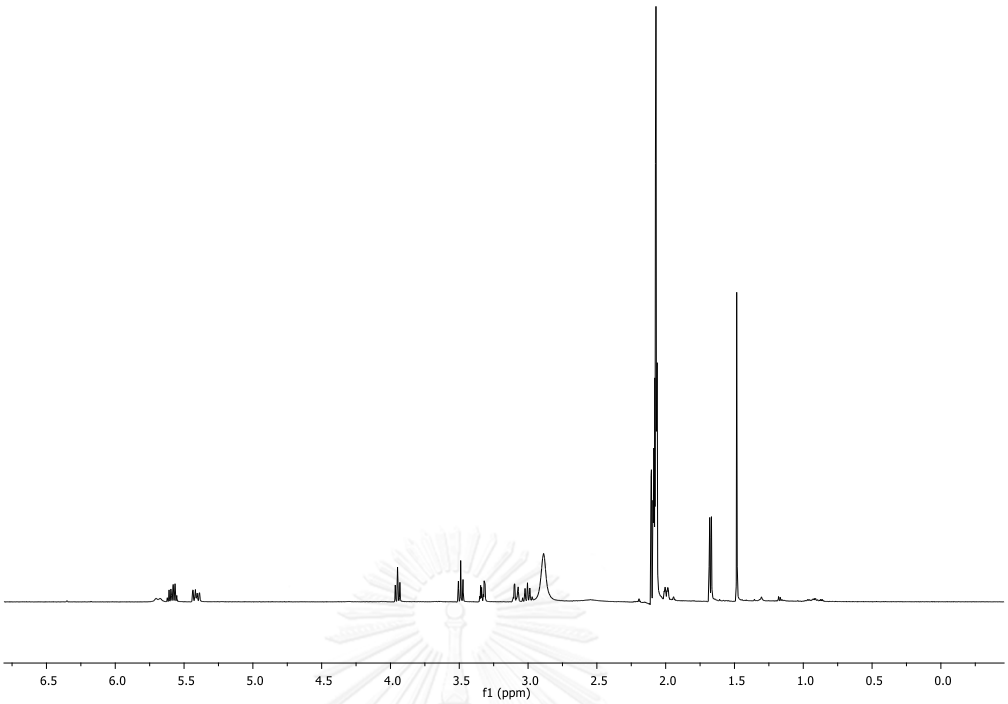

Figure A.96 ^{1}H (500 MHz, acetone-d_6) NMR spectrum of compound **15**

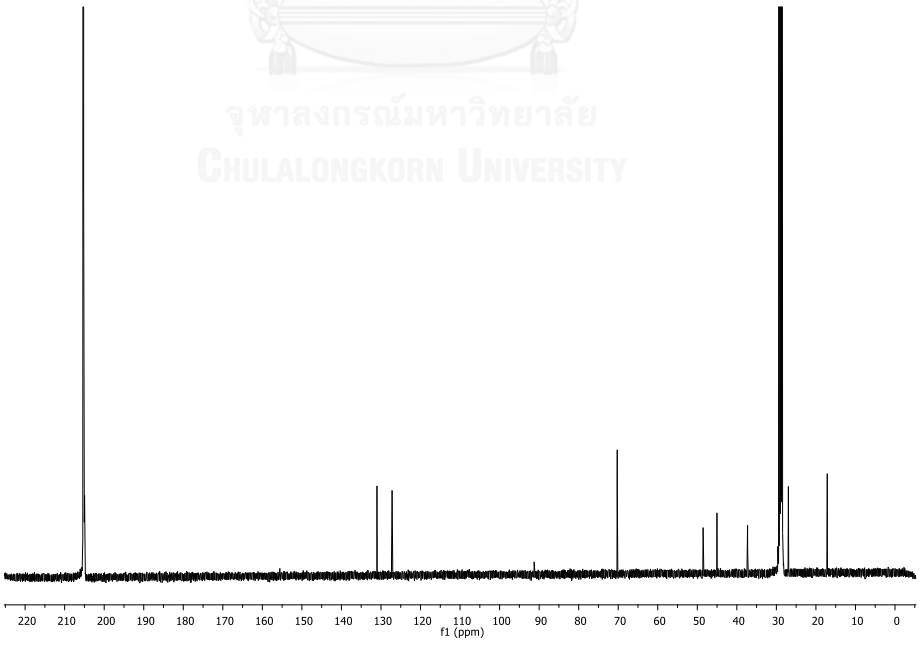

Figure A.97 ^{13}C NMR (acetone-d_6) NMR spectrum of compound **15**

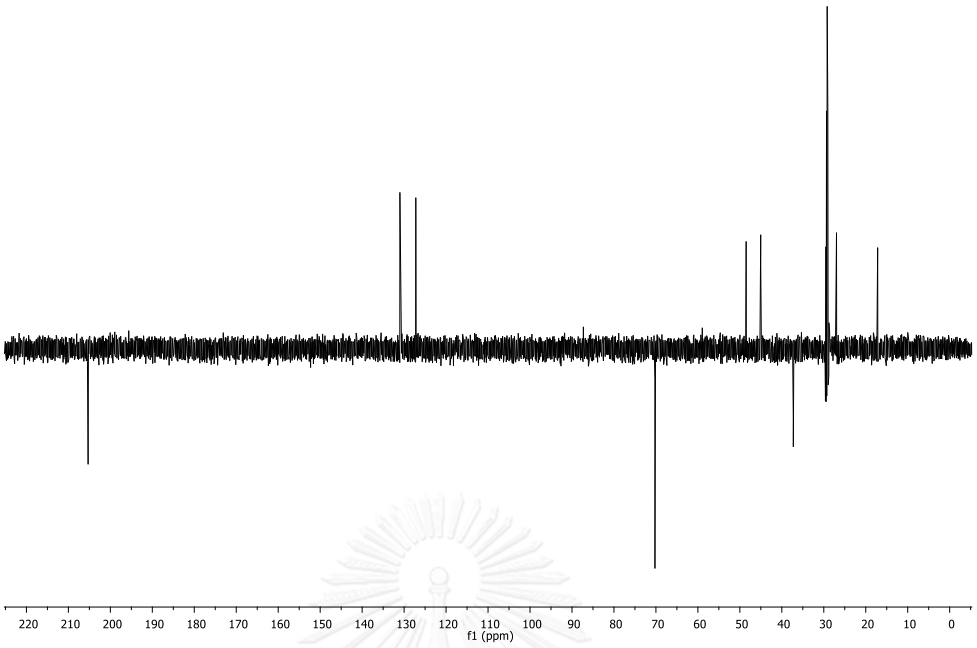

Figure A.98 DEPT spectrum (acetone-d_6) of compound **15**

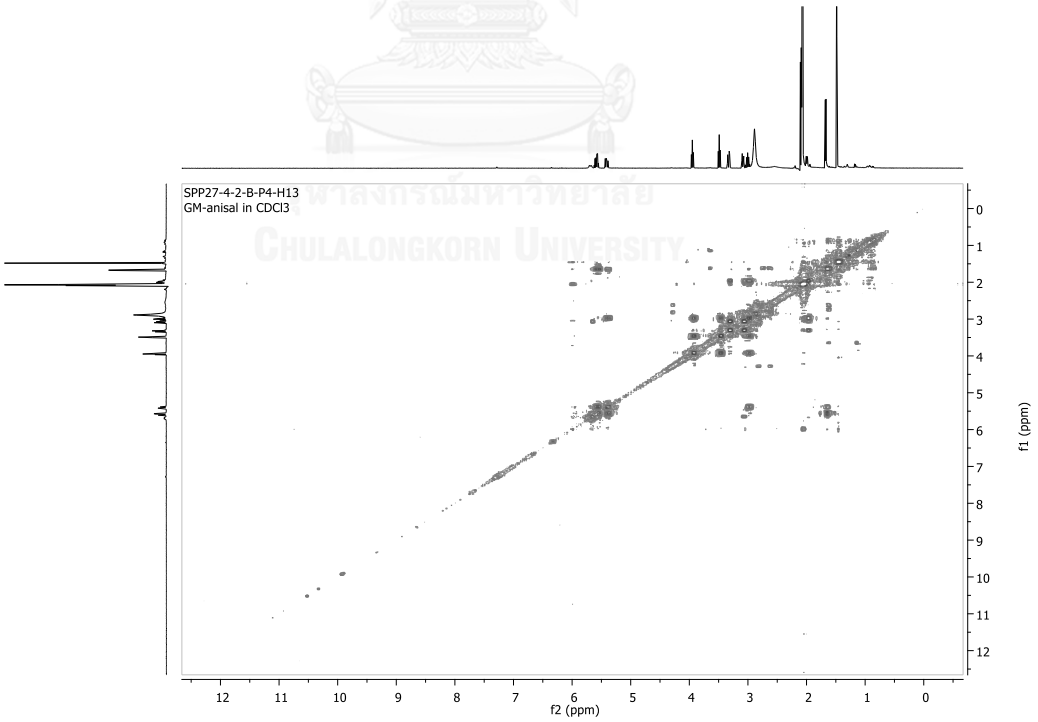

Figure A.99 ^{1}H-^{1}H COSY spectrum (acetone-d_6) of compound **15**

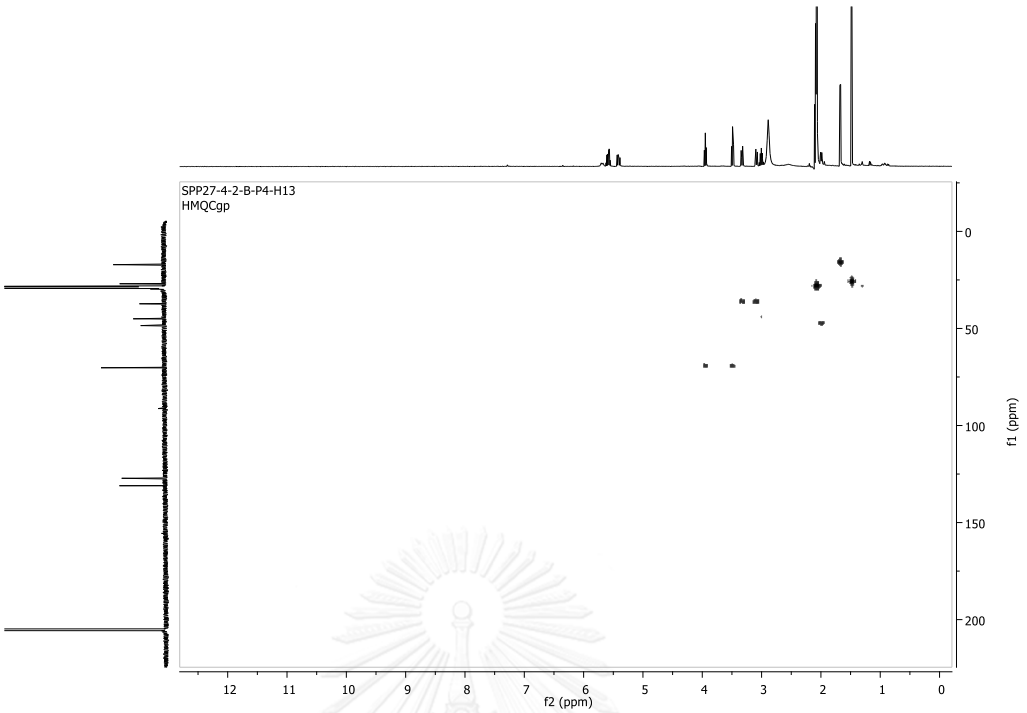

Figure A.100 HMQC spectrum (acetone-d_6) of compound **15**

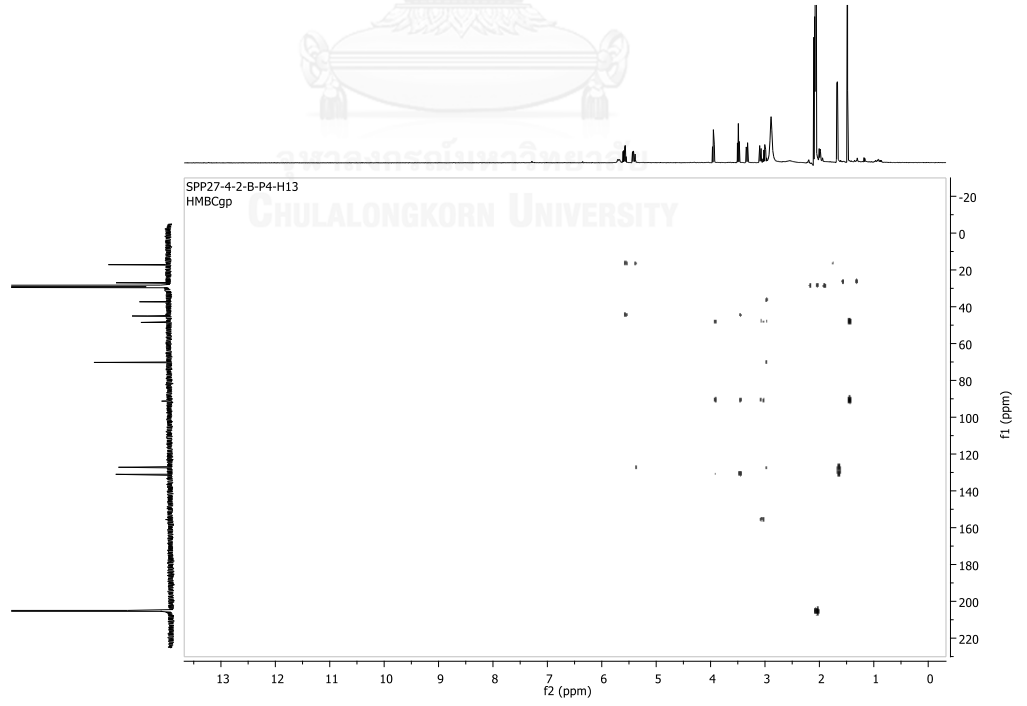

Figure A.101 HMBC spectrum (acetone-d_6) of compound **15**

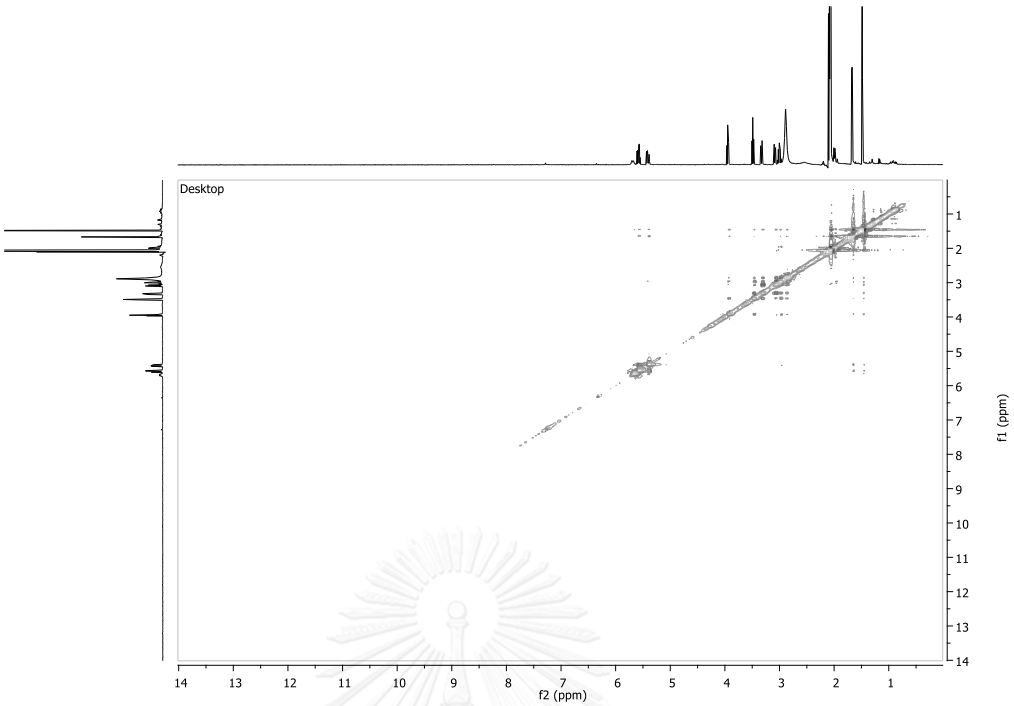

Figure A.102 NOESY spectrum (acetone-d_6) of compound **15**

BIORESOURCES RESEARCH UNIT

High resolution report

		Acquisition Date	4/3/2015 3:50:10 PM
Analysis Name	D:\Data\Taridaporn\SPP271 2 B P4 H13.d		
Method	NaFormate_pos_infusion .m	Operator	Sutichai Ext: 3560
Sample Name	SPP271 2 B P4 H13	Instrument	micrOTOF Bruker
		Calibrate by	Sodium Formate

Acquisition Parameter

Source Type	ESI	Ion Polarity	Positive	Set Nebulizer	1.0 Bar
Focus	Not active			Set Dry Heater	150 ?C
Scan Begin	100 m/z	Set Capillary	5000 V	Set Dry Gas	4.0 l/min
Scan End	1500 m/z	Set End Plate Offset	-500 V	Set Divert Valve	Source

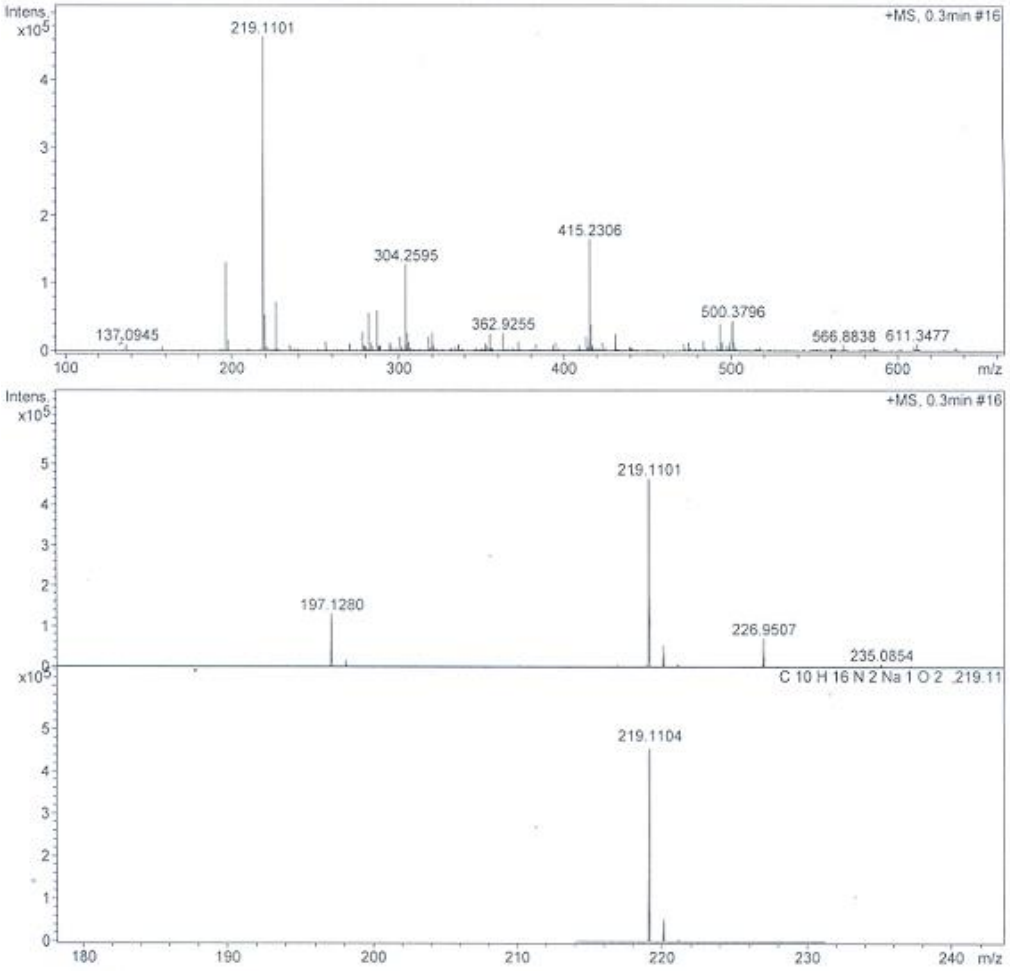

Bruker Daltonics DataAnalysis 3.4 printed: 4/3/2015 3:51:39 PM Page 1 of 1

\Figure A.103 HRESIMS Mass spectrum of compound **15**

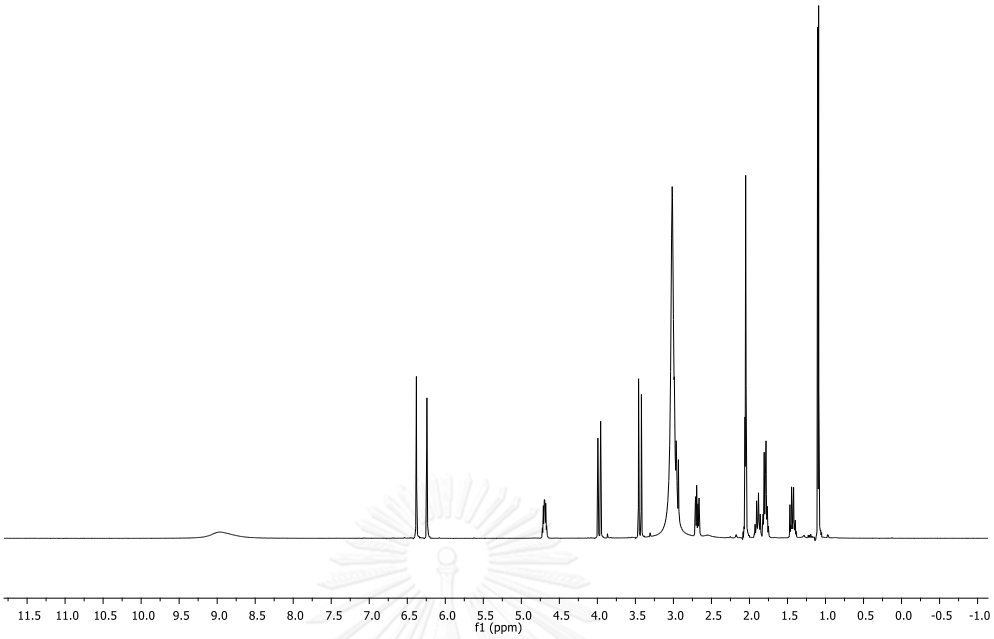

Figure A.104 ^{1}H (500 MHz, acetone-d_6) NMR spectrum of compound **16**

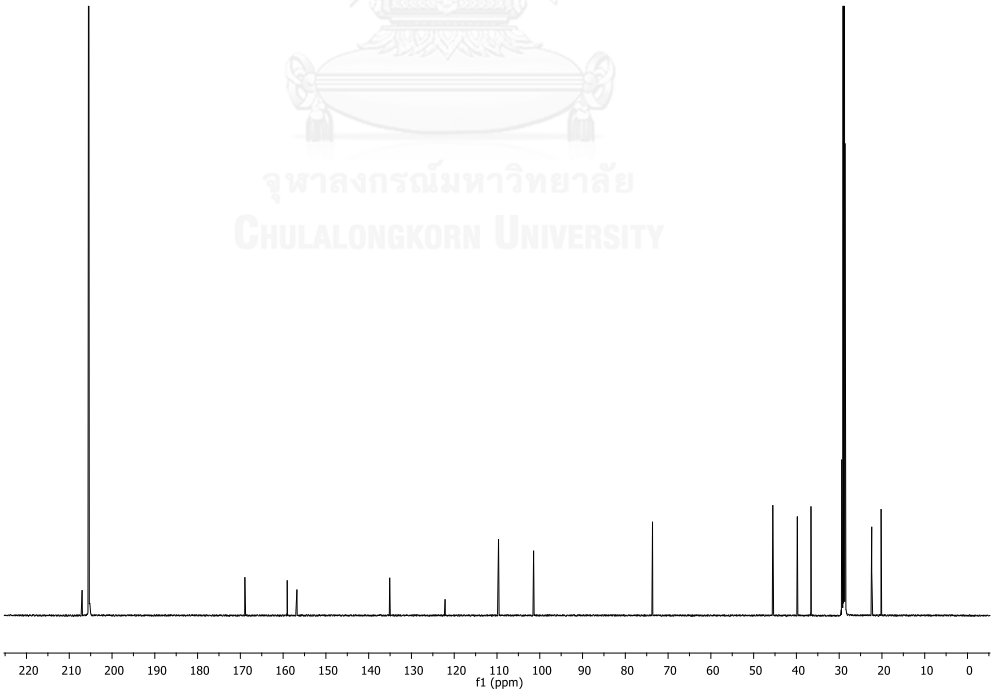

Figure A.105 ^{13}C NMR (acetone-d_6) NMR spectrum of compound **16**

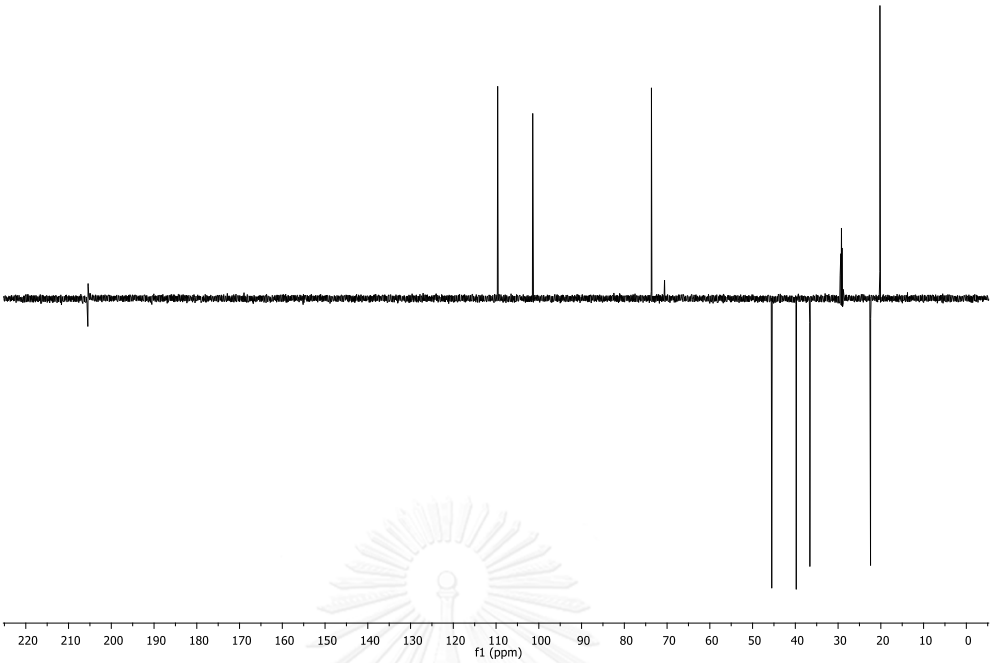

Figure A.106 DEPT spectrum (acetone-d_6) of compound **16**

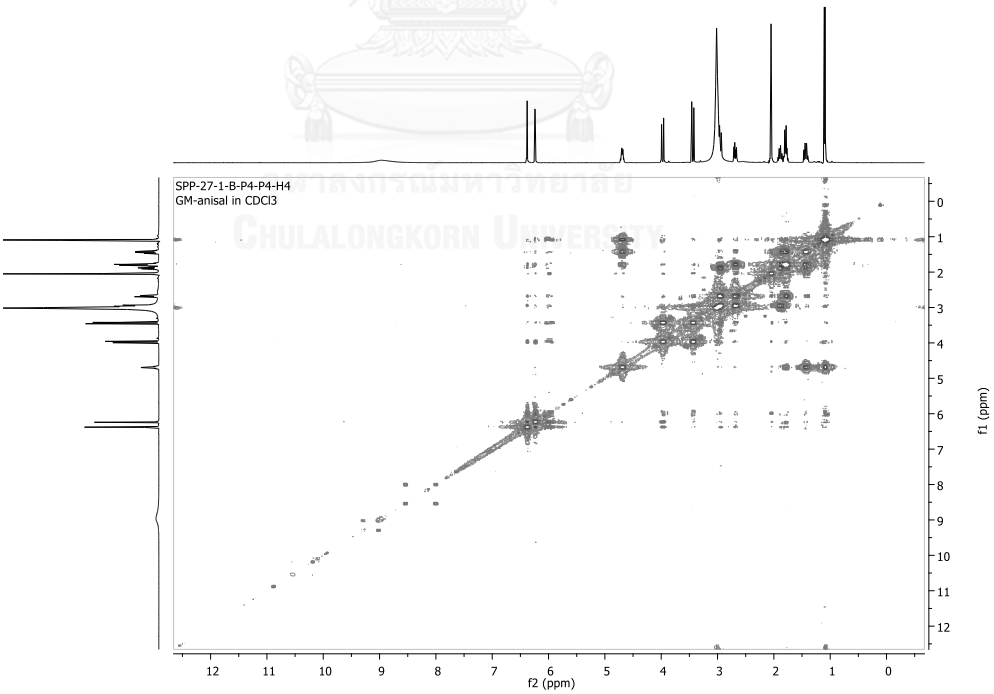

Figure A.107 ^{1}H-^{1}H COSY spectrum (acetone-d_6) of compound **16**

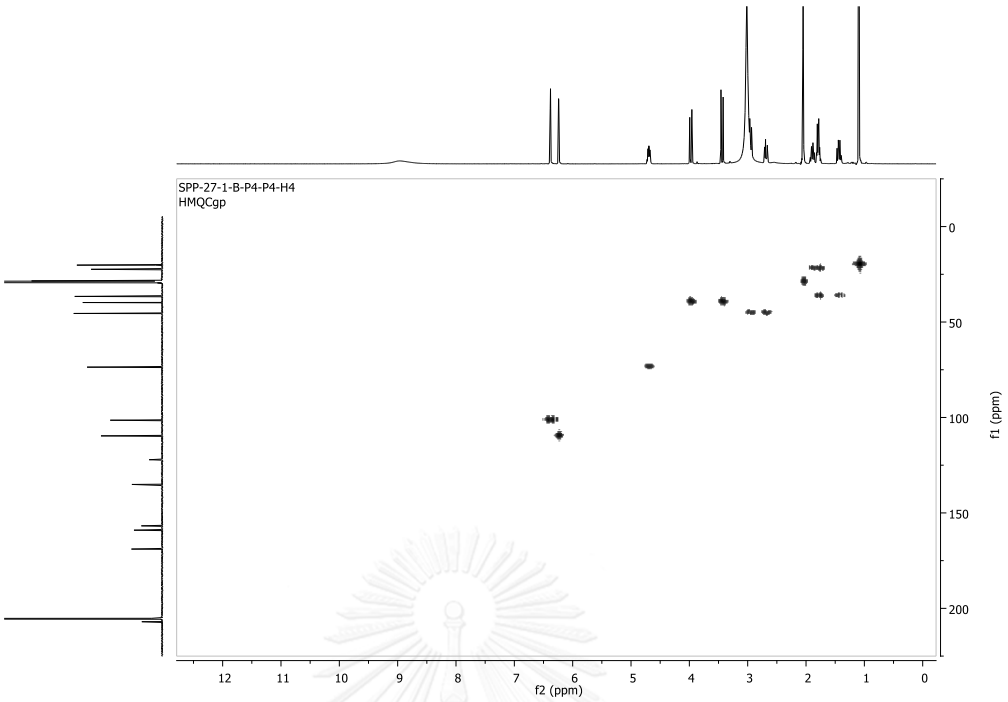

Figure A.108 HMQC spectrum (acetone-d_6) of compound **16**

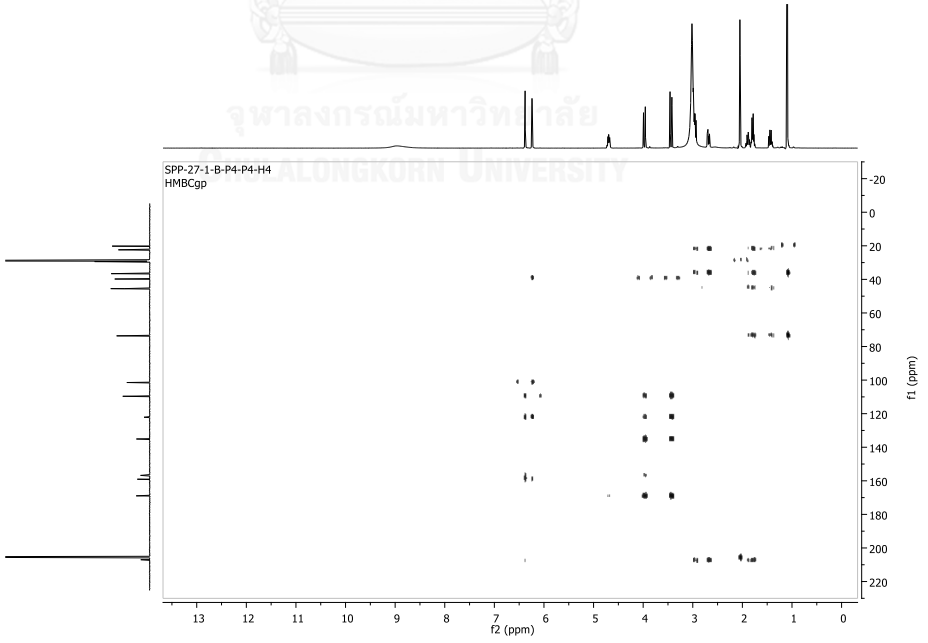

Figure A.109 HMBC spectrum (acetone-d_6) of compound **16**

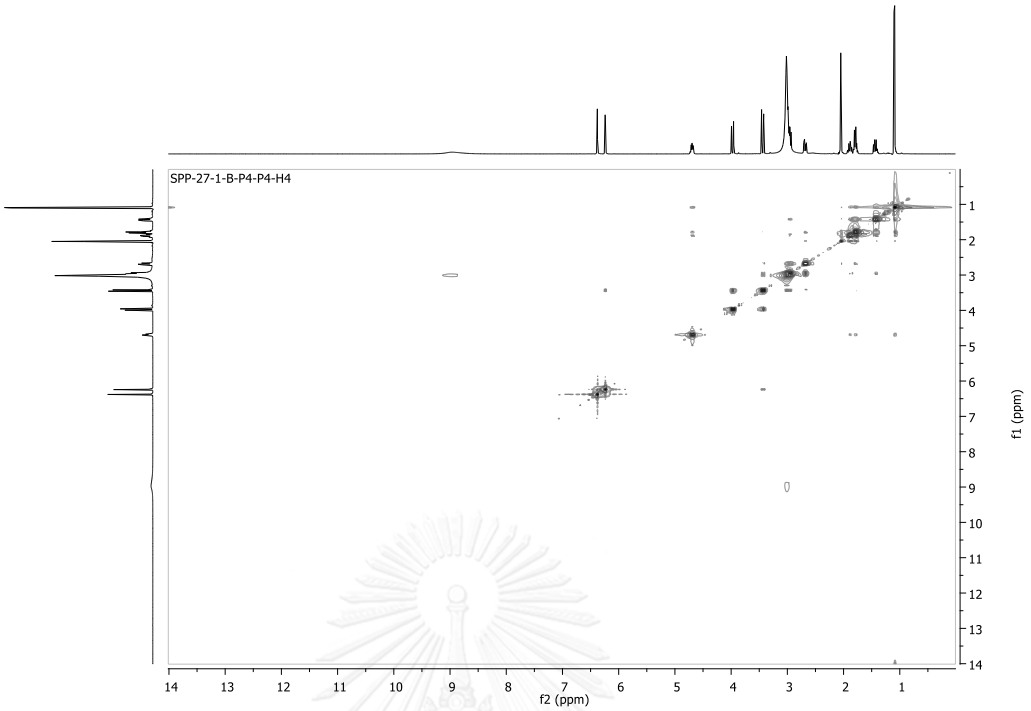

Figure A.110 NOESY spectrum (acetone-d_6) of compound **16**

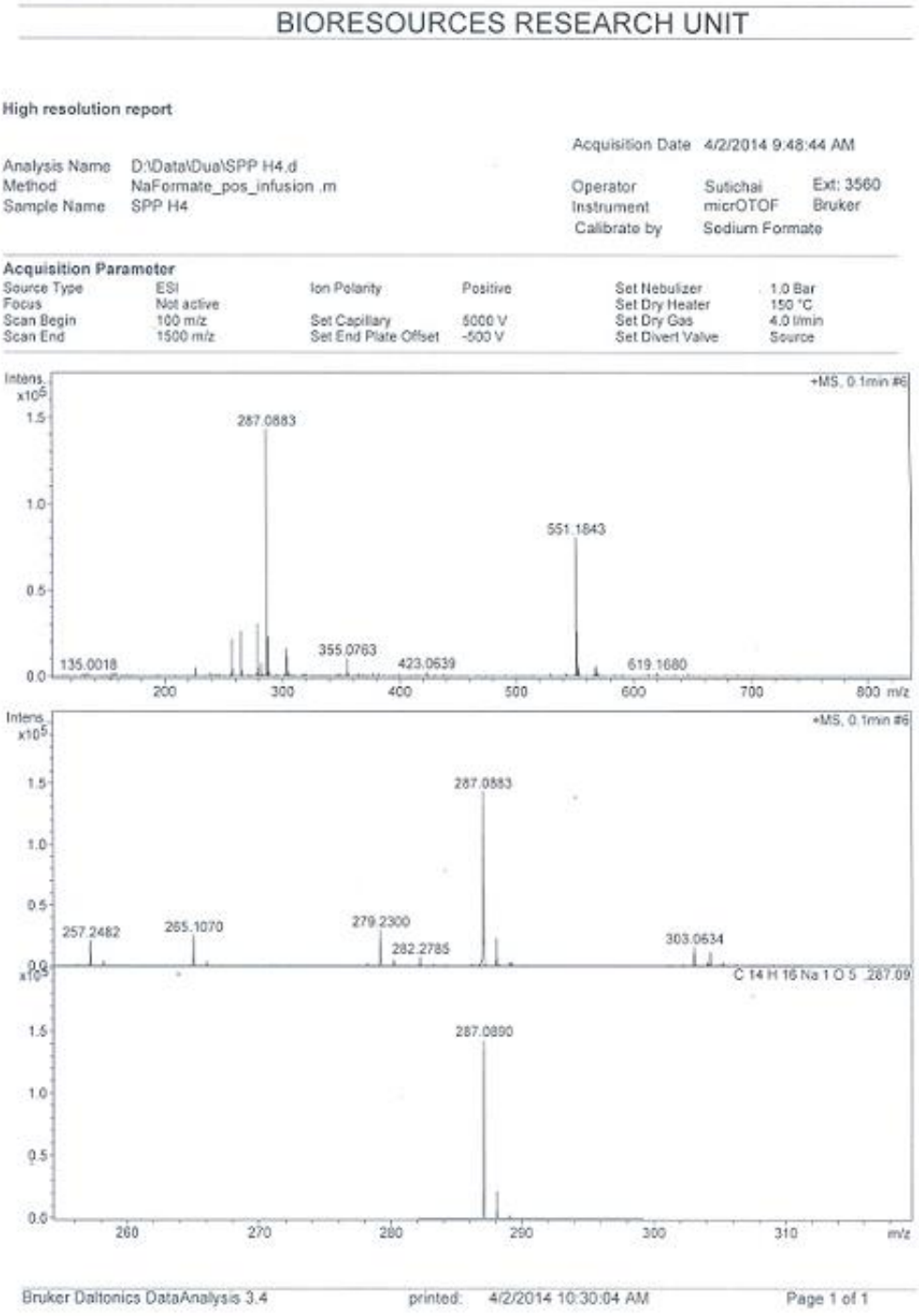

Figure A.111 HRESIMS Mass spectrum of compound **16**

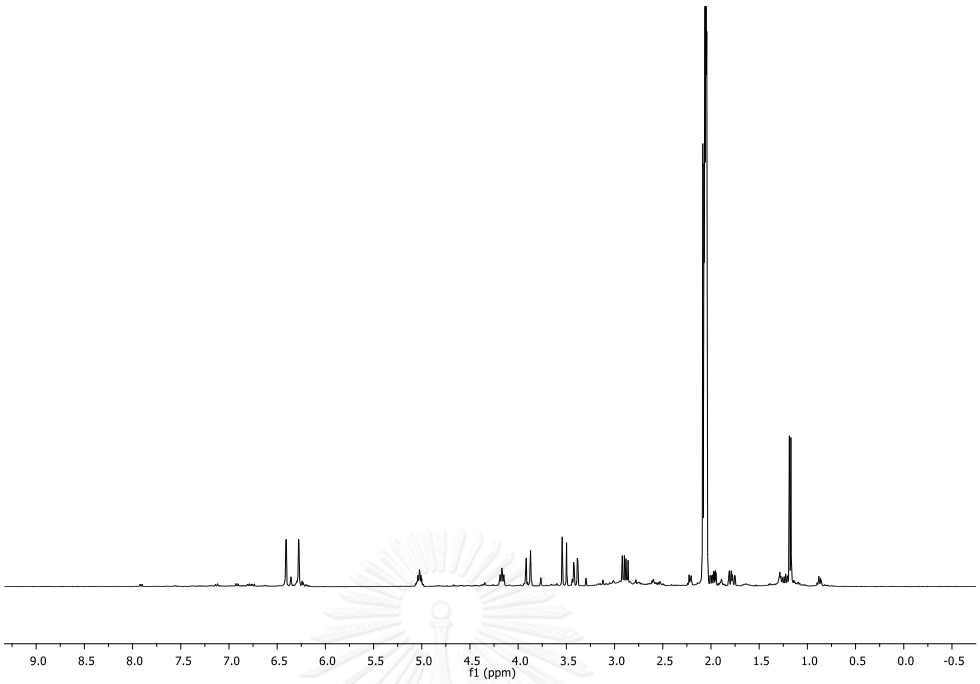

Figure A.112 ^{1}H (500 MHz, acetone-d_6) NMR spectrum of compound **17**

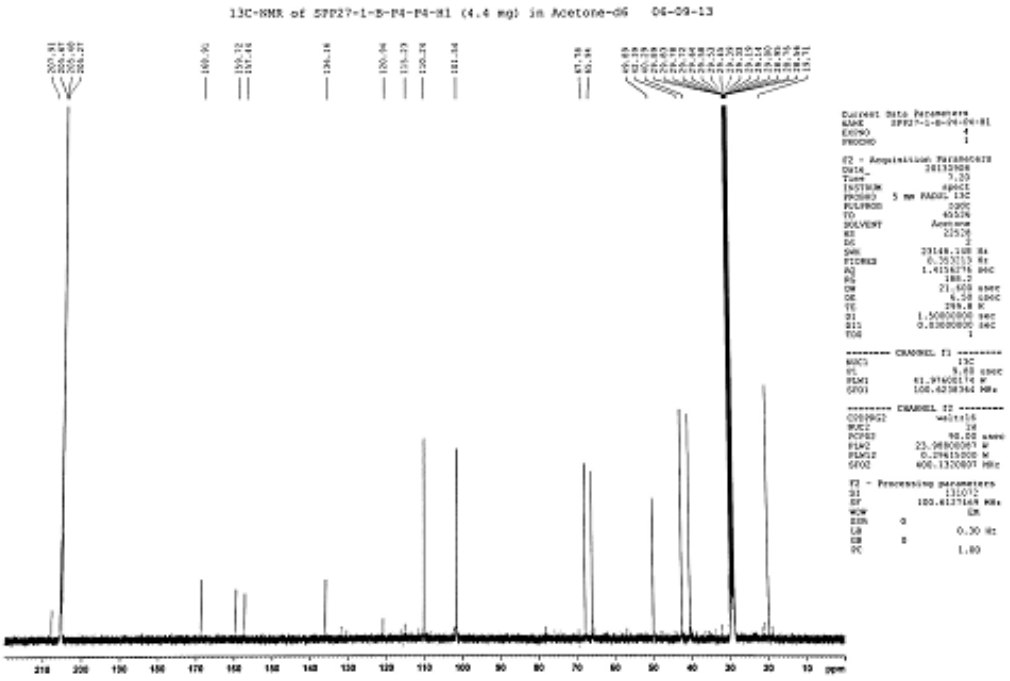

Figure A.113 ^{13}C NMR (acetone-d_6) NMR spectrum of compound **17**

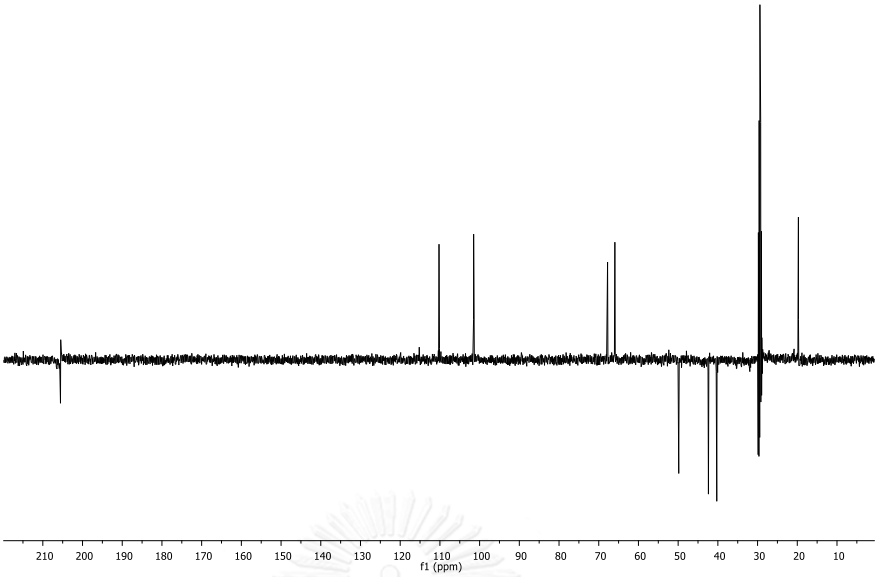

Figure A.114 DEPT spectrum (acetone-d_6) of compound **17**

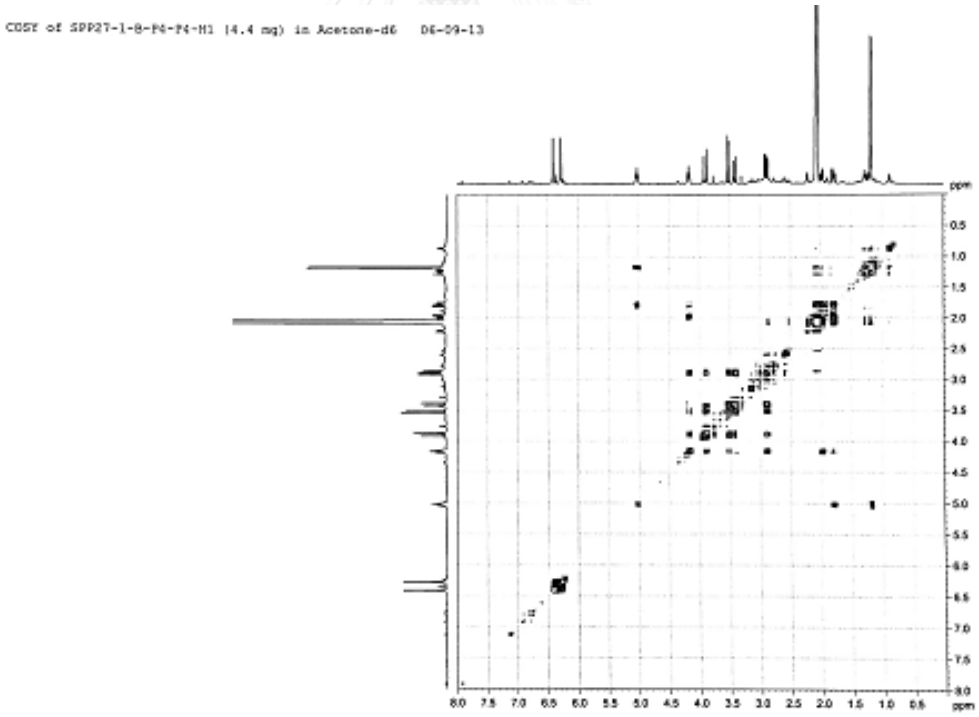

Figure A.115 ^{1}H-^{1}H COSY spectrum (acetone-d_6) of compound **17**

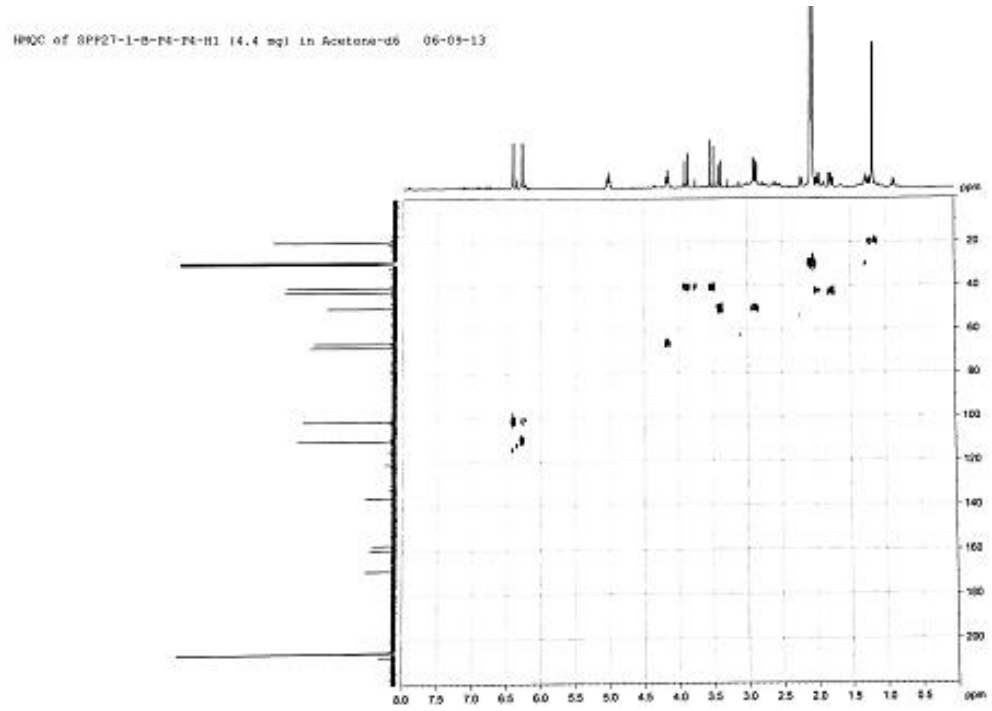

Figure A.116 HMQC spectrum (acetone-d_6) of compound **17**

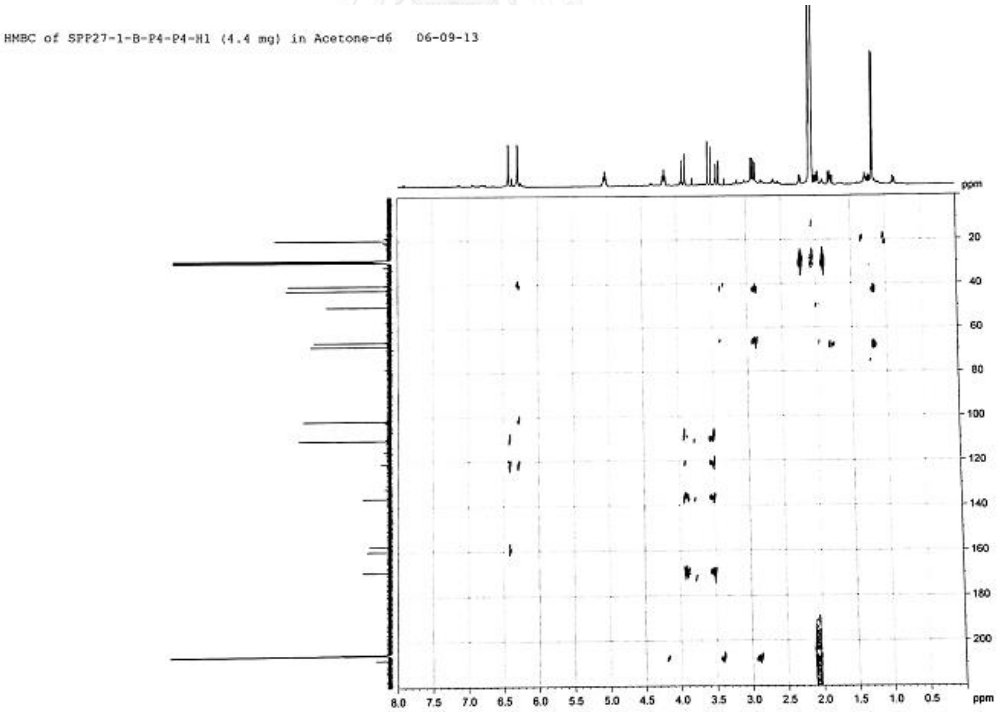

Figure A.117 HMBC spectrum (acetone-d_6) of compound **17**

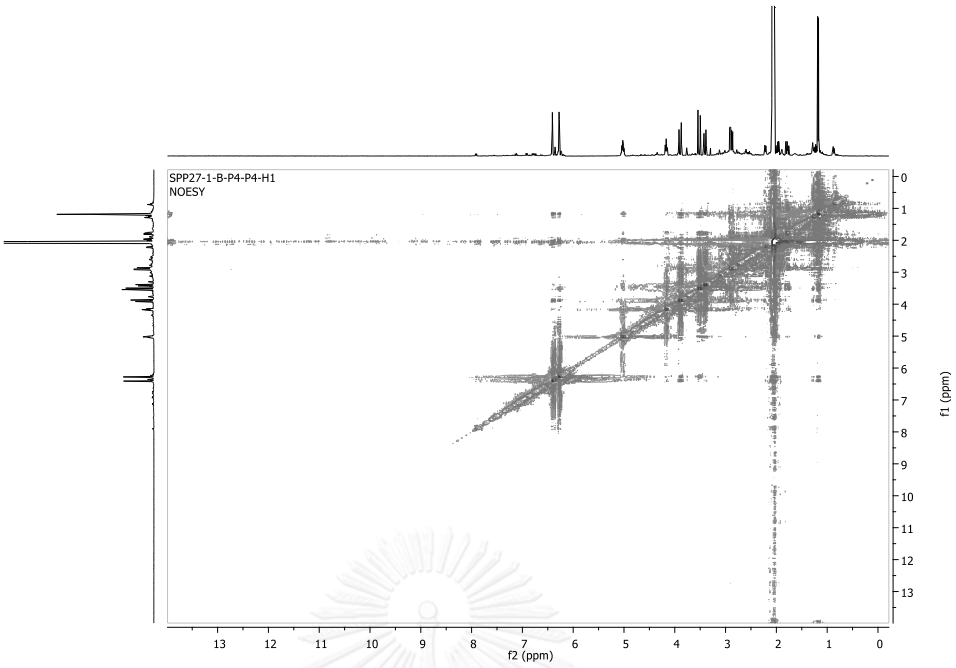

Figure A.118 NOESY spectrum (acetone-d_6) of compound **17**

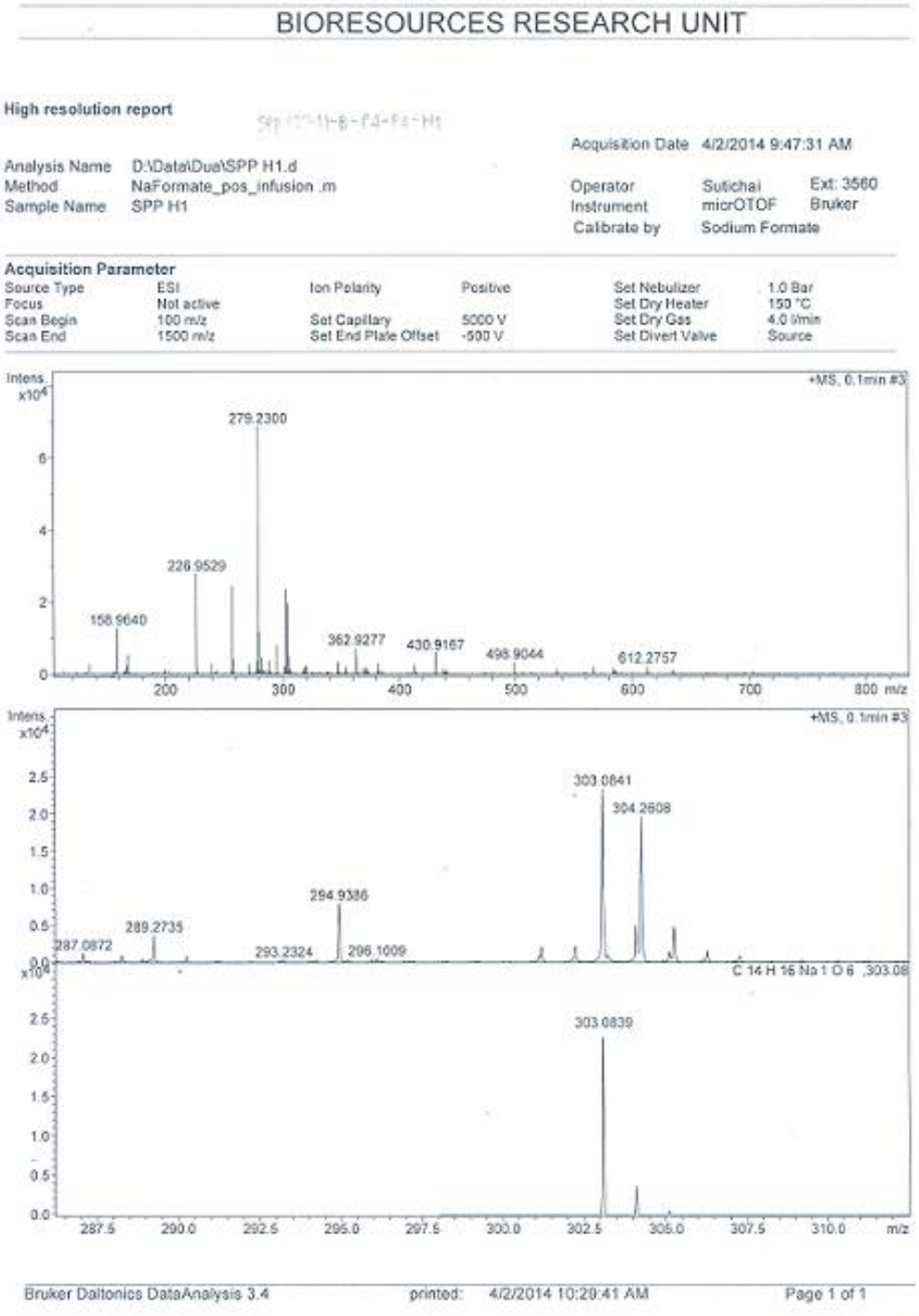

Figure A.119 HRESIMS Mass spectrum of compound **17**

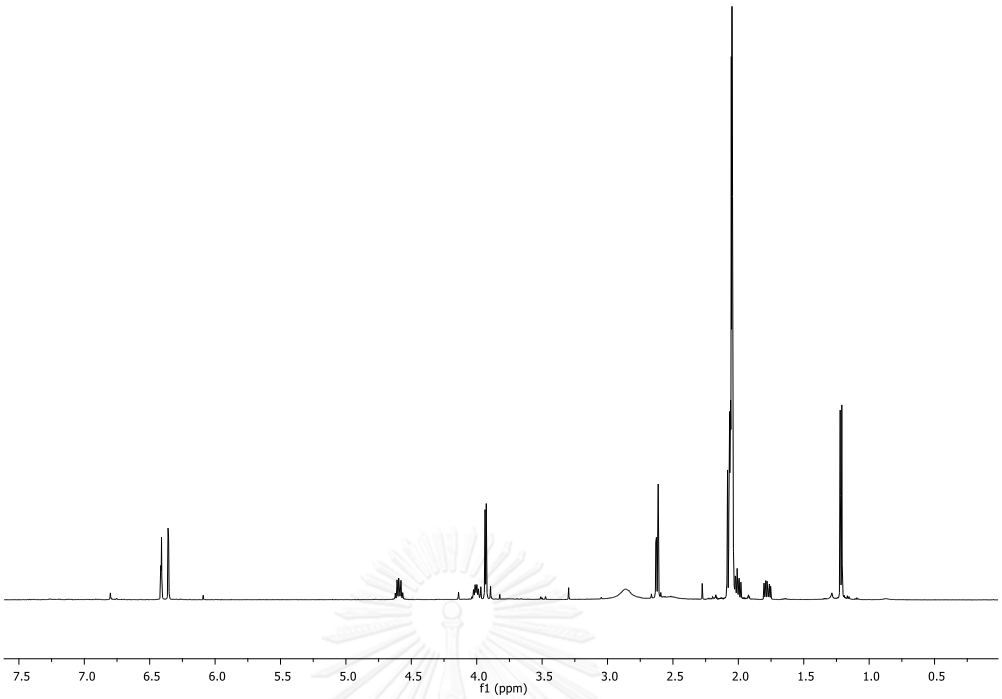

Figure A.120 ^{1}H (500 MHz, acetone-d_6) NMR spectrum of compound **18**

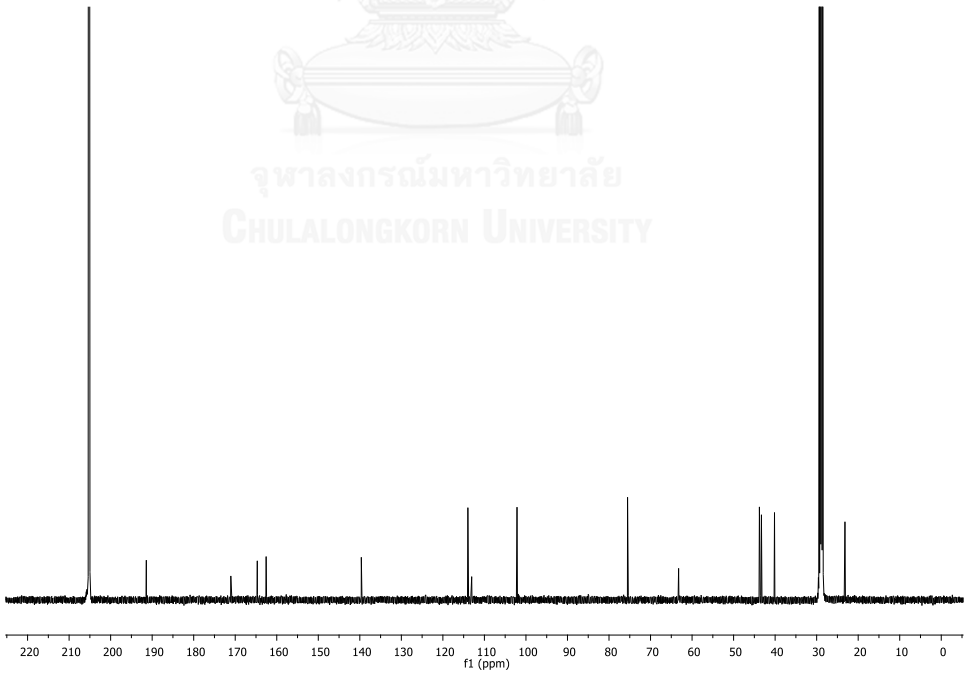

Figure A.121 ^{13}C NMR (acetone-d_6) NMR spectrum of compound **18**

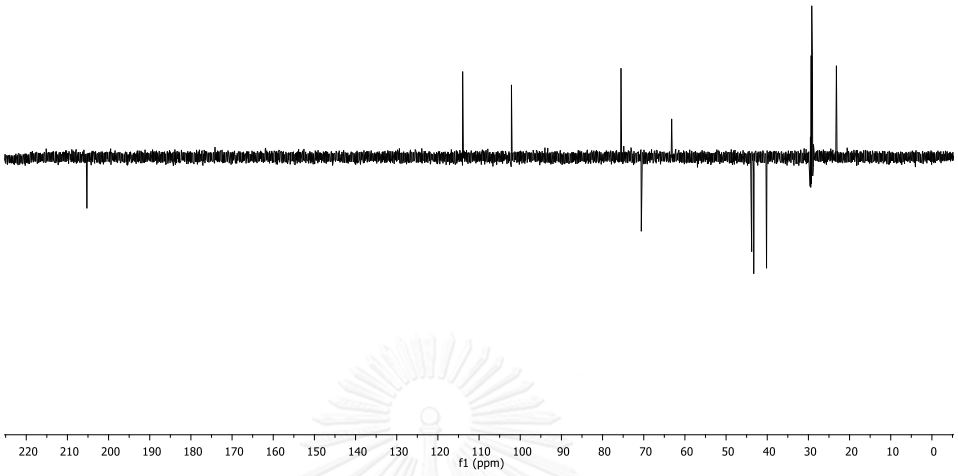

Figure A.122 DEPT spectrum (acetone-d_6) of compound **18**

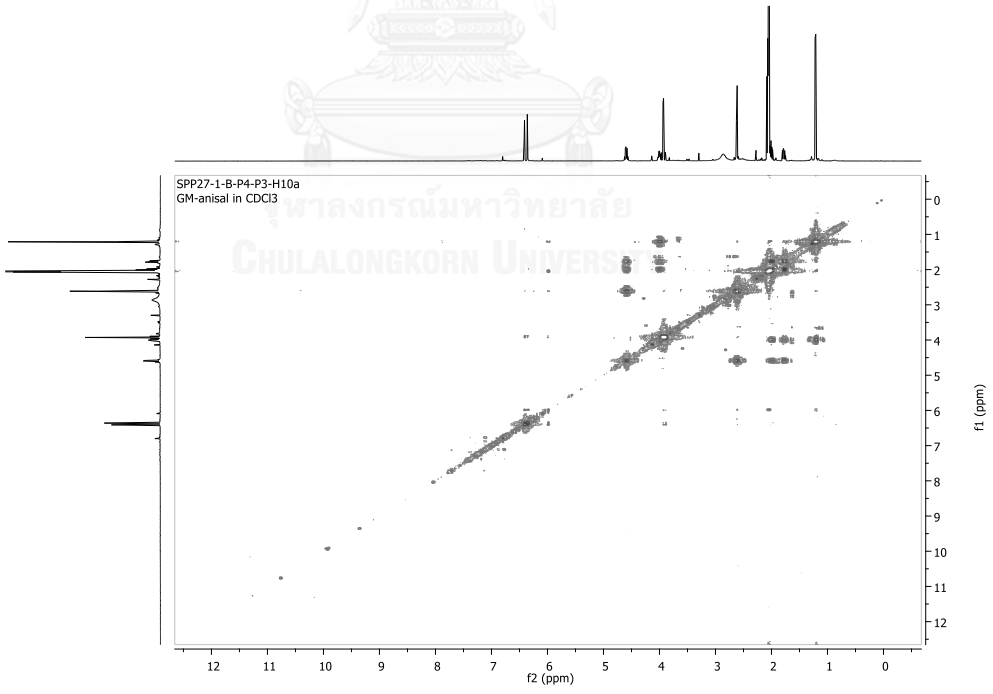

Figure A.123 ^{1}H-^{1}H COSY spectrum (acetone-d_6) of compound **18**

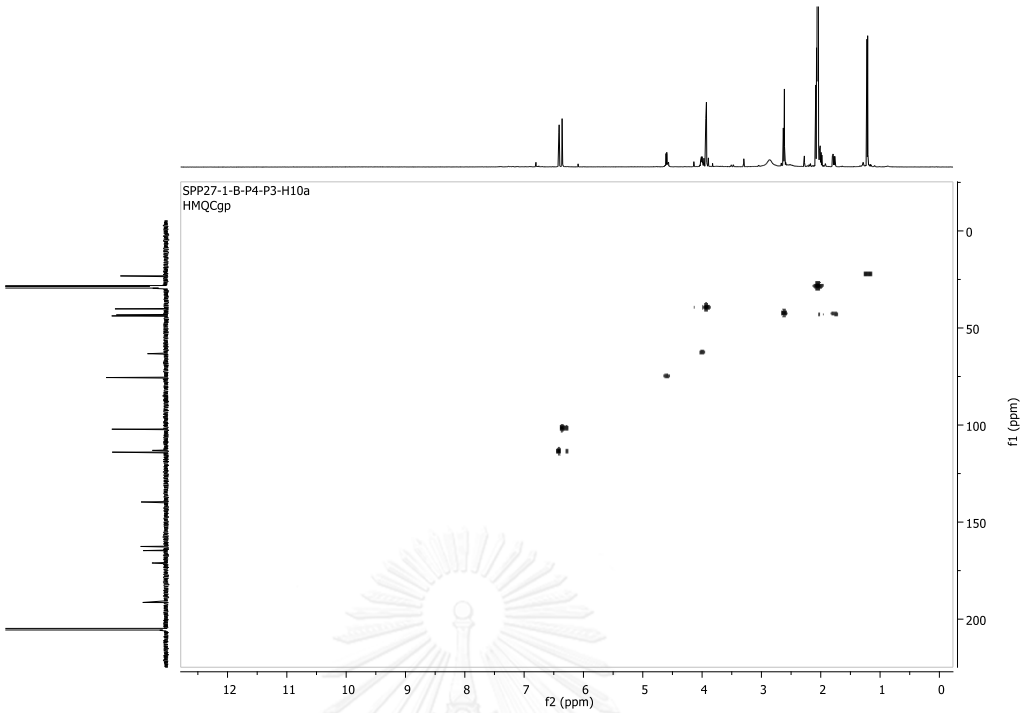

Figure A.124 HMQC spectrum (acetone-d_6) of compound **18**

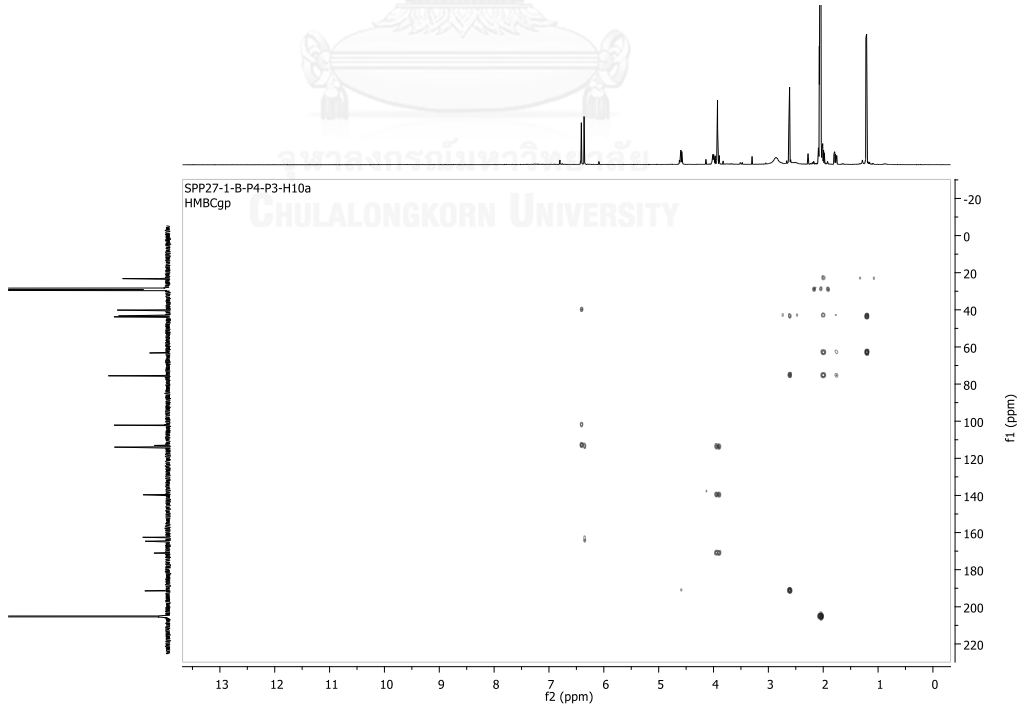

Figure A.125 HMBC spectrum (acetone-d_6) of compound **18**

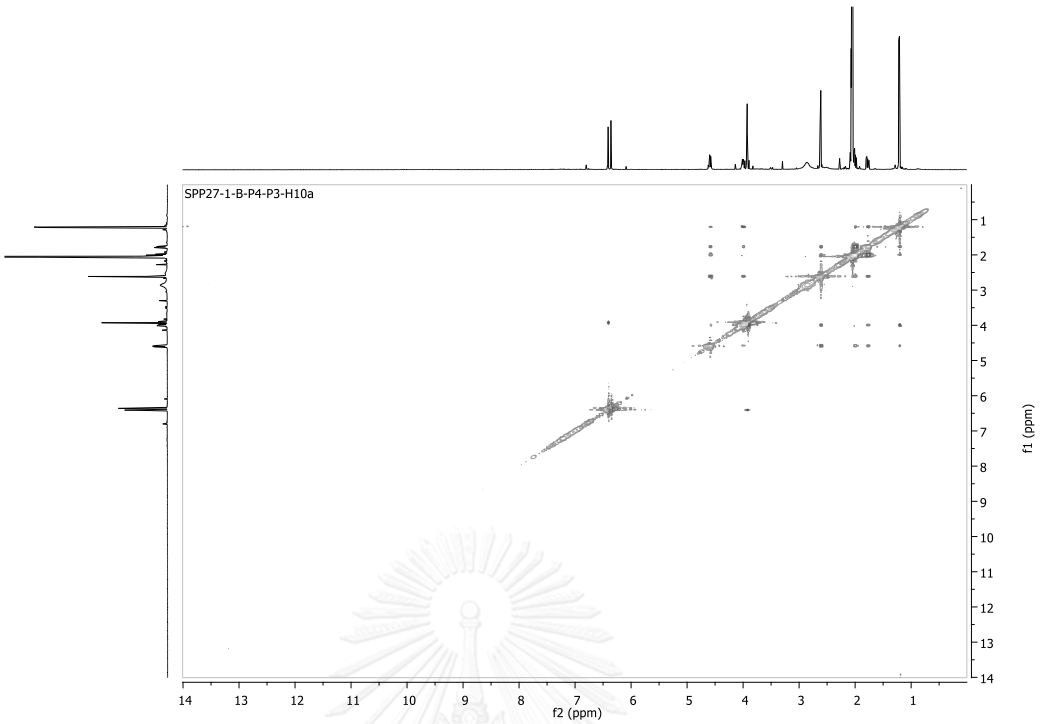

Figure A.126 NOESY spectrum (acetone-d_6) of compound **18**

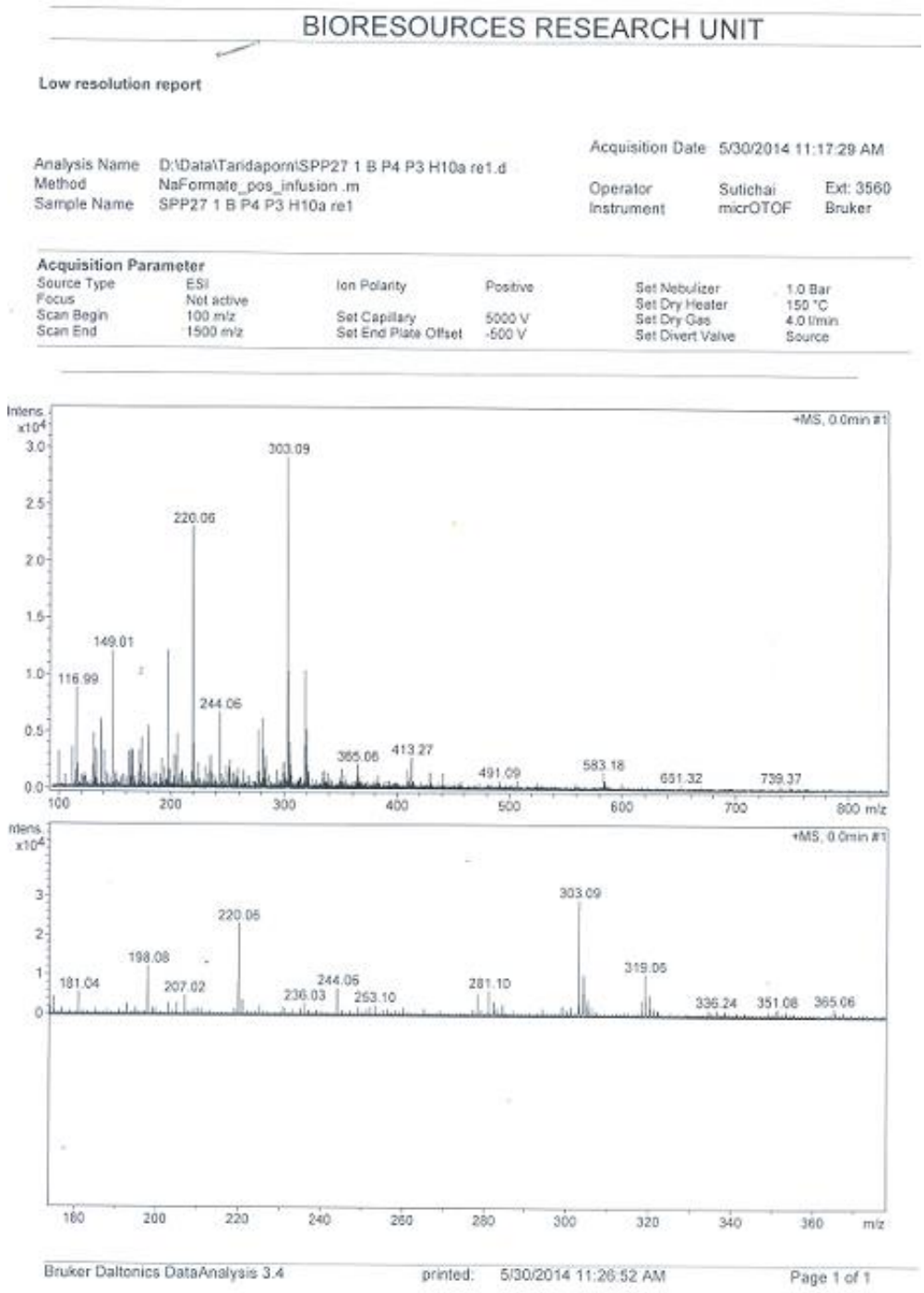

Figure A.127 ESIMS Mass spectrum of compound **18**

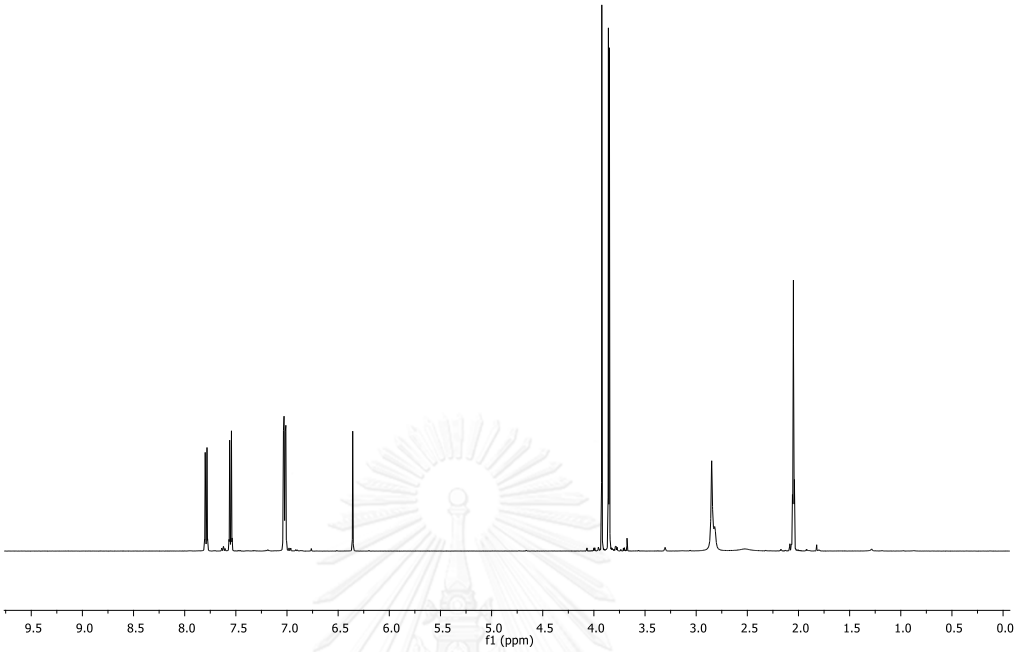

Figure A.128 ^{1}H (500 MHz, acetone-d_6) NMR spectrum of compound **19**

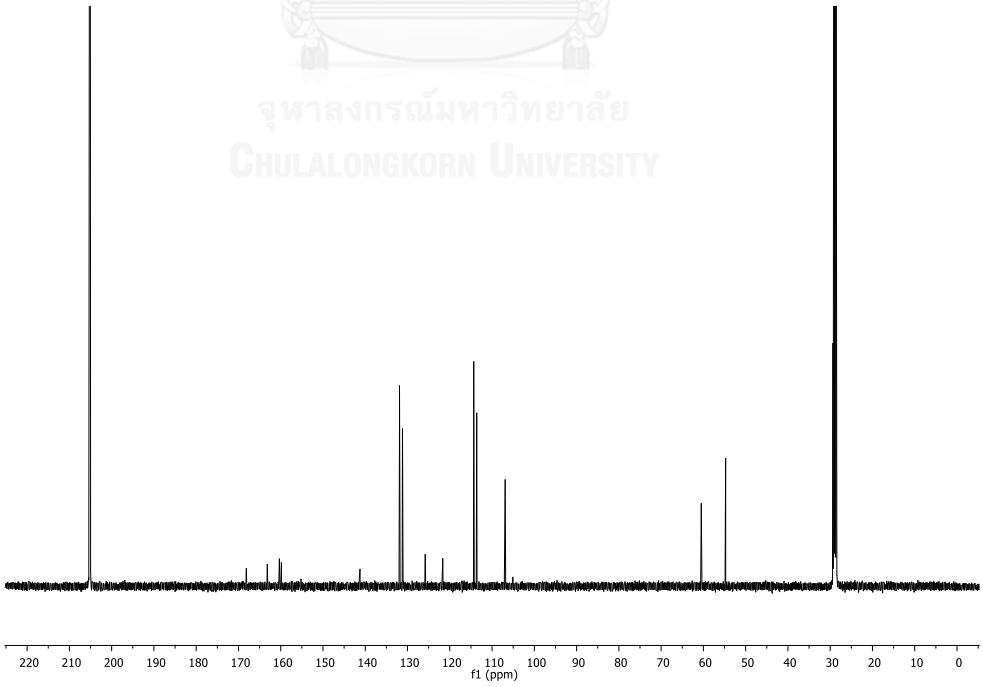

Figure A.129 ^{13}C NMR (acetone-d_6) NMR spectrum of compound **19**

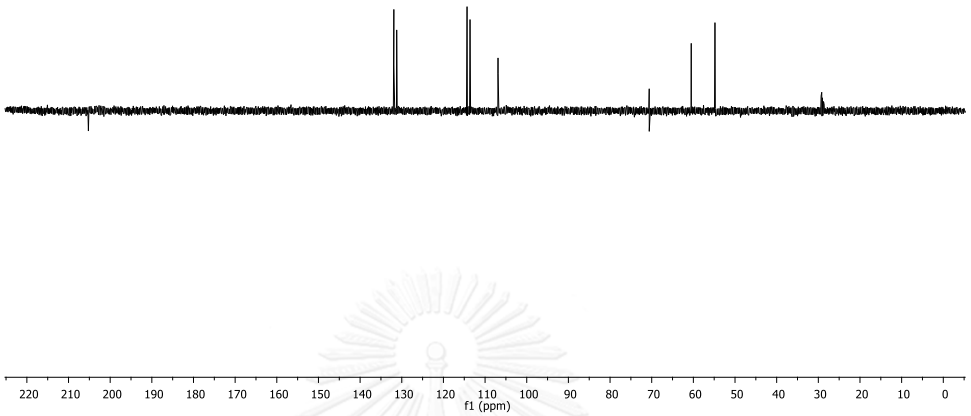

Figure A.130 DEPT spectrum (acetone-d_6) of compound **19**

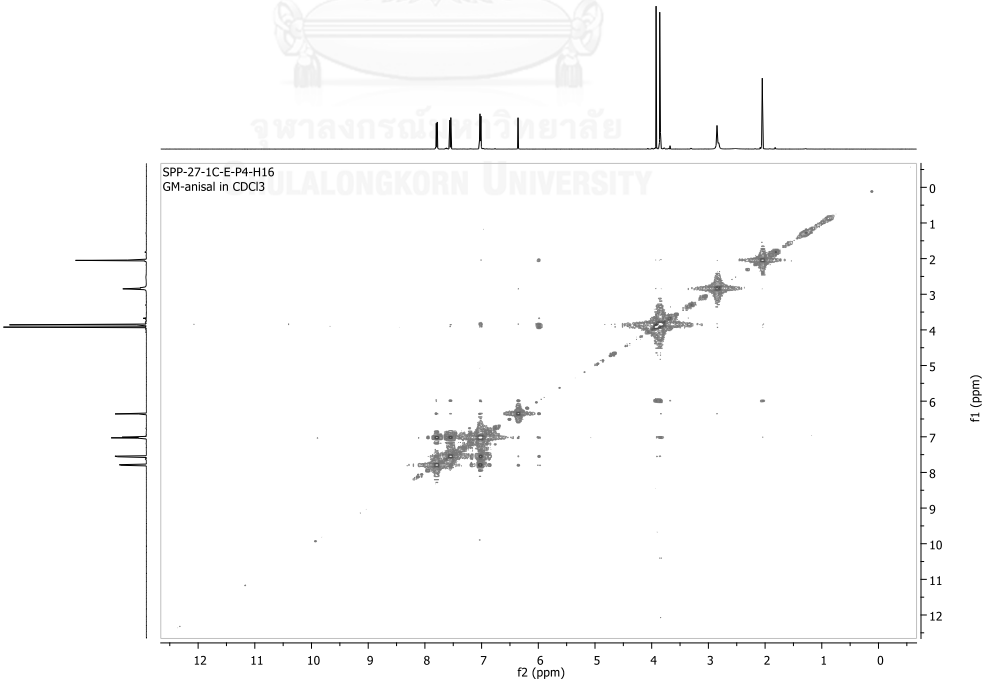

Figure A.131 ^{1}H-^{1}H COSY spectrum (acetone-d_6) of compound **19**

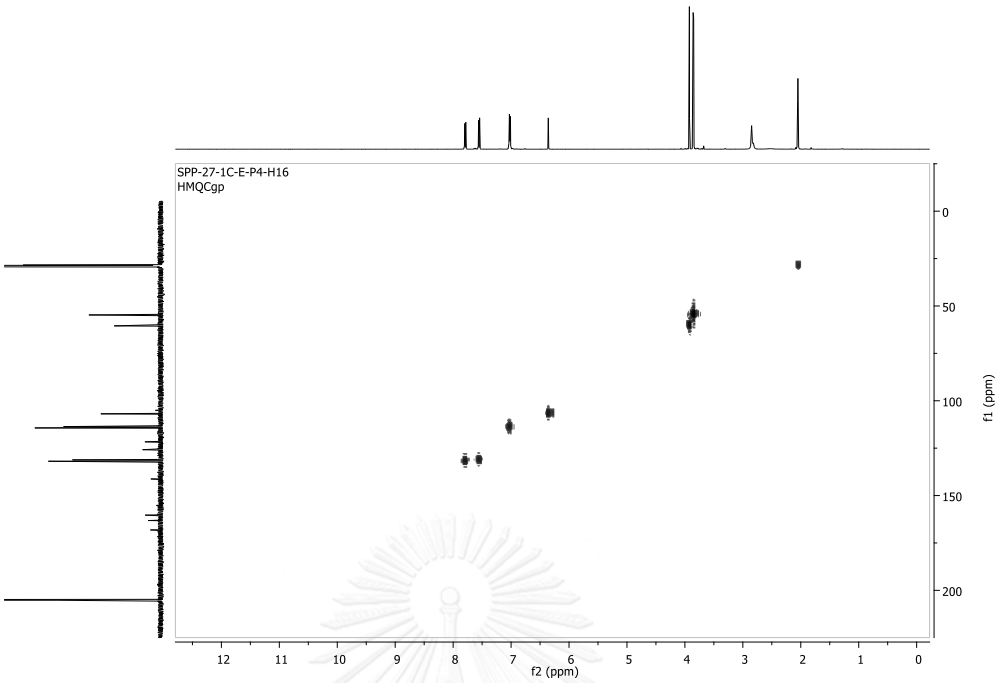

Figure A.132 HMQC spectrum (acetone-d_6) of compound **19**

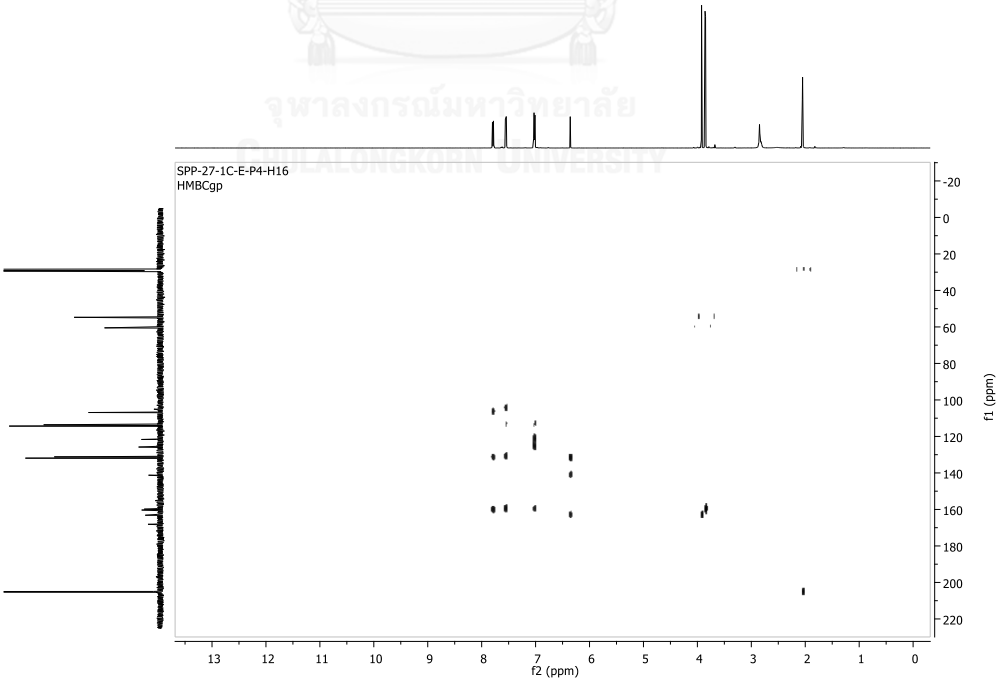

Figure A.133 HMBC spectrum (acetone-d_6) of compound **19**

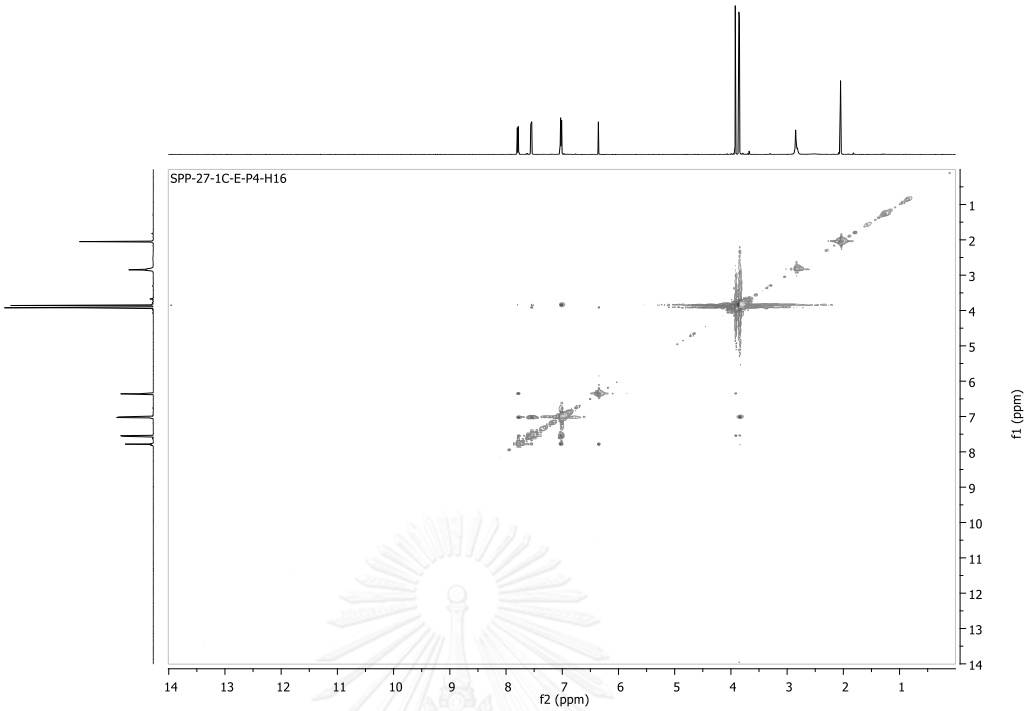

Figure A.134 NOESY spectrum (acetone-d_6) of compound **19**

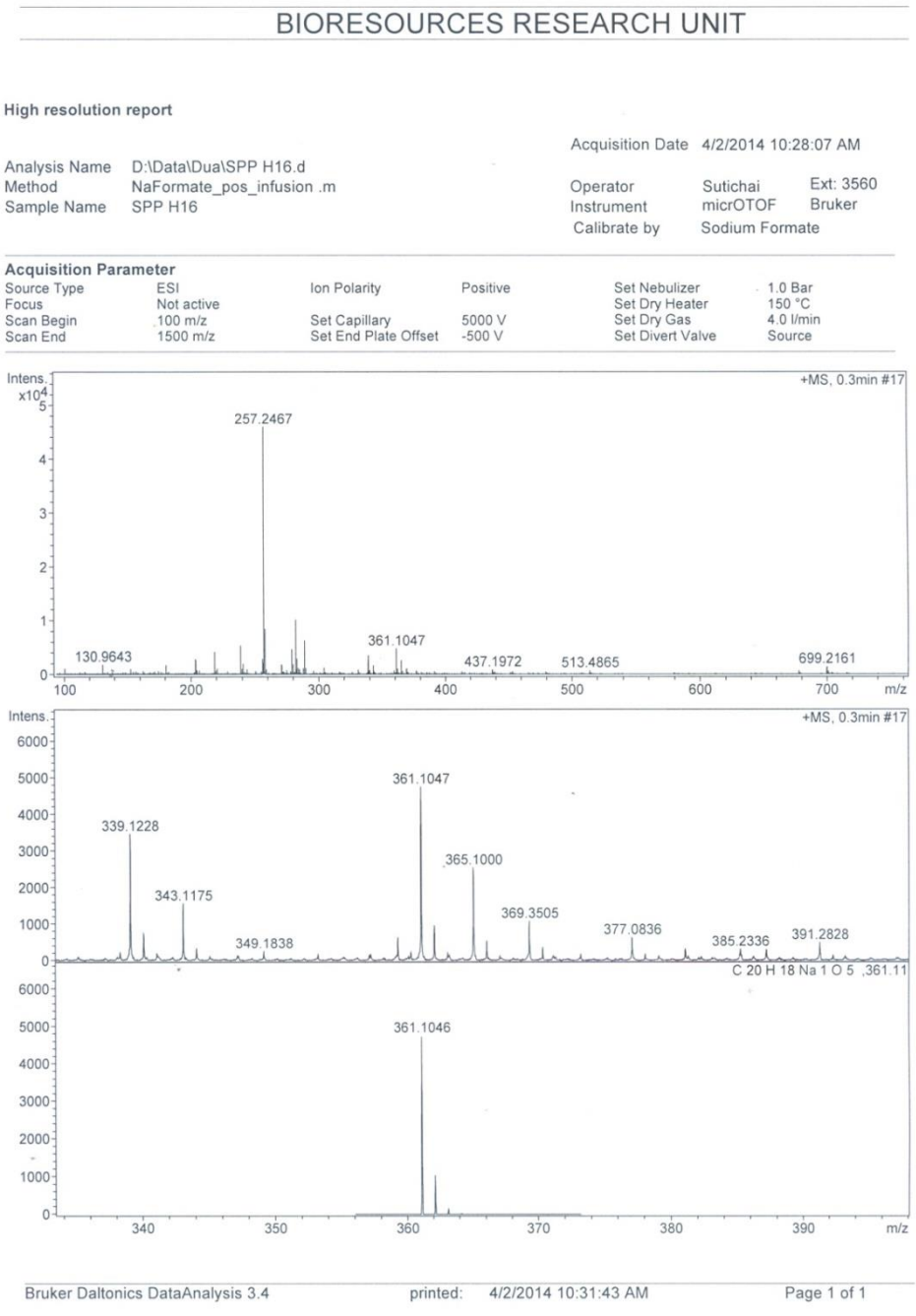

Figure A.135 HRESIMS Mass spectrum of compound **19**

VITA

Ms. Supichar Chokpaiboon was born on July 24, 1981 in Nakhonsawan, Thailand. She was in applied-science program when she attended Satri Nakhonsawan School, and finished her high-school level in 1999. She was graduated with Bachelor's Degree of Science in Food Technology, Institute of Agricultural Technology, Suranaree University of Technology, in 2004. She was graduated in the Master's Degree in Biotechnology program under a scholarship from the Thailand Graduate Institute of Science and Technology (TGIST) of the National Science and Technology Development Agency (NSTDA), in 2009. During the time she was studied in the Doctoral Degree in Biotechnology program under a scholarship from the Thailand Graduate Institute of Science and Technology (TGIST; Grant No. TGIST 01-53-011) of the National Science and Technology Development Agency (NSTDA) and received the 90th Anniversary of Chulalongkorn University Fund (Ratchadaphiseksomphot Endowment Fund) for supporting her research project

Contact address: 84/1 Rodjana Rd., Tambon Takhli, Amphur Takhli, Nakhonsawan 60140

Plublications:

1. Chokpaiboon, S., Sommit, D., Teerawatananond, T., Muangsin, N., Bunyapaiboonsri, T., and Pudhom, K. Cytotoxic Nor-chamigrane and Chamigrane Endoperoxides from a Basidiomycetous Fungus. Journal of Natural Products 73(5) (2010): 1005-1007.

2. Chokpaiboon, S., Sommit, D., Bunyapaiboonsri, T., Matsubara, K., and Pudhom, K. Antiangiogenic Effect of Chamigrane Endoperoxides from a Thai Mangrove-Derived Fungus. Journal of Natural Products, 74(10) (2011): 2290-2294.